2016

Characterization of Human-Induced Vibrations

Benjamin Thomas Davis
University of South Carolina

Characterization of Human-Induced Vibrations

by

Benjamin Thomas Davis

Bachelor of Science
University of South Carolina 2013

Master of Science
University of California, Berkeley 2014

Submitted in Partial Fulfillment of the Requirements

for the Degree of Doctor of Philosophy in

Civil Engineering

College of Engineering and Computing

University of South Carolina

2016

Dedication

To all those who take the road less traveled by,

it makes all the difference [1].

Acknowledgments

Funding

This work is partially supported by a grant from the University of South Carolina Magellan Scholar Program, and additional partial support is provided by a grant from the Alzheimer's Association (ETAC-10-174499).

This work was supported in part by VISN 7 from the United States (US) Department of Veterans Affairs Health Services Research and Development Service. The contents do not represent the views of the US Department of Veterans Affairs or the US Government.

This material is based upon work supported by the National Science Foundation Graduate Research Fellowship Program under Grant Number 1450810. Any opinions, findings, and conclusions or recommendations expressed in this material are those of the author(s) and do not necessarily reflect the views of the National Science Foundation.

Appreciation

My thanks to the following who are presented in no particular order and with the role I knew them in:

- Dr. Juan Caicedo (USC Professor) for his invaluable guidance, support, and encouragement since the beginning of my college career;
- Dr. Victor Hirth (PH Medical Director) for his collaboration and guidance on the project;
- Dr. Bruce Easterling (VAMC Doctor) for his collaboration on the hospital study;

- Dr. Charles Pierce (USC Professor) for inspiring me to be a civil engineer during the Carolina Master Scholars program;
- Johannio Marulanda, Glen Weiger, Gustavo Ospina, and Grady Mathews (PhD Candidates) for helping me thoroughly understand various aspects of engineering;
- Ramin Madarshahian, Albert Ortiz, and Yohanna Mejia (PhD Candidates) for helping refine ideas and conquer stubborn math problems;
- Diego Arocha (MS Student) for creating a benchmark dataset comprising 3575 human-induced vibrations records;
- Michael Fernandez (BS Student) for building the steel test frame FEEL was initially tested on;
- Andrew MacMillan (BS Student) for his help testing the monitoring system before deployment;
- Robert Boykin (BS Student) for lending his computer science skills to help develop the monitoring system;
- Minji Moon (High School Student) for her aid in the initial experiments to develop FEEL;
- Davis Borucki (High School Student) for his aid in the initial experiments to develop FEEL;
- Laney Patterson (High School Student) for being a joy summer after summer helping with experiments;
- Emily Cranwell (Writing Center MS Student) for her English grammar/spelling/writing review and tips so my proposal and dissertation would sound even better;
- Mackenzie Roman (Nuclear Engineer) for her upbeat encouragement and food deliveries;
- Eric and Diane Davis (My Parents) for encouraging me to reach for the stars;
- Emily Davis (My Sister) for her encouragement and support, and keeping me grounded;
- the many study participants across the state of South Carolina;
- countless teachers;
- and all those who kept me going through your encouragement and support.

Abstract

In the US alone, 20% of citizens will be over the age of 65 by the year 2030, and the largest challenge facing this growing demographic is not a new disease but a simple motion - the fall. These events are the premier cause of fatal and nonfatal injuries. In fact, a fall is so common that every 17 seconds an older adult is treated for fall-related injuries, and every 30 minutes, an older adult dies from fall complications. Research has shown a positive outcome of a fall event is largely dependent on the immediate response (<30 minutes) and rescue of the person.

This work explores the concept of utilizing structural vibrations to detect human falls for rapid rescue response. A human-induced vibration monitoring system is developed on the principles of the ideal fall detection system. The system was installed throughout the William Jennings Bryan Dorn Veteran's Administration Medical Center (VAMC) and a private four person family's residence to collect real world human-induced vibrations. Installation resulted in the recording of 16 human falls and 45,000 acceleration events, expanding the database to 220,597 events as of 2016 February 1. This and other information are recorded according to the data management plan presented within to enable future study of human activity from vibrations.

For a successful fall detection system implementation, the accelerometers need the ability to discern good signals to reduce the amount of data analyzed. A method of signal categorization using Support Vector Machines is explored to this end, with 96.8% accuracy over 100 trials. Following signal selection, the ability to detect a fall regardless of the distance from the event to the accelerometer becomes paramount, and is overcome with the introduction of the Force Estimation and Event Localization

(FEEL) Algorithm. The algorithm allows structures to ‘FEEL’ an impact, such as a fall, boasting 96.4% accuracy in locating the impact in over 3575 impacts of eight different types, and a 99% confidence interval for being within -2.0% ± 1.3% of the actual force magnitude. The strength of the algorithm is that it intrinsically embeds the properties of any structure and does not require time synchronization of sensors. Since FEEL operates in the frequency domain, an Environments For Fostering Effective Critical Thinking (EFFECT) active learning module is included to aid in educating future learners.

Table of Contents

List of Tables

List of Figures

List of Symbols

A_{max}	maximum value of amplitude present in a signal
E_s	signal energy in a signal processing sense
FS_{new}	new sampling rate
FS_{old}	original sampling rate
Δ	(accelerometer unit conversion) offset value;
	(RoD) window shift
Δt	signal delay time
Γ	raw 1 g value for the sensor axis
Γ_{-1}	the last calculated raw 1 g value for the sensor axis
α_i	regularization parameter in the range of $0 \leq \alpha_i \leq$C
γ	(SVM) shape parameter;
	(Weibull distribution) scale parameter
$\hat{F}$	force magnitude estimation for an acceleration event
$\hat{F}_{i,j}$	force magnitude estimation for the i-th location and j-sensor
$\hat{L}$	coefficient which indicates the impact's location
λ	failure rate
$\left[\hat{F}_{i,j}\right]$	matrix containing force estimations for the i-th locations and j-sensors
$\mathrm{P}_{xx}(f)$	power spectral density of x
$\mathrm{P}_{xy}(f)$	power spectral density of x to y
$\mathrm{P}_{yx}(f)$	power spectral density of y to x
$\mathrm{P}_{yy}(f)$	power spectral density of y
$\hat{\mathrm{T}}(f)$	transfer function estimate

μ	mean
ρ	independent intercept parameter
ρ_{nan}	density of NaN present in a signal
ρ_{xy}	Pearson product-moment correlation coefficient
σ	standard deviation
$\sigma^{\ddagger}$	vector of standard deviations
τ	offset integer
$\tau_{\hat{F}_{i,j}}$	data point in the signal of the peak in the force estimate
$\tau_{\hat{F}_{i,j}}$	data point in the signal of the peak in the force estimate
$\{L_i\}$	vector of location coefficients
$\{\hat{F}_{i,j}\}$	force estimation vector for the i-th location and j-sensor
n_o	number of overlapping points per window
n_s	number of points present in a signal
n_w	number of points per window
n_{nan}	number of NaN present in a signal
x'	training data
y_i	vector of the form $y \in \{-1, 1\}^n$
$y_{i,g}$	i-th accelerometer value in units of gravity
$y_{i,raw}$	i-th raw value (i.e. before conversion to gravity units) read from the accelerometer
C	(accelerometer unit conversion) scale value for an accelerometer axis; (SVM) penalty parameter
D	signal sorted in descending order
d	signal delay
f	number of failures

i	(FEEL) location;
	(MADr) index of signal;
	(RoD) point in acceleration signal
j	(FEEL) sensor;
	(RoD) window adjusting integer
K	support vector machine kernel function
k	(Weibull distribution) shape parameter;
	(deviation method) point in $\left[\hat{F}_{i,j}\right]$ being compared
N	number of coefficients in the filter
n	(event localization) number of points in window;
	(signal energy) last time step;
	(SVM) number of points of x
S	detrended acceleration signal
T	sensor acceleration trigger threshold
t	(log-normal distribution) time value of interest;
	(normal distribution) time value of interest;
	(reliability) time period that failures f occurred in;
	(signal processing) time;
	(Weibull distribution) time value of interest
x	(SVM) testing data or data to be classified;
	(FEEL) force input
y	acceleration output

List of Abbreviations

ABET	Accreditation Board for Engineering and Technology
ASCE	American Society of Civil Engineers
COV	Covariance
DAQ	Data Acquisition System
DOM	Drawn Over Mandrel
DR	Dispersion Ratio
EFFECT	Environments For Fostering Effective Critical Thinking
FEEL	Force Estimation and Event Localization Algorithm
FFT	Fast Fourier Transform
FIR	Finite Impulse Response
IFFT	Inverse Fast Fourier Transform
LAN	Local Area Network
MAC	Modal Assurance Criterion
MAC Address	Media Access Control Address
MAD	Maximum Amplitude Difference
MADr	Maximum Amplitude Difference Ratio
MTBF	Mean Time Between Failure

MTTF	Mean Time To Failure
MULE	Mobile Ubiquitous LAN Extension
NaN	Not a Number
PC	Personal Computer
PH	Palmetto Health Hospital
QQ	Quantile-Quantile
RBF	Radial Basis Function
RoD	Rate of Dispersion
SDII	Structural Dynamics and Intelligent Infrastructure Laboratory
SDOF	Single Degree of Freedom
SVM	Support Vector Machine
UDP	User Datagram Protocol
US	United States of America
USB	Universal Serial Bus
USC	University of South Carolina
VAMC	William Jennings Bryan Dorn Veteran's Administration Medical Center

Chapter 1

Introduction

1.1 Motivation

In the US alone, 20% of citizens will be over the age of 65 by the year 2030 [2]; the largest challenge facing this growing demographic is not a new disease but a simple motion - the fall. These events are the premier cause of fatal and nonfatal injuries [2, 3, 4], and hospital trauma admissions among older adults [2]. They affect one in three age 65+ every year [2, 4] and over half of those age 80+ [4]. In fact, a fall is so common that every 17 seconds an older adult is treated for fall-related injuries, and every 30 minutes, an older adult dies from fall complications [3].

This accounts for "25% of all hospital admissions and 40% of all nursing home admissions" [4]. Of the population admitted, "40% [...] do not return to independent living [and] 25% die within a year" [4]. That means 65% of those experiencing a fall cannot return to their previous quality of independent living.

Costs stemming from falls are high. Direct medical costs "adjusted for inflation, were $30 billion" in 2012 with an expected increase of annual direct and indirect costs to $67.7 billion (in 2012 dollars) by the year 2020 [3].

The expense does not stop there but further continues to the health impact on the person who fell. Moderate to severe injuries can result from an incident. These include "lacerations, hip fractures, and head traumas" which "can make it hard to get around or live independently, and increase the risk of early death" [2].

Even though only 20-30% of falls result in moderate to severe injuries [2], "a large percentage of non-injured fallers (47%) cannot get up without assistance" [4]. The time spent immobile directly affects the person's health outcome. Within 30-60 minutes of compression from a fall, muscle cells begin to breakdown potentially resulting in dehydration, pressure sores, hypothermia, and pneumonia [4].

Thus, the outcome of a fall becomes dependent upon the immediate response and rescue of those immobile persons [5, 6]. Help after an immobilizing fall increases survival rates by 80% and the probability for the person to return to independent living [4]. If one could largely reduce response time, more older adults could return to their residences in a healthy state rather than sacrifice their individual independence. Rapid response would decrease the medical costs associated with falls, along with the amount of nursing home admissions, and more importantly, the amount of fatalities due to falls.

Those who fall can develop a fear of falling, even if no injuries were sustained. The person may be driven by this fear to limit their activity. Risk of falling consequently increases because of the person's reduced mobility and physical fitness [2, 3]. Several health problems are associated with impaired mobility "including depression, cardiovascular disease, cancer, and injuries secondary to falls and automobile crashes" [2]. Fear can tug at the person's mind, causing "feelings of helplessness and social isolation" to further complicate one's health state [3].

Combating falls is harder than prevention techniques alone. Restraints have been used to restrict a patient's movements in an effort to reduce the chance of falling. However, forcefully limiting movement has a similar outcome as the patient voluntarily limiting his activity due to fear. It does not work. Muscles weaken and physical function declines which increases the falling risk rather than reduce it [3]. Prevention must be done in ways that do not restrict mobility, but the chance of falling remains because every movement has that potential implicitly.

1.2 Current State of Fall Detection Technology

The ever present fall risk directs development towards methods other than prevention. Commercial solutions utilizing worn pendants, like Life Alert, remove the need to be near a phone to call for aid after a fall event. Effectiveness of the system shows when a Life Alert member goes to a retirement home, members go “six years later than an equivalent aged senior” [7]. The system also impacts mental health as 87% of Life Alert users say the protection provided is a main or important factor in the decision to stay at home [7]. However, the system is still limited because of user dependence. Users need to be conscious to press the pendant and need to be wearing the pendant in the first place.

Computer vision techniques with machine learning have been used successfully to 92% accuracy when using simulated falls by able-bodied participants in home environments [8]. Visual techniques are computationally intensive and intrusive, bringing concerns of processing power and user privacy. The machine-learning component when applied to human activity (i.e. a person’s normal schedule) has the possibility to predict a fall and could be used as part of a preemptive measure.

An alternative to using cameras is to use infrared technology which is somewhat less privacy-intrusive [9]. However, household residents’ perception is one of “being watched” so the privacy concern persists [5]. The system utilized was based on user activity and was only 35.7% successful in detection [9]. They described falls that required aid as those where the observed was inactive. Challenges arise as aid may be required in situations where the observed is not completely inactive. For instance, one can break a hip and crawl across the floor in an effort to get to a phone, but in the end the phone is out of reach because the person cannot get up to reach it. The observed in this case needs medical assistance, but by the concept presented, this person would not receive aid.

Worn accelerometers have been suggested as a good way to differentiate between human activities. Rybina et al correctly identified hopping, jumping, and skipping in all cases, running and balancing in 11 out of 12 cases using the Time Domain Correlation Coefficient in a laboratory setting [10]. Other research suggests the method used has a medium/high uncertainty without time synchronization, making it not ideal for fall detection [11]. Another worn accelerometer method using a Hidden Markov Model successfully detected 68 of 74 human falls in laboratory testing [12]. While privacy issues dissipate using acceleration data, other challenges arise from wearing devices. The assumption that the device remains in a fixed position to the wearer does not fully account for devices moving around during human activities. More importantly, compliance issues abound as "patients have low will to wear devices for detecting falls because they feel well before a fall occurs" or consider the device intrusive [6].

The previous directs research towards a less intrusive solution. Floor vibrations have been previously proposed as a way to detect falls, and dummies were used for laboratory testing of the algorithms [5, 13]. One team developed and patented a special device for use in fall detection [5]. However, little information is publicly available to determine the effectiveness of this device.

Techniques presented by Zigel et al added microphones as an additional input to recognize a fall [13]. However, energy methods were employed, which presents challenges if the event is near or far from a sensor. Different transient wave forms can produce the same amount of energy and lead to incorrect identification or missed events. Damping ratios are often assumed by the spectrum employed by Zigel et al, opening the possibility of further error as the characteristics of the structure are not fully realized [14].

1.3 What's Next?

The author seeks to overcome the challenges of other methods towards the ideal human-induced vibration monitoring system. We begin this journey by describing what the ideal system would be:

(1) user-independent to remove the need for any specific user information or user input;

(2) environmentally-based, removing the need for the user to wear any devices and the challenges associated with worn devices;

(3) able to operate on devices that are naturally unobtrusive;

(4) privacy respecting;

(5) inexpensive to operate and maintain, both monetarily and computationally;

(6) and adaptive to any environment (e.g. registers event regardless of distance from event to sensor).

This ideal can be extended when one looks at human fall detection from the angle of structural vibrations for a potential product implementation. The system should additionally seek to:

(1) not require modifications to the structure;

(2) not require modifications to the electrical network of the buildings;

(3) not interfere with normal network operation in the building;

(4) and easy to install.

The natural sensor choice for the ideal system is a wireless smart accelerometer. These sensors are small and can be easily attached anywhere on a structure, allowing them to be unobtrusive whilst monitoring the environment of the user. They are typically inexpensive to operate and maintain (e.g. smart phones often come equipped with an accelerometer), and can perform some analytics on their own. No structural or electrical modifications of the building are needed.

This work utilizes wireless accelerometers to design and implement a human-induced vibration monitoring system towards the end goal of developing the ideal human fall detection system. Systems are installed in two different real world environments - a hospital and a private family residence - resulting in the capture of several fall events. The information is cared for according to a data management plan based with a relational database design to provide flexibility for the future as research progresses.

A human fall detection system using structural vibrations would require the ability for the system to sort good from bad signals, ideally on the sensor level. Signal selection as a preprocessing operation, reduces the amount of information for detection algorithms to work through making the system as a whole more efficient. Methods for using machine learning through Support Vector Machine (SVM) with new signal metrics are developed to enable individual sensors to decide signal quality.

The challenge after initial signal selection thus becomes detecting an impact from a human fall. Acceleration amplitudes the sensor experiences will vary based on the distance between a sensor and an impact. Thus any algorithm for fall detection based in vibrations has to overcome distance to be effective, and ideally would not require time synchronization or estimate structural properties whilst doing so. This led to the development of the Force Estimation and Event Localization Algorithm (FEEL) which accomplishes all those goals and is additionally designed to scale with any number of sensors, which increases the robustness of the system.

FEEL utilizes the frequency domain as part of relating accelerations to a force and location. The concept of frequency domain can be hard to grasp, leading the author to include an education module for teaching the concept. The Environments For Fostering Effective Critical Thinking (EFFECT) framework was chosen for creating the module due to the focus on critical thinking and increasing knowledge transfer, whilst encouraging the student to improve other beneficial professional skills.

Chapter 2

System Design and Implementation

2.1 Introduction

A robust, automated system must be designed for deployment in the real world in order to learn more about human activity through vibrations. The system should emulate the ideals for a human fall detection system as outlined in Section 1.3, so that the system may operate in diverse environments. In a hospital environment like that of William Jennings Bryan Dorn Veteran's Administration Medical Center (VAMC), the additional implementation requirements of the system are very important due to the nature of hospital equipment. The VAMC has numerous networks running and machines operating on various frequency bands that a monitoring system, not being aware of this fact, could interfere with and affect the normal health care operations of the hospital. For the case of private residences, an owner would not necessarily want to alter his home nor have installation personnel spending a large amount of time interrupting his day.

Initial research into a system was conducted by Davis et al [15], and is where the ultimate system design draws its basis. Various network configurations employing wireless accelerometers were explored, ultimately resulting in an adaptive network that allows the capturing of human-induced vibrations within the bounds of the ideal system. This work puts forth a standard for all human activity monitoring systems that has been vetted through installations at both VAMC and a private residence.

The goal for developing this system focused on capturing real world fall events through structural vibrations, with many human falls being captured during the study period. Several fall events are showcased with discussion relating what is seen in the acceleration plots to that of the reported incidents' descriptions, showing the possibility of fall detection through structural vibrations. In addition, the author explores features of the signals and vibration activity trends that closely match the general schedule of the people at each installation location which can lead to broader human activity monitoring for other health care applications.

2.2 Wireless Accelerometer Validation

Before any system was installed, the wireless accelerometer on the Intel Agua Mansa V2.0 sensor board needed to be validated as operating to the wired accelerometer standard. The two accelerometers were sitting side by side on a steel frame table, where a tennis ball was dropped and allowed to come to rest on the table. A NI-9234 DAQ operated a PCB Piezotronics 333B50 accelerometer with 1019 mV/g collecting data at 1651.7 Hz for the wired accelerometer standard. Data was collected for both accelerometers simultaneously as the ball bounced on the table. Time vectors were generated for each signal with the Agua Mansa's time vector being adjusted until a match was obtained between the two signals. The Agua Mansa accelerometer was found to be operating at approximately 316 Hz and matching the wired accelerometer very well as seen in Figure 2.1. Differences in amplitude are due to the sensors having two different sampling rates, which causes the sensors to see different parts of the waveform.

The experiment was repeated using another Agua Mansa sensor, with the results being the same as the first trial. Thus the remainder of the sensors are considered to be operating at the same rate.

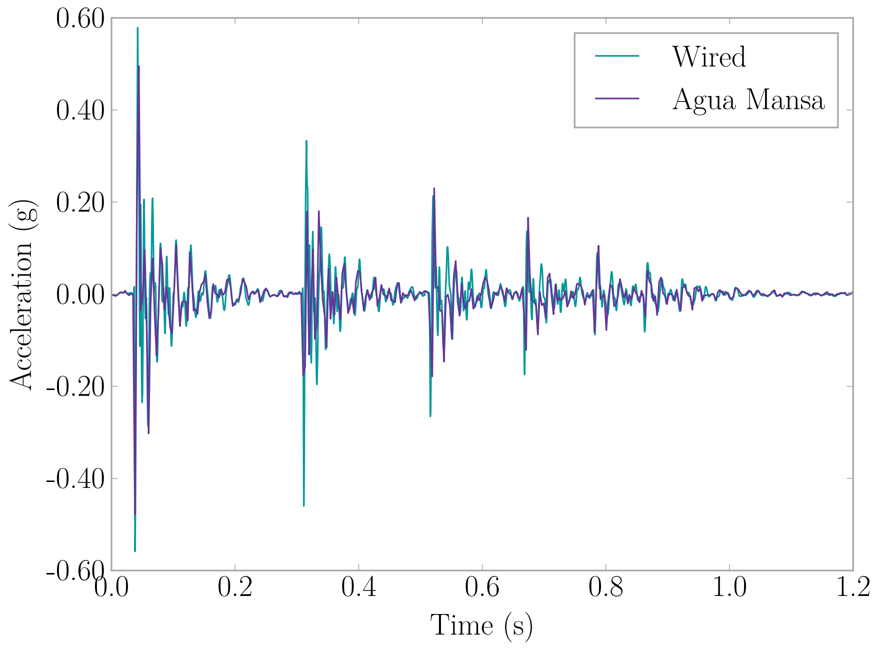

Figure 2.1: PCB 33B50 Wired Accelerometer vs Intel Agua Mansa V2.0

2.3 Installation Details

2.3.1 System

The systems utilized the proposed star network sensing framework with a multi-agent system architecture outlined by Davis et al [15]. The Intel Camp Hill V2.1 processor/radio board in conjunction with the Intel Agua Mansa V2.0 sensor board were employed as the leaf nodes. A multi-agent system architecture was employed allowing each sensor to respond individually to its environment, which in turn aids in reducing false-positives that an interesting event occurred. For example, a sensor located near a household appliance such as a dishwasher would experience lots of vibrations due to the machine's operation. That sensor would have to adjust its beliefs as to what is normal, with this normal being different from that of a sensor that is in a comparatively quiet vibration zone. If both sensors operated under the same beliefs, then every time the dishwasher was operated, the sensor would be telling the base station that an interesting event occurred when all it really was is noise generated by a machine. Accelerometers on board the Agua Mansa had a resolution of 4000 pts/g and a range of ±2 g. Data was sampled at 316 Hz with 12.7 s windows (∼6.35 s of data before and after the event). The large window was chosen in an attempt to capture what happened leading up to an event and motions following.

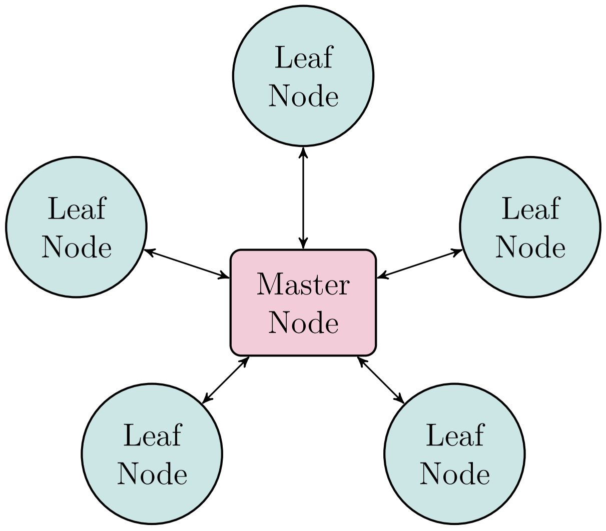

Figure 2.2: System Star Network Topography

Calibration of the wireless sensors was performed in accordance with a static technique from the University of Illinois at Urbana-Champaign [16]. The scale value C for each accelerometer axis is the difference between the 0 g reading and 1 g reading on each respective axis, and the offset value Δ is simply the 0 g reading for the axis.

Values reported by the accelerometer would be converted into units of gravity before being saved into the sensor's buffer. This calculation was performed using Equation 2.1 where $y_{i,g}$ is the i-th acceleration value in gravity units, $y_{i,raw}$ is the i-th raw value (i.e. before conversion to gravity units) read from the accelerometer, Δ is the offset value for the axis, and C is the scale value for the axis. The offset and scale values are determined from static calibration for the accelerometer axis where $y_{i,raw}$ was read [16].

$$y_{i,g} = \frac{y_{i,raw} - \Delta}{C} \tag{2.1}$$

A threshold level of ± 50 pts (typically 0.0125 g) served to indicate a vibration event of note (threshold choice discussed more in Section 2.4). The system is triggered if the condition presented in Equation 2.2 where Γ is the raw 1 g value for the sensor axis, $y_{i,raw}$ is the current (or i-th) raw value read from the accelerometer on the axis, and T is the threshold for the axis.

$$|\Gamma - y_{i,raw}| \geq T \tag{2.2}$$

The value of Γ for each sensor axis changes depending on the orientation of the sensor. Initially, Γ is determined by filling up the sensor's buffer once under "at rest" conditions, and then taking the average of those values. Each time a new value is read from the accelerometer, Γ updates using a version of a running average seen in Equation 2.3 where Γ raw 1 g value for the sensor axis, Γ_{-1} is the last calculated raw 1 g value for the sensor axis, and $y_{i,raw}$ is the i-th raw value (i.e. before conversion to gravity units) read from the accelerometer.

$$\Gamma = \frac{\Gamma_{-1} \cdot y_{i,raw}}{2} \tag{2.3}$$

Each leaf node streamed data over an User Datagram Protocol (UDP) wireless local area network connection provided by the base station computer where all processing was handled, including buffering, triggering, and local storage. UDP connections, by its nature, sometimes lose data when communicating between entities leaving gaps in the signal (see Figure 2.3). The platform combats this by adding in synchronization packages that allow for tracking how many data points should have been seen, that way the unreliable nature of UDP connections can be overcome.

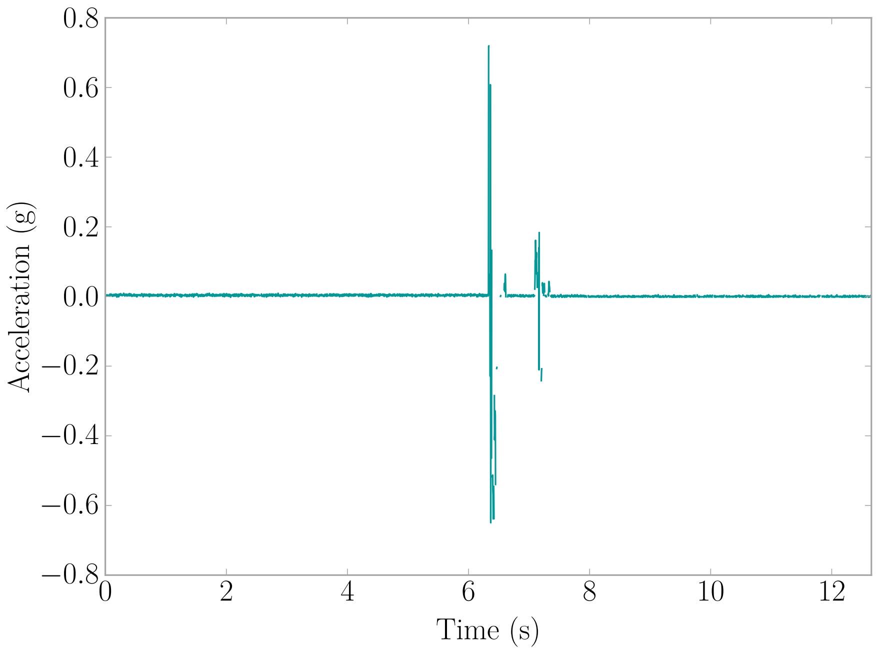

Figure 2.3: Example Signal With Missing Data

Base station roles of the wireless network were fulfilled by Asus Eee PCs running Windows 7 and secured by TrueCrypt encryption software. A custom application developed in PHP Script served to control communication with the sensors, record signal data, and system operational data. A local MySQL database stored all data; an outline is presented in Figure 2.4.

The home installation provided an Internet connection allowing the remote sending of collected acceleration data to a centralized server at the University of South Carolina (USC). In the hospital installation, Internet access was not permitted to the systems, thus, a Data Mobile Ubiquitous LAN Extension (MULE) was employed to ferry data from the hospital and back to the USC server [17]. The Data MULE was an Asus Eee PC running Windows 7 and would use data retrieval software to download information stored on the Base Station laptops in the hospital. Manual data retrieval occurred every two weeks. Data would then be transfered to the main servers and stored in aggregate with all other systems. Figure 2.5 shows the operational flow.

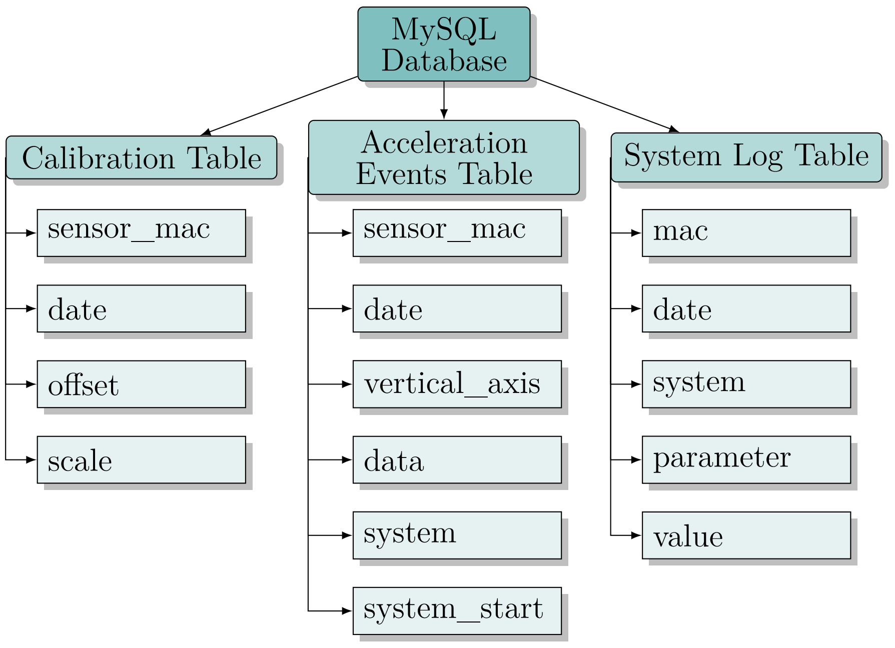

Figure 2.4: Outline of System Database

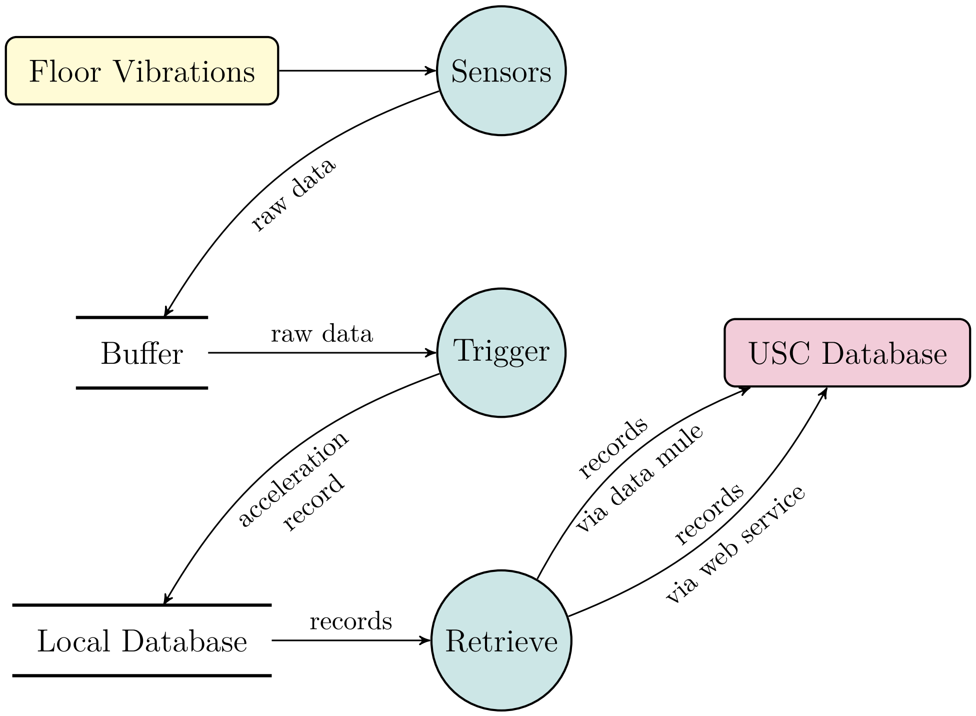

Figure 2.5: System Operational Flow

2.3.2 Home Environment

The home installation occurred on the first story of a two story wood-framed house located in Columbia, South Carolina. A family of four resided there, including two identical twin toddlers 2.5 years of age. Sensors were installed in the living room of the home, a location chosen for its high human activity. Sensors were attached to hardwood floors using double-sided duct tape. Figure 2.6 provides a diagram of the home installation.

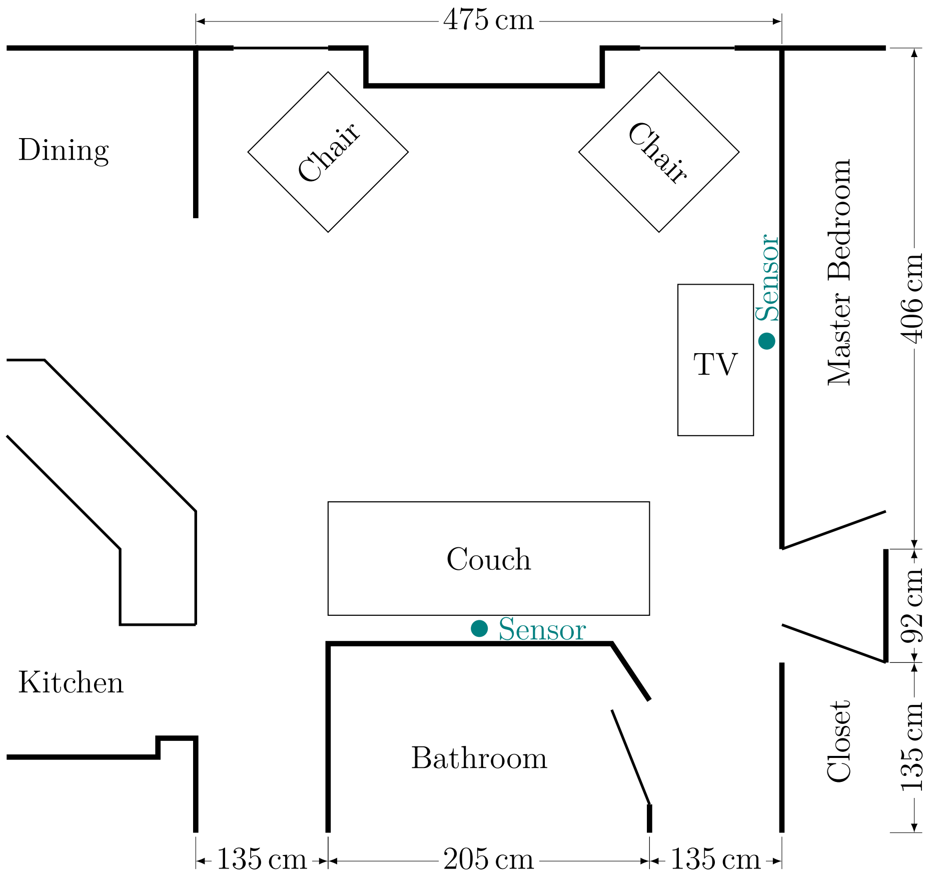

Figure 2.6: Home Layout

2.3.3 Hospital Environment

Systems were installed on the fourth floor of the hospital whose flooring was vinyl layered on top of reinforced concrete. The particular wing monitored contained

20 patient rooms with two beds per room. They centered around a nurses' island containing offices, staging areas, and four nurse stations. Sensors were placed out of site when possible, with two per room attached with double-sided duct tape. Base Stations were placed in equipment closets and locked to high metal shelving. Each base station served six to eight leaf node sensors. Figure 2.7 shows a diagram of a typical patient room in the hospital.

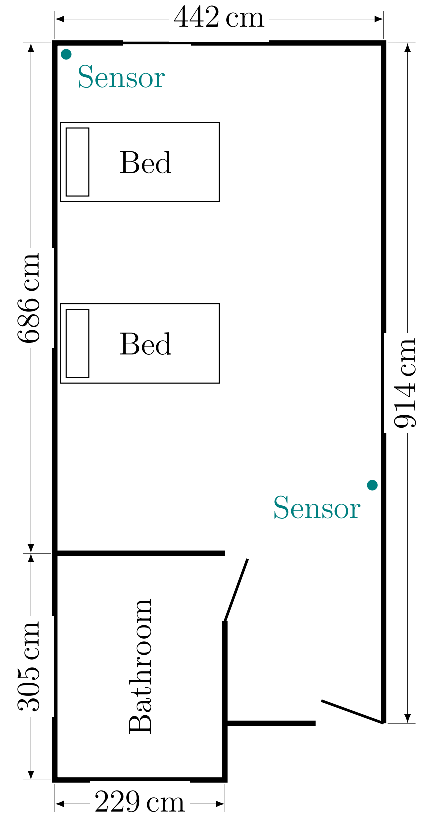

Figure 2.7: Typical Patient Room at Hospital

The hospital wing typically admitted patients who were generally at risk of falling, allowing the systems the best possible chance to catch a fall event. Visitors were permitted between the hours of 8:00 am and 8:30 pm. Hospital personnel moved through daily with 10-20 Medical Doctors, 3-4 Therapists, 1-2 Pharmacists, 2-3 Social Workers, 1-2 Dieticians, and 2 Food Service Staff. In addition, nurses worked 3 shifts/day with about 4 nurses per shift. Numerous patients rotate through as well. This brings a lot of variability to the system and challenges in deployment discussed in Section 2.4.1.

2.4 Common Challenges

The challenges faced by the floor monitoring system have the potential to be very complex as the research not only looks at the structure vibrations itself but aims at inferring the activities that people perform as they interact with their environment and those objects in it. These challenges are augmented when the sensors are installed in a hospital setting where patients and visitors can directly interact with the system. The challenges of having a successful monitoring system are discussed in three categories: (1) Environment, focusing on installed location; and (2) Hardware focusing on the sensing system itself.

2.4.1 Environment Challenges

One of the first challenges phased during sensor installation was the limitation of which outlets were available for use. This limited the location of the sensors as the cables for power were kept to a minimal distance. Spare outlets out of the way, say behind a bed, were few. Sensors were not permitted in particular outlets because they were for emergency power, medical equipment, etc. This left mostly outlet that were in the open or in a hallway where a higher probability of tampering exists because of the visibility of the phone chargers used to power the sensors. Sensors in these areas could also be accidentally hit when a hospital bed is wheeled out of a room or someone thinks the power source is a complementary charger provided by the hospital and attempt to use it. Many of the sensors experiencing the *USB Port Detached* failure mode discussed in Section 2.5 were found in unprotected areas (e.g. hallway). When the sensors were hidden, people had more of a 'out of sight, out of mind' mentality as they did not know the sensors or their chargers existed.

The user interaction with the sensors changed when sensors were installed in patients' homes. Each patient was advised to not touch the equipment. There were zero *USB Port Detached* failure modes in patient homes even when sensors were easily visible. In comparison, only hospital staff (e.g. nurses) were informed about the system equipment in the hospital setting. Movement of patients through the hospital is variable, and sometimes rapid, making informing each individual patient impractical for the research team. The conclusion drawn is that equipment used in a hospital setting needs to look foreign enough to patients that they do not tamper with it, or at the very least, all equipment needs to be well hidden out of the view of patients and visitors.

Another challenge was the low amount of vibrations transfered through the reinforced concrete flooring present in the hospital. The floors design of hospitals tend to be stricter on the amount of vibration allowed because of potentially sensitive medical instruments and patient comfort [18]. Hence, each patient room needed several sensors and a lower threshold level to adequately detect signals.

2.4.2 Hardware Challenges

The use of a star network as outlined in [15], provides challenges due to the operation of a base station in the form of a laptop. Restrictions placed by the hospital removed the possibility of sending data through the Internet to a centralized server. Thus, a laptop was required to collect and store data from the wireless sensors. The limited laptop WiFi range increased the number of laptops required to cover the entire hospital wing to six. This becomes one more item, and a very vital data collection piece, to keep functional; something that can be removed with access to hospital WiFi.

The maintenance of the laptop meant monitoring battery health (to keep system running when electricity goes out) and cleaning out dust accumulation. In addition, the computers needed to be hidden to prevent tampering, locked down to prevent theft, and thoroughly encrypted to protect the data according to the hospital's regulations. These devices were undisturbed to the best of our knowledge due to the proactive stance taken to secure the equipment.

The sensors themselves experienced significant failures over their operating life span. Failures include wireless communication errors and accelerometer reading failures with the Mean Time To Failure (MTTF) of the sensors being approximately 170 days. These failures are most likely because the type of sensors used are prototypes for research purposes and not a commercial standard. The reliability of the sensors can be improved when using industrial level sensors. More on this is discussed in Section 2.5.

Various operational errors of the sensors lead to false-positives as readings crossed the threshold level. Some sensors reported extremely rapid oscillations to the maximum swing level of the hardware as depicted in Figure 2.8. These were certainly not generated by any human activity as the cycling rate is extremely high.

Accelerometers were sometimes over-clocked or malfunctioned to produce a single high value point reading that would trigger the system. Figure 2.9 displays the error. The plot shows that the trigger could not have been caused by human activity as there is no oscillation around zero which would be expected from a floor excitation.

2.5 Sensor Failure Modes

The Camp Hill and Agua Mansa boards experienced several different modes of failure during the life of this study, both physical hardware damage and software issues. Failure modes are presented in order of most common to least for each board in Table 2.1. The sensors installed in a hospital setting mainly experienced the *USB Port Detached* and the *Network Failure* modes.

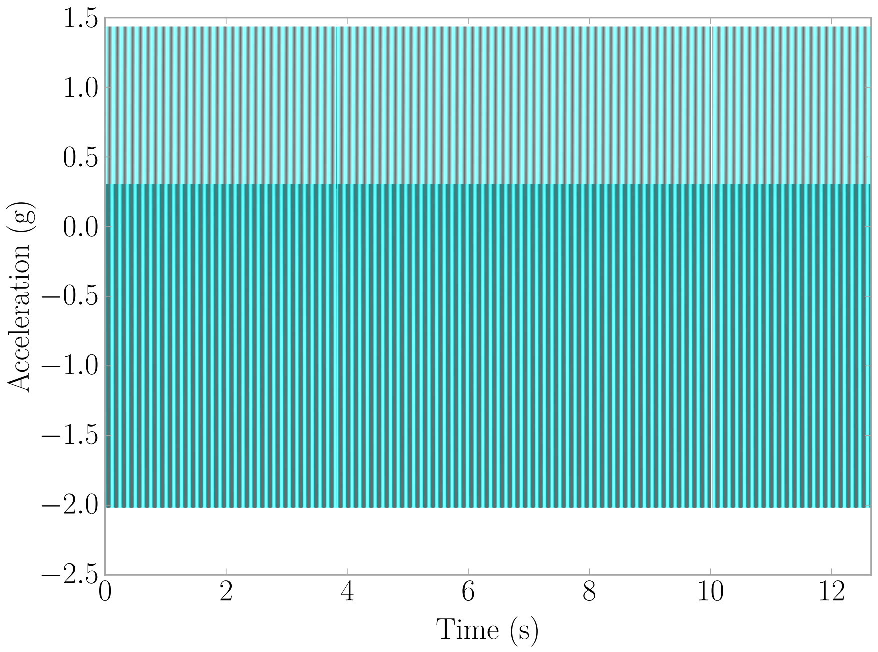

Figure 2.8: Accelerometer Rapid Oscillation

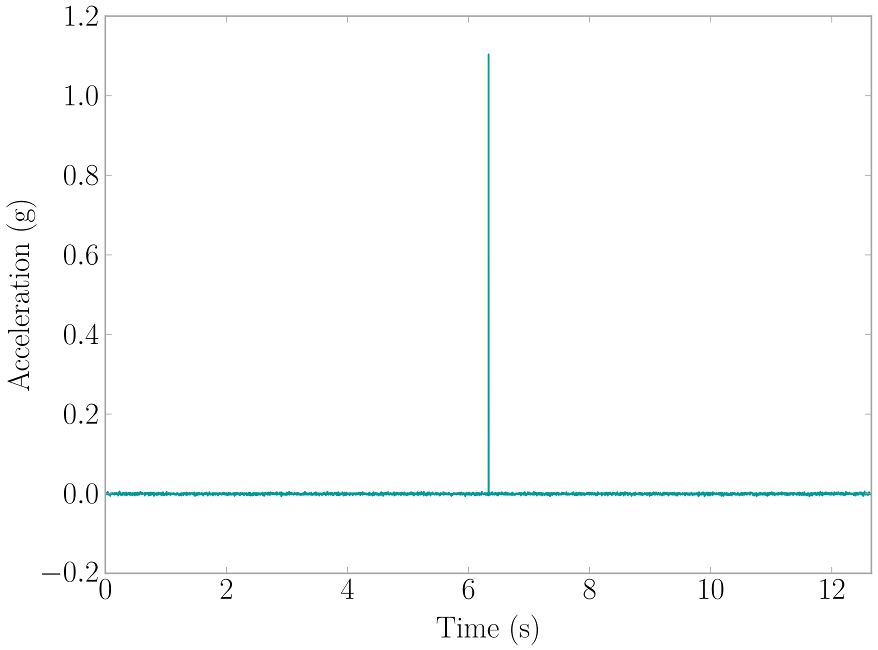

Figure 2.9: Accelerometer Spike

Table 2.1: Sensor Failure Modes

	Type	**Description**
Camp Hill	USB Port Detached	The USB port is ripped off the Camp Hill board
	Network Failure	Camp Hill does not connect to host or drops from network to never rejoin
	Serial Port Communication Failure	Unable to communicate with the processor board using the serial port which prevents programming of the board
	Data Transmission Failure	The Camp Hill connects to the host but does not transmit data
Agua Mansa	Accelerometer Reading Failure	The Agua Mansa is not sending acceleration signals for the Camp Hill to read

As seen in Figure 2.10, there were numerous compliance issues resulting in the physical damaging of the sensors. USB wall chargers were adapted for use to power the sensors on location; however, some patients did not abide by the warning labels and attempted to unplug the sensors so that they could use the charger for their phone or other device. The result was the detachment of the USB port used to power the sensor.

The second ranked mode, Network Failure, and the last ranked mode, *Data Transmission Failure*, are due to issues in the WiFly chip or software on the Camp Hill boards. Additionally, there may be some signals operating in the same band as the Camp Hill causing the network communication issues. Cell phones and medical devices in the hospital were checked to remove the possibility of interference but with the constant influx of patients, anyone could have brought in a device that interfered.

A *Serial Port Communication Failure* arises during the preparation of the sensor for deployment and is an expected defect of the microprocessor. The *Accelerometer Reading Failure* develops from manufacturing defects or the degradation of the Agua Mansa board.

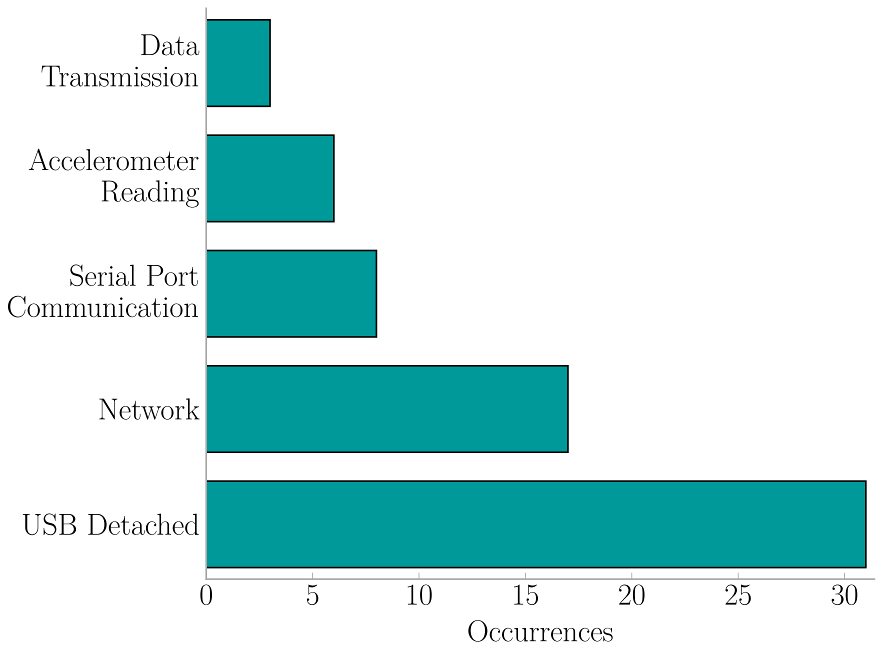

Figure 2.10: Sensor Failure Modes in a Hospital Setting for a Total of 46,214 Sensor Hours

Instrumentation in private rooms showed signs of higher compliance noted in a large reduction in the *USB Port Detached* mode due to the education of the residents whereas in a hospital setting, every new patient would need to be informed about the system. This presented quite a challenge. Software failures were more common in private rooms suggesting the sensors degraded over their lifespan rather than were destroyed due to patient compliance.

Another interesting result is the life time of the sensors in the failure modes tended largely to remain under 100 days of operation as seen in Figure 2.11. Patient stays in the hospital are often not very long. Hence, the *USB Port Detached* failure mode is more likely to occur because the high turnover rate and the impracticality to inform each patient about the system.

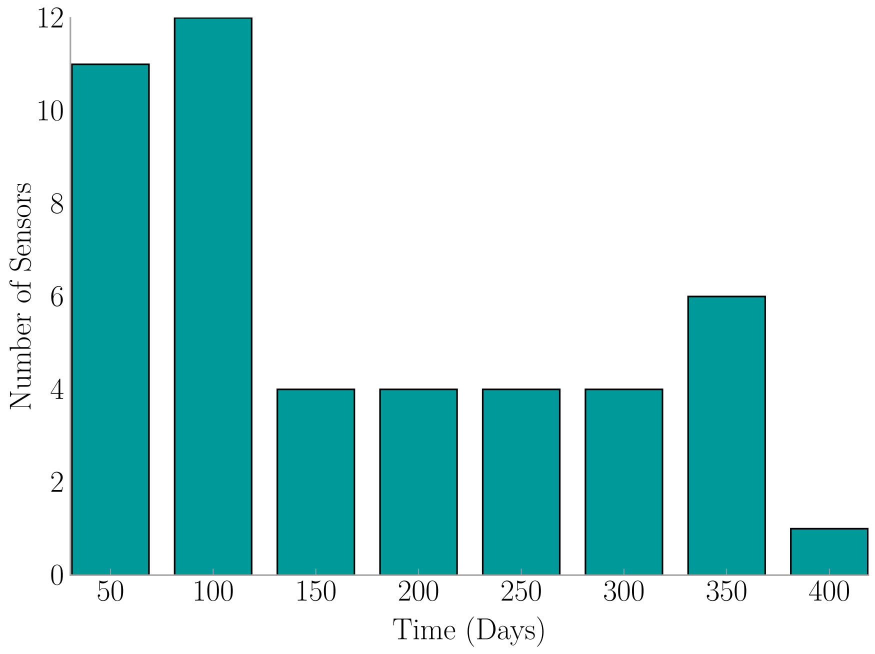

Figure 2.11: Life Time of Failed Sensors in a Hospital Setting (Out of 100 Sensors)

2.6 Sensor Reliability

Before looking at the acquired data, signals containing sensor operational errors were filtered out. These errors are discussed in detail in Section 2.4.2.

2.6.1 Time Distribution

The installation in the household lasted for 167 days, and totaled 6450 sensor monitored hours. Figure 2.12 displays the amount of sensors active per day of the study. Two sensors were active for the majority of the study. Sensors would be restarted and reconnected to the Base Station when maintenance checks of the system occurred, which is evident in the figure by the change in the amount of active sensors.

Systems installed in the hospital operated for 511 days and totaling more than 46,214 sensor monitored hours. Figure 2.13 displays the amount of sensors active each day during the study. The beginning months have many days where only a few

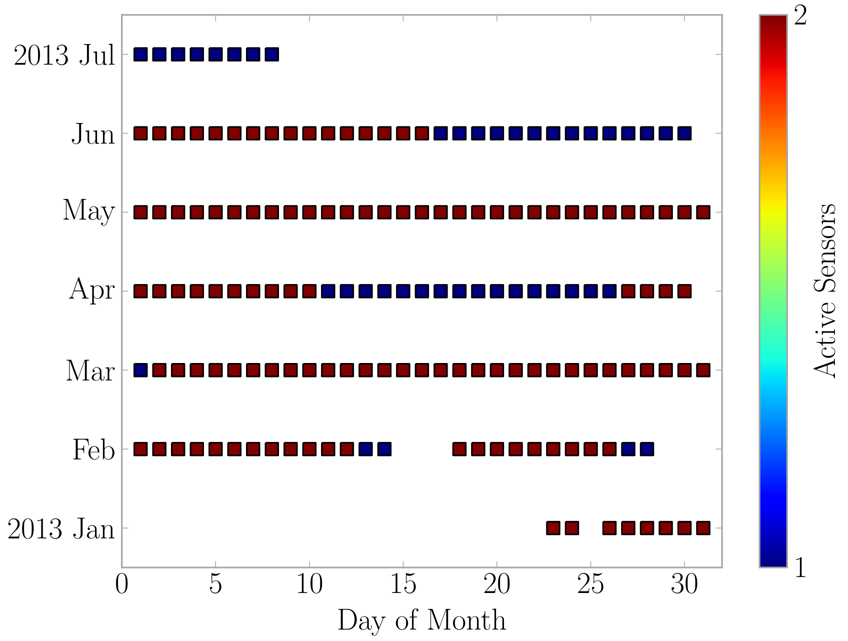

Figure 2.12: Home Installation's Active Sensors

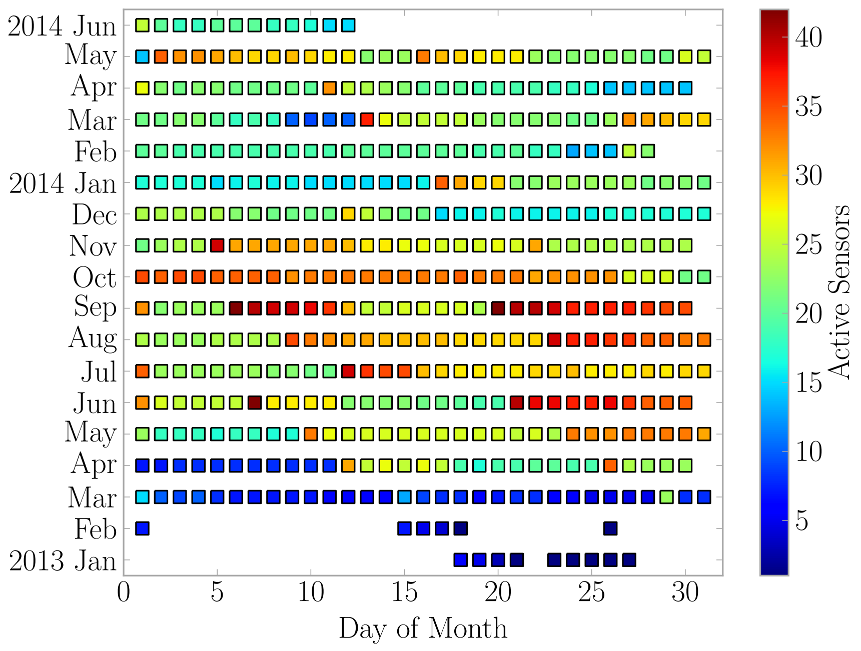

Figure 2.13: Hospital Installation's Active Sensors

sensors were operational due to an initial development phase where a prototype system was deployed to find an optimum monitoring setup. The number of sensors fluctuated as sensors stopped working or were re-assigned to a new location. Monitoring was fairly consistent with about 25 sensors operating daily.

For reliability calculations, only the sensors in the hospital were considered. The household only had three sensors installed, and the conditions for operation are different than that of the hospital. Hence, the sensor sets cannot be mixed. Multiple household installations are needed to generate reliability information for a those sensors installed in an home environment.

2.6.2 Reliability

Failure rate is calculated using Equation 2.4 where f is the number of failures and t is the time period those failures occurred in [19, 20].

$$\lambda = \frac{f}{t} \tag{2.4}$$

The Mean Time Between Failure (MTBF) is calculated using Equation 2.5 where λ is the failure rate from Equation 2.4 [19, 20].

$$MTBF = \frac{1}{\lambda} \tag{2.5}$$

Traditionally, a Weibull distribution is used to model failure rates, and in this case, models the sensors better than other distributions tried. Equation 2.6 provides the formula for the Weibull distribution where t is the time value of interest, γ is the scale parameter, and k is the shape parameter.

$$P(t) = \begin{cases} \frac{k}{\gamma}\left(\frac{t}{\gamma}\right)^{k-1} \mathrm{e}^{-\left(\frac{t}{\gamma}\right)^{k}} & t > 0 \\ 0 & t \leq 0 \end{cases} \tag{2.6}$$

The Weibull distribution was fitted using the *weibull_min* function from SciPy [21], and a Quantile-Quantile (QQ) plot produced in Figure 2.14 showing a relatively linear trend. This indicates the distribution is a good fit for the Camp Hill failures.

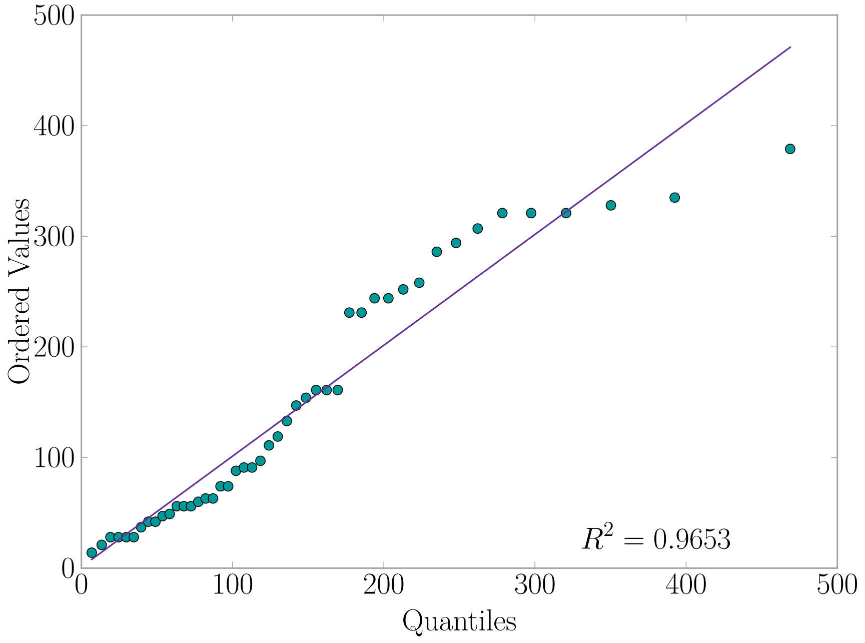

Figure 2.14: QQ Plot for a Weibull Distribution Describing the Failure Rate

A truncated normal distribution was tried as in Equation 2.7 where σ is the standard deviation, μ is the mean, and t is the time value of interest. In this case, the standard deviation was 110.6 days, and the mean was 170.7 days.

$$P(t) = \begin{cases} \frac{1}{\sigma\sqrt{2\pi}}\mathrm{e}^{-(t-\mu)^2/\left(2\sigma^2\right)} & t > 0 \\ 0 & t \leq 0 \end{cases} \tag{2.7}$$

The truncated normal distribution was fitted using the *norm* function from SciPy [21], and then a QQ plot produced in Figure 2.15 that shows the quantiles following a linear pattern. The R^2 value is slightly less than that of the Weibull, making this distribution less suitable to model the failures.

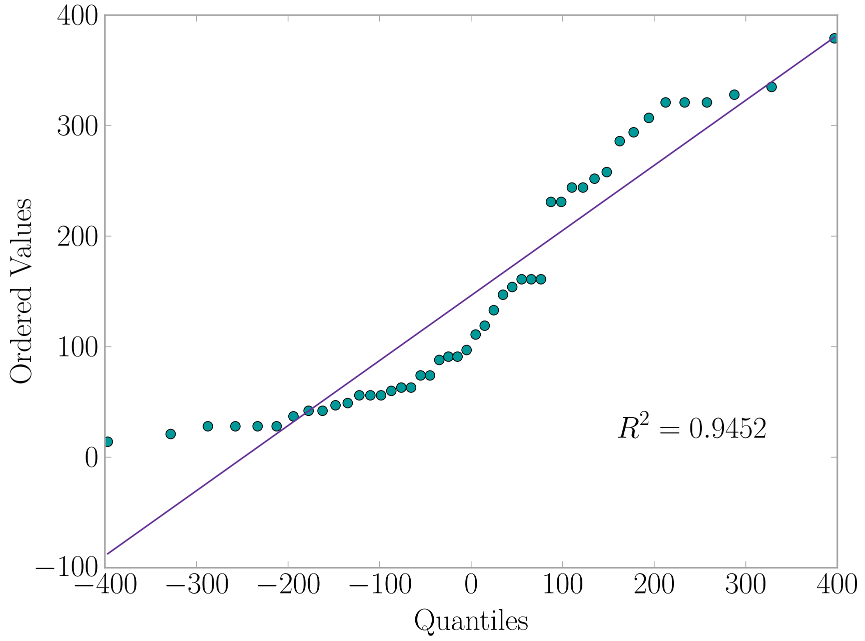

Figure 2.15: QQ Plot for a Truncated Normal Distribution Describing the Failure Rate

A log-normal distribution was tried as in Equation 2.8 where σ is the standard deviation, and t is the time value of interest.

$$P(t) = \frac{1}{t\sigma\sqrt{2\pi}} e^{-\frac{1}{2}(\log t/\sigma)^2} \tag{2.8}$$

The log-normal distribution was fitted using the *lognorm* function from SciPy [21], and then a QQ plot produced in Figure 2.16 that shows the quantiles following a nonlinear pattern. The R^2 value indicates this is not a good fit for the failure data.

The Weibull distribution proved to be the best fit to model the failures. Figure 2.17 plots the Weibull failure model against the sensor failure data. The slight

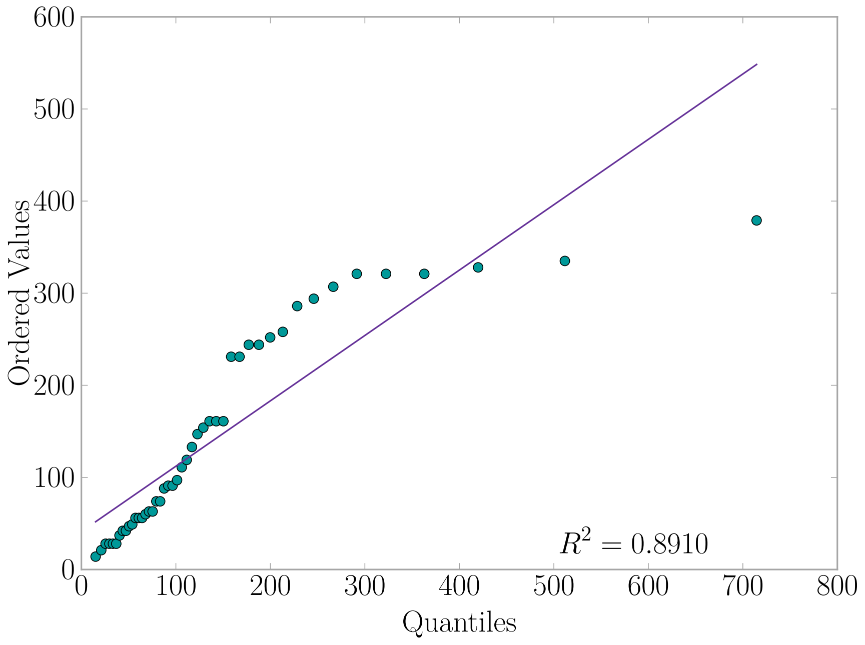

Figure 2.16: QQ Plot for a Log-Normal Distribution Describing the Failure Rate

increase in failures around 300 days is not well modeled by the Weibull and contributes to the nonlinear right tail of the Weibull QQ Plot in Figure 2.14. A wear out failure trend as exhibited in Figure 2.18 was experienced by the sensors. The overall failure rate is $5.06 \times 10^{-3} \frac{\text{failures}}{\text{hour}}$, and the MTBF is 197.7 hours.

Expanding this in a probabilistic sense for the likelihood of measuring a fall that produced a vibration measurable by the sensor, we find that the chance is directly related to the sensor failure rate as demonstrated in Equation 2.9.

$$\begin{aligned} \mathrm{P}\left(\text{Measuring Fall} \mid \text{Measurable Vibration}\right) &= \mathrm{P}\left(\text{Sensor Working}\right) \\ &= 1 - \mathrm{P}\left(\text{Sensor Failure}\right) \end{aligned} \tag{2.9}$$

The assumption made here is that a sensor that is operating correctly will have the capability to correctly identify the impact (identification is being explored in other research), and the fall occurs in the sensor's area of influence.

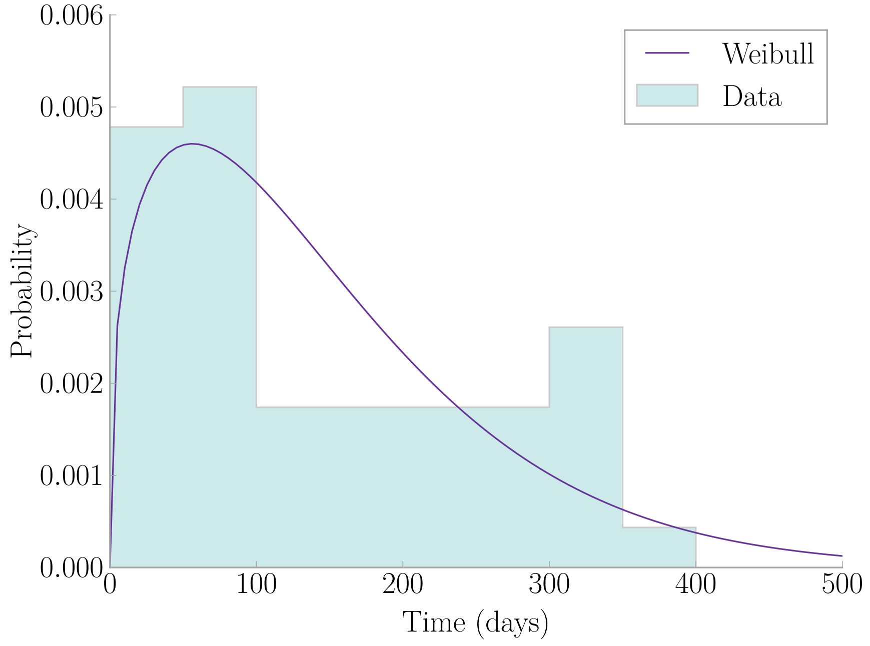

Figure 2.17: Weibull Distribution Failure Model Vs. Sensor Failures

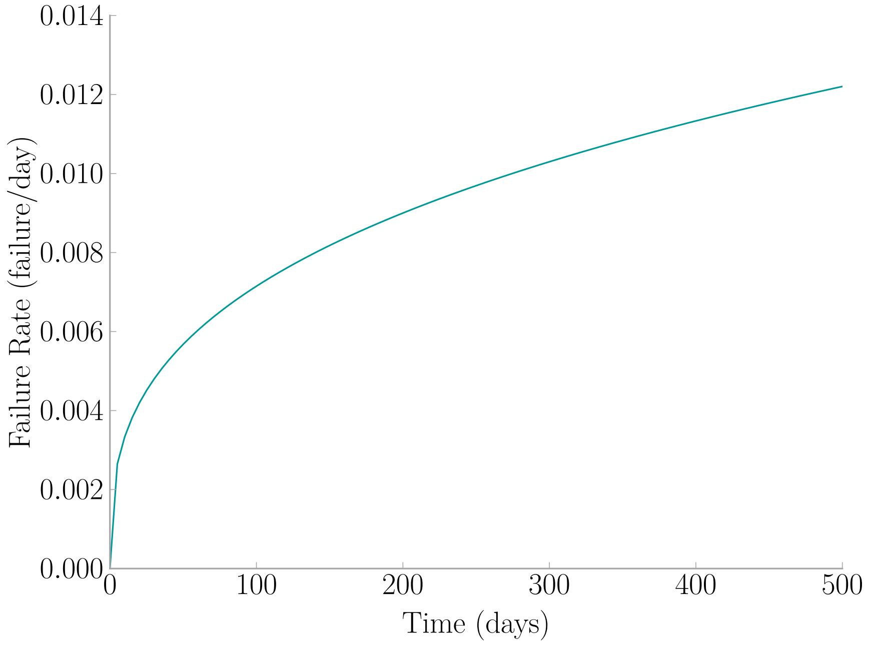

Figure 2.18: Sensor Failure Rate Bathtub Curve

Using the Weibull distribution fitted above, the likelihood of measuring a fall in a year using these sensors is 4.9%. This assumes that the algorithms are completely reliable, and the fall creates measurable accelerations. The MTBF to achieve 99% likelihood comes out to be 8642.4 hours. This equates to $1.16 \times 10^{-4} \frac{\text{failures}}{\text{hour}}$ as an overall failure rate for a sensor, which is what a manufacturer should aim for when producing sensors for a fall detection application.

2.7 Description of Collected Data

A total of 21,413 events were captured in the household. Figure 2.19 displays the distribution of sensor activations during this time period. The beginning of this period experienced around 260 activations a day, while the end of the period experienced around 60 events a day. This disparity has to do with system operational issues towards the end of the study. The laptop started to degrade in performance, and consequently, the ability to receive and store data. In addition, the residents took a vacation from May 19 until June 1 as marked on the graph, which, during this time, no activity was recorded.

Taking all of the activations and compressing them into a week, human activity trends show a discernible pattern as illustrated in Figure 2.20. Three bands of higher activity appear around the hours of 8, 12, and 18. These, evidently correspond with typical daily meal times when there would naturally be a lot of activity in the household preparing dinner and wrangling children to the dinner table. The sensors were located in the first floor in the room next to the kitchen and dinning room, which supports this conclusion. Lighter activity is seen throughout the day time and almost zero activity is seen during typical sleeping hours (between hours of 22 and 6). The twins regularly took naps around the hours of 10 and 15, which are shown to be times of lower activity as well. Also, the family attends Sunday church services around the hours of 9 and 10, which, as the graph displays, have almost zero events.

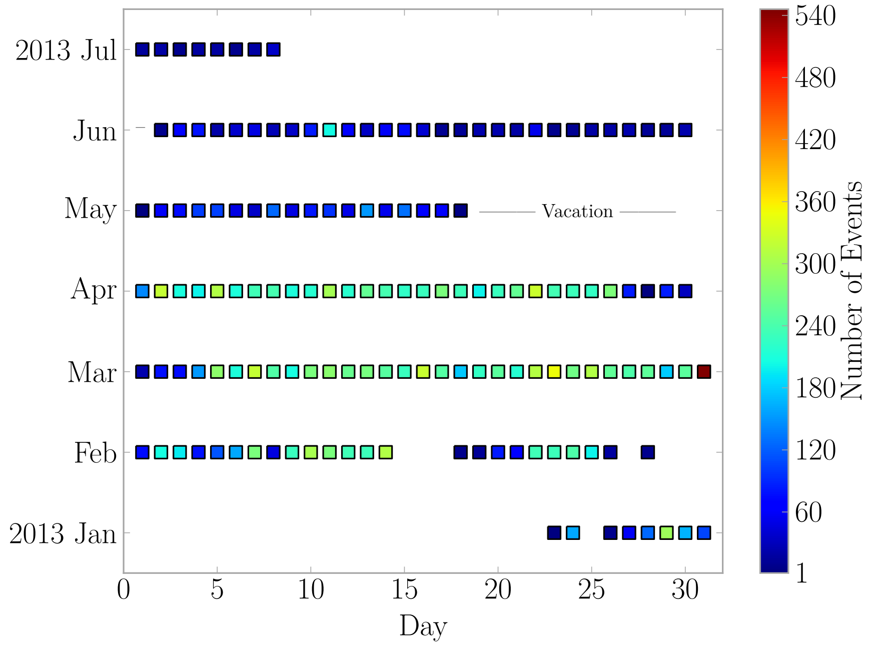

Figure 2.19: Home Installation's Sensor Activations

The patterns demonstrate the potential of using floor vibrations for determining the probability of a specific human activity given a time and day of the week. The probability of specific human activities can be estimated based on prior behavior and the data collected by the sensors. For instance, if an object fell during the middle of the night when the household is typically asleep, the probability that the resulting vibrations were caused by a human jumping will be extremely low.

Over the course of the hospital study, a total of 25,415 acceleration events were collected. Figure 2.21 shows the distribution of events to be fairly regular after 2013 April 13, when the final system was installed. The VAMC system recorded around 1500 acceleration events per day after this time. There are some days that have an extremely high amount of events captured. These days experienced a high number of sensor errors (see Section 2.5). These days appear with a high number of events because only the records containing the sensor errors were filtered out of the data set (i.e. data from one sensor), leaving the data from the other sensors. The remaining

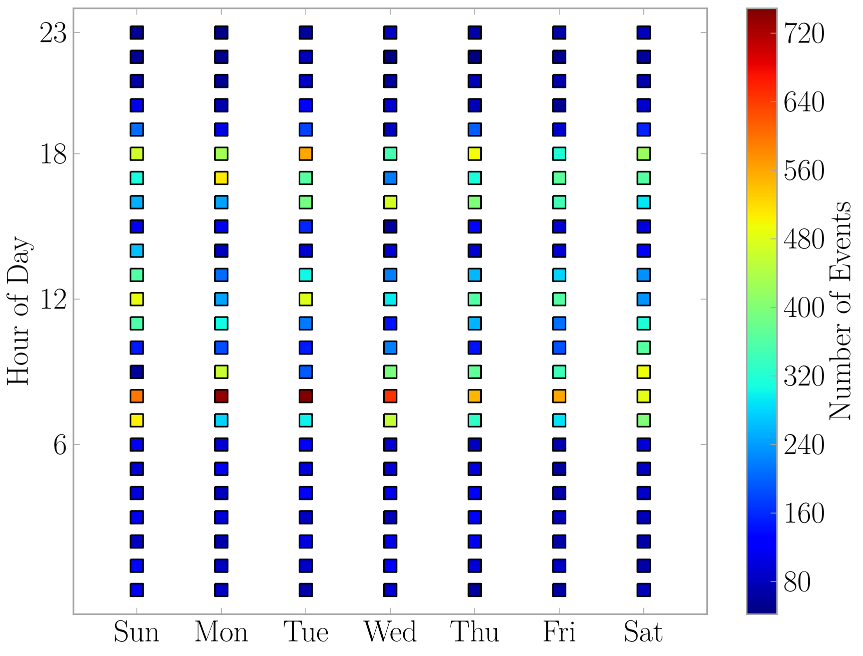

Figure 2.20: Home Installation's Activity Density

signals are low magnitude signals with a small signal to noise ratio.

A distinct pattern develops when the entire data set is broken down by hour of the day and overlapped; a pattern which matches what one would expect to see in a hospital setting (see Figure 2.22). A large amount of events were recorded during normal business hours on the weekdays and a smaller amount of events are present on the weekends during all hours. This demonstrates the possibility of using floor vibrations to study a high traffic area's activity patterns. These patterns could further be used for a number of uses. For example, to refine any human fall detection methodology by introducing probabilities of falls based on the hospital's routines. For instance, if a large amount of activity is present around hour 10 normally, then the probability that a fall would go unnoticed at this time is low, but if a spike of acceleration occurred at hour 23, then there would be a higher probability of fall going unnoticed and a monitoring system would raise an alarm.

Different environments produce different activity patterns, which means systems

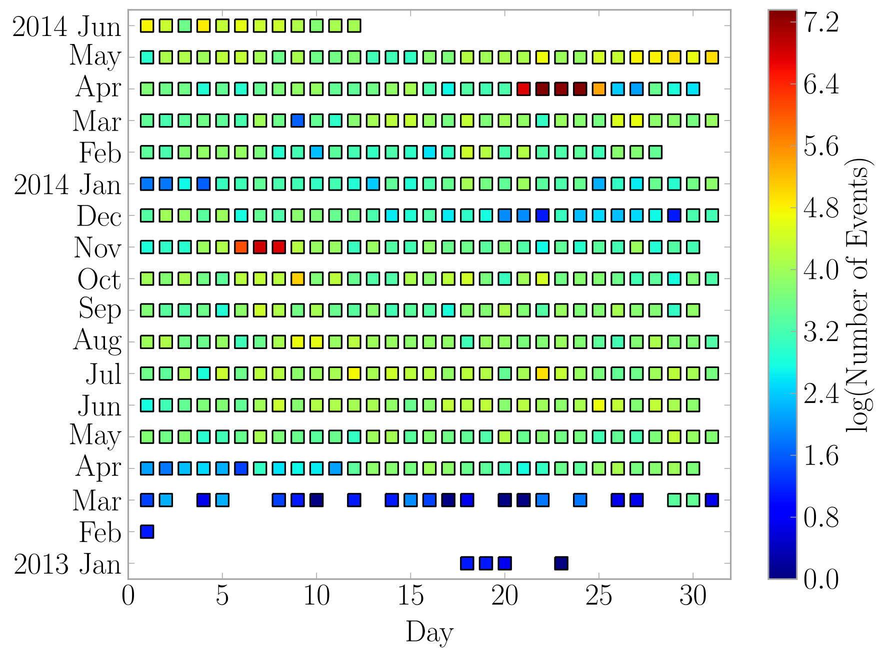

Figure 2.21: Hospital Installation's Sensor Activations

of sensors will need to learn their own specific environment in order to accurately identify and even predict actions such as a human falls. This can be vividly seen by comparing Figure 2.20 and Figure 2.22. For instance, during the nap time hours of the household, there is little activity because the twins are asleep; however, during those same hours in the hospital, things are still very much happening as the hospital never fully sleeps.

2.8 Features of Collected Data

Before looking at the acquired data, signals containing sensor operational errors were filtered out. The errors are discussed in Section 2.4.

2.8.1 Features Explored

Two typical signal features were used to explore trends in the collected data: maximum amplitude and signal energy.

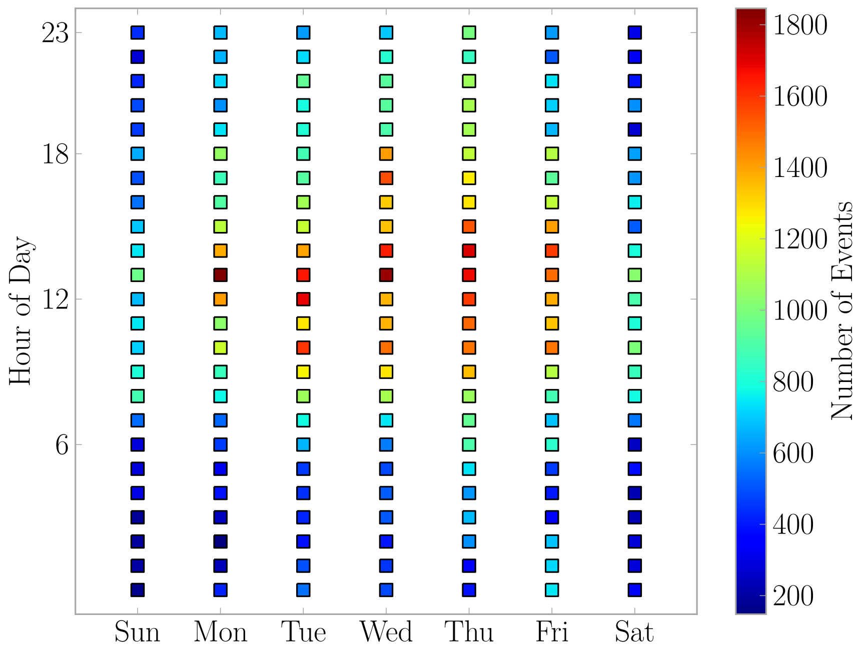

Figure 2.22: Hospital Installation's Activity Density

Maximum Amplitude The maximum value of amplitude present in the signal, calculated using Equation 2.10 where *S(t)* is the detrended acceleration signal, and t is time.

$$A_{max} = max(|S(t)|) \tag{2.10}$$

Signal Energy The energy of the signal, in a signal processing scope, calculated using Equation 2.11 where *S(t)* is the detrended acceleration signal, t is time, and n is the last time step. The trapezoidal rule for numerical integration was utilized.

$$E_s = \int_0^n |S(t)|^2 dt \tag{2.11}$$

2.8.2 Features of Home Data

Most of the amplitudes seen during the home installation, were under 0.5 g. This is to be expected considering the main activity in the household was two three year olds running around and jumping. Their floor impacts would be small due to their size. There were a few larger amplitudes seen, which probably correspond to the two parents. Of particular interest, is even though one parent stayed at home with the children, there were not many large vibrations. This indicates that most day-to-day activity in a household causes very little acceleration on the floor structure.

The overall trend points towards the use of sensors with good resolution and a ±2 g range. A smaller sensor range could potentially be used for home installations, but would risk missing larger amplitude signals such as those caused by a human fall. Note that amplitudes present in recorded signals that were below 0.05 g were ignored in Figure 2.23 as they are considered to be noisy signals, and the few values that were above 2 g as these are outside the range of the sensor, likely sensor malfunctions.

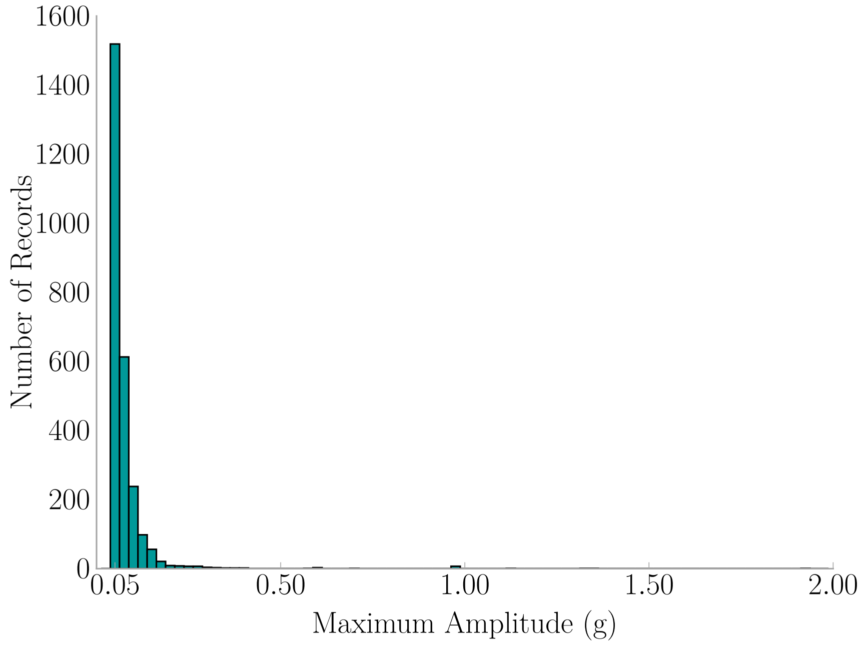

Figure 2.23: Home Installation's Maximum Amplitude per Record

The signal energy for each record was calculated to give a measure of how much activity a sensor caught in each record. The majority of signals, a lot of which are noise, had very low signal energy, while those with activity tended to have relatively higher values. Figure 2.24 displays this trend. Note that outlier values, those above $0.0005\,\mathrm{g}^2\,\mathrm{s}$ are not displayed. There were very few of these signals and corresponded with records containing cyclic patterns, which are most likely caused by a machine, and thus were not included here.

The two signal features were plotted against each other in Figure 2.25 to see if there was a correlation between the two. Groupings would allow machine learning techniques coupled with probabilistic methods to generate the likelihood a fall occurred and other activities occurred. Research is ongoing in this regard.

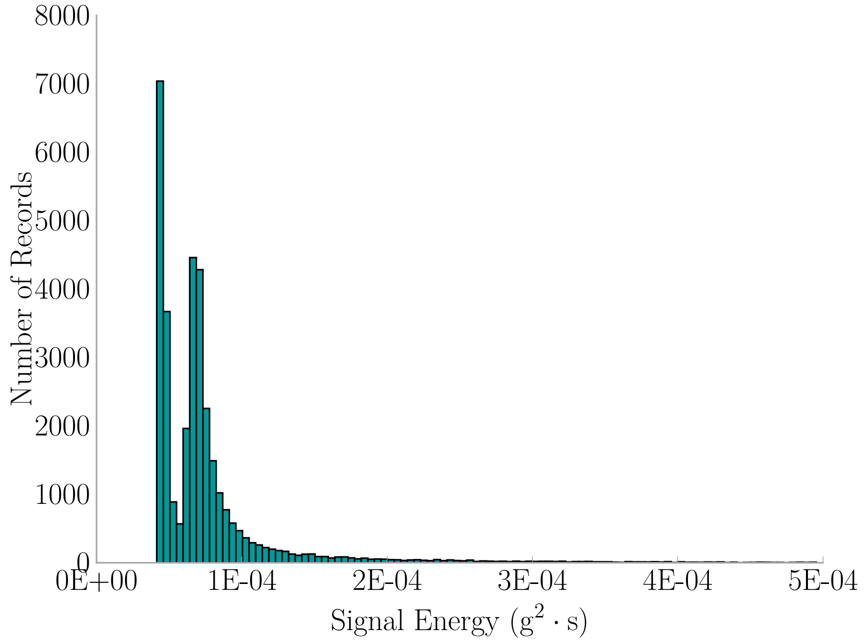

Figure 2.24: Home Installation's Signal Energy Per Record

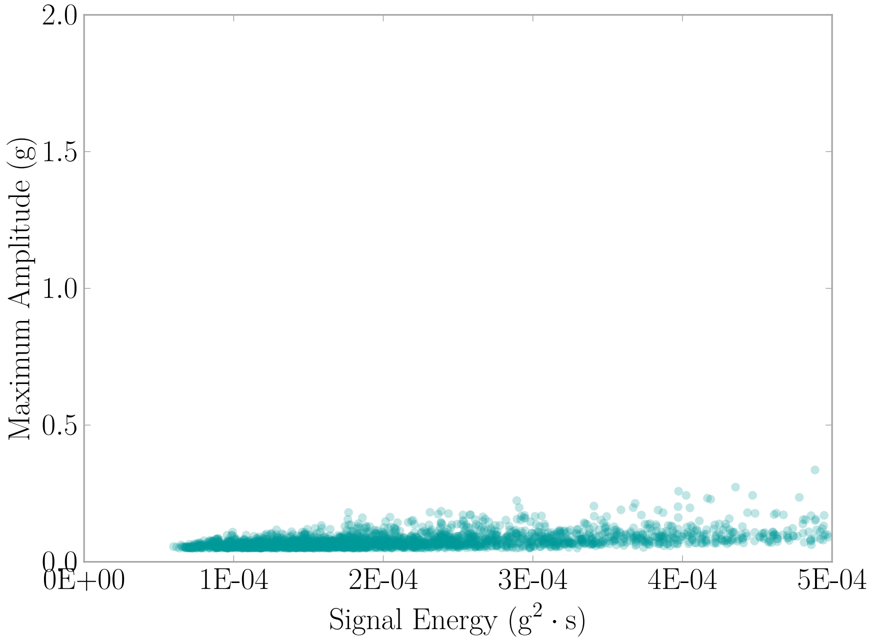

Figure 2.25: Home Installation's Maximum Amplitude Vs. Signal Energy

2.8.3 Features of Hospital Data

Amplitudes present in records capture from the hospital tended to be small in magnitude (<0.5 g), with a bunch of outlying records having around 2 g. The lower amplitudes were expected due to the nature of the stiffness of reinforced concrete flooring, and the tight regulations on hospitals to limit vibrations [18]. The larger amplitudes were caused by a mixture of impacts close to the location of the sensor, and patients picking up the sensors, perhaps thinking they USB power sources were chargers for their phones (see Section 2.4).

The overall trend points towards the use of sensors with good resolution and a ±2 g range. Note that amplitudes present in recorded signals that were below 0.05 g were ignored in Figure 2.26 as they are considered to be noisy signals, and the few values that were above 2 g as these are outside the range of the sensor, likely sensor malfunctions.

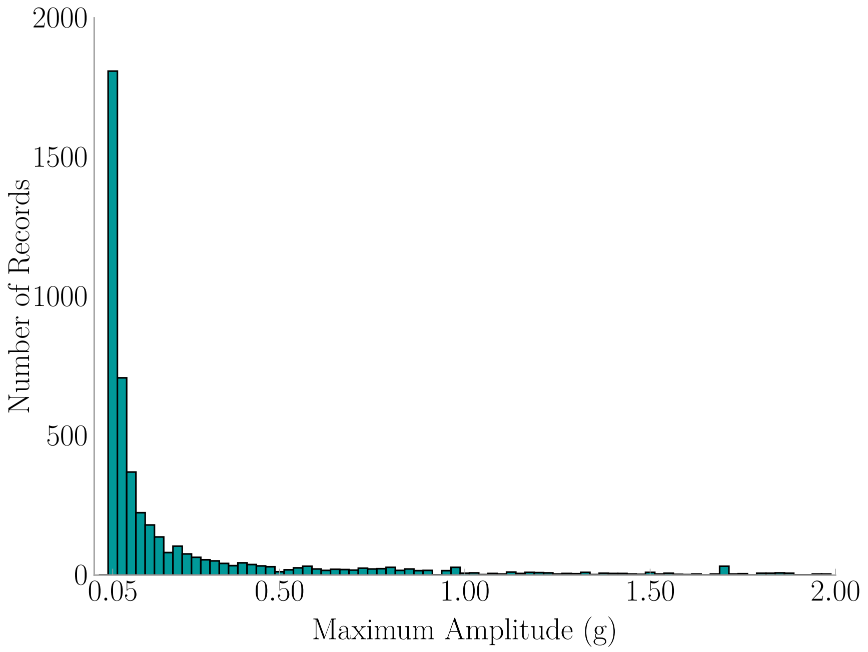

Figure 2.26: Hospital Installation's Maximum Amplitude Per Record

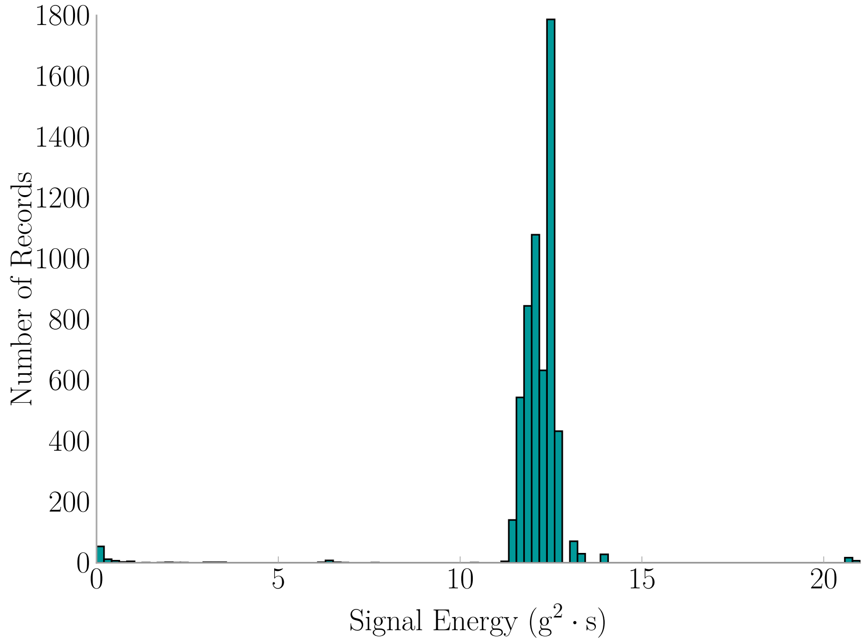

Figure 2.27: Hospital Installation's Signal Energy Per Record

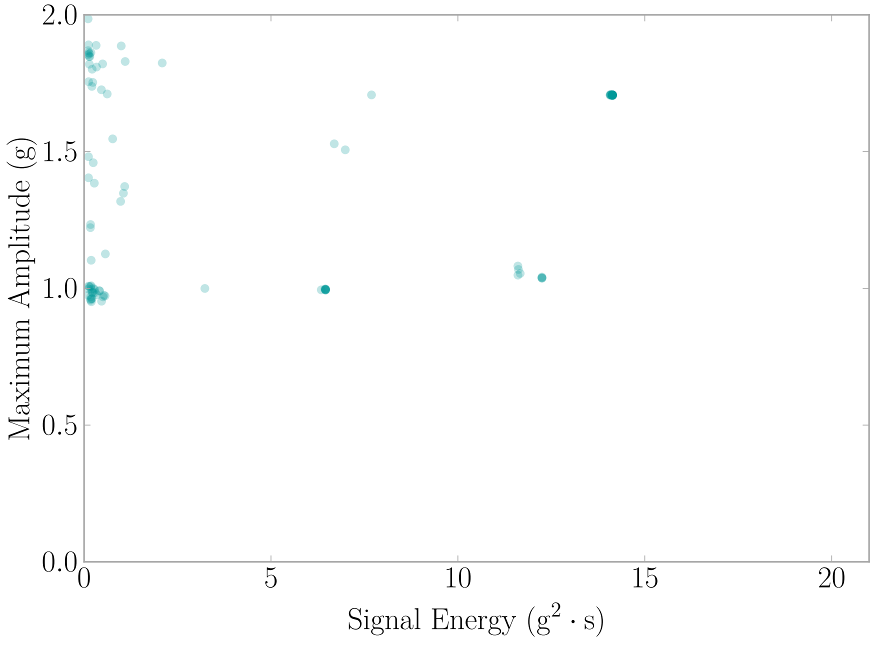

Figure 2.28: Hospital Installation's Maximum Amplitude Vs. Signal Energy

Signal energy present in the hospital installation are grouped mostly between $8\,g^2\,s$ and $15\,g^2\,s$, indicating accelerations observed have a similar amount of activity. Note that values below $0.1\,g^2\,s$ were removed as records with those values are considered to be noise.

The two signal features were plotted against each other in Figure 2.28 to see if there was a correlation between the two. Groupings would allow machine learning techniques coupled with probabilistic methods to generate the likelihood a fall occurred and other activities occurred. Research is ongoing in this regard.

2.9 Hospital Reported Human Falls

For the length of the study, 50 fall events were reported by the hospital staff (see Table A.1). The estimated time of each fall was given to researchers to be used to correlate with collected acceleration records. Challenges arose because the of human error when reporting the time and because the times reported are the time the patient was found and not necessarily the actual time of the event. Hospital patients are monitored on a regular schedule along with constant patrols and emergency pendants the patients can press to call for nurse assistance which aids to reduce reported time error. Additionally, the base station computers' time may also be off since they were not connected to the Internet where the computers could get constant time updates based on an atomic clock. Researchers thus look at a ±1 hour window based on the reported time to account for these potentials for error. Of those 50 reported, four occurred before the room had a system installed and one did not have enough information to identify the system that would have recorded the event. Researchers found records correlating with 16 reports of the remaining 45 records.

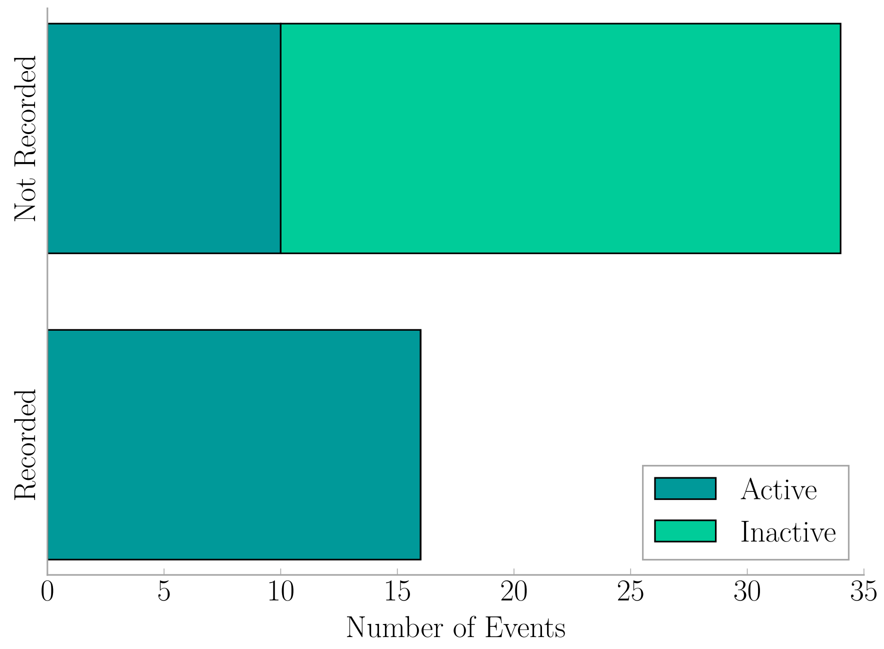

Figure 2.29: Comparison of Hospital Reported Falls to System Captured Falls

Sometimes during operations, the sensors would fail (see Section 2.5) and become inactive leading to missed fall events, and other times, the event was missed entirely even though the sensors were active. The latter may be due to the larger error in time reporting than accounted for (discussed above) or the impact from the fall resulting in a slight vibration that the sensors could not detect. Figure 2.29 demonstrates these challenges. Sensors were active during 26 reported events, but only capturing 16 of those 26. This equates to a ∼62% successful capture rate.

2.10 Real Falls vs Recorded Falls

2.10.1 Recorded Falls

Table 2.2 compares the reported to the collected events and rates the researcher's confidence (0 being no confidence, 5 being very confident) that the fall event was captured based on the collection time and the actual signal. Figure 2.30 visualizes the dates demonstrating human error in the reporting process.

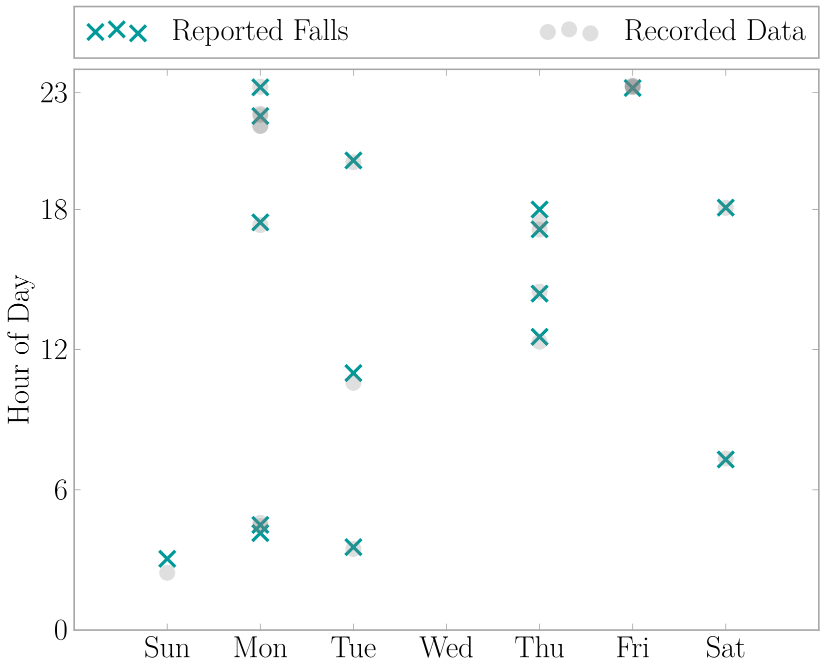

Figure 2.30: Visualization of Reported Falls Vs. Captured Falls

Table 2.2: Reported Falls Vs. Recorded Data Events

ID	**Records ±1 hr**	**Confidence (0-5)**	**Figures**
16	2013-06-17 21:57:19 2013-06-17 21:58:54 2013-06-17 22:03:19 2013-06-17 22:10:07	4	Section B.1
18	2013-06-20 17:14:23	5	Section B.2
20	2013-06-28 23:23:57 2013-06-28 23:24:42 2013-06-28 23:28:42 2013-06-28 23:30:38	5	Section 2.10.2, Section B.3
26	2013-07-25 17:49:29	5	Section B.4
28	2013-07-30 04:45:49	5	Section B.5
32	2013-08-27 10:58:35	2	Section B.6
33	2013-08-29 14:48:57	5	Section 2.10.2, Section B.7
34	2013-08-31 18:07:07	5	Section B.8
35	2013-09-22 02:45:21	5	Section B.9
36	2013-10-03 12:34:31	3	Section B.10
39	2013-10-22 20:02:20	0	Section B.11
41	2013-10-26 07:34:28	1	Section B.12
42	2013-10-28 23:25:33	1	Section B.13
44	2013-11-25 17:33:49	5	Section 2.10.2, Section B.14
46	2013-12-03 03:47:22	1	Section B.15
48	2013-12-09 04:59:04	1	Section B.16

2.10.2 Sample Records

A few collected records stand out to the research team and are presented in this section. The remainder of collected fall events are presented in Appendix B.

Fall Reported on 2013-06-28 23:20 (ID 20)

According the description of this event, the patient was found kneeling next to the bed after attempting to get up and walk around. This is an interesting sequence of events with several captured records in close proximity to the reported time the fall occurred. The first signal shown in Figure 2.31 looks like a jostling movement which is interpreted to be the patient shifting towards the edge of the bed.

The patient attempted to get up to stretch his legs after shifting to the edge of the bed. Instead, he fell to the floor to land (we assume) on his knees. Figure 2.32 shows a signal that looks like one knee hit with the majority of the person's weight, and another knee followed more gently after the initial impact of the first.

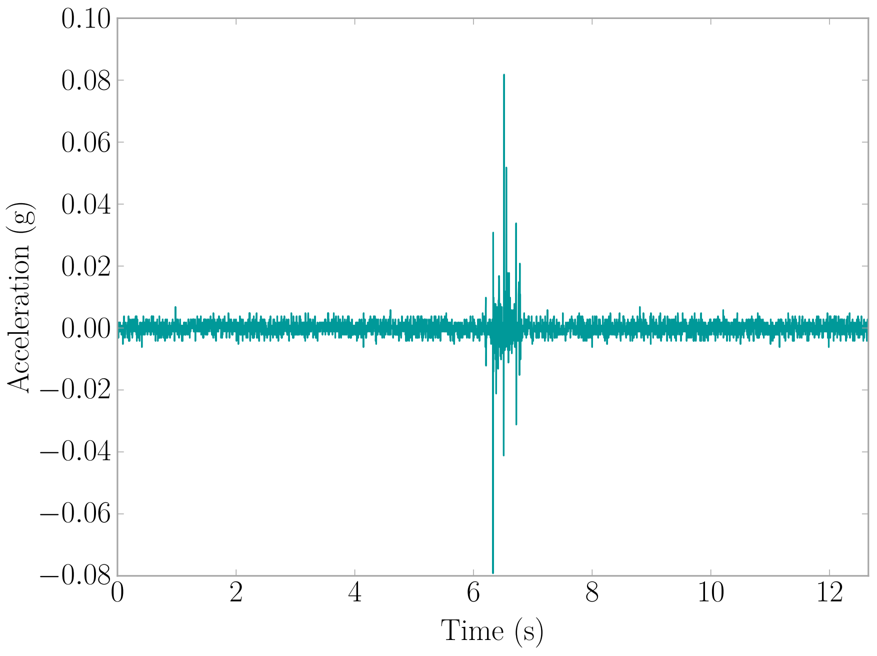

Figure 2.31: Fall Event 2013-06-28 23:23:57

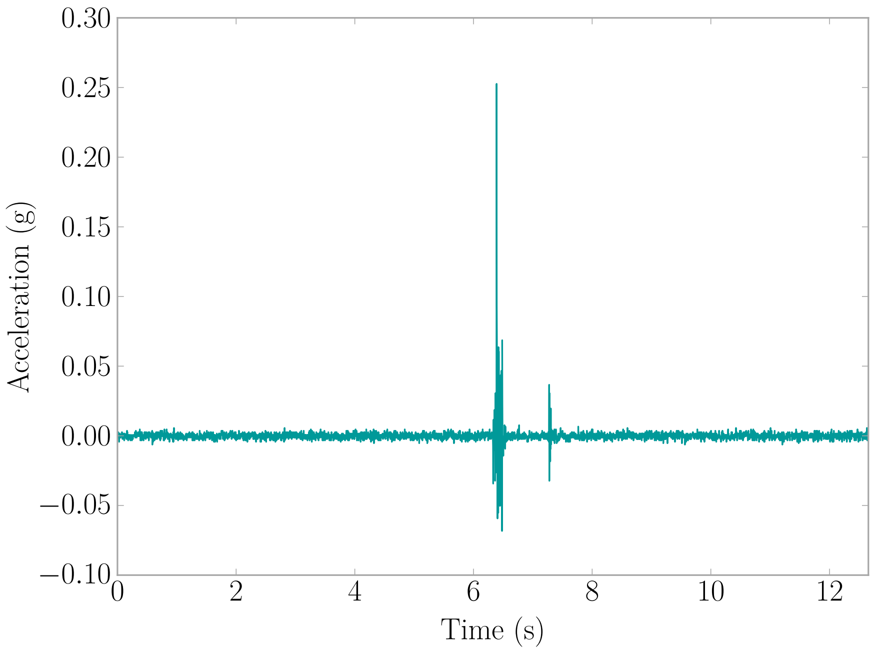

Figure 2.32: Fall Event 2013-06-28 23:24:42

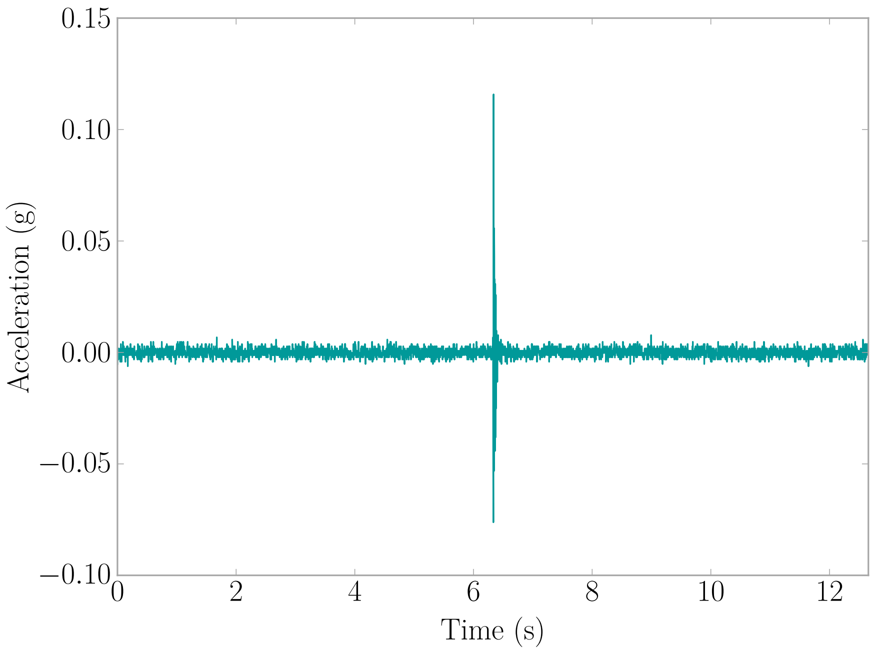

Figure 2.33: Fall Event 2013-06-28 23:28:42

Within a few minutes, the patient may have attempted to get back up onto the bed but was unsuccessful leading to another impact on the floor as he dropped back down. Figure 2.33 shows a downward impact with a slightly higher downward amplitude (∼0.08 g) than the first time the patient fell in Figure 2.32 which suggests more force was applied to the floor, like the full weight of the patient.

Fall Reported on 2013-08-29 14:40 (ID 33)

A nurse was helping the patient, in this instance, to the bedside commode. They did not make all the way and the patient lost balance falling to the floor. The fall was broken by the nurse who eased the patient onto the floor lessening the impact. What is of interest for this event the mode which involves one person ‘damping’ the impact and that two sensors, one inside (Figure 2.34) and one outside of the room (Figure 2.35), showed similar acceleration patterns.

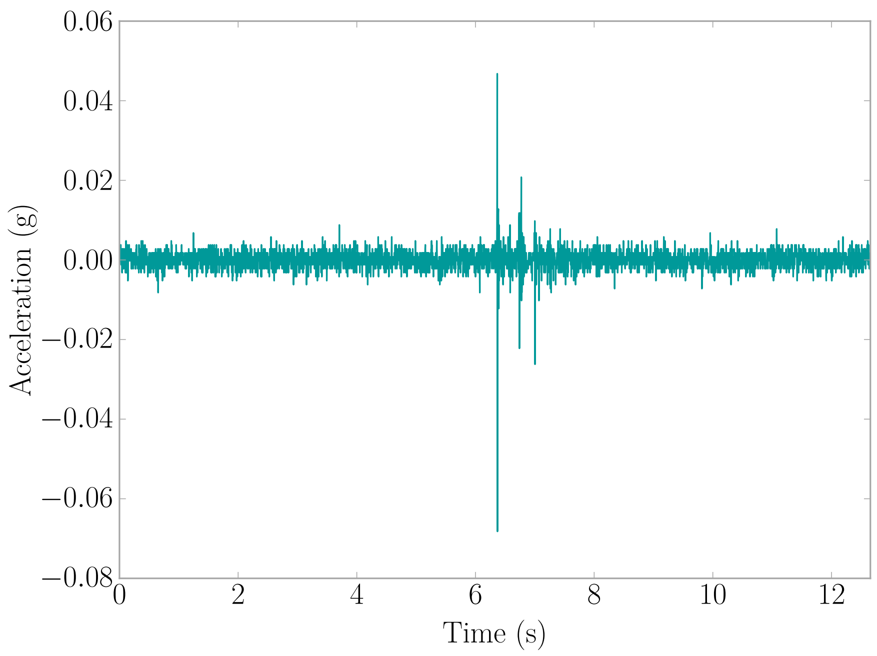

Figure 2.34: Fall Event 2013-08-29 14:48:57 - Sensor Inside Room

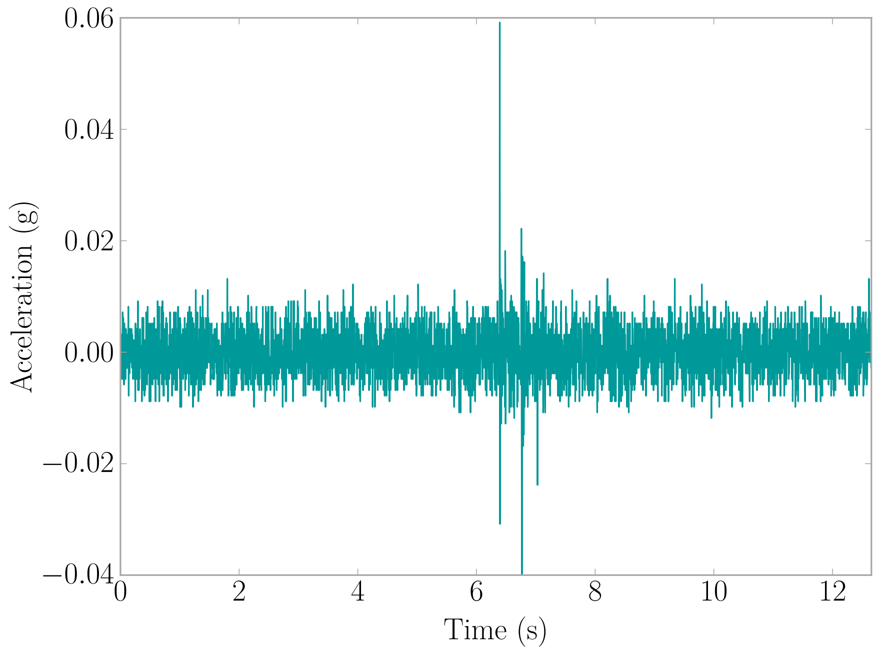

Figure 2.35: Fall Event 2013-08-29 14:48:57 - Sensor Outside Room

Notice how each sensor picked up three consecutive hits at approximately the same time within the record, with the sensor that is in the room of the event experiencing slightly higher accelerations than that of the sensor outside the room. The response demonstrates the low reliability of determining a fall directly from amplitude alone but points towards the possibility of using records from multiple sensors to develop a probability that the event occurred. A research topic the team is currently investigating.

Fall Reported on 2013-11-25 17:45 (ID 44)

The patient in this scenario bent over to pick up some trash off the floor before losing his balance and falling down. Assuming the he bent at the waist and tumbled in the direction of his bending, the natural defensive response would be to attempt to break the fall using ones arms before the rest of the body lands. Figure 2.36's signal displays that pattern with the first peak being smaller than the second.

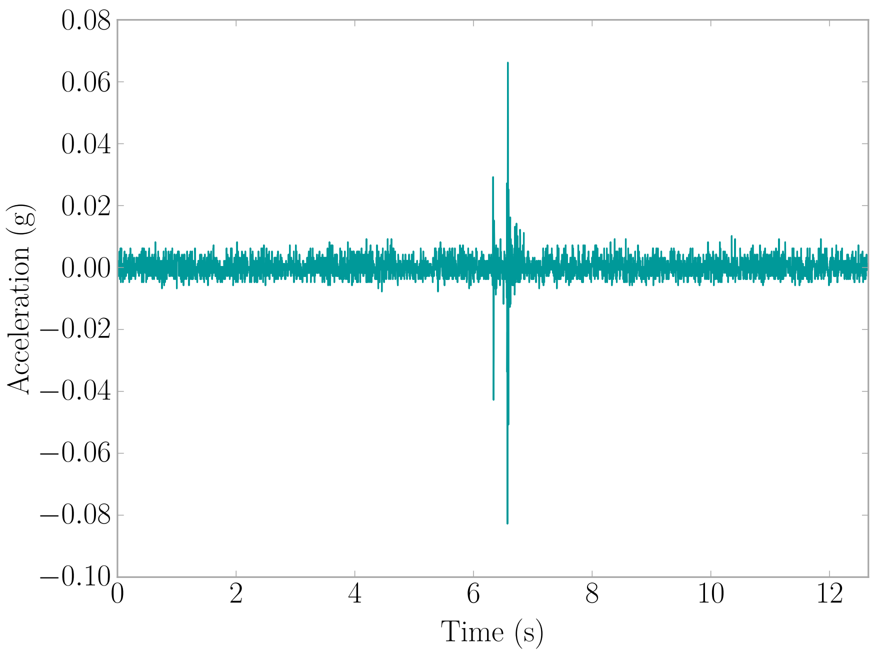

Figure 2.36: Fall Event 2013-11-25 17:33:49

2.11 Conclusion

The star network system used appears to work well for gathering vibration data from human activities whilst emulating the ideal system. Allowing each sensor to operate independently, enabled the sensors to dynamically adjust their threshold levels based on noise (electronic and environmental) without affecting the operation of the whole system. The Camp Hill/Agua Mansa sensors had a low success rate (∼62%) when it came to capturing human falls, with falls being based on hospital reports alone. Falls missed whilst the sensors are operating were likely due to low-force impacts which would not result in severe injury. The remaining falls were missed due to inactivity of the sensors that stemmed from several failure modes, the largest of which involved a person mistaking the sensor's power supply for a phone charger they could use and physically damaging the sensor when attempting to detach the power cord. Overall, the sensors experienced a wear out failure trend with a failure rate of

$5.06 \times 10^{-3} \frac{\text{failures}}{\text{hour}}$ and a MTBF is 197.7 hours. The likelihood of this sensor to capture a fall in its current state is 4.9%. In order to have a 99% likelihood of capturing a fall, a sensor's MTBF should be 8642.4 hours based on a Weibull distribution.

Other aspects of the sensor emerged, including recommendations of buffer size, sampling rate, and sensitivity for wireless accelerometers for human activity monitoring, in particular human fall detection. These factors are chosen as they are general enough that every wireless sensor working with human-induced vibrations would utilize them. Factors such as operational temperature range are not explored as they are specific to the environment one would install the sensor and should be made on a case-by-case basis.

The current recommendation for a buffer size (e.g. amount of time needed to fully capture a vibrations from a fall) is 3 s [6]. This suggestion holds up when looking at the 16 fall events captured by the system for purely capturing the vibrations of the fall. One may wish to increase the buffer size for handling various fall detection algorithms, however. Sampling rate of the sensors was 316 Hz, working well in both the home and hospital installations. This rate is not a typical hardware enabled rate for wireless accelerometers, so it is suggested to use the more common rate of 400 Hz which will also give signals some more definition. Sensitivity of the installed sensors, the remaining aspect, was 0.25 mg resolution and a range of ±2 g. The range proved more than enough in the falls the systems experienced, with no cutting off of the signals. However, the resolution was not enough in several of the cases, and several events were missed potentially due to the fall having low-force which a higher resolution sensor could have registered. A suggested resolution of 1 µg is put forth to have better definition in the signal, particularly for falls resulting in low amplitude vibrations.

Preliminary looks at human activity monitoring through structural vibrations shows promise. Schedules of the people in hospital and the home installations match closely to what the system saw in vibrations as seen in the heat maps presented. Further research into predictive activity models would open up many avenues for development of privacy-respecting technology towards more intelligent infrastructure.

Chapter 3

Data Management For Structural Vibration Monitoring of Human Activity

3.1 Introduction

A large amount of data is produced from a large scale installation of the vibration monitoring system described in Chapter 2. Thus, a way to keep track of all the data in a meaningful way so that researchers can focus more on analysis and not on organization of all the data is needed. This is called data curation and is "the active and ongoing management of data through its life cycle of interest and usefulness to scholarship, science, and education" [22]. The field itself "includes authentication, archiving, management, preservation, retrieval, and representation" [22]. As a first step towards curation of the data generated by this work, a data management plan was devised and implemented. The devised strategy focused on flexibility for scalability through a relational database architecture, as well as leveraging secure websites interfaces for tracking other information related to the project. Additionally, a Python package was created to streamline access to the database allowing for researchers to gather information with ease.

3.2 Management Plan

All data gathered and generated is housed on servers of the Structural Dynamics and Intelligent Infrastructure Laboratory (SDII) at the University of South Carolina (USC). The following sections describe the data being collected and its management.

3.2.1 Data from Installed Systems

Monitoring human-induced vibrations in multiple locations across multiple installed systems produces a large amount of data, which needs to be well managed so researchers can easily access and draw conclusions from the data. The first is the operational data from the systems themselves including acceleration data from the sensors, orientation of the sensors, and logs of system activity. Next, the participant reported fall events need to be housed in relation to the collected data so information the systems collected can be directly related to each fall. Both of these data types are managed in a database using the architecture described in Section 3.3.

In addition to the data collected and generated by the installed monitoring systems, information about each sensor installation (e.g. hospital room or a private residence) is recorded. Approximate location of the sensors are marked on a diagram of the particular area, and the type of construction for the building is included. This data is maintained both on physical paper and digital documents on the servers without any identifiable patient information. Researchers visit installations to maintain the systems periodically. The trips often included some discussion with participants. Both the researchers' check of the systems and participants' comments are recorded in a Drupal-based website [23]. Identifiable participant information (e.g. weight, height, or age) is not recorded as the goal of the dataset is to capture a fall irrespective of the physical characteristics of the person who fell.

3.2.2 Data from Researchers

Researchers working with the database need the capability of appending data to the main database. This includes quantitative and qualitative data generated when exploring the data. Therefore, additional tables were designed to allow researchers this extra capability. The *event_parameters* table, for example, provides a simplified way to relate this information to the various acceleration events captured. See

Section 3.3 for more discussion and description about this and other tables.

3.2.3 Data Access

Access to the data is controlled through log in credentials for each user. This allows for the control of what each user can do with the database so as to prevent accidental changes. In addition, each installed system maintains a local database that mirrors the one housed with SDII as an additional precaution. A Python package (*ssh_database_utilities*) standardizes data access to the database which additionally aids in reducing unwanted accidental changes to stored information. The package documentation is available in Appendix M. For those given more direct access to the database, sample queries are provided in Appendix C.

3.3 Database Architecture

A relational database was chosen to store and access the experimental data, using MySQL as the backend [24]. The enhanced entity relationship diagram is presented in Figure 3.1. This database structure is used at the site where data is collected in the base stations and in the main database. The following paragraphs describe the tables in more detail, and are organized in alphabetical order for easy reference. The term 'event' means the monitoring system was triggered to record accelerations from its sensors thus indicating one or more recorded signals, and the term 'hit' means an impact present in a signal.

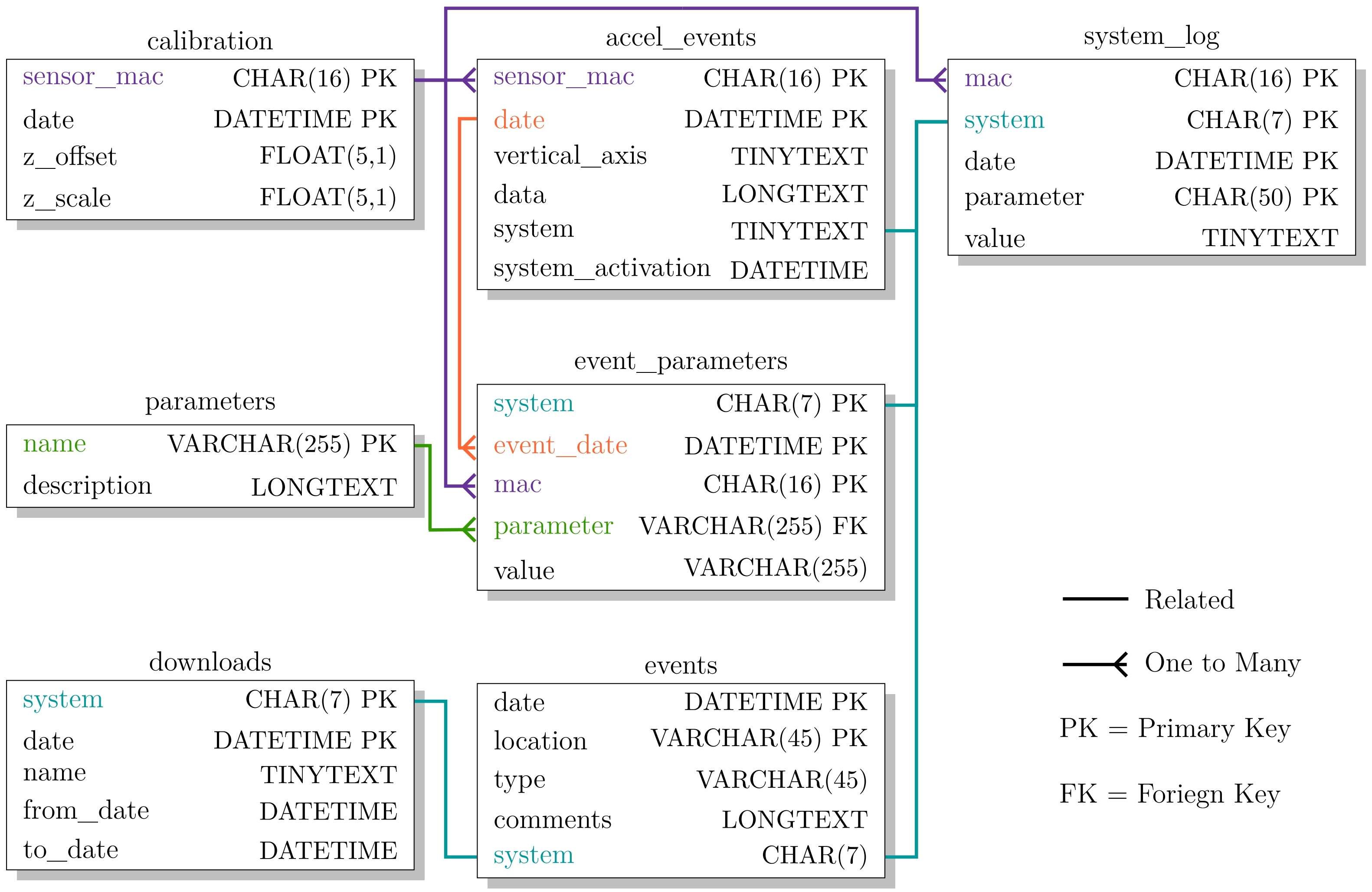

Figure 3.1: Enhanced Entity Relationship Diagram for Human Activity Database

ACCEL_EVENTS Here, all the data collected from the sensors is stored including information about the orientation of the sensor and the system the sensor belongs to. Each table row has a system and system_activation for referencing items stored in the system_log table. Knowing when the system was activated allows one to grab information from the log pertaining to a specific operational period of the system. The acceleration data captured is first converted into units of gravity through the calibration table, and then, is stored as a space delimited string in the field *data*.

CALIBRATION The Agua Mansa sensors report data to the base station in pts/g, where the data needs to be converted into units of acceleration. This table stores the calibration information with the base station using the latest dated calibration values for unit conversion. Sensor Media Access Control Addresses (MAC Addresses) must be available in the calibration table before data is recorded into the *accel_event* table. Base station programs enforce this policy. For more information on calibration and conversion formulas see Section 2.3.1.

DOWNLOADS This table is used to track when data from a system for a specific time period has been transfered from the base station to the SDII servers. When downloading data, the user enters his name or, in the case of the web service, the name *webservice* is entered. Subsequent downloads of data from a base station reference the table to reduce the amount of data to transfer in each download, and thus the amount of time it takes for the download process. This is used in the base station for use with the Data Mobile Ubiquitous LAN Extension (MULE), and the main server for use with the web service (see Section 2.3.1 for more details).

EVENTS All reported human-induced vibration events are recorded here with information on the system that saw the event, the date and time the event occurred, comments from the reporter, and the location of installation. No patient information (e.g. name, weight) is stored to protect privacy. The field *type* intentionally is flexible if other significant human activity besides a human fall is reported as this can be of interest for refining fall detection algorithms or research into other activity.

EVENT_PARAMETERS Acceleration events have various parameters, or metrics, that can be used to describe them. Calculated metrics from the *parameters* table are stored in this table for signals present in *accel_events*. This includes parameters like maximum amplitude and signal category. Access the *parameters* database table for a current list of available metrics created by this research and their descriptions. Table 3.1 provides the parameters available at the time of this writing.

PARAMETERS The parameter table defines parameters and removes the chance that a it can be misspelled. Other tables reference this one via foreign keys to ensure integrity. Table 3.1 describes the parameters, available as of 2016 February 1, in alphabetical order by their database names.

Table 3.1: Acceleration Parameters

Name	DB Name	Description
Amplitude Hits	amphit	Amplitude within the record (g); There is one number per hit
Maximum Amplitude	ampmax	Max of the absolute value of the signal (g); See Section 4.2.2
Manual Category	category-manual	Category of signal manually classified: (0) not sure what category, (1) noise, (2) some activity but indistinct peaks or shape, (3) distinct peaks and shape, (4) sensor error; Used for training an SVM

continued on next page...

Name	DB Name	Description
SVM Category	category-svm	Category of signal created by the SVM: (0) not sure what category, (1) noise, (2) some activity but indistinct peaks or shape, (3) distinct peaks and shape; See Chapter 4
Dispersion Ratio	dr	The ratio of desired signal to environmental noise; See Section 4.2.5
Error	errornorm	Normalized error of the exponential curve
Location	location	Location of the event; For example, a specific room in a house
Max Amplitude Difference	mad	The max change between descending sorted, absolute values of the signal (g); NaN are ignored; See Section 4.2.3
Accepted Hits	naccept	Number of hits accepted during analysis
NaN Density	nandensity	The density of NaN values in the record; See Section 4.2.1
Number Rejected	nreject	Number of potential hits rejected during analysis
Rate of Dispersion	rod	How much dispersion is present within a signal; See Section 4.2.4
Signal Energy	senergy	Energy present in a signal processing sense (g^2 s); See Section 2.8.1
Hit Time	thit	Time of impacts within the record (in seconds since the beginning of the record); There is one number per hit
Natural Freq. and Damping	wnzetahit	Estimation of $\omega_n \zeta$ for each hit within the record

SYSTEM_LOG The system log tracks activity of the system, including errors and installation dates, during a system's operation. This is for both the base station and the sensors themselves. Base stations (i.e. the laptops) store a blank string, 0, or their MAC Addresses for the field *mac*. Sensors store in the log using their own MAC Addresses so parameters such as reliability or actual sampling rate can be determined (see Chapter 2). The table does not reference another table by foreign key unlike that of the *parameter* and *event_parameter* table relationship. This allows for maximum flexibility when programming the system so that new log info can be added at will. Thus, parameter names in this table tend to be more verbose and self-descriptive for clarity. Table 3.2 describes the parameters in the system logs, as of 2016 February 1, in alphabetical order of their database names.

Table 3.2: Parameters in the System Log Table

DB Name	Description
data_received	Number of data points received from the sensor in the time span error_log_length
error_log_length	Length of time between system log saves (s); Saved when system starts
installed	Indicates system installed, reference the date of the log for when the install occurred
lost_sync	Number of times the base station lost synchronization with a sensor in the time span error_log_length
malformed_data	Number of bad data packets received by the base station for the sensor in the time span error_log_length

continued on next page...

DB Name	Description
malformed_sync	Number of bad synchronization packets received by the base station for the sensor in the time span error_log_length
maximum threshold	Indicates the maximum threshold for the bandpass acceleration threshold (pts/g); Saved when system starts
minimum threshold	Indicates the minimum threshold for the bandpass acceleration threshold (pts/g); Saved when system starts
overflow	Number of times the accelerometer overflowed the sensor's buffer in the time span error_log_length
reset	Number of times a sensor reset itself in the time span error_log_length
sample_rate	The expected sample rate; Saved when system starts
soft_version	Base station software version; deprecated
suite_version	System Tool Suite Version; Saved when system starts
sync_received	Number of synchronization packets received by the base station for the sensor in the time span error_log_length
threshold	Acceleration threshold to cross for activation (pts/g); Saved when system starts
trigger_count	Number of times a sensor was triggered in the time span error_log_length
trigger_level	Acceleration value that triggered the sensor (pts/g)
uninstall	Indicates the end of a system's installation period, reference the date of the log for when the install occurred

continued on next page...

DB Name	Description
webservice-accel_events-duplicates	Number of duplicate acceleration event records the web service tried to upload
webservice-accel_events-failure	Indicates the web service failed to upload acceleration events
webservice-accel_events-sent	Number of acceleration event records the web service sent
webservice-accel_events-timeout	Number of timeouts the web service had when trying to send acceleration event data
webservice-calibration-duplicates	Number of duplicate calibration records the web service tried to upload
webservice-calibration-failure	Indicates the web service failed to upload calibrations
webservice-calibration-sent	Number of calibration records the web service sent
webservice-calibration-timeout	Number of timeouts the web service had when trying to send calibration data
webservice-downloads-duplicates	Number of duplicate download records the web service tried to upload
webservice-downloads-failure	Indicates the web service failed to upload downloads
webservice-downloads-sent	Number of download records the web service sent
webservice-downloads-timeout	Number of timeouts the web service had when trying to send downloads data
webservice-system_log-duplicates	Number of duplicate system log records the web service tried to upload
webservice-system_log-failure	Indicates the web service failed to upload system logs

continued on next page...

DB Name	Description
webservice-system_log-sent	Number of system log records the web service sent
webservice-system_log-timeout	Number of timeouts the web service had when trying to send system logs data

3.4 Conclusion

The data management plan outlined in this chapter, has worked well over the many years of the human activity through structural vibrations study and provides a foundation for future data curation. Researchers have the infrastructure to handle and analyze the multitude of acceleration records collected, as well as tools for easy access to data while mitigating the possibility of accidental changes in the data. Identifiable participant information is not recorded, providing privacy and promoting research towards user-independent fall detection. The flexibility and scalability of this plan will provide valuable research infrastructure for years to come.

Chapter 4

Acceleration Event Filtering

4.1 Introduction

The Structural Dynamics and Intelligent Infrastructure Laboratory (SDII) at the University of South Carolina (USC) houses 536,686 acceleration records constituting 220,597 distinct events as of 2016 February 1, with more being gathered daily. These records are collected as a joint effort between SDII, Palmetto Health Hospital (PH), and the William Jennings Bryan Dorn Veteran's Administration Medical Center (VAMC) to capture human-induced vibrations from a variety of environments including hospitals, nursing homes, and personal residences. The aim of the effort is to investigate human activity as it relates to changes in medical conditions using vibrations of the structural as the sole point of reference. Needless to say, vibration based human monitoring systems produce a considerable amount of data which create the challenge of identifying relevant records to study or consider for further action.

Data is often collected using wireless accelerometers, and with that comes additional challenges as wireless communication is not always reliable leading to dropped packets on the network meaning parts of the signals can be missing. Another challenge comes from the reliability of the sensors which can degrade over time under continuous operation and transmit error-ridden data (details discussed in Section 2.5). Hence, signal metrics were developed and employed through a Support Vector Machine (SVM) to sort the database of signals into categories, greatly reducing the amount of human labor required to get to the 'meat' of the database.

4.2 Acceleration Signal Metrics

In addition to typical characteristics of the signal such as amplitude, several metrics were developed for describing the records which would then be used by the SVM to learn what the researcher judged to be a good signal. The metrics NaN Density and MADr served to indicate the cleanliness of the signal with respect to potential sensor errors. The remainder of the metrics were used to describe the level of activity present. A signal with little activity is often unwanted for processing techniques as the data does not contain much information beyond what the sensor quantization levels are, hence, a way to filter out weak signals is necessary to help the analyst find quality signals quickly or for computer code to select signals autonomously. All these metrics are calculated after the mean of the signal has been subtracted to each point.

4.2.1 NaN Density

Sometimes with wireless accelerometers, there will be lost data because of dropped communication packets. Synchronization techniques allow for the host to determine missing packets and how many data points are lost. The lost data points are replaced with a place-holder such as the symbol *NaN* which stands for 'Not a Number.' The more missing packets, the less reliable the data is. In an effort to easily identify the signals with a multitude of missing data points, the metric NaN Density was created. It simply counts the number of NaN place-holders and ratios it to the number of points in the entirety of the record. Equation 4.1 displays the calculation where n_{nan} is the number of points in the signal that indicate missing data, and n_s are the total number of points in the acceleration signal.

$$\rho_{nan} = \frac{n_{nan}}{n_s} \tag{4.1}$$

As can be seen from above, the lower the amount of lost data packets, the lower the ratio with 0.0 being a record without any missing packets. See Figure 2.3 for a signal missing data.

4.2.2 Maximum Amplitude

This is a simple metric that determines the maximum absolute value of the signal as shown in Equation 4.2 where max() is the maximum value function, *S(t)* is the detrended acceleration signal, and t is time.

$$A_{max} = \max\left(|S(t)|\right) \tag{4.2}$$

4.2.3 Maximum Amplitude Difference Ratio (MADr)

This metric determines the maximum change between values of consecutive points within the acceleration signal. Sometimes, the accelerometer may malfunction and produce a fictitious high-value amplitude point or a 'spike' (see Figure 2.9). Acceleration records from real events would follow a shape similar to an impulse response function. Thus the Maximum Amplitude Difference (MAD) gives a sense of discontinuities in the signal that are not due to a physical action.

First, the descending-sorted absolute value of the acceleration signal *S(t)* is calculated using Equation 4.3 where desc() is the descending order sorting function.

$$D = \operatorname{desc}\left(|S(t)|\right) \tag{4.3}$$

Next, Equation 4.4 expresses the calculation of Maximum Amplitude Difference (MAD) where max() is the maximum value function, D_i is calculated in Equation 4.3, and i is the index within D.

$$\text{MAD} = \max\left(D_i - D_{i-1}\right) \tag{4.4}$$

Finally, take this value in ratio with the maximum amplitude like in Equation 4.5 where MAD is the maximum amplitude difference calculated using Equation 4.4, and A_{max} is the maximum amplitude in the signal calculated using Equation 4.2.

$$\text{MADr} = \frac{\text{MAD}}{A_{max}} \tag{4.5}$$

The closer the MADr is to 1.0, the sharper the change between consecutive points is. Typically, a ratio greater than 0.95 indicates a 'spike' in the data.

4.2.4 Rate of Dispersion (RoD)

The maximum change of the dispersion present of the signal can serve as an indication of how spread the acceleration signal is. First, a vector of standard deviations $\sigma^{\ddagger}$ is computed like in Equation 4.6 where $\sigma()$ is the standard deviation, S_i is the i-th point of the acceleration signal, and j is an integer that adjusts the window location where the standard deviation is calculated.

$$\{\sigma^{\ddagger}\} = \left\{\begin{array}{c} \sigma\left(S_{i:i+n_w}\right) \\ \sigma\left(S_{i+\Delta:i+\Delta+n_w}\right) \\ \vdots \\ \sigma\left(S_{i+j\Delta:i+j\Delta+n_w}\right) \end{array}\right\} \tag{4.6}$$

The window shift Δ is calculated using Equation 4.7

$$\Delta = n_w - n_o \tag{4.7}$$

where n_w is the number of points per window, and n_o is the number of overlapping points per window. RoD is calculated using Equation 4.8 where τ is an integer.

$$\text{RoD} = \max\left(\left|\sigma^{\ddagger}_{i+\tau} - \sigma^{\ddagger}_{i}\right|\right) \tag{4.8}$$

An example of what the metric calculation process looks like is presented in the following with two signal examples to demonstrate how the rate changes: free vibration (Signal A) in Figure 4.1a, and a harmonic vibration (Signal B) in Figure 4.1b. For the example, the value of n_w is 250, n_o is 249, and τ is 100. Notice how the Rate of Dispersion (RoD) in Signal A is several magnitudes higher than that of the more regular vibration of Signal B which has more regular dispersion of data points (Figure 4.1e and Figure 4.1f). This demonstrates how changes in accelerations present in a signal can be indicated using RoD.

4.2.5 Dispersion Ratio (DR)

This metric attempts to characterize the strength of the desired signal compared against other sources of vibration considered 'environmental noise.' In the case of human activity, environmental noise would be something like a washing machine running, and a desired signal would be free vibration wave forms resulting from impacts. One challenge associated with evaluating the amount of environmental noise is that one needs to have a record that is only noise. The amount of environmental noise is different for each sensor installation, and it might even change as a function of time. It is not practical to manually study noisy signals for each case and determine the level of environmental noise. An alternative method is presented here where the vector of standard deviations is calculated using Equation 4.6 and values are extracted to create a ratio between the signal of interest and the environmental noise in the same record. The dispersion ratio is defined in Equation 4.9 where max() is

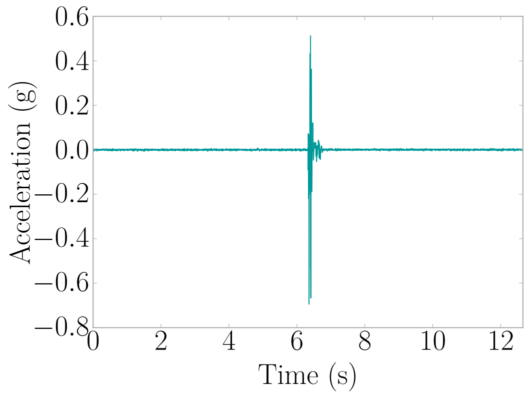

(a) Signal A

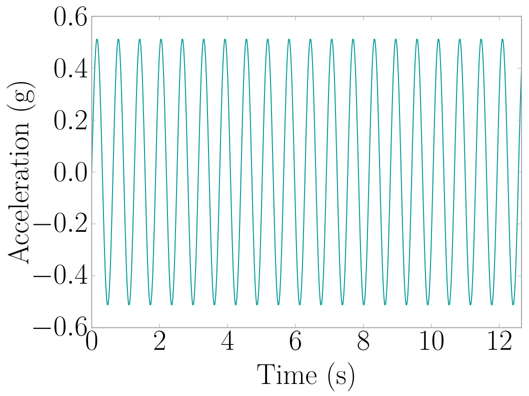

(b) Signal B

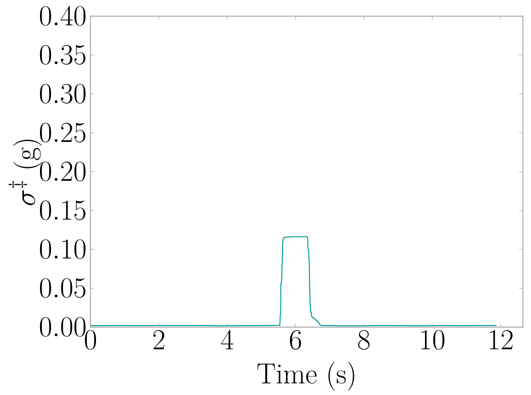

(c) $\sigma^\ddagger$ for Signal A

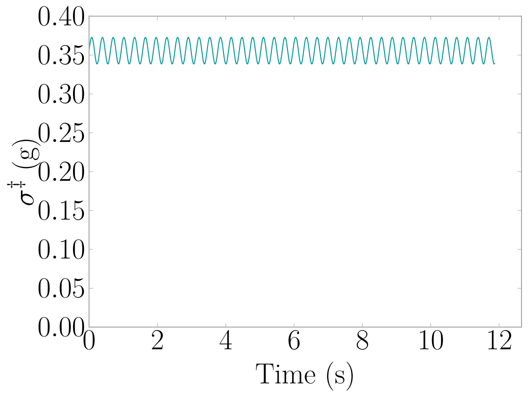

(d) $\sigma^\ddagger$ for Signal B

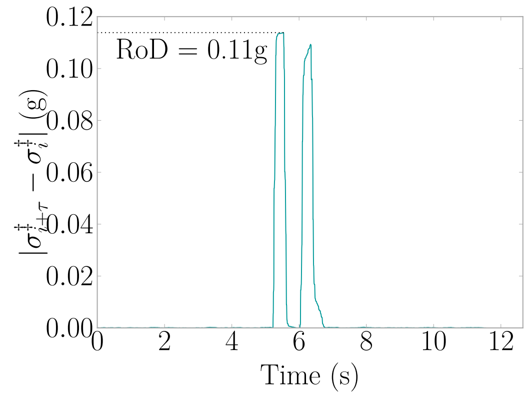

(e) RoD for Signal A

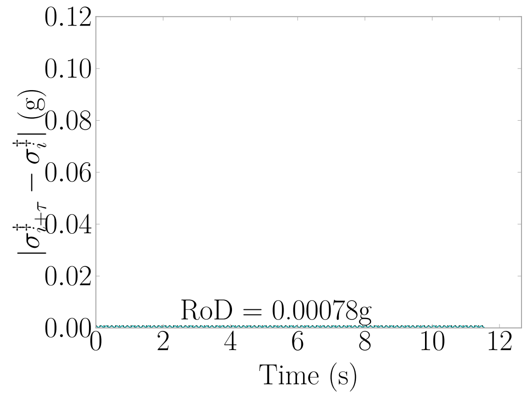

(f) RoD for Signal B

Figure 4.1: Example of How to Calculate RoD

the maximum value function, min() is the minimum value function, and $\sigma^{\ddagger}$ is the vector calculated using Equation 4.6.

$$\mathrm{DR} = \frac{\max\left(\sigma^{\ddagger}\right)}{\min\left(\sigma^{\ddagger}\right)} \tag{4.9}$$

The idea is that the shifting window will grab segments with only environmental noise present and some windows that have data of interest. Environmental noise is then considered to be where a smaller standard deviation is present (e.g. base line readings of a sensor when no activity is present), and good signal is where the data has higher variations which results in a larger standard deviation value.

Figure 4.2 presents an example for calculating DR using the same parameters as in the example for RoD (Section 4.2.4). In Figure 4.2a, the environmental noise and signal of interest are identified. The calculation of $\sigma^{\ddagger}$ occurs, and then the ratio of maximum to minimum values of $\sigma^{\ddagger}$ is taken to determine DR in Figure 4.2b.

4.3 Support Vector Machines

The concept of SVMs was first developed by researchers of AT&T Bell Laboratories as "a training algorithm that maximizes the margin between the training patterns and the decision boundary" [25]. Further research would develop the base algorithm into a flexible and accurate machine learning technique providing the ability for classification, and it would see use in financial forecasting, predicting medication adherence, and mobile communications [26, 27, 28, 29, 30]. The algorithm can be trained, or learn by example, much like a human-being which gives SVMs the ability to label, and hence classify, information presented to it. Metrics can be gathered from an entity in question, which the SVM can use to 'connect the dots' indicating the entity in question belongs to which group [31].

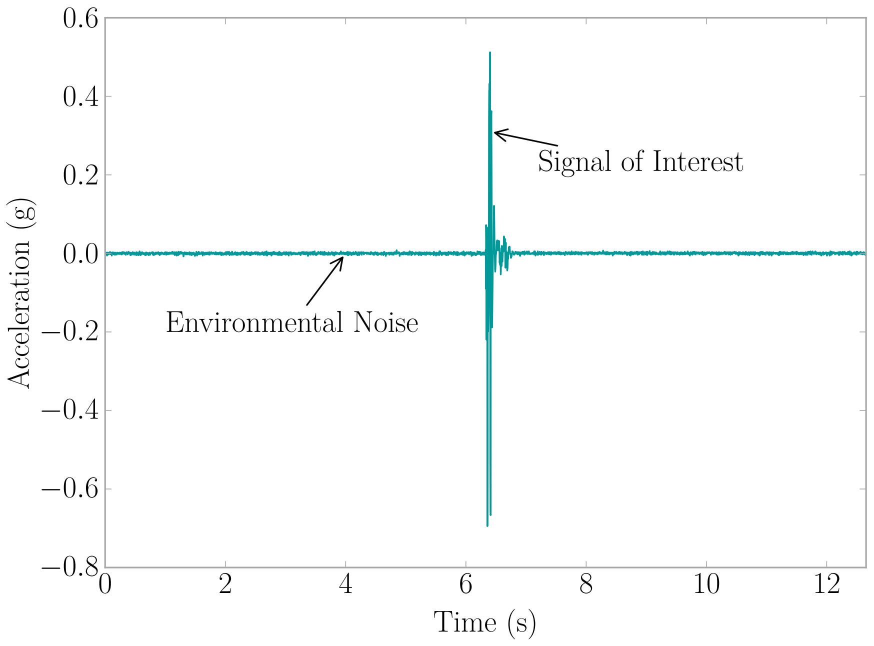

(a) Original Signal

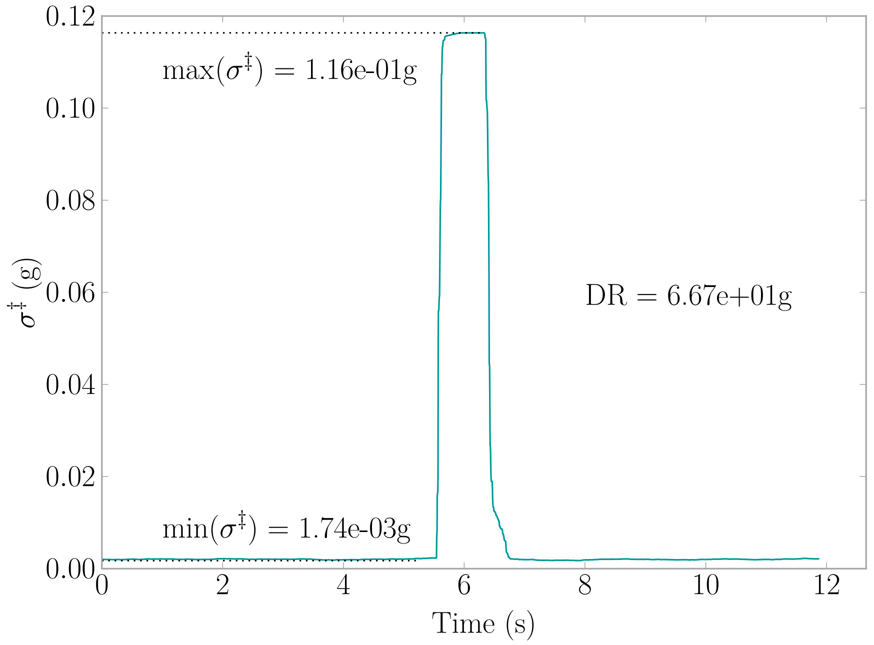

(b) DR for Signal

Figure 4.2: Example of How to Calculate DR

SVMs can use many kernel functions for designing boundaries with the training data [26, 32]. The four kernels tested were linear, radial basis function (RBF), polynomial (3rd degree), and sigmoid. The RBF outperformed the other kernels in robustness, and had the most highest scoring best training sets (see Section 4.4). The linear kernel came in second place in both aspects considered. Therefore, the following discussion is presented with the linear and RBF.

The linear kernel is described by

$$K\left(x, x'\right) = x \cdot x' \tag{4.10}$$

where x' is the training and x is the testing data. The RBF is described by

$$K\left(x, x'\right) = e^{-\gamma|x-x'|^2} \tag{4.11}$$

where x' and x represent the training and testing data respectively. These are regulated by the shape parameter γ [26, 32, 33]. This "projects data from a low-dimensional space to a space of higher dimension" [31] which increases the ability of the SVM to determine decision boundaries, and thus increase the accuracy of classification.

Kernels are fed into a decision function having the form of

$$f\left(x\right) = \operatorname{sign}\left(\sum_{i=1}^{n} y_i \alpha_i K\left(x, x'\right) + \rho\right) \tag{4.12}$$

where sign () is the function described by Equation 4.13, x is the data to be classified, n is the number of points of x, y_i is a vector of form $y \in \{-1, 1\}^n$, α_i is the regularization parameter in the range of $0 \leq \alpha_i \leq C$ with C being the penalty parameter, $K\left(x, x'\right)$ is the kernel function, and ρ is an independent intercept parameter [32]. Python package Scikit-Learn v0.16.1 provides SVM functions used here [32].

$$\operatorname{sign}(x) = \begin{cases} -1 & \text{if } x \leq 0 \\ 0 & \text{if } x = 0 \\ 1 & \text{if } x \geq 0 \end{cases} \tag{4.13}$$

4.4 Filtering of Acceleration Signals

Metrics from Section 4.2 were generated for all the available data and saved into a relational database for future access. Data was first filtered using MADr to ignore signals with data caused by sensor malfunctions (MADr < 0.95) and the NaN Density metric to find complete signals ($\rho_{nan} = 0$), that being the signals not having any missing data points. Researchers then randomly selected 200 signals from the database without knowing the metric values. The signals were plotted and manually categorized using the following categories shown in Table 4.1.

Table 4.1: Signal Categories

Category	Description	Count
1	Exhibiting lots of noise with little to no data	160
2	Some activity but indistinct peaks or shape	22
3	Distinct peaks or shape	18

In this way, the SVM can learn the categories assigned by the researcher. The SVM would relate categories to metric values and be able to sort the remainder of the 536,686 records of the database. Examples of the categories from Table 4.1 are presented in Figure 4.3.

The Pareto Principle, a guideline often used in economics and has seen use in computer science, was chosen to validate the method where the split of the data set becomes 80% training and 20% validation [34]. Data was randomly split into the training and validation categories using the Scikit-Learn function *train_test_split()*

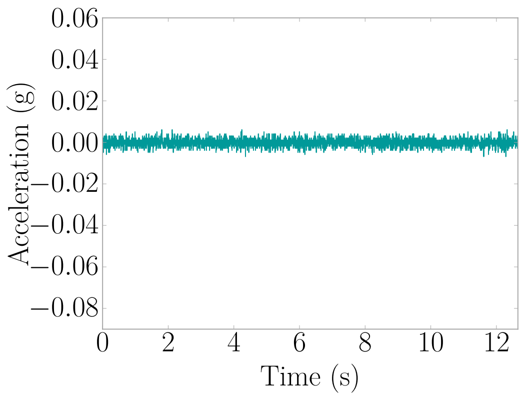

(a) Category 1 - Little to No Data

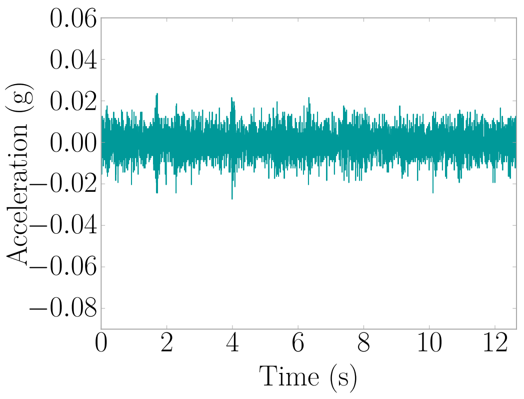

(b) Category 2 - Indistinct Peaks

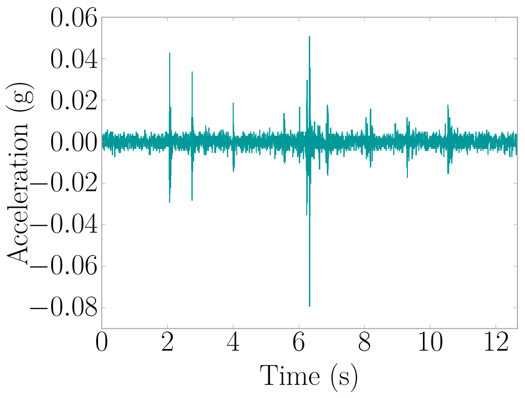

(c) Category 3 - Distinct Peaks

Figure 4.3: Signal Category Examples

for 100 times changing the pseudo-random number generator state each iteration from 0-99. The effectiveness of all possible combinations of A_{max}, RoD, and DR (see Section 4.2) were evaluated. The accuracy stats of each combination for the linear kernel is presented in Table 4.2, and RBF kernel is presented in Table 4.3. The other two kernels are presented in Table D.1 and Table E.1.

The RBF performed better than the linear, and in two cases ($\mathrm{A_{max}}$; $\mathrm{A_{max}}$, RoD) significantly better by about 10%. RoD provided the lowest performance by having the lowest mean accuracy and highest standard deviation of all the combinations. The best metric combinations included DR as it had the highest mean accuracy and lowest standard deviations.

Table 4.2: SVM Linear Kernel Metric Combination Stats (100 Trials)

	Accuracy (%)	
Metric Combinations	Mean	St. Dev.
A_{max}	83.9	5.6
RoD	80.0	6.3
DR	95.7	3.3
A_{max}, RoD	84.0	5.6
RoD, DR	95.7	3.3
A_{max}, DR	95.7	3.2
A_{max}, RoD, DR	95.7	3.2

Table 4.3: SVM RBF Kernel Metric Combination Stats (100 Trials)

	Accuracy (%)	
Metric Combinations	Mean	St. Dev.
A_{max}	94.3	3.9
RoD	83.8	5.6
DR	96.4	3.3
A_{max}, RoD	94.7	3.9
RoD, DR	96.4	3.3
A_{max}, DR	96.8	3.4
A_{max}, RoD, DR	96.8	3.4

Figure 4.4 and Figure 4.5 offer insight into the distribution of scoring for the trials of the linear and RBF kernel, respectively; the other two kernels are presented in Figure D.2 for the polynomial and Figure E.1 for the sigmoid. Both kernels had a larger distribution of scores for metrics A_{max} and RoD, with the combination of there of tending towards a distribution like that of A_{max}. This phenomenon is also seen with the introduction of DR, the best performing metric, where combinations including DR tend to have score distributions, like that of DR alone.

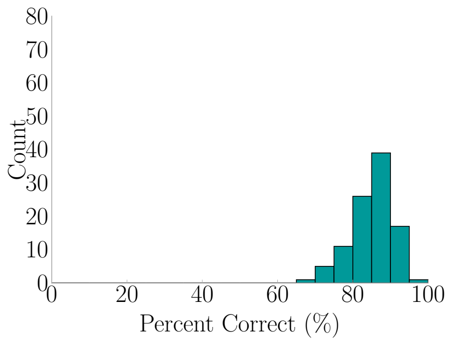

(a) A_{max}

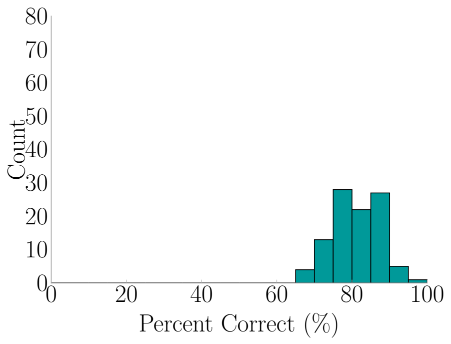

(b) RoD

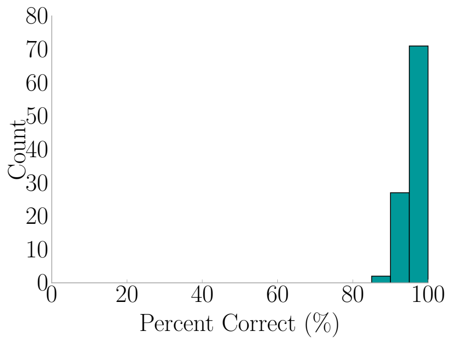

(c) DR

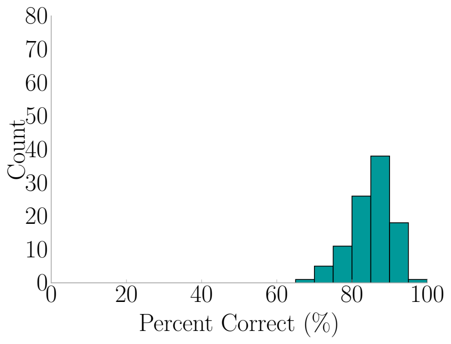

(d) A_{max} and RoD

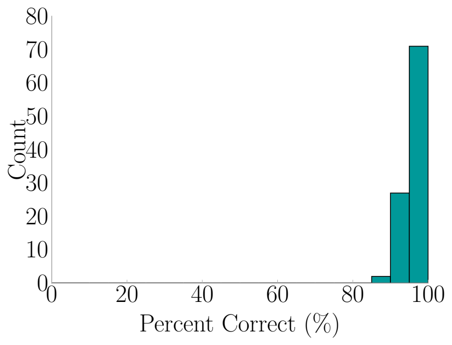

(e) RoD and DR

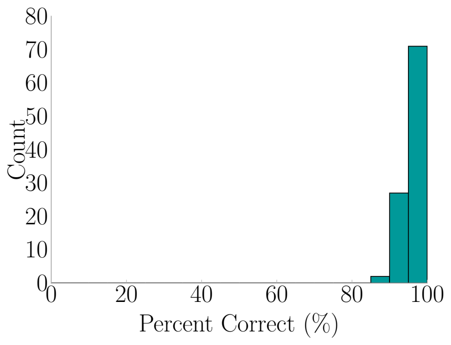

(f) A_{max} and DR

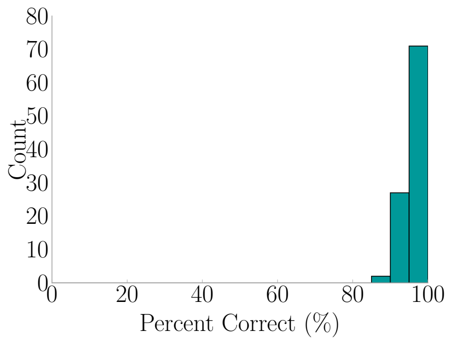

(g) A_{max}, RoD, and DR

Figure 4.4: Score Distribution for Linear Kernel Metric Combinations (100 Trials)

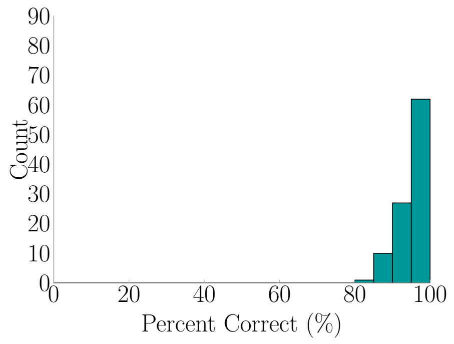

(a) A_{max}

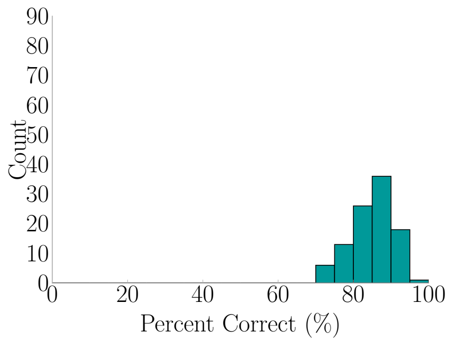

(b) RoD

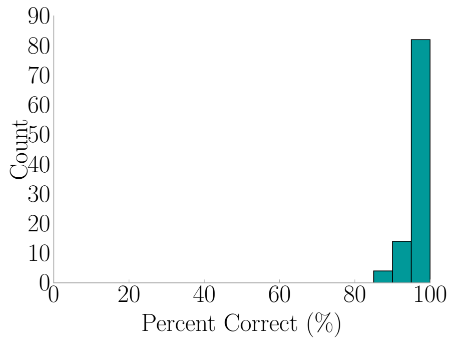

(c) DR

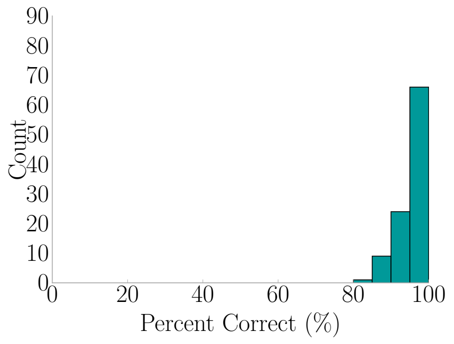

(d) A_{max} and RoD

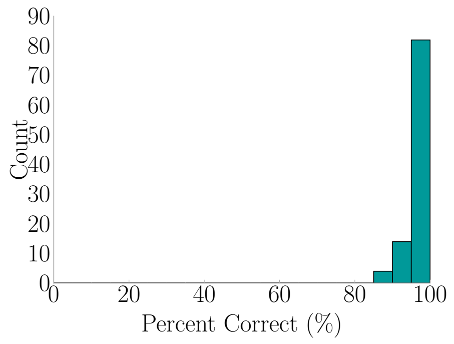

(e) RoD and DR

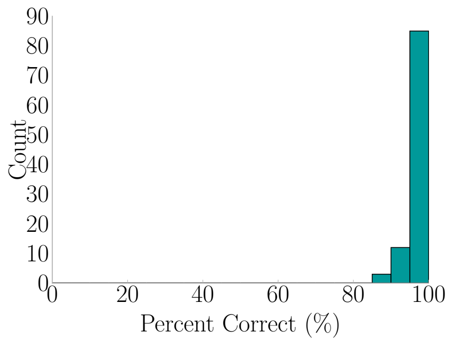

(f) A_{max} and DR

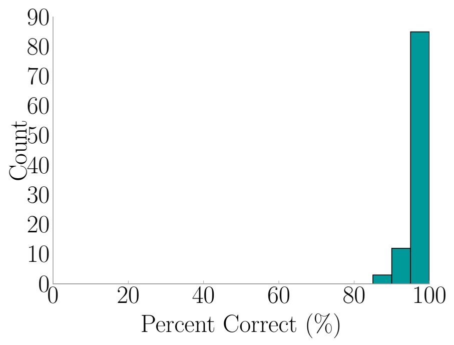

(g) A_{max}, RoD, and DR

Figure 4.5: Score Distribution for RBF Kernel Metric Combinations (100 Trials)

Figure 4.6 visually explores each metric, to aid in understanding category separation using the metrics. The diagonal bar plots show the distribution of categories with respect to a particular metric. As one looks from the first bar plot with A_{max} and on down to DR, groupings of values for each category can be seen. The scatter plots off the diagonal, display the relationship between each metric. RoD and DR, being derived from the same base function, show a near linear relationship; whereas comparing them with A_{max} shows a slight dispersion along a straight line.

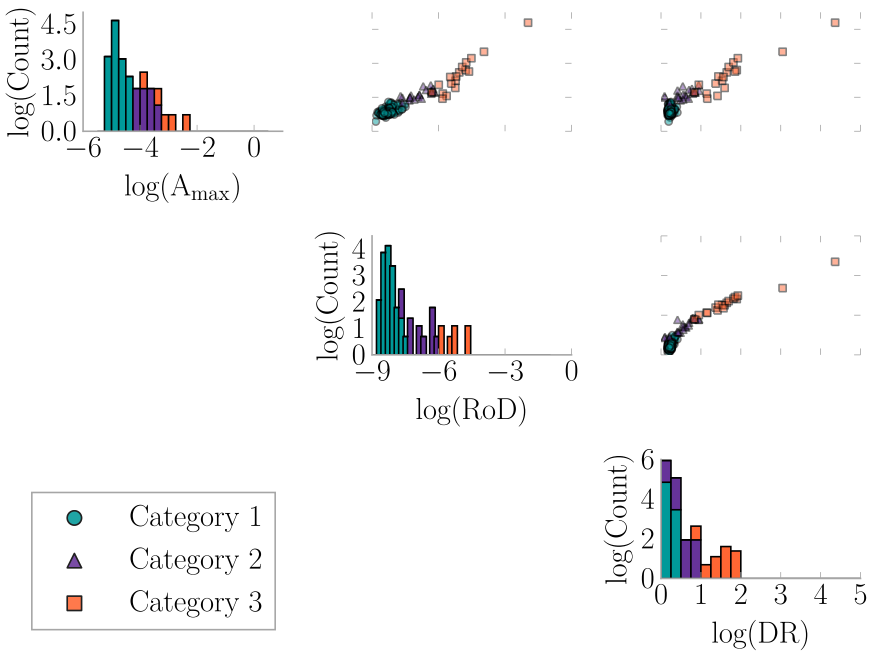

Figure 4.6: Metric Comparison of Manually Categorized Records

SVMs are sensitive to the category split among the training data. Thus, it is possible to have extremely high accuracy (97% and above) when classifying signals. The best combination for training data, being defined as training the SVM to reach the highest accuracy, is presented in Table 4.4 for the linear kernel and Table 4.5 for the RBF kernel. The other two kernels are presented in Table D.2 and Table E.2. Every combination achieved very high accuracy, with the results again pointing towards DR being the best metric, achieving 100% for every combination it is involved in.

Table 4.4: SVM Linear Kernel Best Training Set for Each Metric Combination

Metric Combinations	C1	C2	C3	Accuracy (%)
A_{max}	121	21	18	97.5
RoD	121	21	18	97.5
DR	129	18	13	100.0
A_{max}, RoD	121	21	18	97.5
RoD, DR	129	18	13	100.0
A_{max}, DR	129	18	13	100.0
A_{max}, RoD, DR	129	18	13	100.0

Table 4.5: SVM RBF Kernel Best Training Set for Each Metric Combination

Metric Combinations	C1	C2	C3	Accuracy (%)
A_{max}	121	21	18	100.0
RoD	121	21	18	97.5
DR	128	18	14	100.0
A_{max}, RoD	121	21	18	100.0
RoD, DR	128	18	14	100.0
A_{max}, DR	128	18	14	100.0
A_{max}, RoD, DR	128	18	14	100.0

Table 4.6 and Table 4.7 display the worst scoring category split observed during the trials for the linear and RBF kernels, respectively. The remaining two kernels are presented in Table D.3 and Table E.3. From these results, one can further see the robustness of each metric for the SVM to better determine the hyperplanes between categories.

Table 4.6: SVM Linear Kernel Worst Training Set for Each Metric Combination

Metric Combinations	C1	C2	C3	Accuracy (%)
A_{max}	134	11	15	67.5
RoD	134	15	11	65.0
DR	131	15	14	87.5
A_{max}, RoD	134	11	15	67.5
RoD, DR	131	15	14	87.5
A_{max}, DR	131	15	14	87.5
A_{max}, RoD, DR	131	15	14	87.5

Table 4.7: SVM RBF Kernel Worst Training Set for Each Metric Combination

Metric Combinations	C1	C2	C3	Accuracy (%)
A_{max}	132	16	12	82.5
RoD	134	11	15	70.0
DR	132	16	12	85.0
A_{max}, RoD	132	16	12	82.5
RoD, DR	132	16	12	85.0
A_{max}, DR	127	17	16	85.0
A_{max}, RoD, DR	127	17	16	85.0

The following two figures are provided as an example of how the hyperplanes formed for the linear and RBF kernels. Both kernels perform well in finding regions that indicate a category, with only a few manually categorized signals crossing the hyperplane into another category's region.

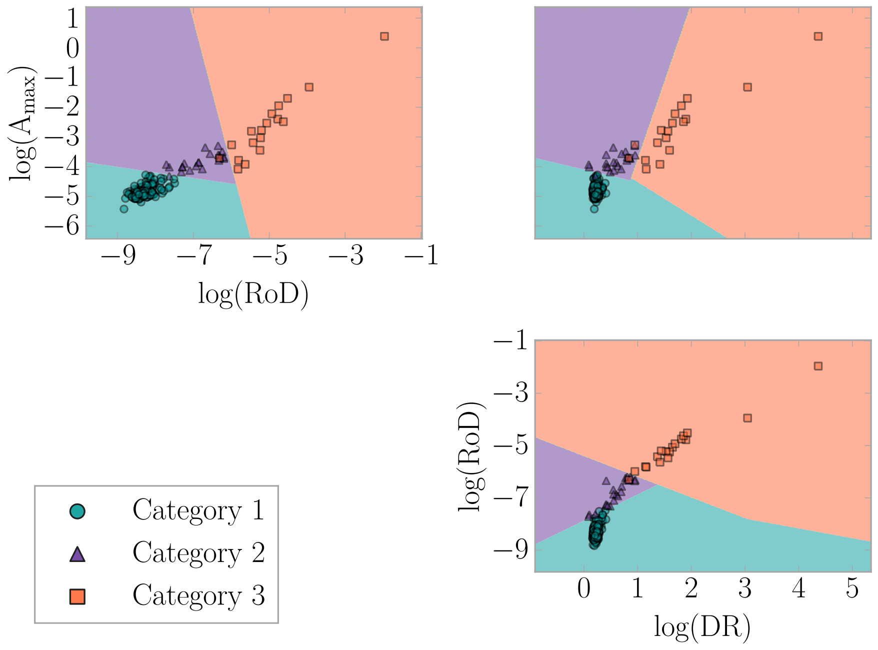

Figure 4.7: SVM Linear Kernel Metric Combination Hyperplanes

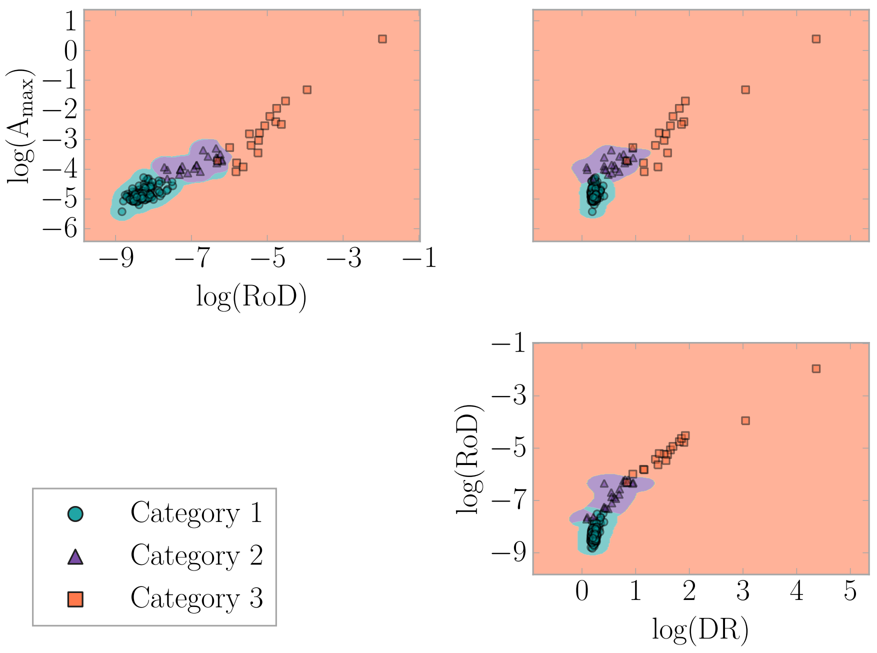

Figure 4.8: SVM RBF Kernel Metric Combination Hyperplanes

4.5 Conclusion

At the time of this writing, the SVM, using the DR metric, has worked through all 536,686 acceleration records much faster than if the same records were processed manually. Preprocessing removed 273,422 records that were missing data points or were identified as sensor malfunctions. This leaves 203,964 records in category one; 33,972 in category two; 25,321 in category three; and 7 records ignored as the value of DR was infinity indicating a signal containing all the same value, something that could also be filtered out in preprocessing in the future. Examples of SVM classified signals are seen in Figure 4.9. Relatively few manually classified training samples are required for the SVM to learn from, making this a very time-efficient method not requiring much user input. In the case of this study, only 200 signals were used for training - a mere 0.04% of the entire dataset.

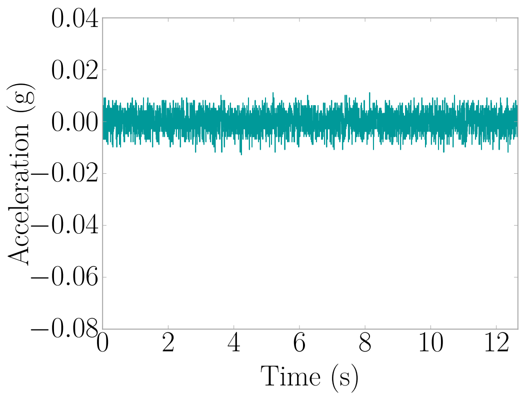

(a) Category 1 - Little to No Data

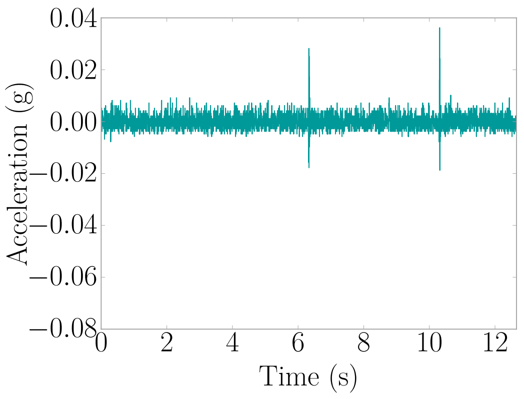

(b) Category 2 - Indistinct Shape

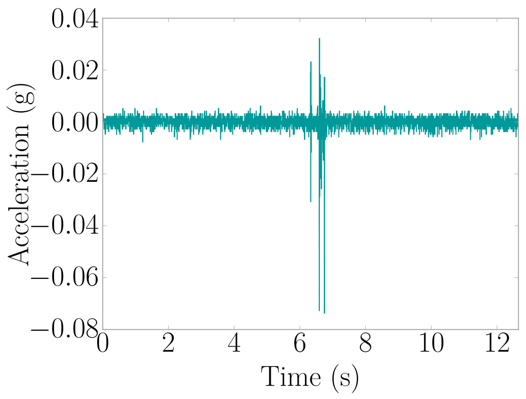

(c) Category 3 - Distinct Peaks

Figure 4.9: SVM Classified Signal Category Examples

The following metric comparison plot in Figure 4.10 shows the breakdown of SVM classified categories when the RBF kernel was trained using DR only, as this setup is considered optimal based on accuracy score, standard deviation, and number of metrics in a combination. The results are interesting in that one can see a more distinct separation of categories classified for DR, whereas the other categories have significant overlap.

Of interest to the author is the ability of the SVM to filter out signals with lots of environmental noise in a human fall detection application while retaining signals with possible fall events in them. Figure 4.11 takes the fall signals that have been identified in the database during the VAMC hospital study (see Appendix A) and

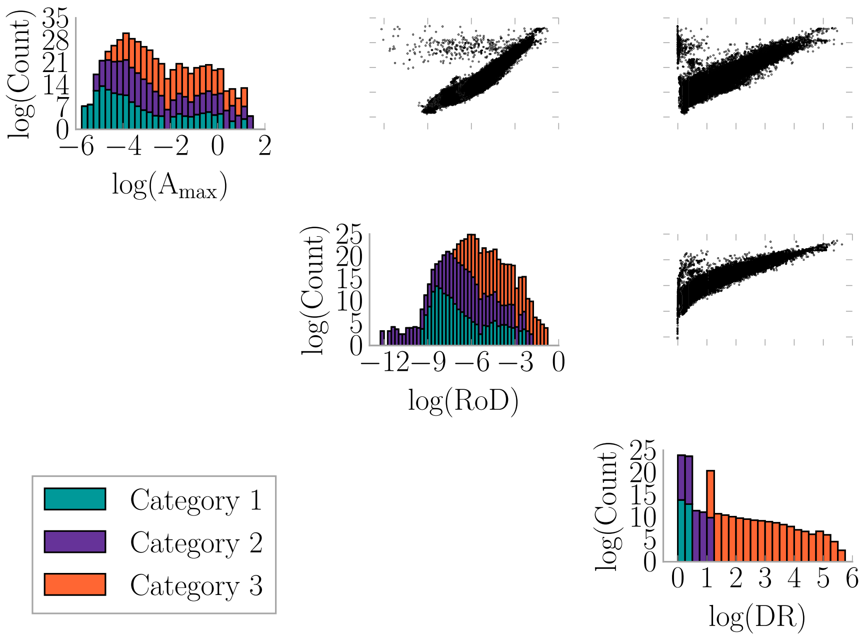

Figure 4.10: Metric Comparison of SVM Classified Records Where DR Was Used for Training

indicates what the SVM classified each signal from the sensors in the system that observed the event verse what the author categorized the signal to be. A more detailed breakdown is available in Table F.1 for this data with figures indicated in the table for easy reference. Note that signals marked as environmental noise by the author are not included in the bar graph but are included in the table. A few sensor's signals that researchers have visually identified as having fall data where ignored during preprocessing as they had missing a few data points, and preprocessing was set to strictly ignore signals missing data points. The effectiveness of the SVM could still be high if this rule was relaxed some, something to be explored in future work. In all other cases, fall signals were identified in either category two or three with only one signal being classified as category one, closely matching that of the manually designated categories. The SVM results demonstrate a desirable outcome for a fall detection application.

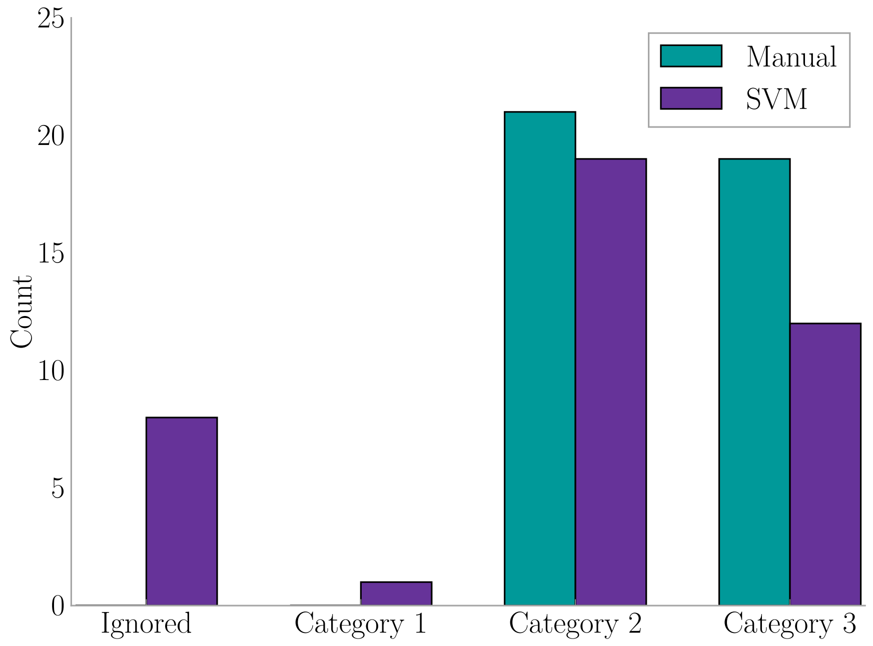

Figure 4.11: Recorded Fall Events Manual Vs. SVM Categories

Support Vector Machines appear to be effective and viable approach to sorting through massive amounts of data generated from a vibration monitoring system given metrics that are descriptive of the signals being classified. RoD was the worst performing metric explored, having low mean accuracy for both linear and RBF kernels. A_{max} was the second best performing metric in this study as higher amplitude signals typically indicated real data in our study. Ultimately DR came out to be the most robust and effective metric in this study. Combining metrics together can produce a slight increase in the overall accuracy.

Part of having an effective SVM, is to choose the right kernel using the right metrics for the application. Being a new approach, the research explored four kernels to find that the radial basis function performed the best not only in robustness (defined as having high mean accuracy and low standard deviation over 100 trials), but also in having extremely high accuracy possible using each metric with a specific training set.

Chapter 5
The FEEL Algorithm

5.1 Introduction

An important part for treatment and rescue pertaining to fall detection is estimating the magnitude of the impact and its location within the structure. Doctors could utilize the force information to determine the severity of injuries and take appropriate action to prevent further exacerbation. Diagnosis and treatment of injuries thus have the potential to be quicker with the impact's force magnitude. Rescuers can use the impact location information to more quickly find the fallen person, a useful tool particularly when the fallen cannot yell for help. In addition, the force estimate can also be used to differentiate between a person falling and objects being dropped.

The challenges of current state-of-the-art fall detection algorithms using structural vibrations (discussed in Section 1.2) stem from the estimation of properties that vary by structure (e.g. energy methods use structural damping estimations). Even with ample experimentation and modeling of a structural system, the physical properties, such as stiffness and damping, are still challenging to obtain. Thus, an algorithm using floor vibrations should intrinsically embed within itself the attributes of any structure.

5.2 Force Estimation and Event Localization (FEEL) Algorithm

The FEEL Algorithm was designed to intrinsically embed structural properties into transfer function estimates between calibrated locations and sensors. Forces and the dynamic response of the structure are related during the calibration process, which eliminates challenges with distance between a sensor and an impact's location assuming the response is measurable. Time synchronization of sensors can be difficult, thus FEEL was designed to not require it. The algorithm becomes more easily scalable because of this. Scalability also brings with it greater robustness as more sensors can be added to the mix to provide more information. A minimum of two sensors are required to apply FEEL due to the pair matching method for estimating the location and force of impact. FEEL has been implemented as the Python package *feel* with documentation being provided in Appendix N and has been filed as U.S. Patent Application No. 62/324,468 [35]. The process diagram for navigating the algorithm's operation is shown in Figure 5.1, with more detail on each step provided in the following sections.

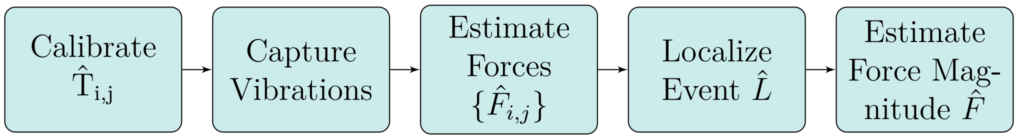
Calibrate $\hat{\mathrm{T}}_{\mathrm{i,j}}$
Capture Vibrations
Estimate Forces $\{\hat{F}_{i,j}\}$
Localize Event $\hat{L}$
Estimate Force Magnitude $\hat{F}$

Figure 5.1: FEEL Algorithm Process Diagram

5.2.1 Calibration

The FEEL Algorithm works by first dynamically characterizing the structure. Calibration yields transfer functions between forces at plausible fall locations and accelerations at the sensor locations. Force records obtained from an impulse hammer and the resulting floor vibrations are recorded for use in the transfer function estimate presented in Equation 5.1

$$\hat{\mathrm{T}}(f) = \frac{\mathrm{T}_{xy}(f) + \mathrm{T}_{yx}(f)}{2} \tag{5.1}$$

where

$$\mathrm{T}_{xy}(f) = \frac{\mathrm{P}_{xy}(f)}{\mathrm{P}_{xx}(f)} \tag{5.2}$$

$$\mathrm{T}_{yx}(f) = \frac{\mathrm{P}_{yy}(f)}{\mathrm{P}_{yx}(f)} \tag{5.3}$$

x is input (force), y is output (accelerations), $\mathrm{P}_{xy}(f)$ is the cross power spectral density of x to y, $\mathrm{P}_{xx}(f)$ is the power spectral density of x, $\mathrm{P}_{yy}(f)$ is the power spectral density of y, and $\mathrm{P}_{yx}(f)$ is the cross power spectral density of y to x [36, 37]. The averaging of $\mathrm{T}_{xy}(f)$ and $\mathrm{T}_{yx}(f)$ reduces the amount of noise and measurement error present in the transfer function estimate.

5.2.2 Force Estimation

To estimate the force, one takes the acceleration signal S and applies the $\hat{\mathrm{T}}(f)$ for the each location of impact as seen in the following

$$[I_{i,j}] = \frac{\mathrm{FFT}(S)}{\left[\hat{\mathrm{T}}_{i,j}(f)\right]} \tag{5.4}$$

$$\left[\hat{F}_{i,j}\right] = \mathrm{IFFT}\left([I_{i,j}]\right) \tag{5.5}$$

where FFT() is the Fast Fourier Transform, IFFT() is the Inverse Fast Fourier Transform, $\left[\hat{F}_{i,j}\right]$ is the force estimation matrix, i is the location, and j is the sensor.

5.2.3 Event Localization

The location of events in other disciplines has traditionally been treated as a ‘time of flight’ problem. Sensors are time synchronized and the difference between the arrival of a wave is used for localization [38, 39]. This technique has proven successful in other areas of engineering but has significant challenges. In particular, the sensors need to be synchronized and the wave speed needs to be known. This would increase the complexity of the sensing system, and ultimately the potential cost of production. Therefore, the author aimed at developing a method that does not depend on time. The method compares force estimates for different locations using data from different sensors. The location that estimates the same force, likely corresponds to the location of impact.

The FEEL Algorithm event localization requires at least two sensors. The author attempted many methods to compare the force estimates and found the use of the Correlated Force Estimates Method to be the most robust due to its redundancy, with reliability increasing with the more sensors used. Other techniques explored during the development of the FEEL Algorithm are presented in Appendix G.

Correlated Force Estimates Method

The method begins by determining the window of the force estimation to consider based on the maximum amplitude within the acceleration window. Alternatively, one could use a threshold crossing method to choose a window within the force estimate, like taking the time where the signal first crosses out of a 'noise' level previously defined.

Symmetrical or asymmetrical windows may be used. The windows may also be taken on a per sensor basis, by choosing one sensor as a reference and using its window for all the sensors, or any combination thereof. The author suggests using a symmetrical window and using one sensor as a reference. This is due to the fact that the FEEL Algorithm is time-independent, meaning the force estimates at each sensor will show peaks at the same time across all estimates, and the method is based on the shape of the peak in the force estimates, making a symmetrical window ideal for capturing the similarity of symmetrical peaks. The force estimates do usually maintain a similar shape at the location of impact, which lends localization towards this method.

After portions of each force estimate are selected, the normalized correlation coefficient matrix is formed using only the real portion of the force estimate like in Equation 5.6

$$\{L_i\} = \max \begin{bmatrix} 0 & \rho_{xy}(\hat{F}_{i,1}(n), \hat{F}_{i,2}(n)) & \cdots & \rho_{xy}(\hat{F}_{i,1}(n), \hat{F}_{i,j}(n)) \\ & 0 & \cdots & \rho_{xy}(\hat{F}_{i,2}(n), \hat{F}_{i,j}(n)) \\ & & \ddots & \vdots \\ \text{sym.} & & & 0 \end{bmatrix} \tag{5.6}$$

where

$$\rho_{xy} = \frac{\text{COV}\,(x, y)}{\sqrt{\sigma_x \sigma_y}} \tag{5.7}$$

is the Pearson product-moment correlation coefficient, cov() is the covariance, σ is the standard deviation, x and y are vectors, $\{L_i\}$ is the vector of maximum normalized correlation coefficient for each location i, max() is the maximum value function, $\hat{F}_{i,j}$ is the force estimation of the i-th location at the j-th sensor, and n is the number of points in the window [21, 40].

The normalized correlation coefficients are then compared by location with the largest value being the location of impact as in Equation 5.8 where $\hat{L}$ is the highest correlation coefficient, and max() is the maximum value function.

$$\hat{L} = \max(\{L_i\}) \tag{5.8}$$

The advantage of this approach stems from the pair matching in the correlation matrix. Each force estimate is compared to the other, providing redundancy when more sensors and consequently, more force estimates are available. There may be times when very poor force estimates appear, so by taking the best pair of estimates (i.e. the pair having the highest correlation value), error in locating the impact reduce greatly. Furthermore, the acceleration records do not have to be time-synchronized, reducing the complexity of the data acquisition system. The Correlated Force Estimates Method thus provided the more robust localization of the methods tested.

5.2.4 Force Magnitude Estimation

Once the location has been identified as in Section 5.2.3, the two closest matching pair of force vectors are used to estimate the force magnitude. The estimation of the force can be biased with a constant value in the acceleration measurements. Yet, the force magnitude estimate of the i-th location and j-th sensor can be estimated using

$$\hat{F}_{i,j} = \max\left(\{\hat{F}_{i,j}\}\right) - \min\left(\{\hat{F}_{i,j}\}\right) \tag{5.9}$$

where max() is the maximum value function, $\{\hat{F}_{i,j}\}$ is the real portion of the force estimation vector produced by Equation 5.5, and min() is the minimum value function. Figure 5.2 demonstrates a biased force estimation. Applying Equation 5.9, one can see the accuracy of the force magnitude estimate increases for the location and sensor.

The force magnitude for the specific acceleration event is taken to be the average of the two sensor's force estimation magnitudes whose force estimation vectors more closely match as seen in Equation 5.10

$$\hat{F} = \frac{\hat{F}_{i,1} + \hat{F}_{i,2}}{2} \tag{5.10}$$

where $\hat{F}_{i,1}$ and $\hat{F}_{i,2}$ are the two force estimate magnitudes who closely match relative to other pairings at the identified impact location i.

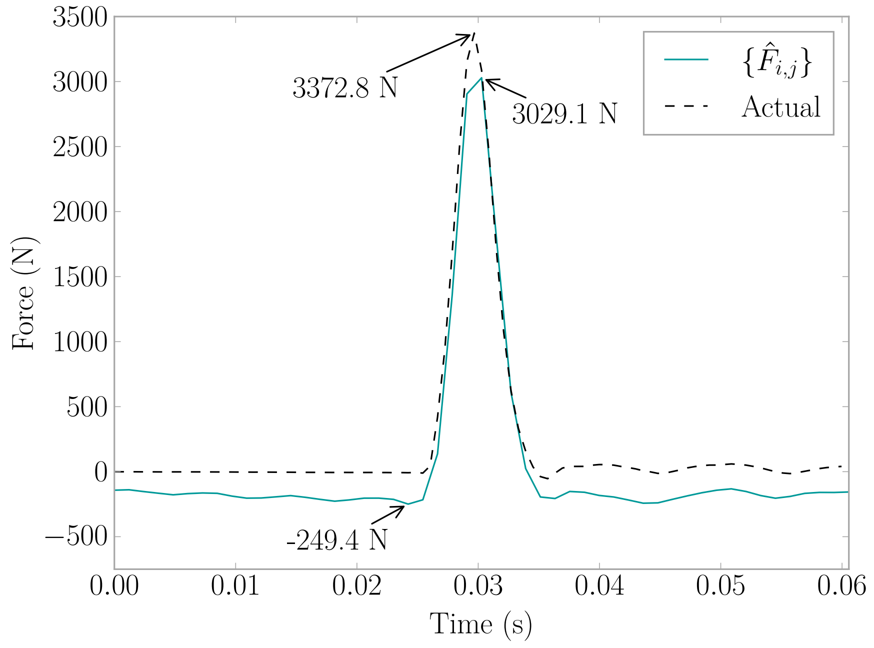

Figure 5.2: Biased Force Estimate Example

5.3 Low-Pass Finite Impulse Response Filter Design and Fourier Method Resampling

Sometimes, before processing signals, it is desirable to apply a low-pass filter to reduce noise from high frequencies and prevent aliasing in the signal during resampling [41]. A low-pass Finite Impulse Response (FIR) filter was thus designed using the window method for use in processing acceleration signals before applying FEEL [42, 43]. The Kaiser Window Function was used to apply the filter [44] with a beta value of 16.67 and window order of 8682. Figure 5.3 displays the frequency response of the filter having a transition band of 10 Hz, a stop band attenuation of 160 dB, a cutoff frequency of 208 Hz, and based on a signal sampling rate of 2049 Hz.

Resampling was performed using the Fourier Method to reduce sampling rates to

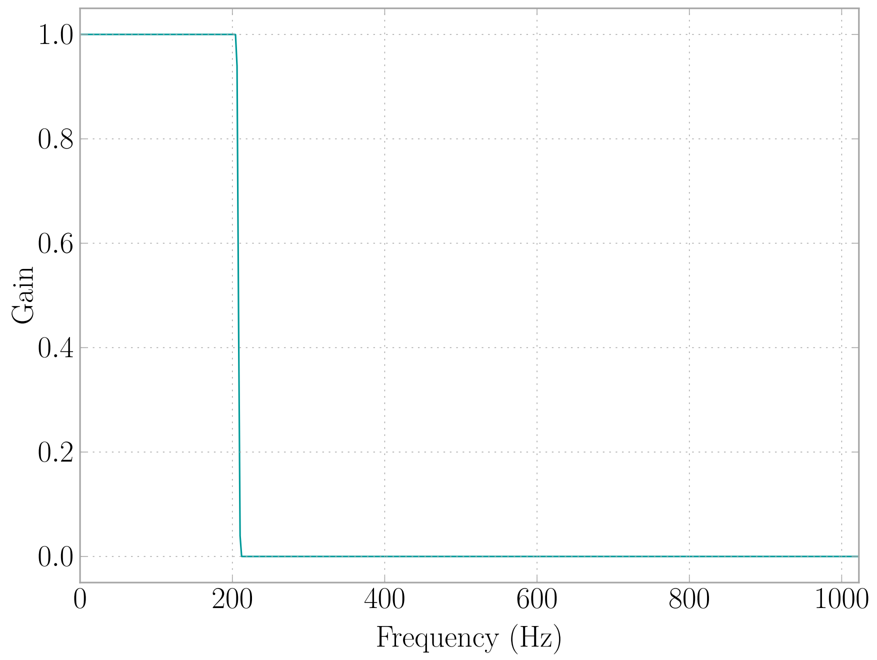

Figure 5.3: Low-Pass FIR Filter Frequency Response

400 Hz after the filter was applied to the data [21, 45]. A signal delay was calculated using Equation 5.11 where N is the number of coefficients in the filter, d is the number of data points in the delay, FS_{new} is the new sampling rate, and FS_{old} is the original sample rate of the signal [21].

$$d = \left(\frac{N-1}{2}\right)\left(\frac{FS_{new}}{FS_{old}}\right) \tag{5.11}$$

The above signal delay equations give the number of samples the filtering process have been affected by the filter's initial conditions, and it is suggested to round the values if a whole number is not produced from the equations. To get the amount of time the signal delay equates to, use Equation 5.12 where d is the signal delay calculated in Equation 5.11.

$$\Delta t = \frac{d}{FS_{new}} \tag{5.12}$$

The filter and resampling mentioned here are both provided in the *feel* Python package for convenient use. See Appendix N for more details.

5.4 Verification Experiments

The FEEL Algorithm was tested on a small scale steel structure at the Structural Dynamics and Intelligent Infrastructure Laboratory (SDII) at the University of South Carolina (USC) in two trials. The structure is shown in Figure 5.4 and was built using 3.18 cm (1.25 in) outer diameter, 0.478 cm (0.188 in) wall DOM cold-rolled tube steel as the beams and 2.54 cm (1 in) NC 2C threaded rods to connect the beams to the 6.35 cm (2.5 in) cubic 1018 cold-rolled bar. The tubes and cubes were thread in an 20.32 cm (8 in) pitch. The structure is suspended on steel supports and allowed to rotate around the horizontal axis using mounted bearings. Even though the dynamic characteristics of the structure do not match those of a residential dwelling, the objective of the tests described here is to verify if the algorithm would work before moving to a full scale structure. Three PCB Piezotronics 333B50 accelerometers with a sensitivity of 1000 mV/g were attached to the structure using magnetic mounts at nodes 8, 9, and 12. A 2.22 N (0.5 lb) PCB Piezotronics Impulse Force Hammer having a sensitivity of 2.33 mV/N (10.35 mV/lb) was used to excite the structure,. Data was collected at a rate of 2049 Hz, filtered using a FIR, and downsampled to 400 Hz as in Section 5.3. The lower rate was chosen in order to model a more realistic scenario.

5.4.1 Preliminary Trial

The first trial served to indicate the viability of the FEEL Algorithm. Transfer functions were calculated using the method outlined in Section 5.2.1 at node 7 (Figure 5.5) and node 10 (Figure 5.6) for all three sensors using a n_{fft} value of 2048 and a n_{overlap} value of 1024. The data used for the transfer functions was captured in one continuous record containing forces and accelerations. Five impacts were performed,

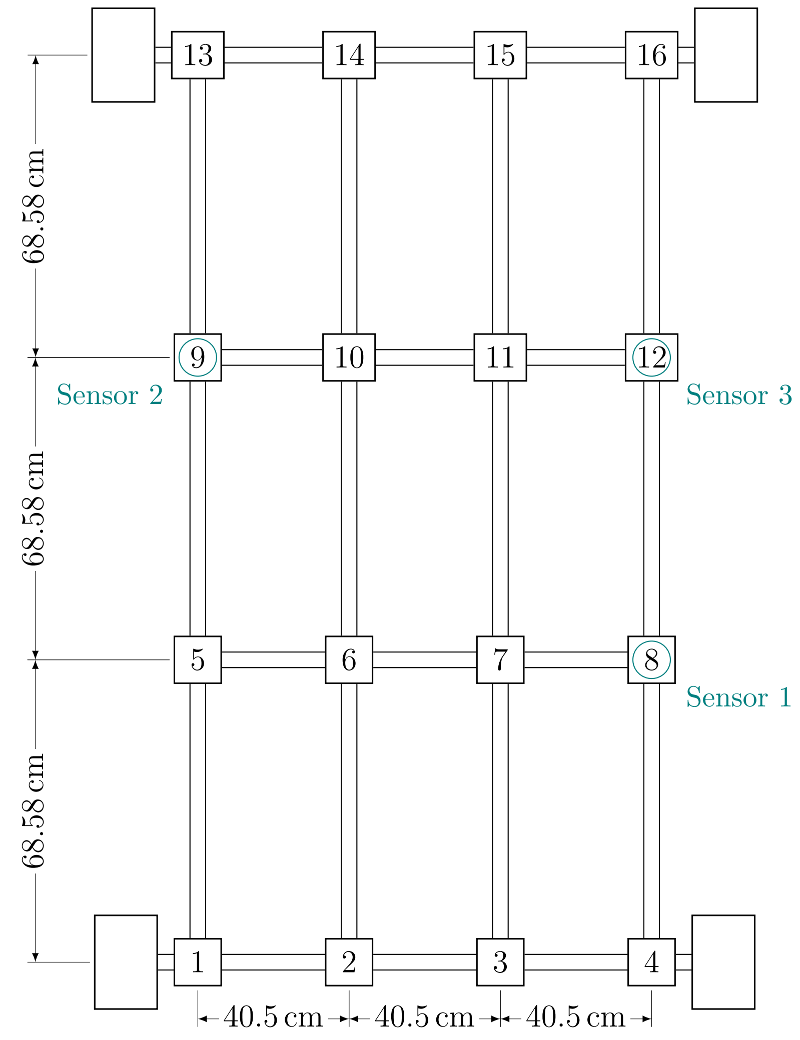

Figure 5.4: Steel Test Frame Layout

with the structure being allowed to return to rest after each hammer hit.

The transfer functions were then used to estimate the force of impact using the method in Section 5.2.2. Figure 5.7 displays the node 7 impact results, and Figure 5.8 displays the node 10 impact results. The force estimations for both impacts were used to identify the location of an impact based on the Correlated Force Estimates Method in Section 5.2.3. The location results for node 7's impact are displayed in Figure 5.9, and node 10's impact displayed in Figure 5.10. The correct location is highlighted in orange. The force magnitude was calculated as in Section 5.2.4 and results displayed in Table 5.1. FEEL was successful in identifying the location and force of the impacts.

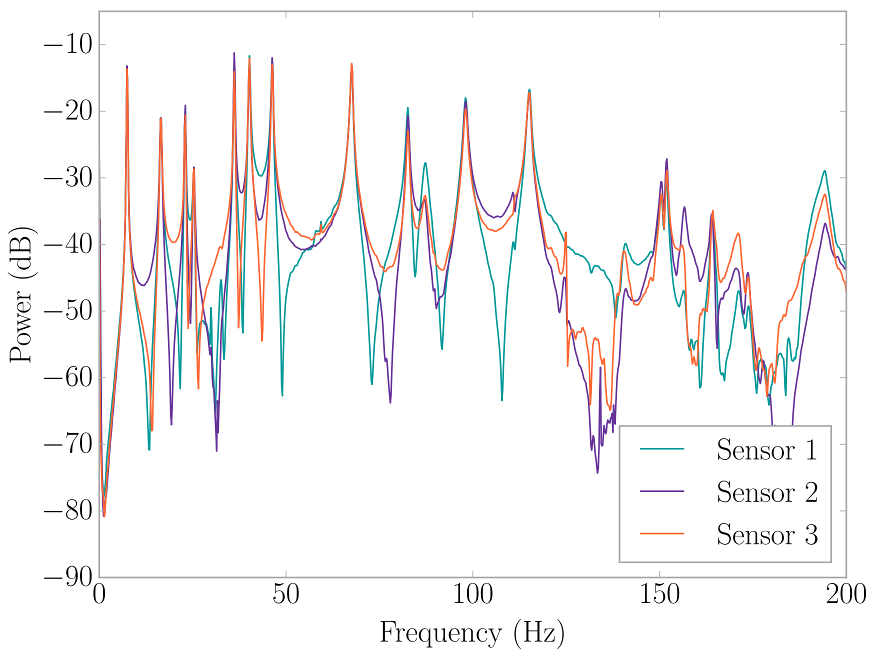

Figure 5.5: $\hat{\mathrm{T}}_{7,\mathrm{j}}$ for j From 1 to 3

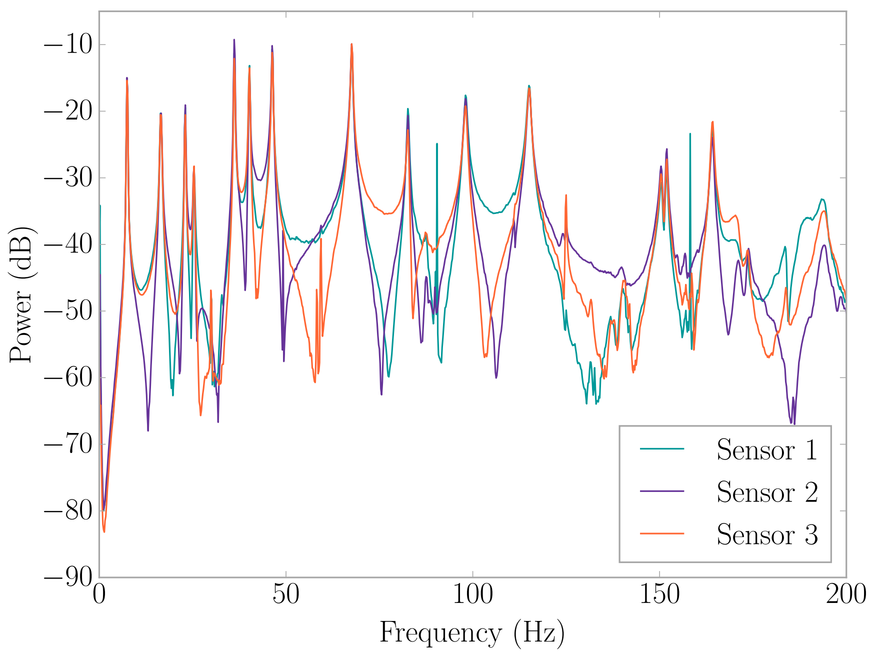

Figure 5.6: $\hat{\mathrm{T}}_{10,\mathrm{j}}$ for j From 1 to 3

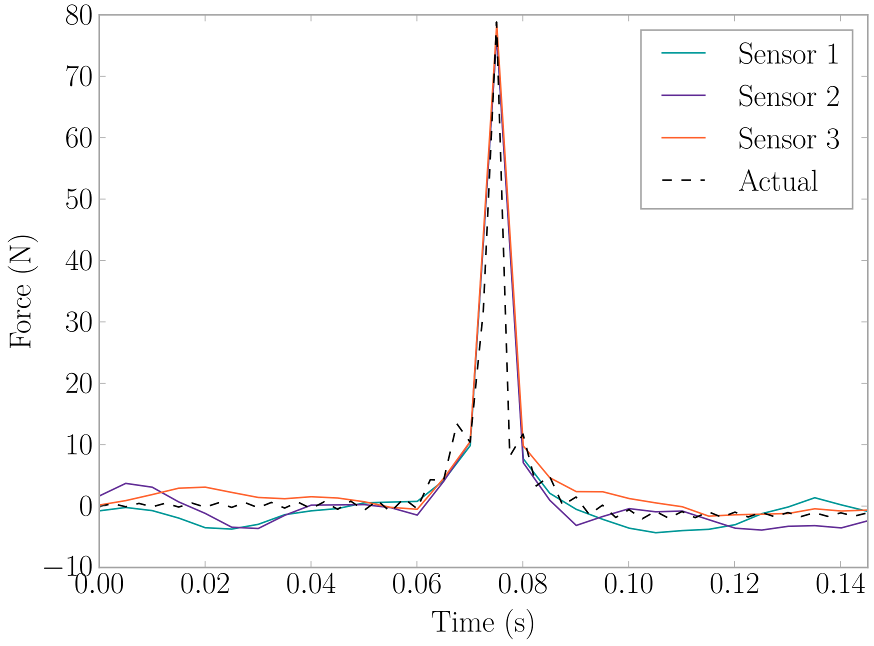

(a) $\hat{F}_{7,j}$

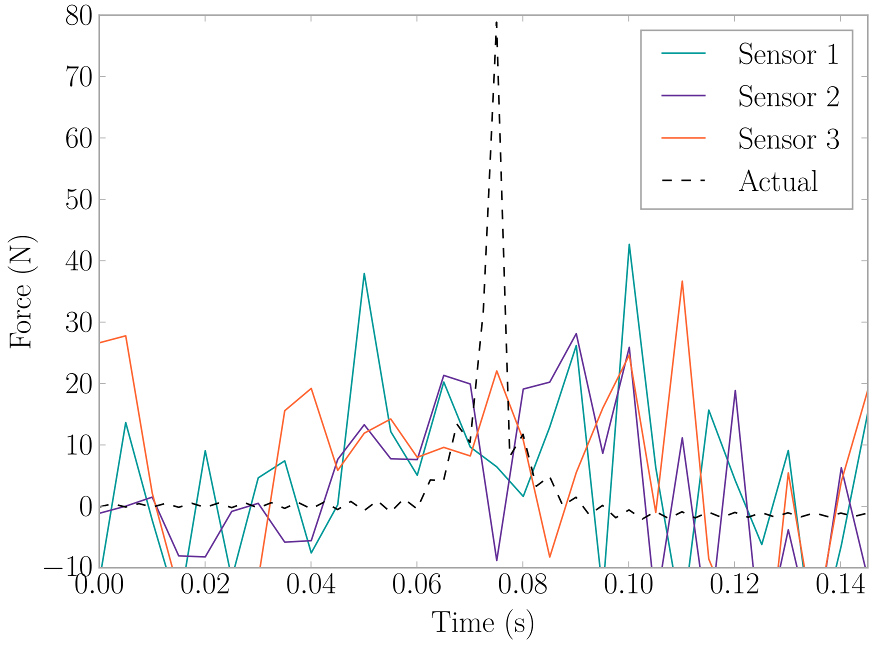

(b) $\hat{F}_{10,j}$

Figure 5.7: Force Estimations for an Impact on Node 7

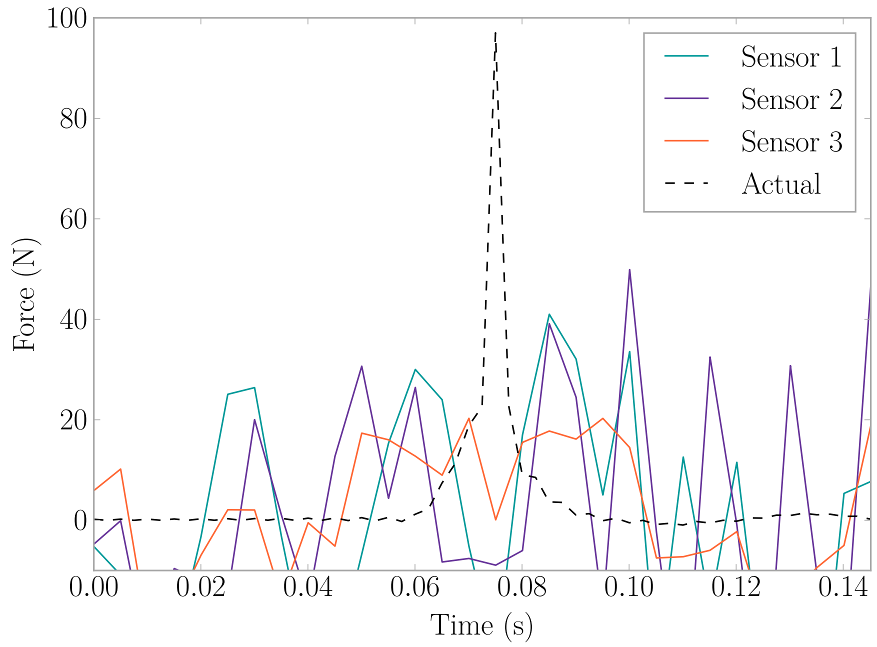

(a) $\hat{F}_{7,j}$

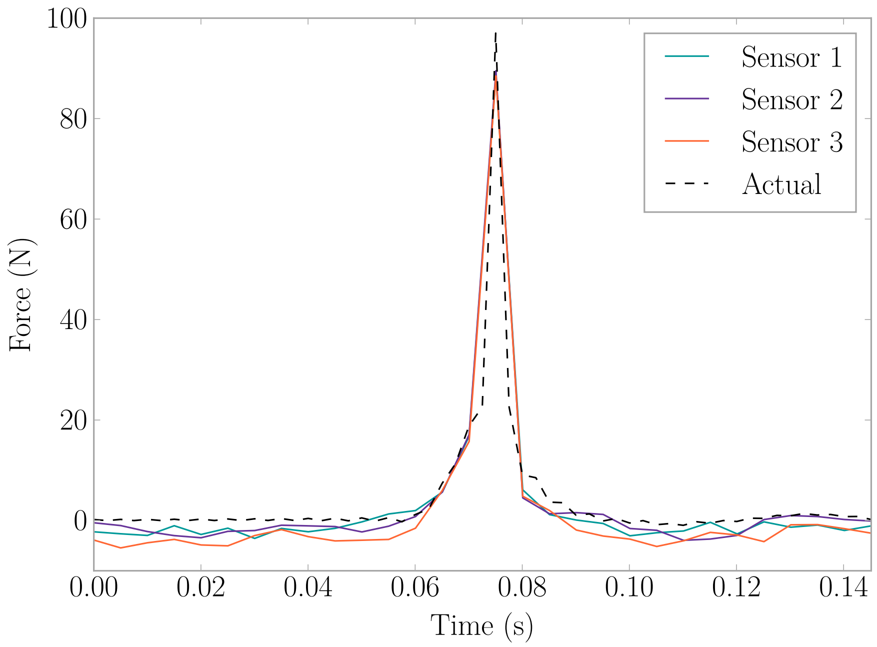

(b) $\hat{F}_{10,j}$

Figure 5.8: Force Estimations for an Impact on Node 10

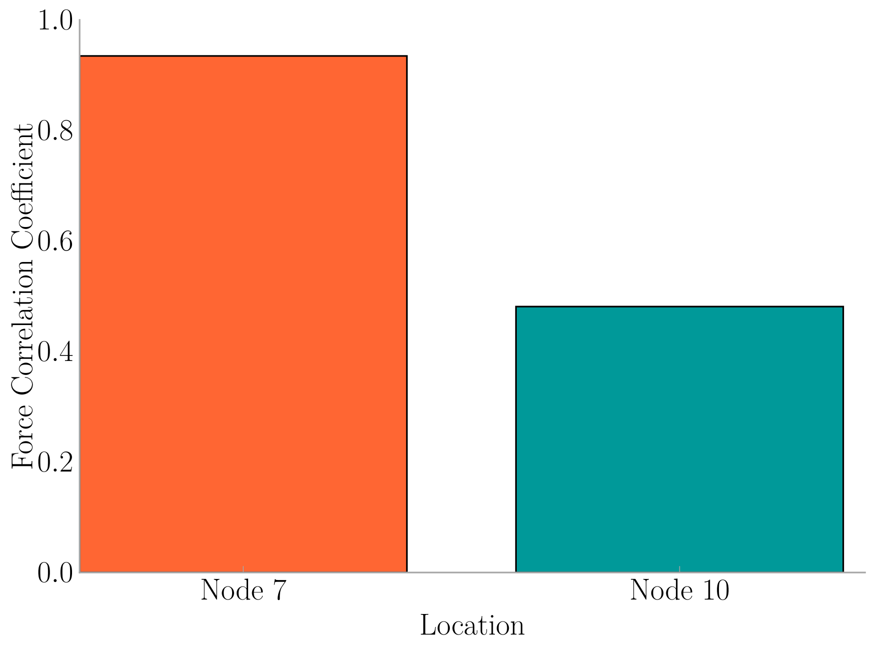

Figure 5.9: L_i for an Impact on Node 7

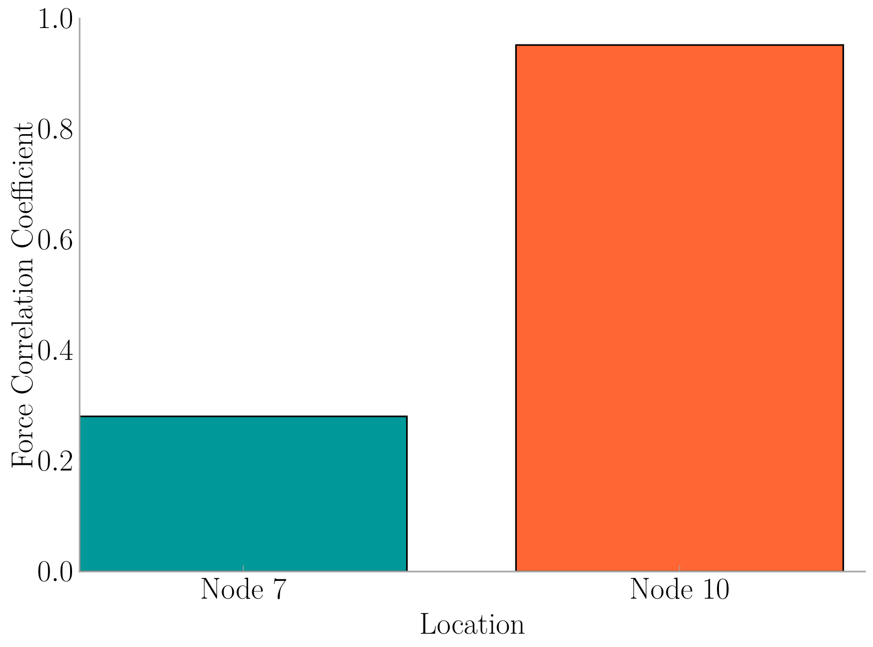

Figure 5.10: L_i for an Impact on Node 10

Table 5.1: Steel Frame Preliminary Trial Force Magnitude Estimate Results

Impact	Actual (N)	$\hat{F}$ (N)
Node 7	78.8	80.0
Node 10	97.0	91.7

5.4.2 Trial Using Eight Locations

The FEEL Algorithm was applied, when impacts were exerted, to 8 of the 16 nodes present on the steel frame in Figure 5.4. Nodes 1, 4, 5, 8, 9, 12, 13, and 16 were not taken into consideration as they were assumed to be under a wall. Each of the remaining nodes was excited 20 times using the impulse force hammer, with 10 records being used to generate transfer functions. Each hit was stored as a record containing 10 s of data from the time of impact. The rest of the procedure progressed as in Section 5.4.1. Transfer functions are presented in Figure 5.11. Note that the transfer functions from Node 7 and Node 10 look different that those from the steel frame preliminary trial of Section 5.4.1. This is due to the different techniques for combining data for the generation of each transfer function. Here, the transfer functions were generated using several records spliced together (one for each impact), whereas in the preliminary trial, the record was continuous.

An impact on node 2 is presented as an sample of this trial. Figure 5.12 shows the force estimates for all locations, and Figure 5.13 shows the force correlations by location with the identified location being highlighted in orange. The methodology was successful in estimating the location of impact as well as the force. The remaining impacts may be found in Appendix H, and a summary of results is provided in Table 5.2.

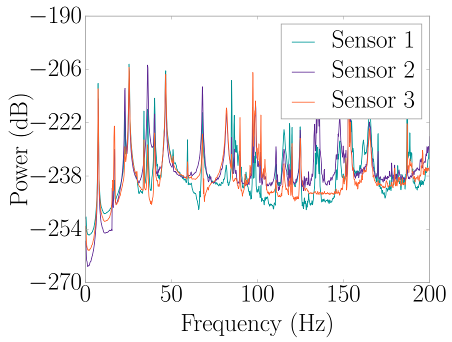

(a) $\hat{\mathrm{T}}_{14,j}$

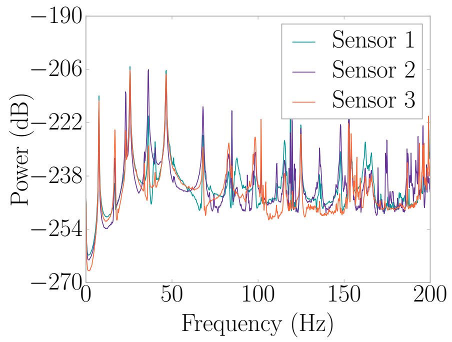

(b) $\hat{\mathrm{T}}_{15,j}$

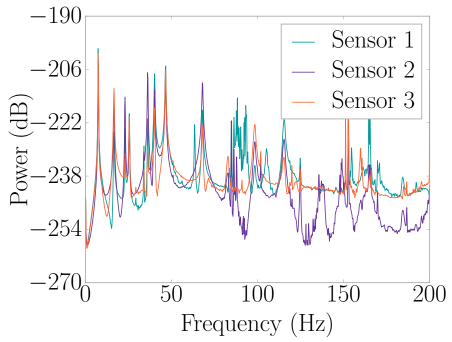

(c) $\hat{\mathrm{T}}_{10,j}$

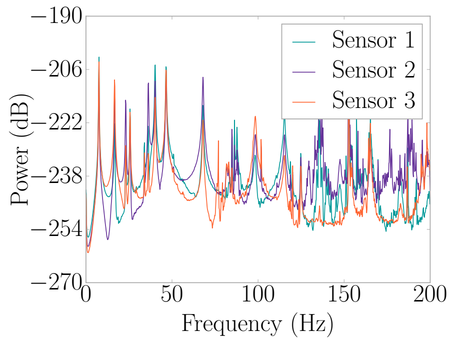

(d) $\hat{\mathrm{T}}_{11,j}$

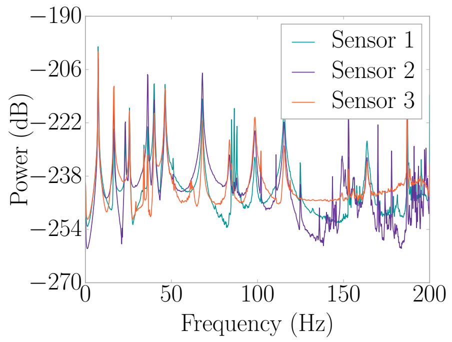

(e) $\hat{\mathrm{T}}_{6,j}$

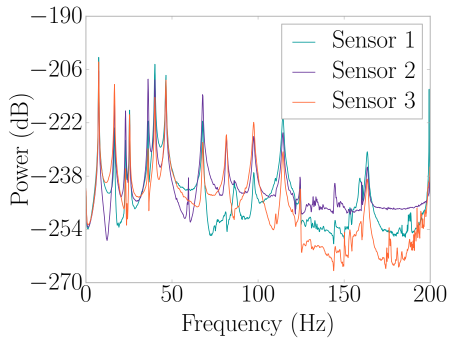

(f) $\hat{\mathrm{T}}_{7,j}$

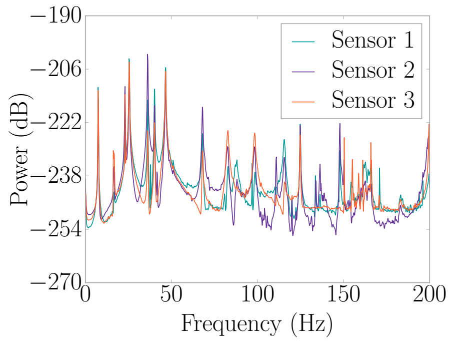

(g) $\hat{\mathrm{T}}_{2,j}$

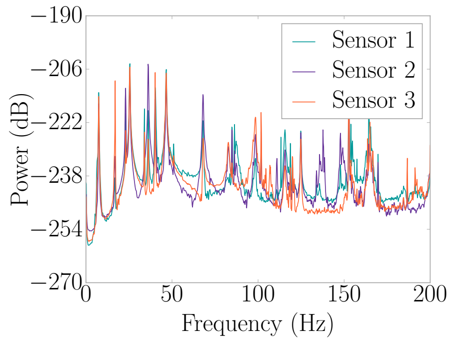

(h) $\hat{\mathrm{T}}_{3,j}$

Figure 5.11: Steel Frame Transfer Functions

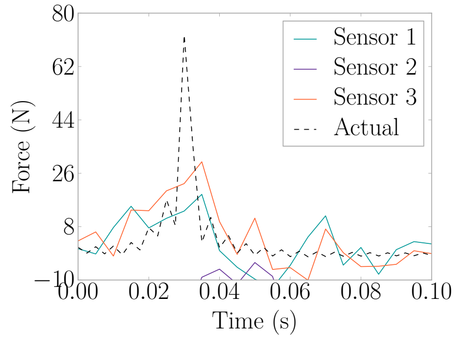
(a) $\hat{F}_{14,j}$

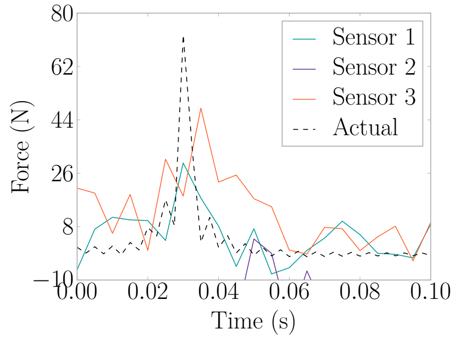
(b) $\hat{F}_{15,j}$

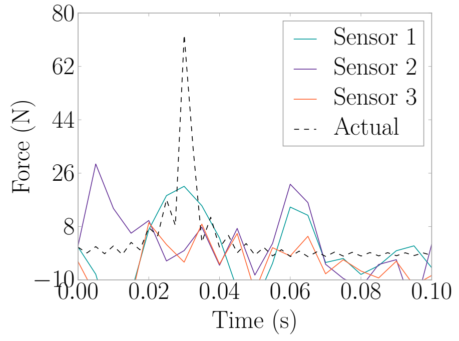
(c) $\hat{F}_{10,j}$

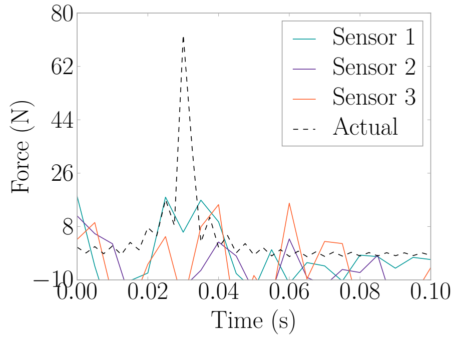
(d) $\hat{F}_{11,j}$

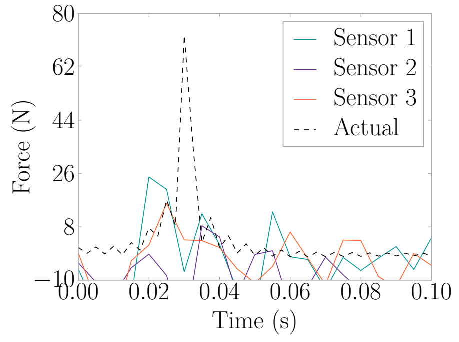
(e) $\hat{F}_{6,j}$

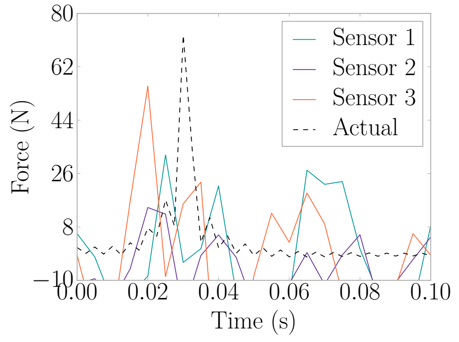
(f) $\hat{F}_{7,j}$

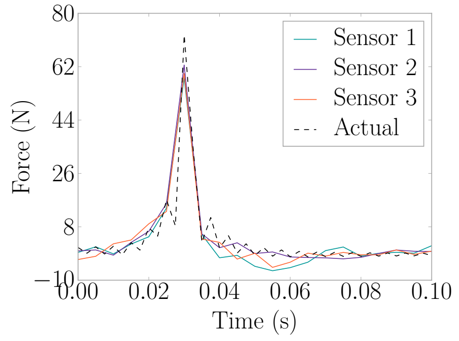
(g) $\hat{F}_{2,j}$

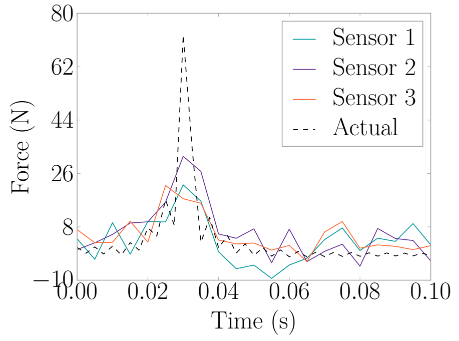
(h) $\hat{F}_{3,j}$

Figure 5.12: Force Estimates by Node for an Impact on Node 2

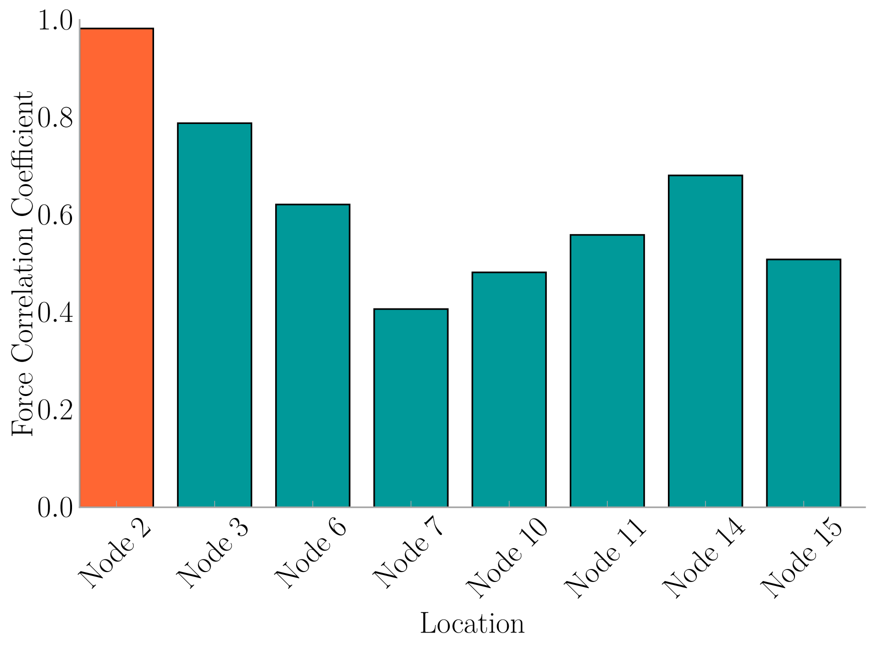

Figure 5.13: L_i for an Impact on Node 2

The results from the steel frame indicate the viability of the FEEL Algorithm. Each impact set correctly identified the node the impact occurred on, and closely estimated the maximum force of the impact. Sometimes a node near the impact, such as node 2 in Figure H.1, shows some convergence of the three sensors. This demonstrates that each transfer function has an area of influence, which will be explored in future work.

Table 5.2: Steel Frame Trial Using Eight Locations Results Summary

Impact	$\hat{L}$	Actual (N)	$\hat{F}$ (N)
Node 2	Node 2	72.7	63.4
Node 3	Node 3	13.6	10.7
Node 6	Node 6	26.0	22.5
Node 7	Node 7	88.4	83.9
Node 10	Node 10	12.9	11.1
Node 11	Node 11	18.0	19.0
Node 14	Node 14	24.4	23.7
Node 15	Node 15	38.5	29.6

5.5 Implementation Experiments

This section discusses the performance of the FEEL Algorithm in a full scale structural environment based on the human-induced vibration benchmark dataset developed by Arocha [46]. The experiments were performed in the second story office of the USC Structures Laboratory, measuring 777 cm (25.5 ft) by 638 cm (20.9 ft), that has reinforced concrete floors covered in vinyl tiles. The experimental layout is presented in Figure 5.14. Three PCB Piezotronics 333B50 accelerometers with sensitivity of 1000 mV/g were installed on the floor near the walls. Data was collected at a rate of 1651.7 Hz with 2 s windows. Five locations were chosen on the floor for the experiment. A total of 3575 impact events of eight different types were available. The events include hammer impacts (Section 5.5.1), ball drops (Section 5.5.2), bag

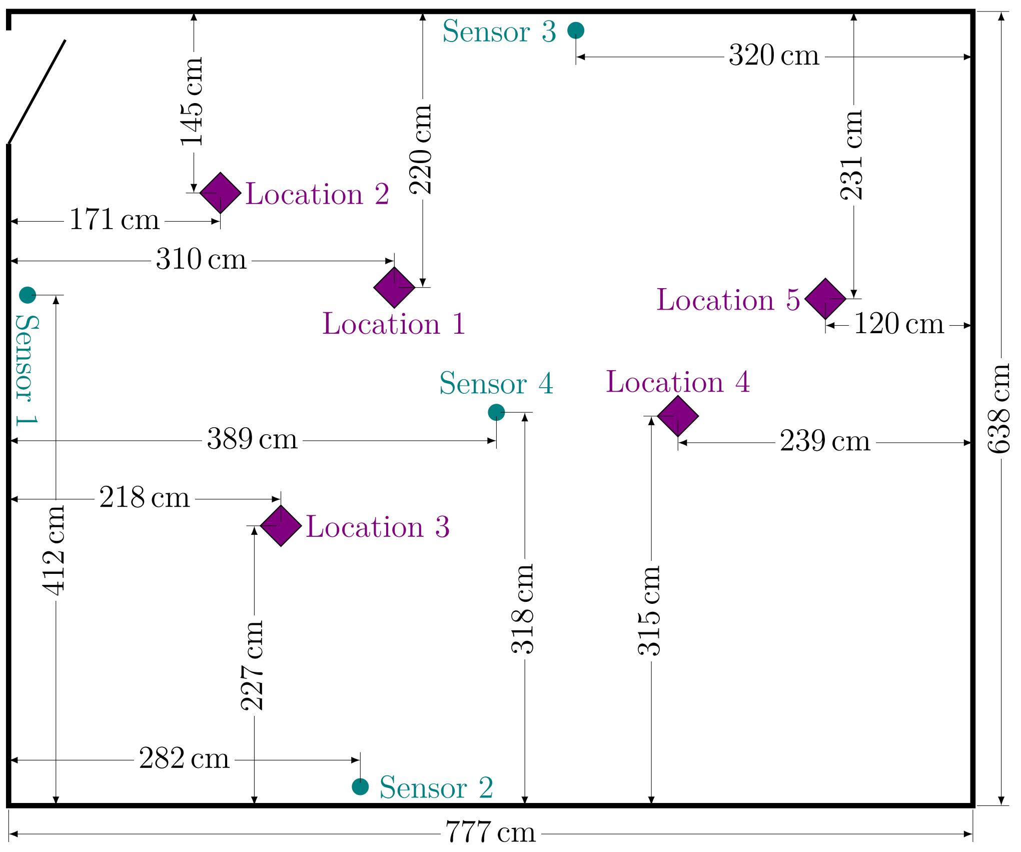

Figure 5.14: Implementation Experimental Layout

drops (Section 5.5.3), and human jumps (Section 5.5.4). Event types are outline in Table 5.3 and example acceleration records are provided in Figure 5.15.

Table 5.3: Implementation Experiment Event Types

Event Name	Mass (kg)	Details
hammer	5.49	
ball-low	0.56	1.42 m drop
ball-high	0.56	2.10 m drop
bag-low	0.45	1.42 m drop
bag-high	0.45	2.10 m drop
d-jump	80	male
j-jump	55	female
w-jump	85	male

5.5.1 Force Hammer Trials

Transfer functions were developed for each of the five locations (see Figure 5.16) using a PCB Piezotronics Impulse Force Hammer Model 086D50 with a sensitivity of 0.2305 mV/N (1.025 mV/lb) and the ability to excite to a frequencies up to 800 Hz. Five separate impacts were combined into one long force vector for calculation of the transfer functions as seen in Figure 5.16. Then, 15 separate impacts per location (total of 75 impacts) were used to validate the FEEL Algorithm. Results for a single impact on location one are presented where Figure 5.15h displays the acceleration signals, Figure 5.17 displays force estimations, and Figure 5.18 displays the force correlation coefficients with the identified location in orange. Examples for the remaining locations are presented in Appendix I.

A histogram of the difference between the estimated force magnitudes and those measured with the force hammer are shown in Figure 5.19, with a mean of 183.9 N (41.3 lb) and a standard deviation of of 184.3 N (41.4 lb). The estimates largely tend to be within 200 N (45 lb) of the measured force for each impact, with 72.0% of estimates falling within this range. Figure 5.20 displays the distribution of the force

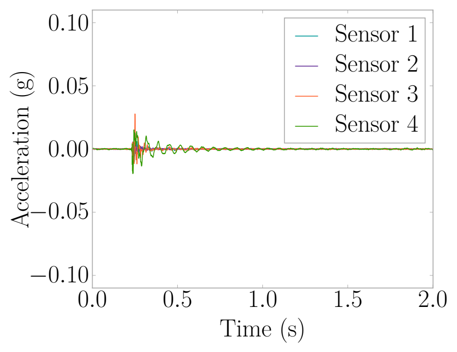

(a) Ball-Low

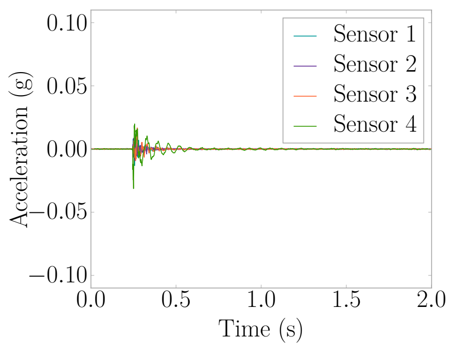

(b) Ball-High

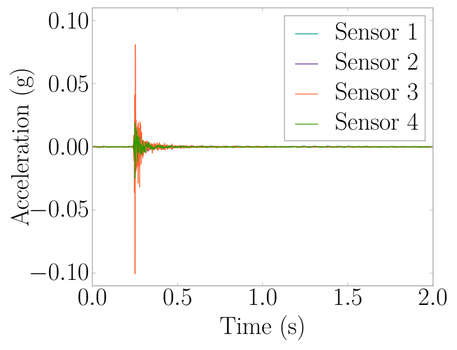

(c) Bag-Low

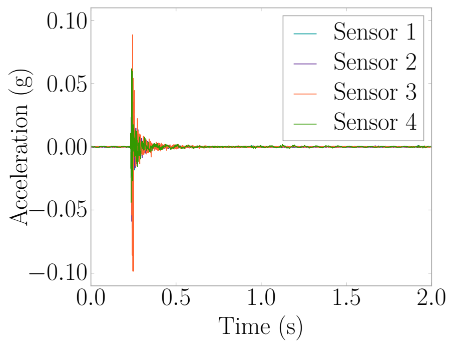

(d) Bag-High

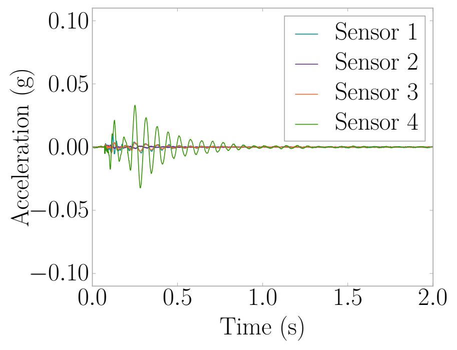

(e) D-Jump

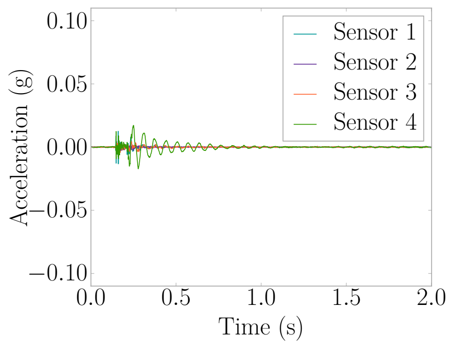

(f) J-Jump

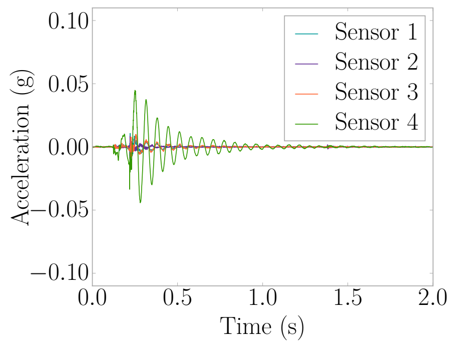

(g) W-Jump

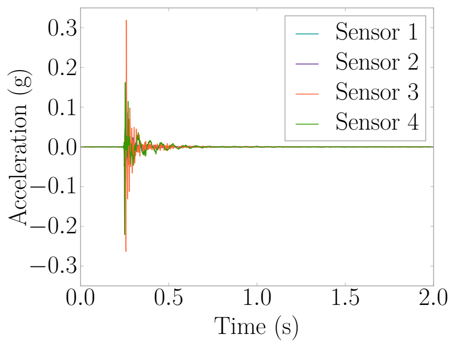

(h) Hammer

Figure 5.15: Implementation Experiment Example Accelerations

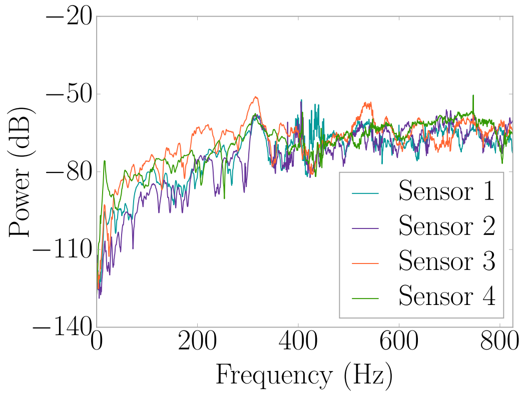

(a) $\hat{T}_{1,j}$

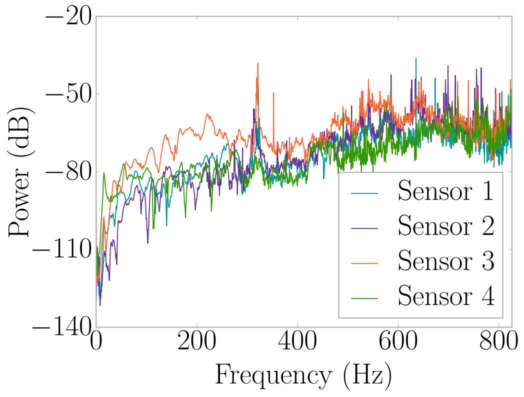

(b) $\hat{T}_{2,j}$

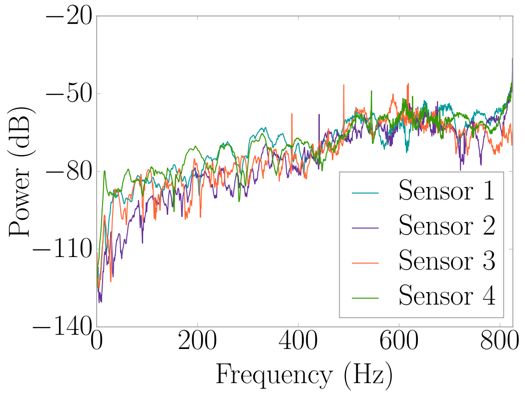

(c) $\hat{T}_{3,j}$

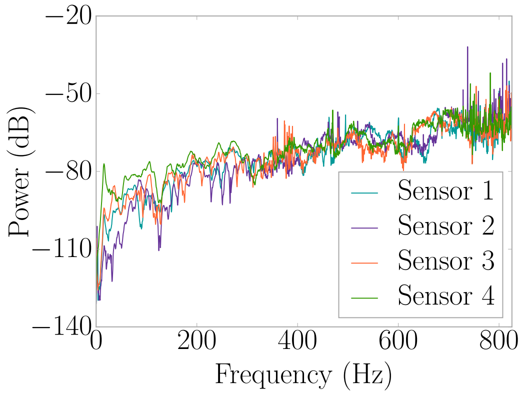

(d) $\hat{T}_{4,j}$

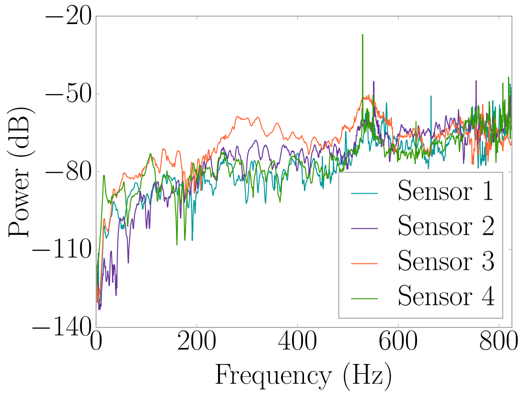

(e) $\hat{T}_{5,j}$

Figure 5.16: Concrete Floor Transfer Functions

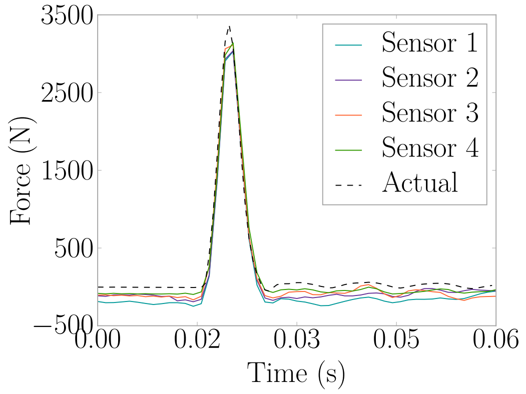

(a) $\hat{F}_{1,j}$

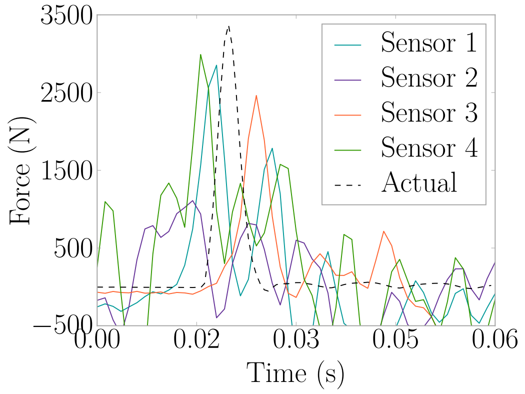

(b) $\hat{F}_{2,j}$

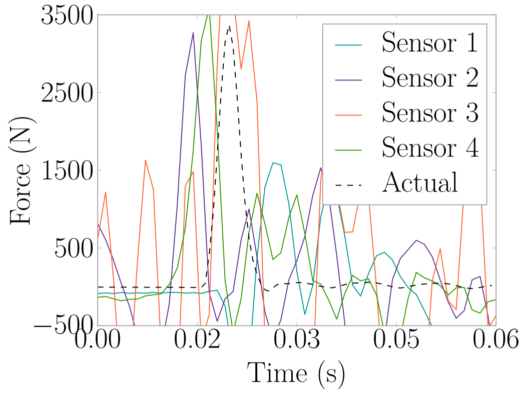

(c) $\hat{F}_{3,j}$

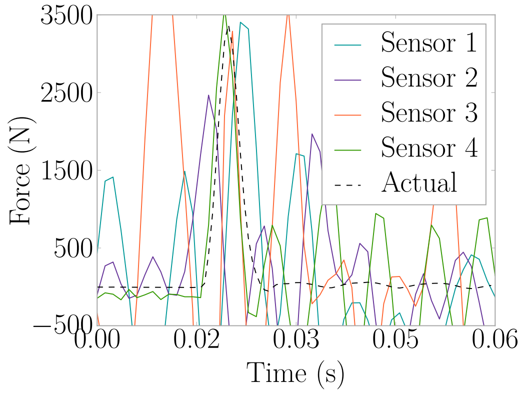

(d) $\hat{F}_{4,j}$

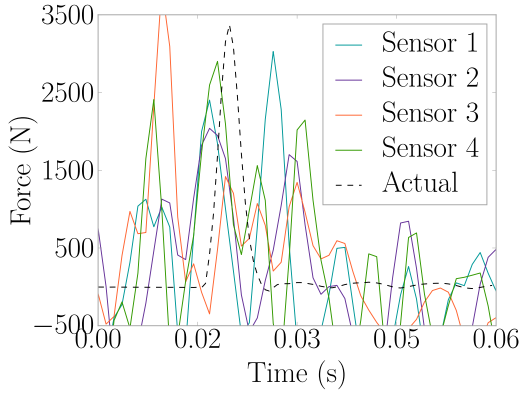

(e) $\hat{F}_{5,j}$

Figure 5.17: Hammer Impact Force Estimations for an Impact on Location 1

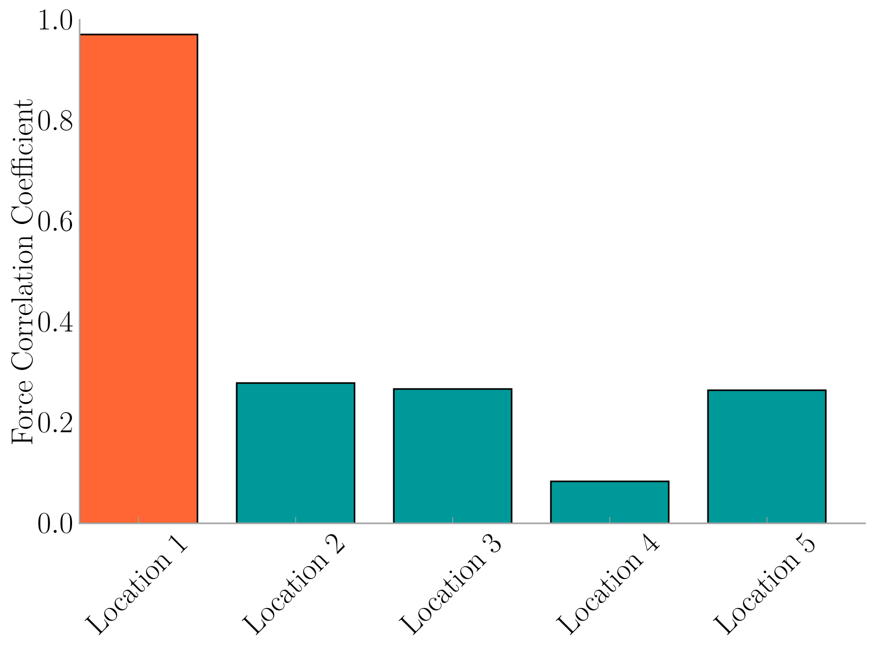

Figure 5.18: Hammer Impact L_i for an Impact on Location 1

magnitude estimate error which has a mean of -2.0% and a standard deviation of 4.4%. This gives a 99% confidence interval for the force magnitude estimate being within -2.0% ± 1.3% of the actual force magnitude.

A confusion matrix was developed to determine how well the FEEL Algorithm determined the location of each hit, which is presented in Table 5.4. All 75 hammer impacts were correctly located.

Table 5.4: Confusion Matrix for Locating Hammer Impacts

		Identified				
		Location 1	Location 2	Location 3	Location 4	Location 5
Actual	Location 1	**15**	0	0	0	0
	Location 2	0	**15**	0	0	0
	Location 3	0	0	**15**	0	0
	Location 4	0	0	0	**15**	0
	Location 5	0	0	0	0	**15**

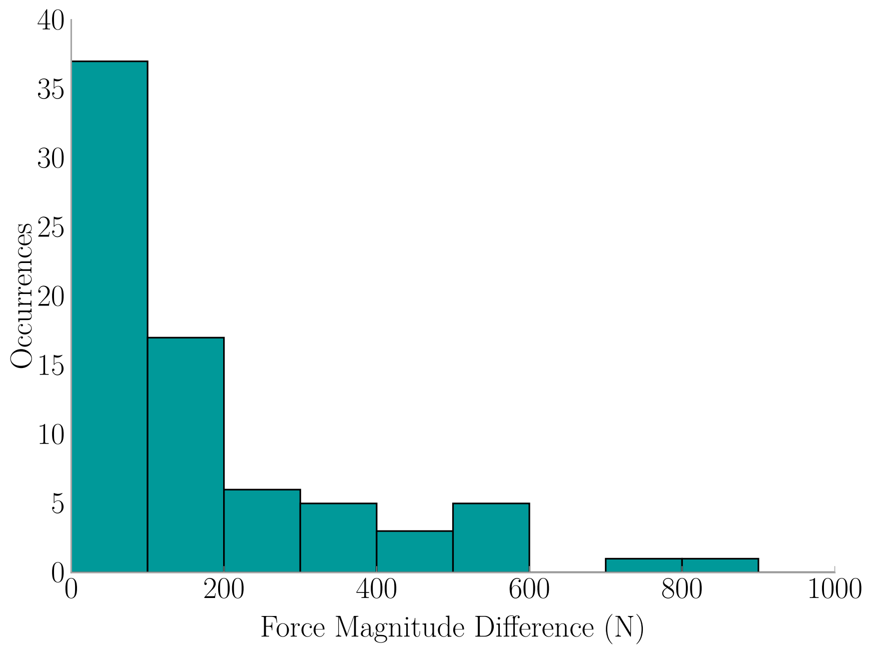

Figure 5.19: Hammer Impacts Force Magnitude Estimation Difference

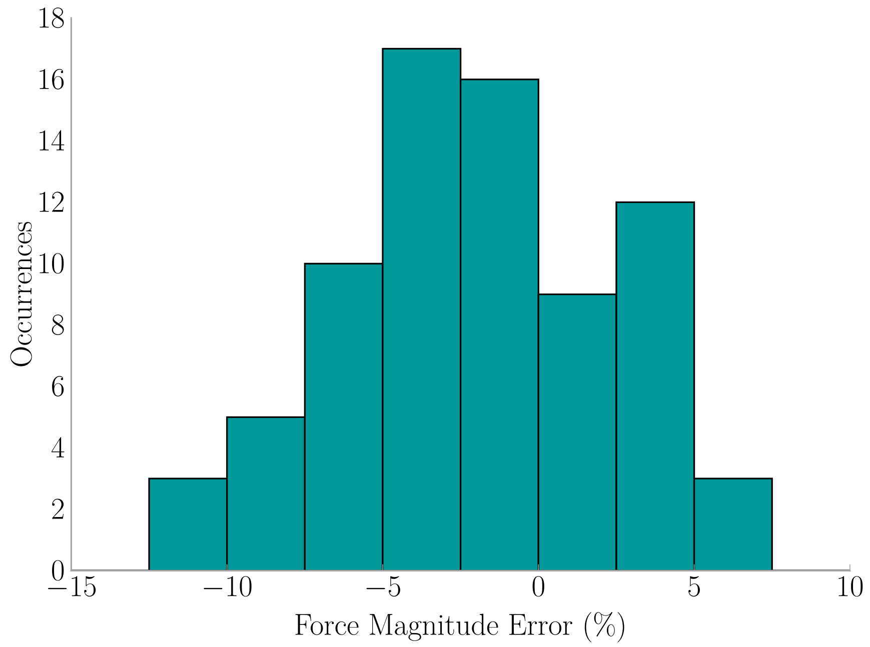

Figure 5.20: Hammer Impacts Force Magnitude Estimation Error

5.5.2 Ball Drop Trials

A basketball weighing 0.56 kg (1.23 lb) was dropped from two different heights at each location for 100 repetitions. The trial named *ball-low* indicates a drop height of 1.42 m (4.63 ft), and the trial named *ball-high* indicates a drop height of 2.10 m (6.89 ft).

A sample impact for ball-low at location one is presented with Figure 5.15a showing the vibrations the floor experienced, Figure 5.22 showing the force estimations at each location, and Figure 5.21 showing the resulting correlation coefficients where the orange bar is the identified location. Note that unlike with the hammer excitation, no force record is available for comparison.

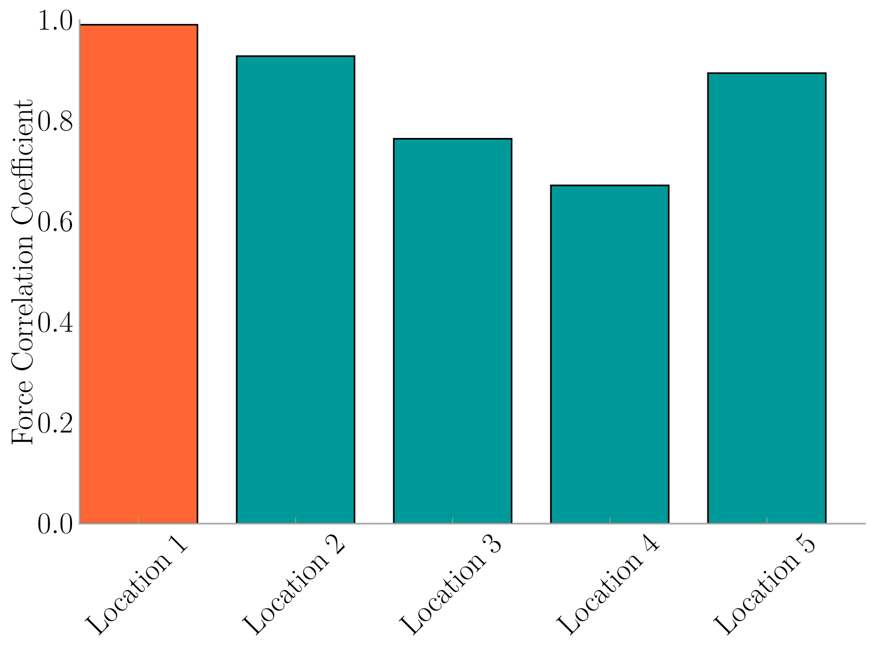

Figure 5.21: Ball-Low L_i for an Impact on Location 1

A confusion matrix was generated to demonstrate the accuracy of the FEEL Algorithm for location when the impact was caused by ball-low in Table 5.5. All 500 ball-low impacts were correctly identified giving a 100% success rate.

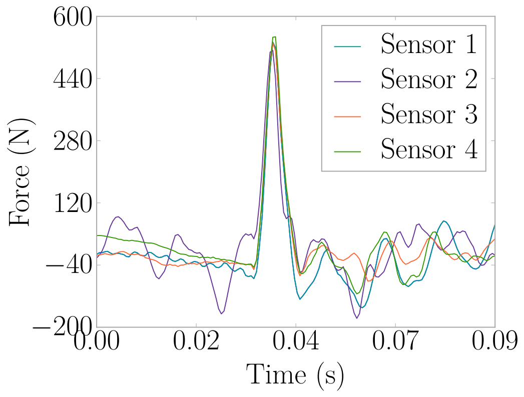

(a) $\hat{F}_{1,j}$

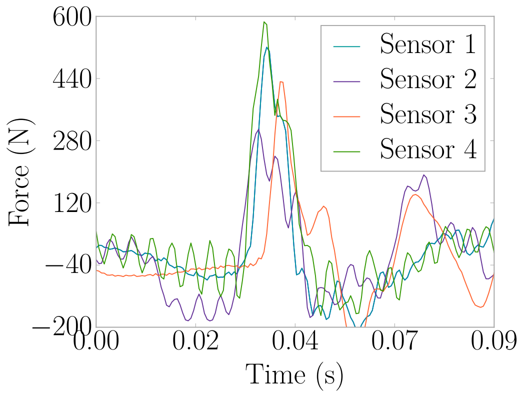

(b) $\hat{F}_{2,j}$

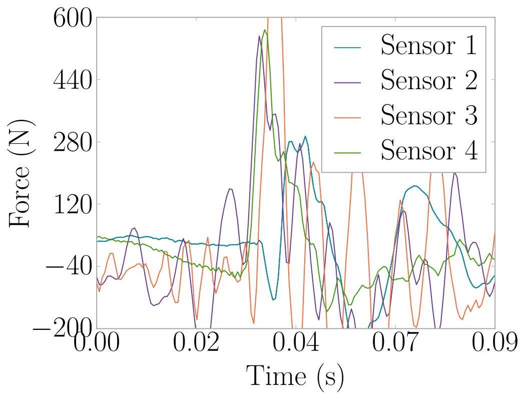

(c) $\hat{F}_{3,j}$

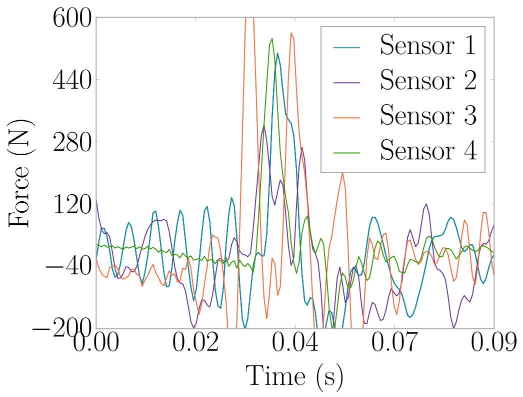

(d) $\hat{F}_{4,j}$

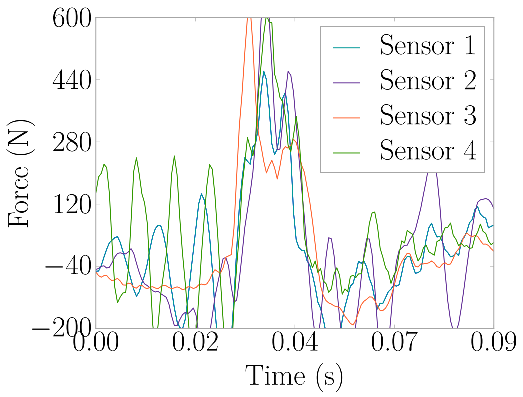

(e) $\hat{F}_{5,j}$

Figure 5.22: Ball-Low Force Estimations for an Impact on Location 1

Table 5.5: Confusion Matrix for Locating Ball-Low Impacts

		Identified				
		Location 1	Location 2	Location 3	Location 4	Location 5
Actual	Location 1	**100**	0	0	0	0
	Location 2	0	**100**	0	0	0
	Location 3	0	0	**100**	0	0
	Location 4	0	0	0	**100**	0
	Location 5	0	0	0	0	**100**

A histogram of the estimated force magnitudes shown in Figure 5.23 demonstrates a tight grouping of the force estimates around 500 N-600 N (123 lb-135 lb) having a mean of 569.5 N (128.0 lb) and standard deviation of 41.3 N (11.5 lb). The variation in estimates is due to how the ball drop experiment was performed as well as errors in FEEL. The experiment was performed by a person holding and releasing the ball. This means there will be some variation in the force as the person holds the ball at a slightly different heights, and the ball bounces at slightly different spots each time.

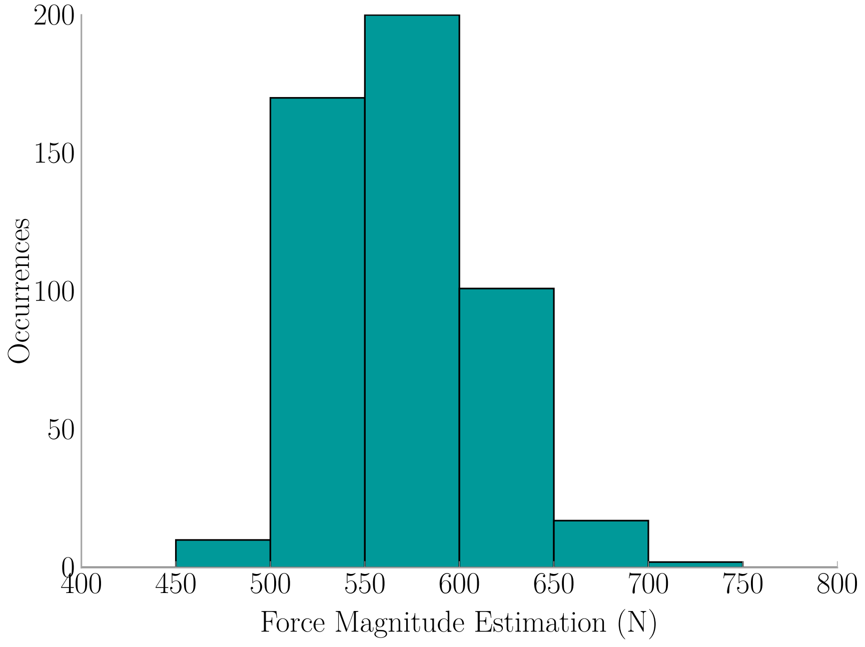

Figure 5.23: Ball-Low Force Magnitude Estimation Histogram

A sample impact for ball-high at location four is presented with Figure 5.15b showing the vibrations the floor experienced, Figure 5.25 showing the force estimations at each location, and Figure 5.24 showing the resulting correlation coefficients where the orange bar is the identified location.

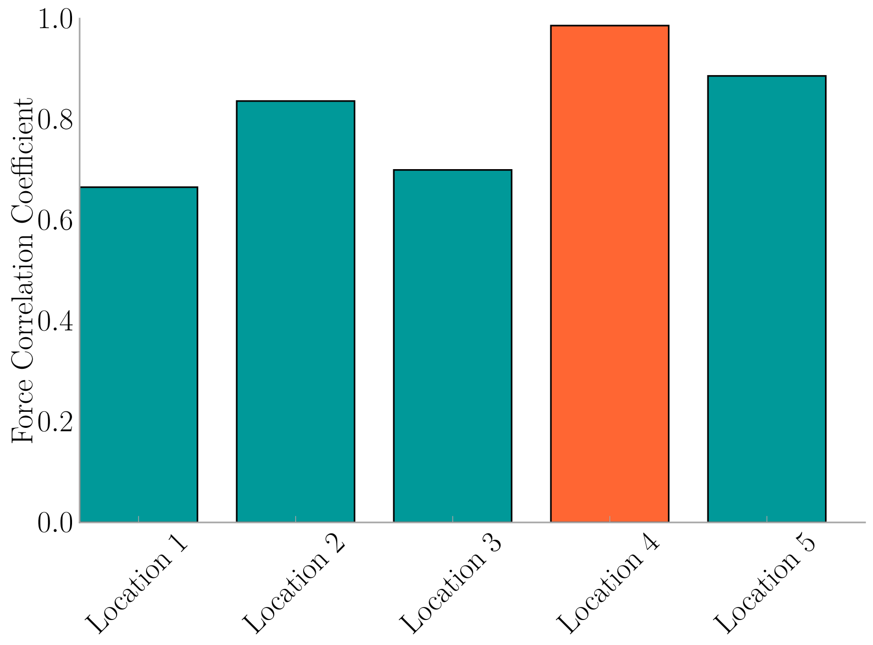

Figure 5.24: Ball-High L_i for an Impact on Location 1

A confusion matrix was generated to demonstrate the accuracy of the FEEL Algorithm for localization in the case of ball-high in Table 5.6. Of the 500 ball-high impacts, 499 were correctly identified which is a 99.8% success rate.

Table 5.6: Confusion Matrix for Locating Ball-High Impacts

		Identified				
		Location 1	Location 2	Location 3	Location 4	Location 5
Actual	Location 1	**100**	0	0	0	0
	Location 2	0	**100**	0	0	0
	Location 3	1	0	**99**	0	0
	Location 4	0	0	0	**100**	0
	Location 5	0	0	0	0	**100**

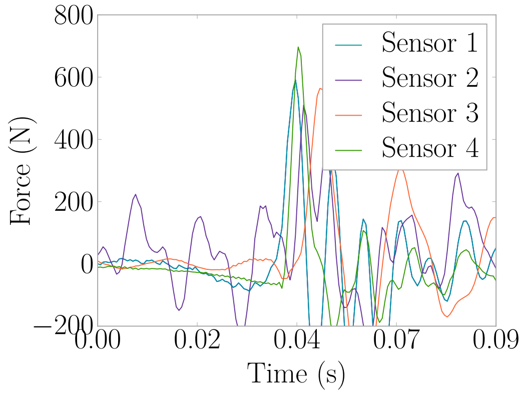

(a) $\hat{F}_{1,j}$

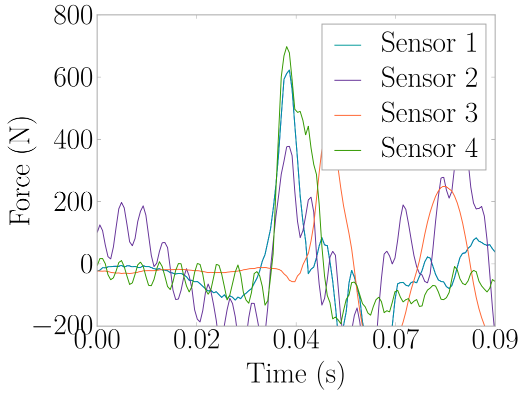

(b) $\hat{F}_{2,j}$

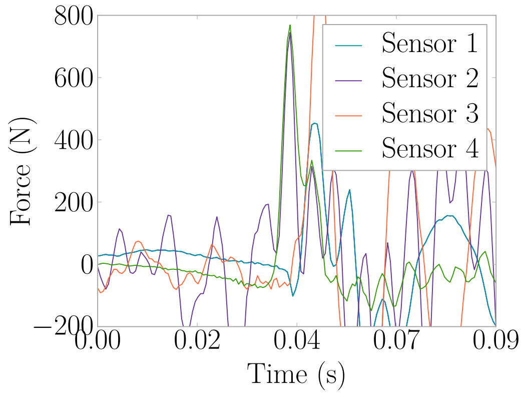

(c) $\hat{F}_{3,j}$

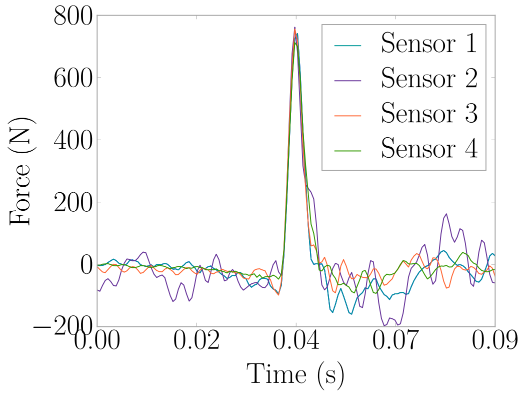

(d) $\hat{F}_{4,j}$

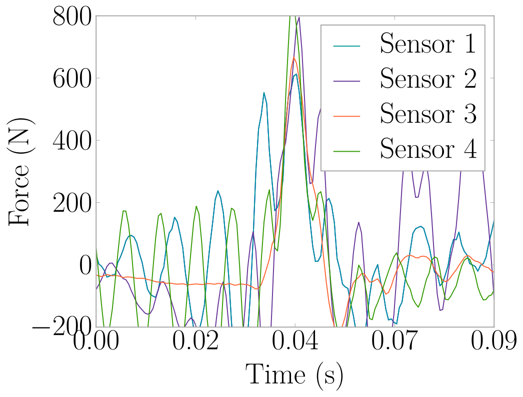

(e) $\hat{F}_{5,j}$

Figure 5.25: Ball-High Force Estimations for an Impact on Location 1

The force estimations center around 700 N (157 lb) having a mean of 713.2 N (160.3 lb) and standard deviation of 56.5 N (12.7 lb). Variations in the estimates here stem from how the ball-high trial was performed, like that of the ball-low trial, where a person held the ball at approximately the same height each time.

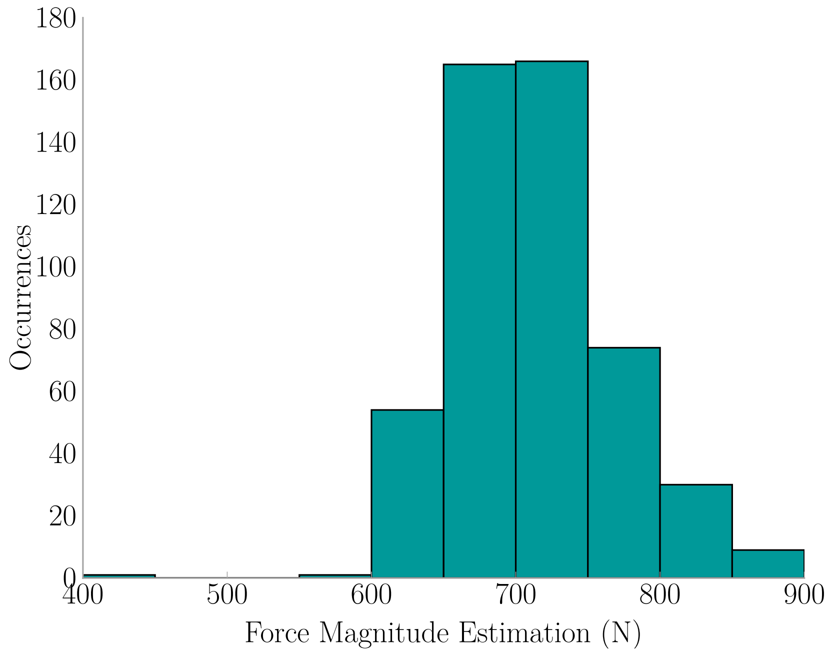

Figure 5.26: Ball-High Force Magnitude Estimation Histogram

5.5.3 Bag Drop Trials

A bag of k'nex weighing 0.45 kg (0.99 lb) was dropped from two different heights at each location for 100 repetitions. The trial named *bag-low* indicates a drop height of 1.42 m (4.63 ft), and the trial named *bag-high* indicates a drop height of 2.10 m (6.89 ft). This bag was selected because it provides an impact with a very different coefficient of restitution than the basketball.

A sample impact for bag-low at location two is presented with Figure 5.15c showing the vibrations the floor experienced, Figure 5.27 showing the force estimations at each location, and Figure 5.28 showing the resulting correlation coefficients where

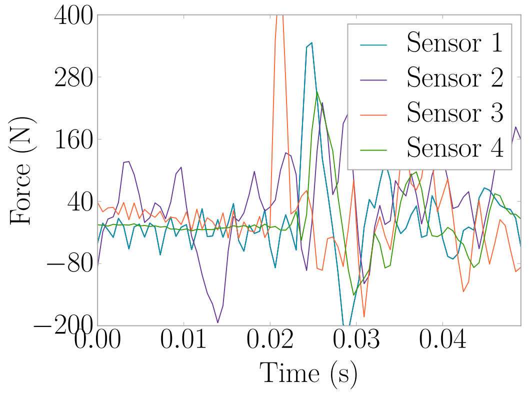

(a) $\hat{F}_{1,j}$

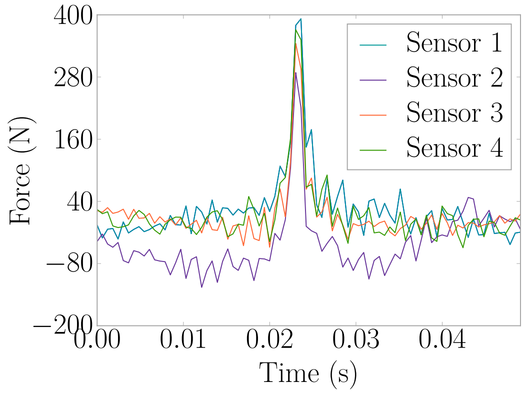

(b) $\hat{F}_{2,j}$

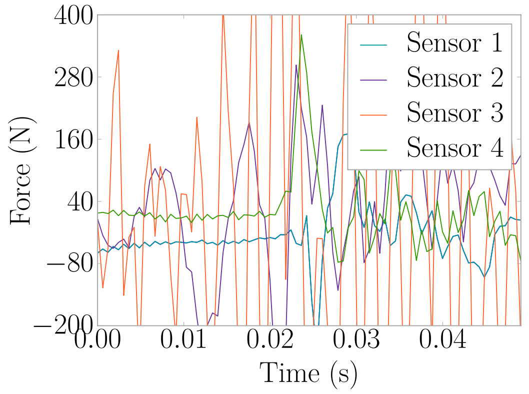

(c) $\hat{F}_{3,j}$

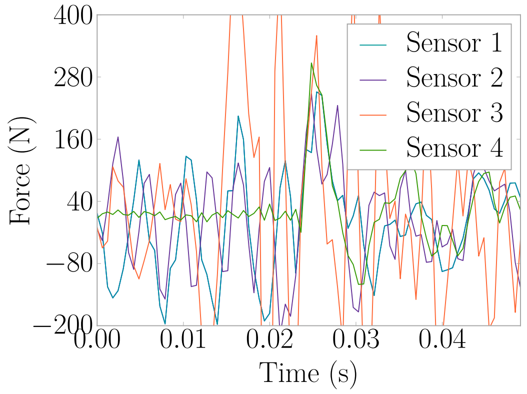

(d) $\hat{F}_{4,j}$

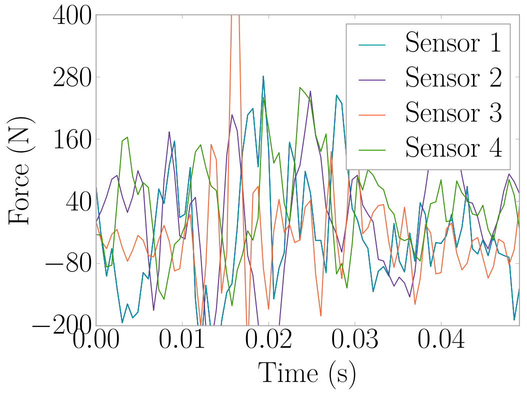

(e) $\hat{F}_{5,j}$

Figure 5.27: Bag-Low Force Estimations for an Impact on Location 2

the orange bar is the identified location. Notice that the force correlation coefficient for the k'nex bag was much smaller than those found for the basketball. However, the method was still successful at determining the location of impact.

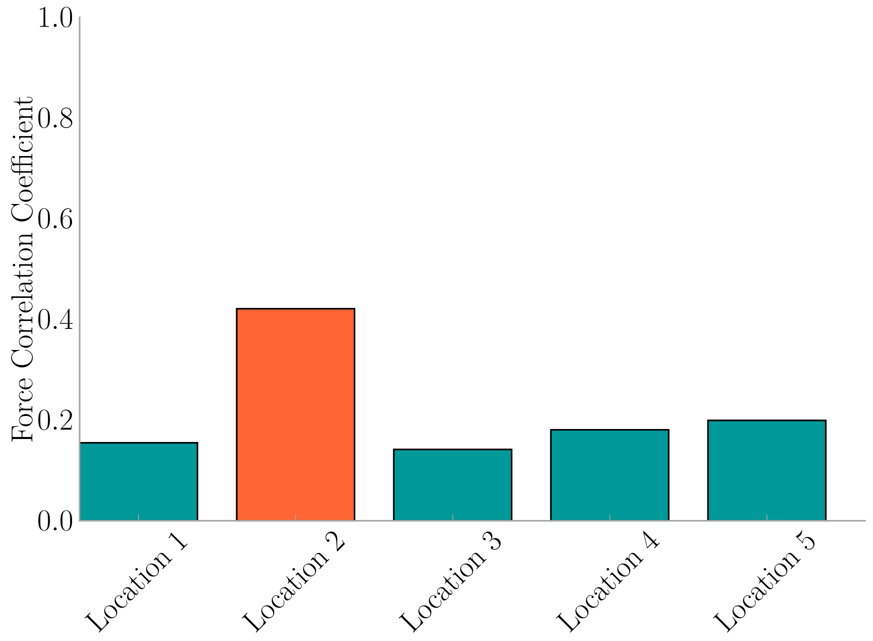

Figure 5.28: Bag-Low L_i for an Impact on Location 2

A confusion matrix was generated to demonstrate the accuracy of the FEEL Algorithm for localization with the bag-low test in Table 5.7. Of the 500 bag-low impacts, 498 were correctly identified which is a 99.6% success rate.

Table 5.7: Confusion Matrix for Locating Bag-Low Impacts

		Identified				
		Location 1	Location 2	Location 3	Location 4	Location 5
Actual	Location 1	**98**	1	0	0	1
	Location 2	0	**100**	0	0	0
	Location 3	0	0	**100**	0	0
	Location 4	0	0	0	**100**	0
	Location 5	0	0	0	0	**100**

The force estimations center around 300 N-400 N (67 lb-90 lb), having a mean of 356.6 N (80.2 lb) and standard deviation of 158.7 N (35.7 lb) as in Figure 5.29.

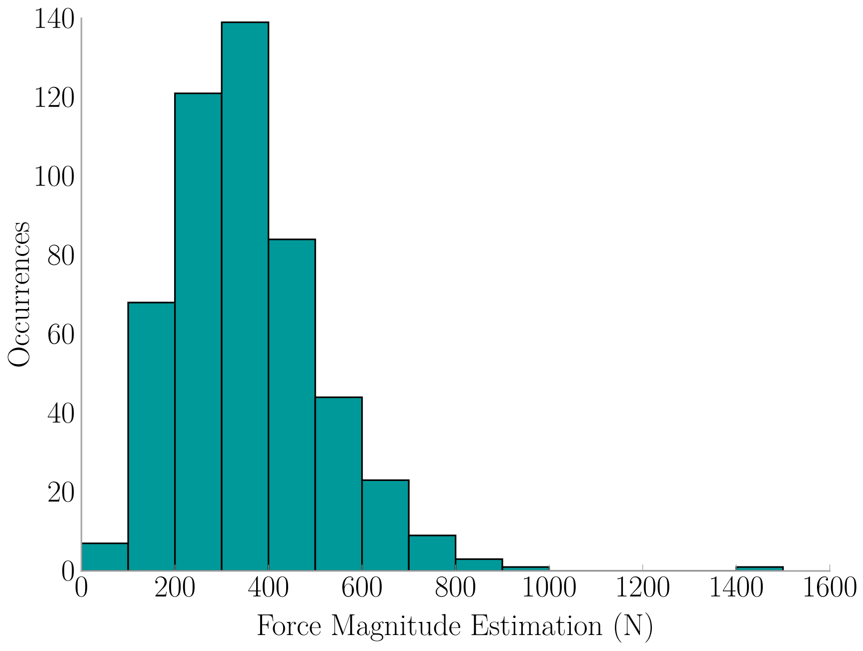

Figure 5.29: Bag-Low Force Magnitude Estimation Histogram

A sample impact for bag-high at location five is presented with Figure 5.15d showing the vibrations the floor experienced, Figure 5.30 showing the force estimations at each location, and Figure 5.31 showing the resulting correlation coefficients where the orange bar is the identified location.

The location confusion matrix was generated to demonstrate the accuracy of the FEEL Algorithm for localization for bag-high in Table 5.8. Of the 500 bag-high impacts, 494 were correctly identified which is a 98.8% success rate.

The force estimations center around 300 N-400 N (67 lb-90 lb), having a mean of 444.7 N (100.0 lb) and standard deviation of 314.1 N (70.6 lb) as in Figure 5.32.

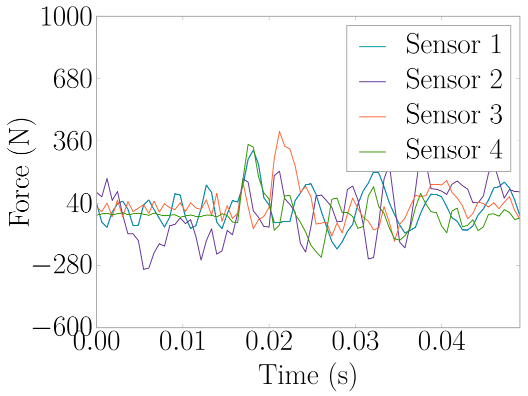

(a) $\hat{F}_{1,j}$

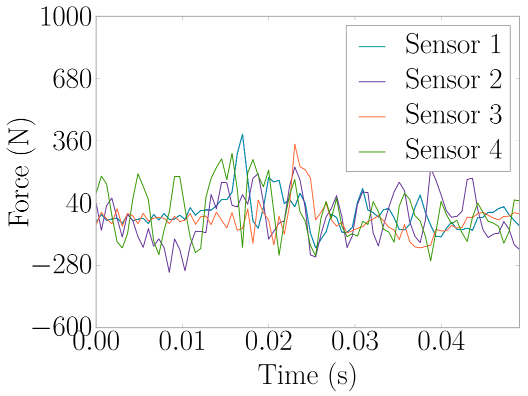

(b) $\hat{F}_{2,j}$

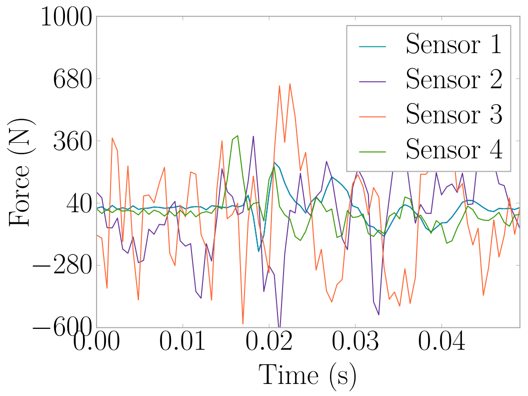

(c) $\hat{F}_{3,j}$

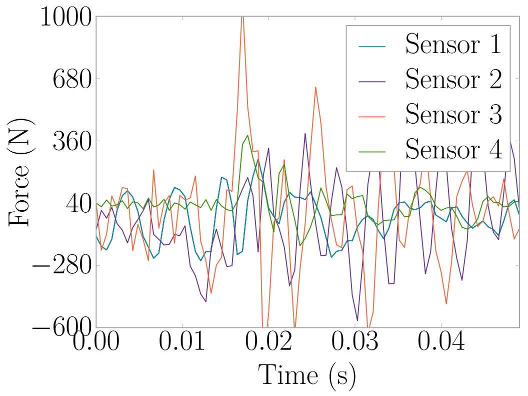

(d) $\hat{F}_{4,j}$

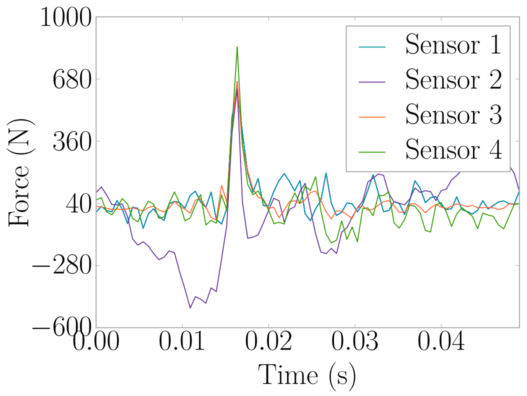

(e) $\hat{F}_{5,j}$

Figure 5.30: Bag-High Force Estimations for an Impact on Location 5

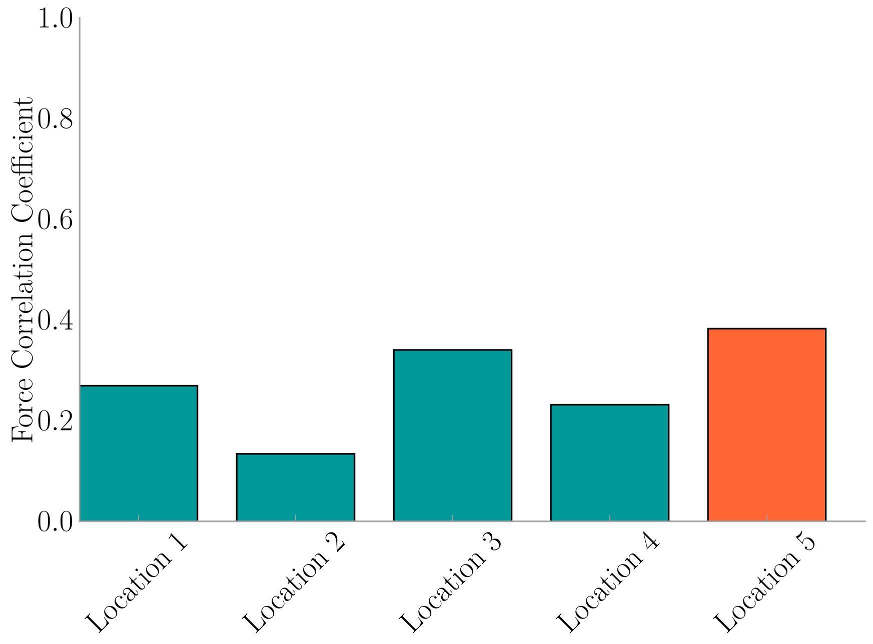

Figure 5.31: Bag-High L_i for an Impact on Location 5

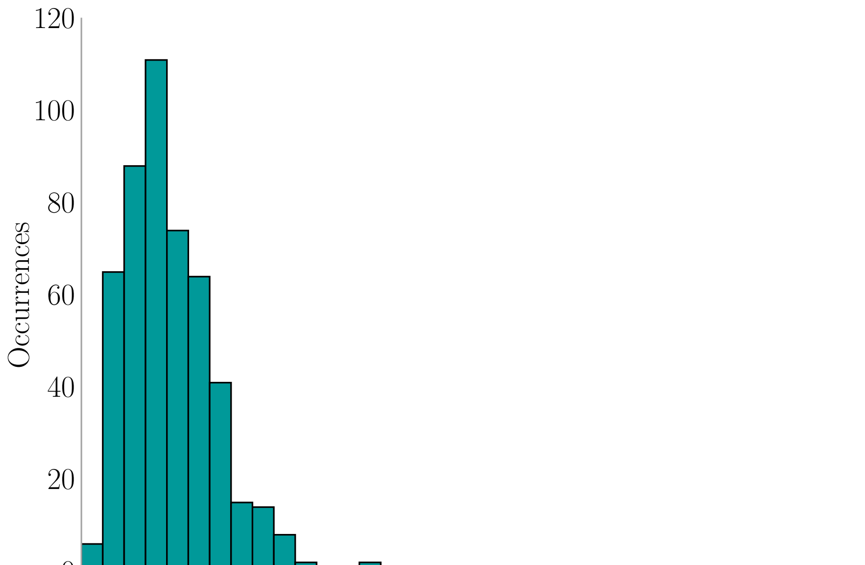

Figure 5.32: Bag-High Force Magnitude Estimation Histogram

Table 5.8: Confusion Matrix for Locating Bag-High Impacts

		Identified				
		Location 1	Location 2	Location 3	Location 4	Location 5
Actual	Location 1	**96**	2	1	0	1
	Location 2	0	**100**	0	0	0
	Location 3	0	1	**98**	0	1
	Location 4	0	0	0	**100**	0
	Location 5	0	0	0	0	**100**

5.5.4 Human Jump Trials

Three different people jumped at each location 100 times. The trial names indicate the following: *d-jump* is a male weighing 80 kg (176 lb), *j-jump* is a female weighing 55 kg (121 lb), *w-jump* is a male weighing 85 kg (187 lb). The jump height of each person varied, and the way the person landed varied as well. This allowed for testing the FEEL Algorithm and exploring its robustness.

A sample impact for d-jump at location one is presented with Figure 5.15e showing the vibrations the floor experienced, Figure 5.33 showing the force estimations at each location, and Figure 5.34 showing the resulting correlation coefficients where the orange bar is the identified location.

The location confusion matrix was generated to demonstrate the accuracy of the FEEL Algorithm for localization for the d-jump test in Table 5.9. Of the 500 d-jump impacts, 476 were correctly identified which is a 95.2% success rate. The algorithm had the most error at location one where it only had 86% success.

The force estimations center around 700 N-800 N (157 lb-180 lb), having a mean of 711.4 N (159.9 lb) and standard deviation of 226.9 N (51.0 lb) as in Figure 5.35. Since this trial is record of human-induced vibrations, there is bound to be some variation as the person jumping would not have jumped to the same height every time. The spread of estimates is closer together than that of the bag-high trials.

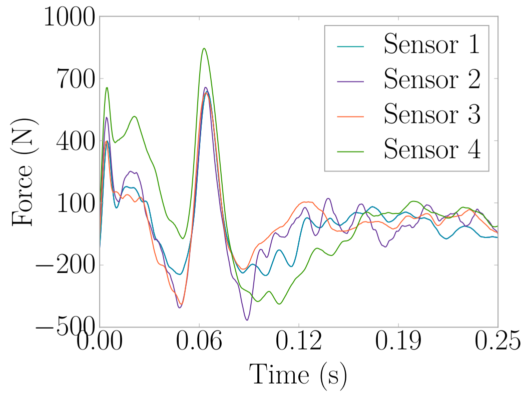

(a) $\hat{F}_{1,j}$

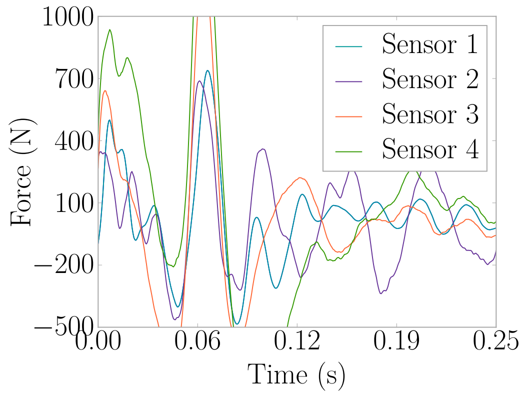

(b) $\hat{F}_{2,j}$

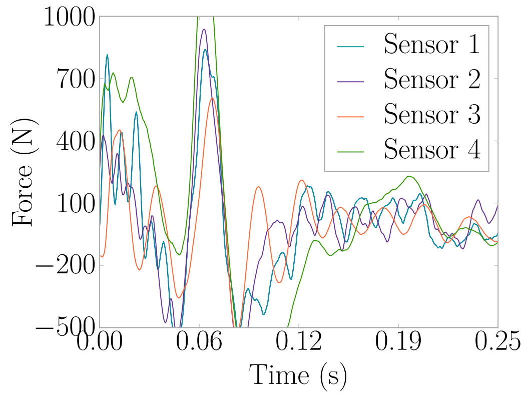

(c) $\hat{F}_{3,j}$

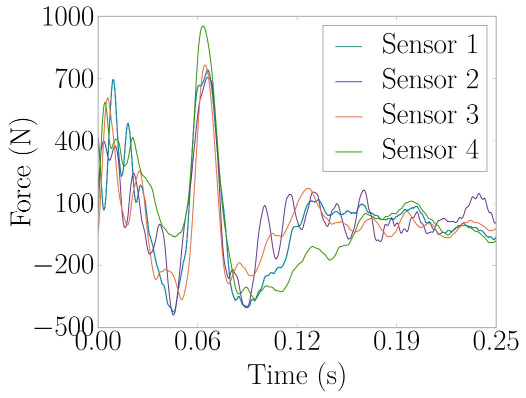

(d) $\hat{F}_{4,j}$

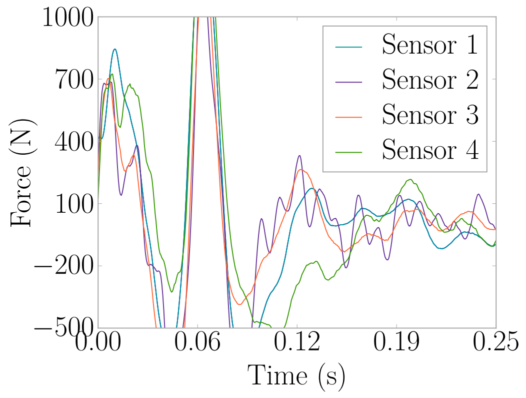

(e) $\hat{F}_{5,j}$

Figure 5.33: D-Jump Force Estimations for an Impact on Location 1

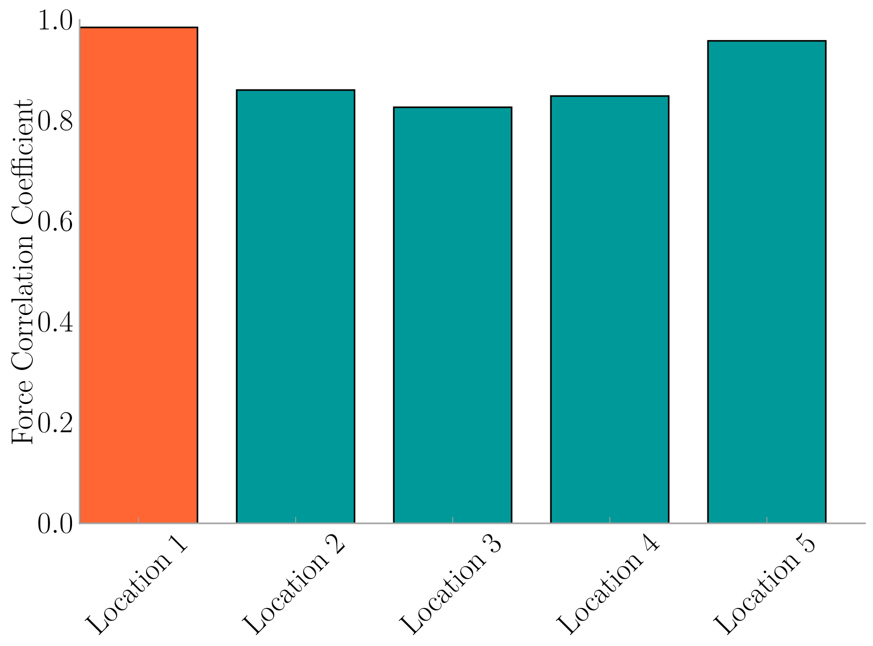

Figure 5.34: D-Jump L_i for an Impact on Location 1

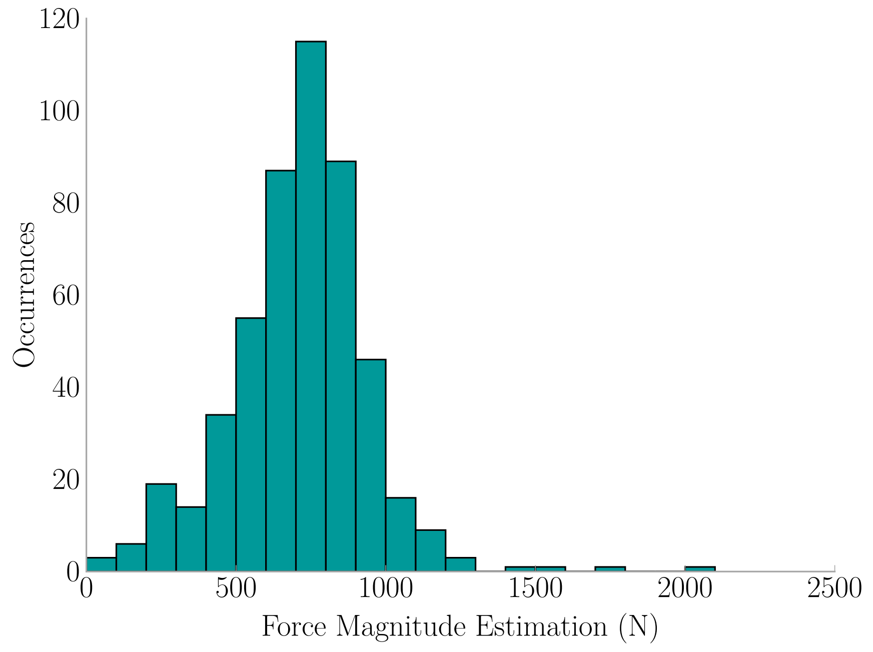

Figure 5.35: D-Jump Force Magnitude Estimation Histogram

Table 5.9: Confusion Matrix for Locating D-Jump Impacts

		Identified				
		Location 1	Location 2	Location 3	Location 4	Location 5
Actual	Location 1	**86**	0	0	2	12
	Location 2	0	**100**	0	0	0
	Location 3	0	0	**91**	1	8
	Location 4	0	0	0	**99**	1
	Location 5	0	0	0	0	**100**

A sample impact for j-jump at location two is presented with Figure 5.15f showing the vibrations the floor experienced, Figure 5.37 showing the force estimations at each location, and Figure 5.36 showing the resulting correlation coefficients where the orange bar is the identified location.

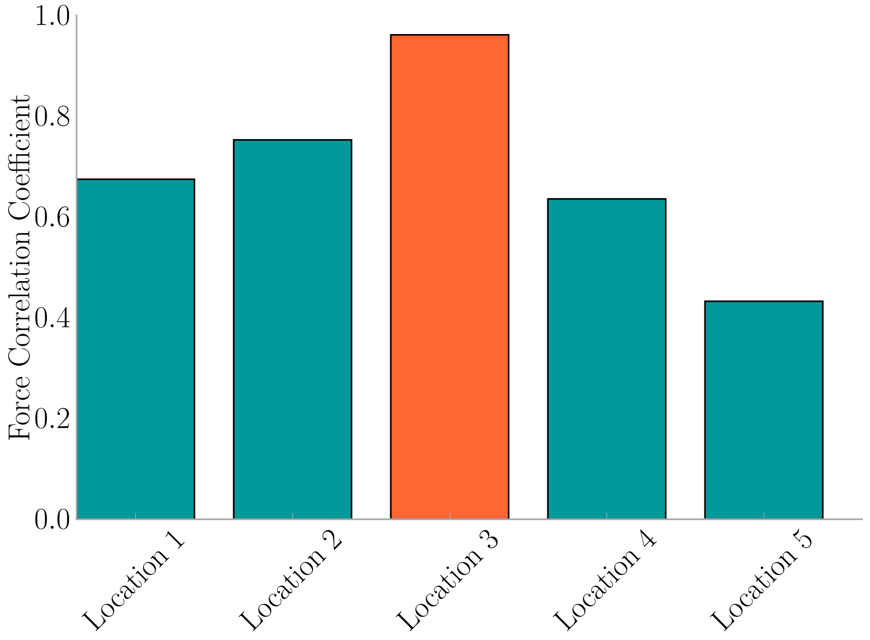

Figure 5.36: J-Jump L_i for an Impact on Location 3

The location confusion matrix was generated to demonstrate the accuracy of the FEEL Algorithm for localization in Table 5.10. Of the 500 j-jump impacts, 477 were correctly identified which is a 95.4% success rate. Location one continued to be the lowest performing location of those tested.

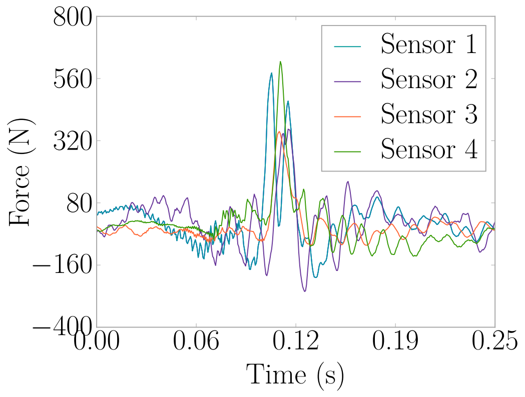

(a) $\hat{F}_{1,j}$

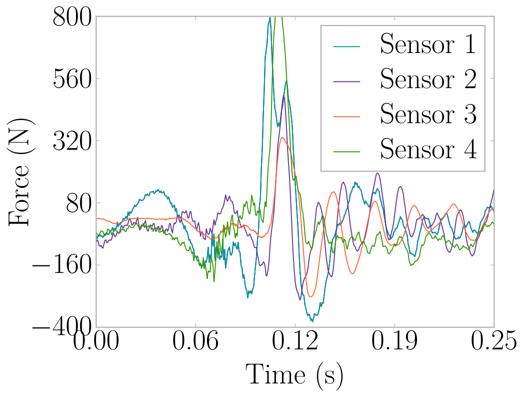

(b) $\hat{F}_{2,j}$

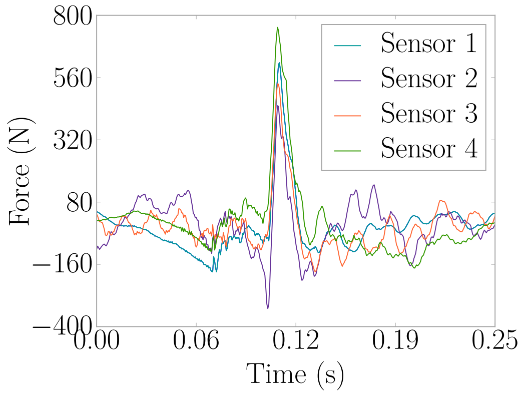

(c) $\hat{F}_{3,j}$

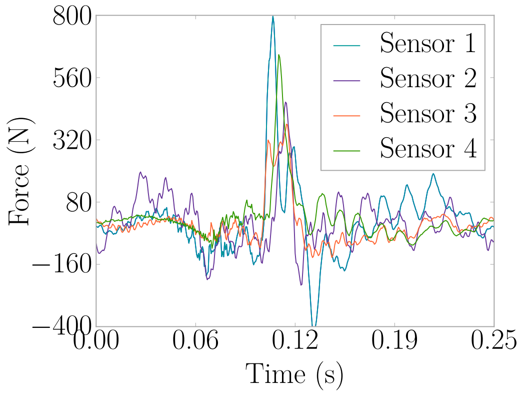

(d) $\hat{F}_{4,j}$

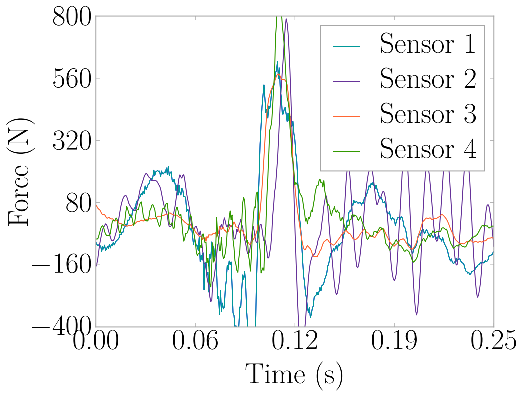

(e) $\hat{F}_{5,j}$

Figure 5.37: J-Jump Force Estimations for an Impact on Location 3

Table 5.10: Confusion Matrix for Locating J-Jump Impacts

		Identified				
		Location 1	Location 2	Location 3	Location 4	Location 5
Actual	Location 1	**92**	3	0	0	5
	Location 2	0	**100**	0	0	0
	Location 3	2	0	**98**	0	0
	Location 4	0	2	1	**94**	3
	Location 5	2	4	0	1	**93**

The force estimations tend to be around 100 N-200 N (22 lb-45 lb), having a mean of 227.1 N (51.1 lb) and standard deviation of 244.8 N (55.0 lb) as in Figure 5.38. The variation reason is the same as that of d-jump. The interesting point here is that the estimates tend to be lower in magnitude which makes sense considering the lighter weight of the person jumping compared to the other two jumpers.

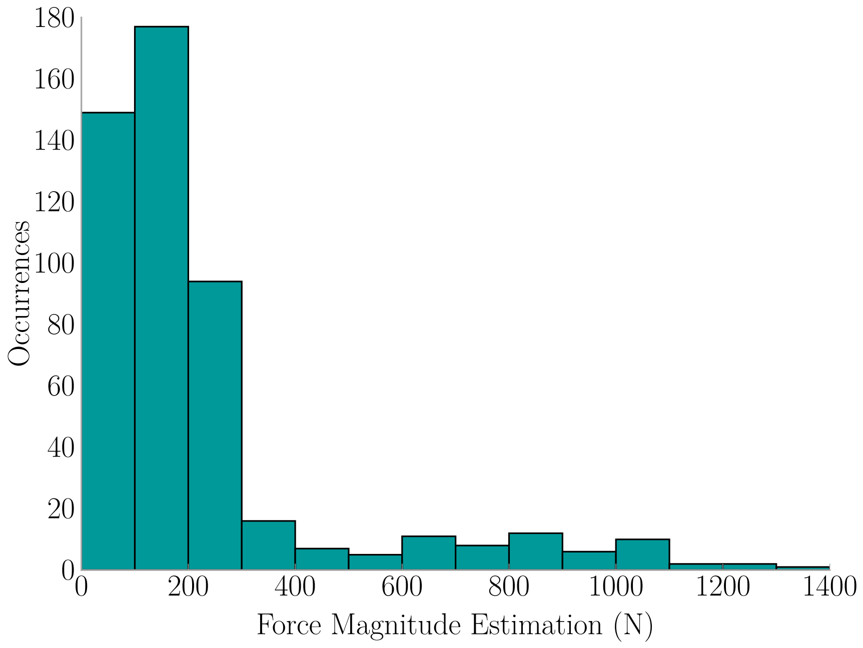

Figure 5.38: J-Jump Force Magnitude Estimation Histogram

A sample impact for w-jump at location four is presented with Figure 5.15g showing the vibrations the floor experienced, Figure 5.39 showing the force estimations

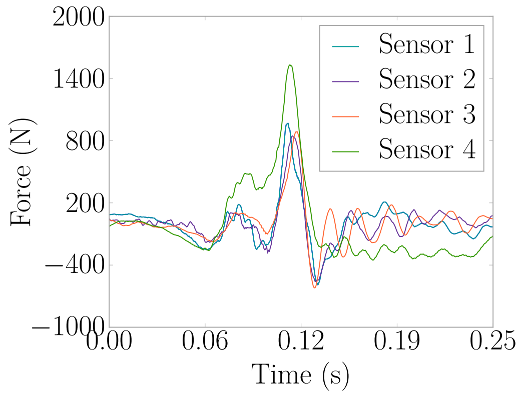

(a) $\hat{F}_{1,j}$

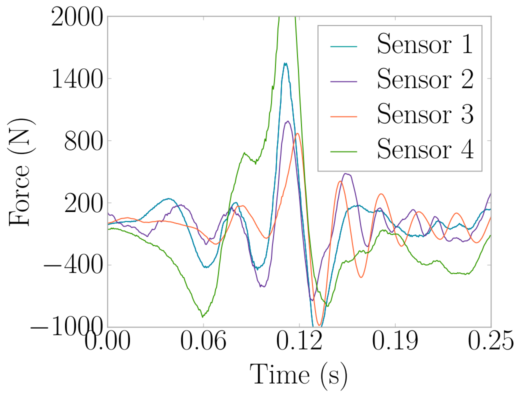

(b) $\hat{F}_{2,j}$

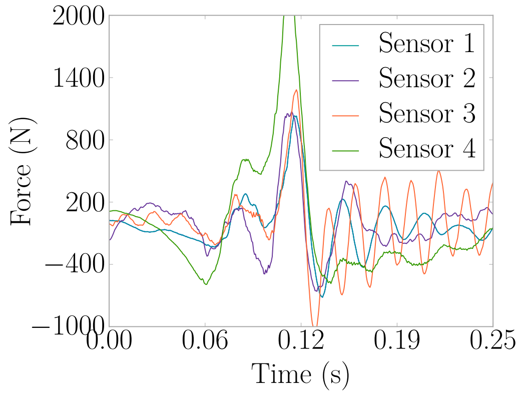

(c) $\hat{F}_{3,j}$

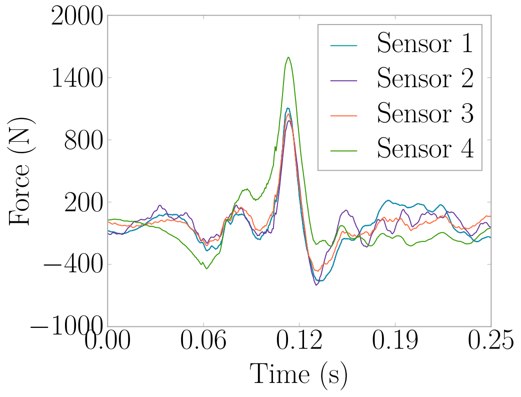

(d) $\hat{F}_{4,j}$

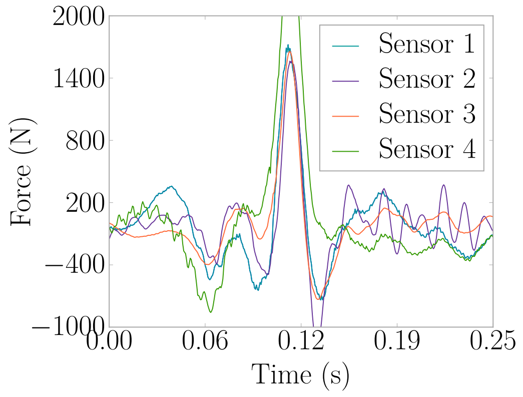

(e) $\hat{F}_{5,j}$

Figure 5.39: W-Jump Force Estimations for an Impact on Location 4

at each location, and Figure 5.40 showing the resulting correlation coefficients where the orange bar is the identified location.

Notice how in Figure 5.39 how the shapes of the force are quite similar. This is reflected in Figure 5.40 where the correlations are also very similar. A possibility arises here that there could be few calibration points in an area. The force could possibly be estimated, and the room identified as the location of impact from less information. This will be explored in future work.

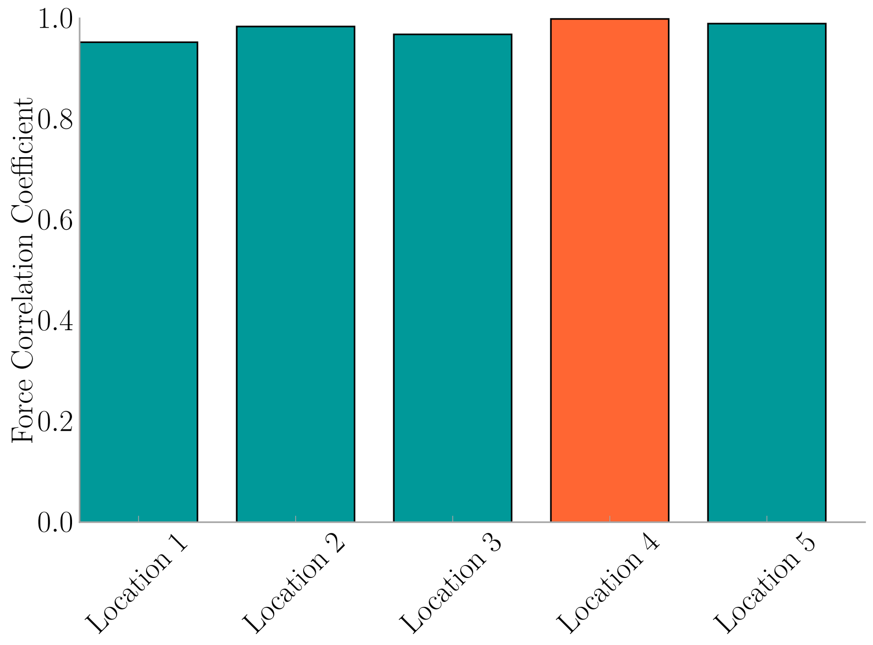

Figure 5.40: W-Jump L_i for an Impact on Location 4

The location confusion matrix was generated to demonstrate the accuracy of the FEEL Algorithm for localization for w-jump in Table 5.11. Of the 500 w-jump impacts, 428 were correctly identified which is a 85.6% success rate. Location one again had the lowest performance of the locations tested.

Table 5.11: Confusion Matrix for Locating W-Jump Impacts

		Identified				
		Location 1	Location 2	Location 3	Location 4	Location 5
Actual	Location 1	**45**	6	4	13	32
	Location 2	1	**98**	0	0	1
	Location 3	3	3	**90**	0	4
	Location 4	0	0	1	**96**	3
	Location 5	0	1	0	0	**99**

The force estimations center around 900 N-1000 N (202 lb-225 lb), having a mean of 947.1 N (212.9 lb) and standard deviation of 421.5 N (97.8 lb) as in Figure 5.41. The variation in magnitudes is due to the same reason as that of d-jump and j-jump trials. This test had the heaviest person jumping which the histogram demonstrates with the majority of jumps being higher in magnitude than the other two participants.

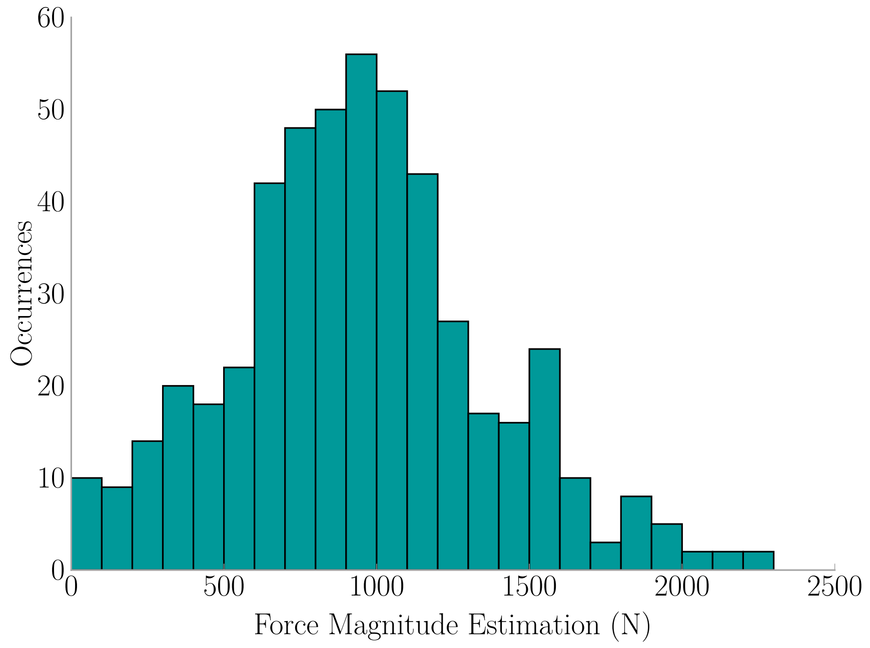

Figure 5.41: W-Jump Force Estimation Histogram

5.6 Implementation Experiment Resampled

The following describes the effect of resampling on the performance of FEEL.

5.6.1 Using Sampling Frequency of 400 Hz

The data collected during the experiment presented in Section 5.5, was downsampled to 400 Hz using the Fourier Method [21, 45]. This would determine if the higher frequencies present in the data affect the force estimate and event localization. The results presented below point towards the new rate being more effective than the original sampling rate. It is then verified that the FEEL Algorithm can be implemented at a relatively low sampling frequency to reduce computational cost.

The experiment first started with the force estimate difference for the hammer impacts as a signifier of force magnitude estimation accuracy shown in Figure 5.42. With the new sampling frequency of 400 Hz, the differences became much smaller having a mean of 109.9 N (24.7 lb) and standard deviation of 99.1 N (22.3 lb). The accuracy improved placing 85.3% of force differences within the 200 N (45 lb) range, an increase of 13.3% from the original estimates presented in Figure 5.19. The 99% confidence interval for force magnitude estimation error also improved becoming -1.7% ± 1.0% based on Figure 5.43 where the mean is -1.7% and the standard deviation is 3.5%.

The next measure was event localization accuracy which is displayed in a confusion matrix of Table 5.12. Originally across all action types, there were 3447 correctly located out of 3575 records for a 96.4% overall accuracy rate. Resampling brought the location accuracy down to 90.7% correct, or 3244 out of 3575. The event localization accuracy still remains very high showing that the FEEL Algorithm can be used for localization at lower sampling rates.

The results indicate that as one lowers the sampling rate, the location accuracy decreases, while the force magnitude estimation accuracy increases. Sampling rate

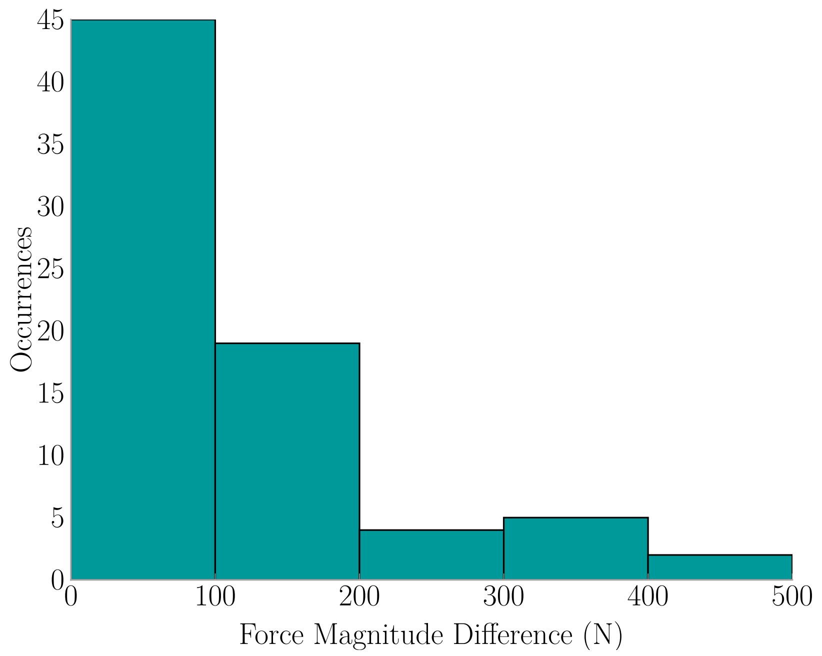

Figure 5.42: Force Magnitude Estimation Difference for Concrete Floor Impacts Using Data Downsampled to 400 Hz

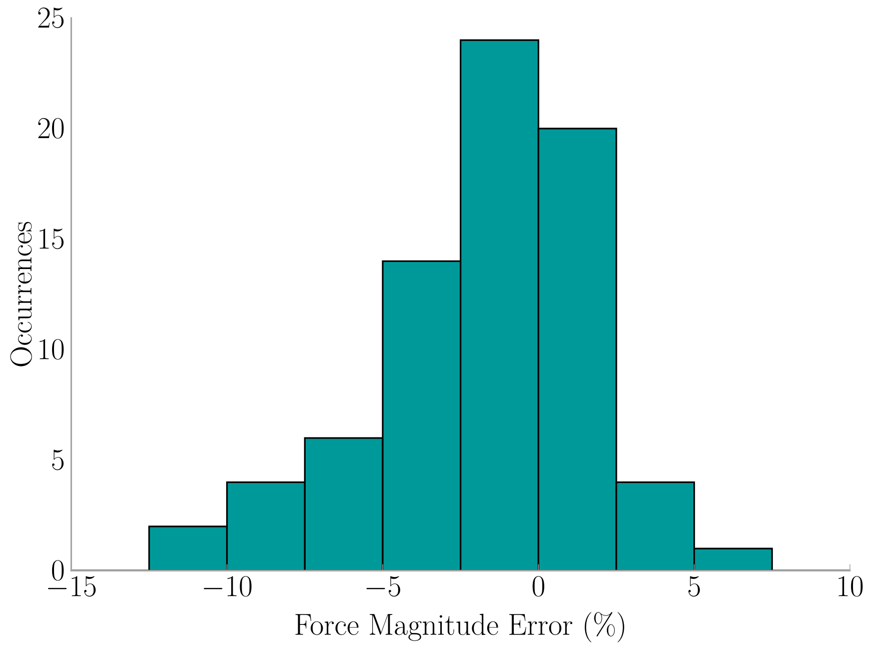

Figure 5.43: Force Magnitude Estimation Error for Concrete Floor Impacts Using Data Downsampled to 400 Hz

Table 5.12: Concrete Floor Confusion Matrix for Location Using Data Downsampled to 400 Hz

		Identified				
		Location 1	Location 2	Location 3	Location 4	Location 5
Actual	Location 1	**499**	14	18	60	124
	Location 2	8	**700**	0	3	4
	Location 3	8	13	**668**	14	12
	Location 4	0	5	0	**699**	11
	Location 5	6	20	2	9	**678**

optimization is outside the scope of this scholarly work but is something to be looked into if the desired application of the FEEL Algorithm requires the highest possible accuracy for both force estimation and event localization.

5.6.2 Upsampling From 400 Hz to 1651.7 Hz For Force Accuracy

When all data in the concrete floor experiment was downsampled to 400 Hz using the Fourier Method [21, 45], the recorded force magnitude from the impulse hammer was consequently also reduced. The accuracy might have improved between the downsampled data, but in actuality the real, true force magnitude was not there. Thus, to overcome this challenge, the 400 Hz data from Section 5.6.1 was upsampled to the original sampling frequency of 1651.7 Hz. The transfer functions used to estimate the force were generated from the original data that used the 1651.7 Hz sampling rate. Resulting was an accuracy rate near to that seen using just the original data (see Section 5.5), with 61.3% of estimations being within 200 N (45 lb) as in Figure 5.44. The results had a mean of 291.7 N (65.6 lb) and standard deviation of 406.5 N (91.4 lb). This is a 10.7% difference in accuracy than that of using the original data which had 72% of force differences fall within that range. Figure 5.45 displays the force magnitude estimate error having a mean is -4.5% and the standard deviation is 4.8%. The 99% confidence interval for the force magnitude estimate error is thus -4.5% $\pm$ 1.4%.

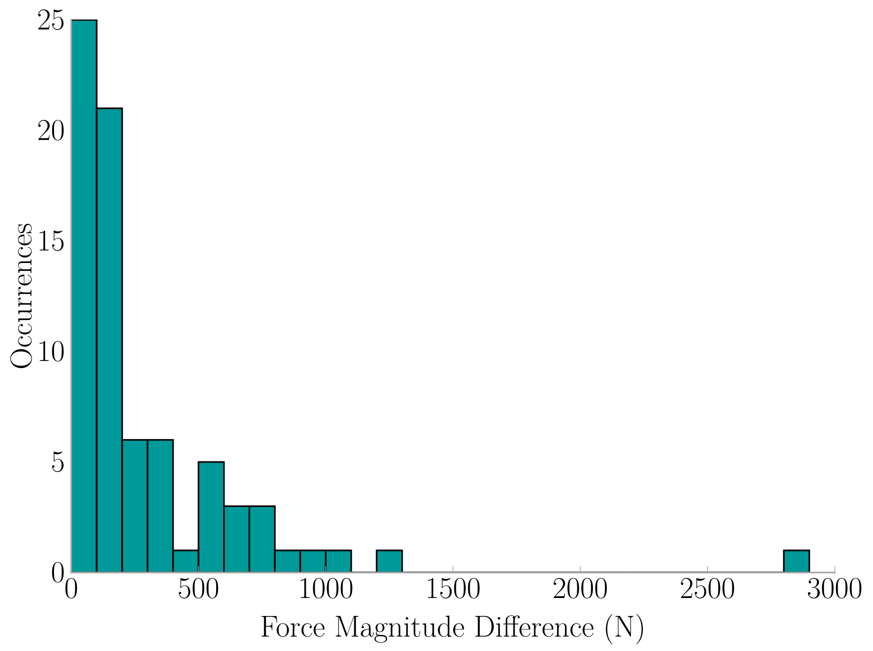

Figure 5.44: Force Magnitude Estimation for Concrete Floor Impacts Using Data Upsampled From 400 Hz to 1651.7 Hz

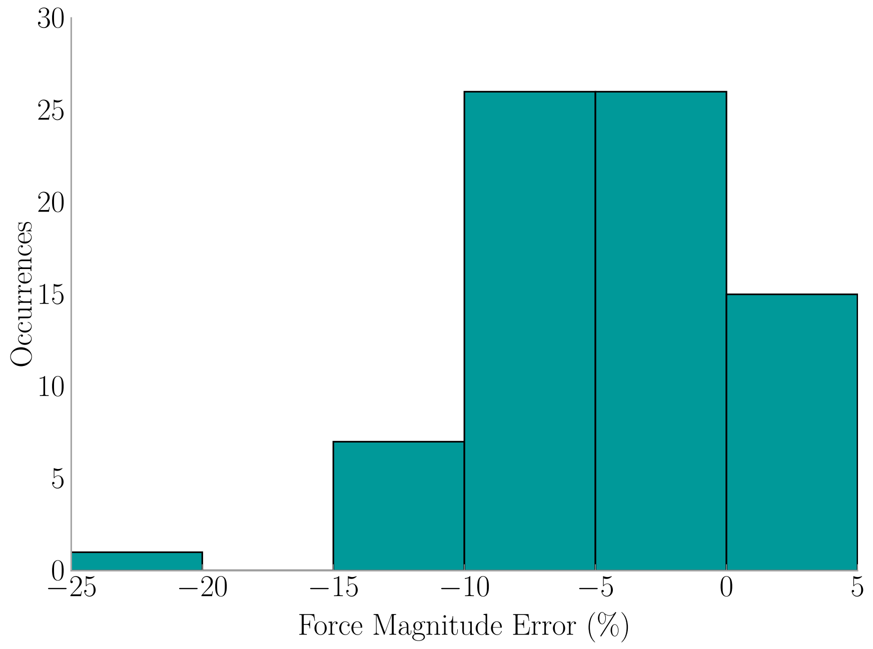

Figure 5.45: orce Magnitude Estimation Error for Concrete Floor Impacts Using Data Upsampled From 400 Hz to 1651.7 Hz

The location confusion matrix is displayed in Table 5.13. Using the upsampled data, the location accuracy decreased from 96.4%, seen in the original dataset, to 35.2%. The conclusion here is that data can be sampled at a low frequency and then upsampled to capture a magnitude closer to that of the real true impact force with a small loss in accuracy, but location accuracy significantly decreases when data is upsampled.

Table 5.13: Concrete Floor Confusion Matrix for Location Using Data Upsampled From 400 Hz to 1651.7 Hz

		Identified				
		Location 1	Location 2	Location 3	Location 4	Location 5
Actual	Location 1	**314**	109	109	93	90
	Location 2	132	**305**	138	34	106
	Location 3	149	164	**236**	88	78
	Location 4	196	116	104	**197**	102
	Location 5	130	160	149	70	**206**

5.7 Implementation Retest Experiment

Two years after the original concrete floor experiment seen in Section 5.5 was performed, a second set of experiments were performed to explore the effect that different arrangement of furniture and people has on the transfer functions. The experiment was set up to use the same equipment, sampling rate, and experimental layout (see Figure 5.14) as the first time. Various actions akin to those in the original were performed. A summary is presented in Table 5.14.

Table 5.14: Concrete Floor Retest Experiment Event Types

Event Name	Mass (kg)	Details
ball	0.6	100 cm drop
e-jump	85	female
g-jump	73	male
hammer	5.5	
l-jump	51	female

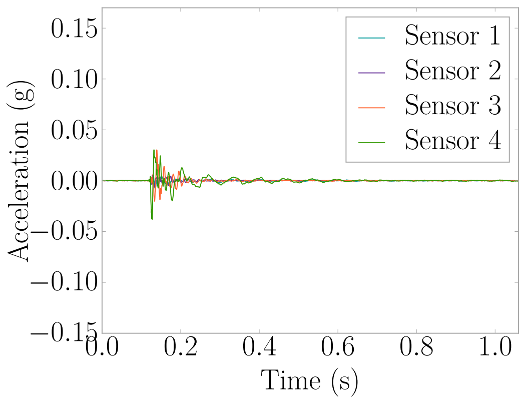

(a) Ball

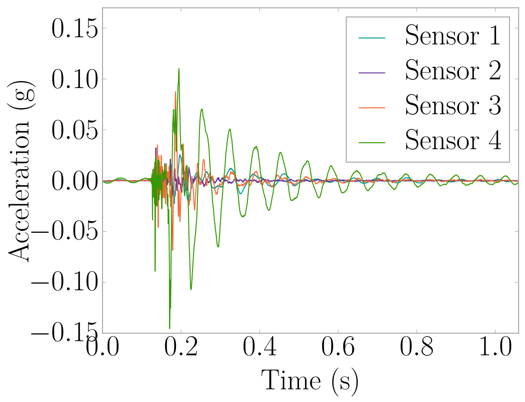

(b) E-Jump

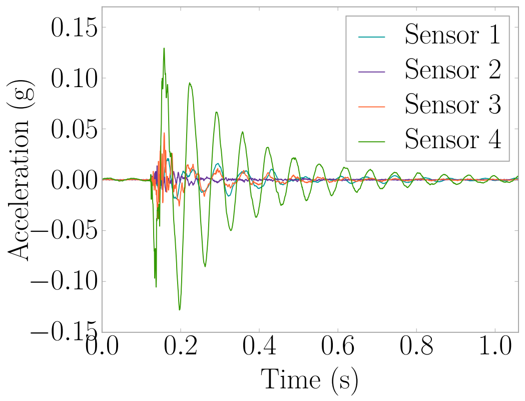

(c) G-Jump

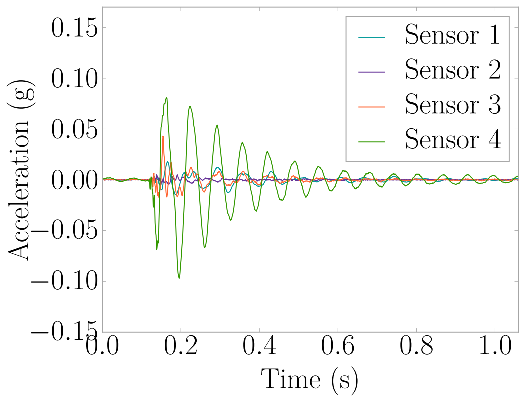

(d) L-Jump

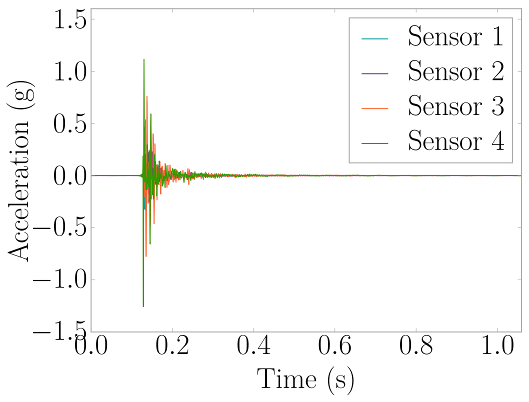

(e) Hammer

Figure 5.46: Concrete Floor Retest Experiment Example Accelerations

Each event type had five repetitions performed at five different locations for a total of 25 records per event, and giving 125 available records in total. Figure 5.46 gives example accelerations for each event type.

The transfer functions from the original dataset (Section 5.5) were applied to the 125 records of the retest dataset. Table 5.15 provides the confusion matrix for location identification, with the shaded regions indicating local areas. The ability to identify location dropped from average 96.8% correct to 70.4% with locations four and five showing the most change. With large redistribution of the loading in the room, the transfer functions have thus changed significantly at locations 4 and 5. Local area identification demonstrates 80% accuracy and indicates a good ability to perform regional localization in the face of significant change in loading.

Table 5.15: Implementation Retest Confusion Matrix for Location

		Identified				
		Location 1	Location 2	Location 3	Location 4	Location 5
Actual	Location 1	**20**	1	1	1	2
	Location 2	0	**25**	0	0	0
	Location 3	0	6	**19**	0	0
	Location 4	1	1	1	**11**	11
	Location 5	5	0	7	0	**13**

Force magnitude estimation is compared to the measured hammer force in Figure 5.47. The differences had a mean of 1533.1 N (344.7 lb) and a standard deviation of 1736.7 N (390.4 lb), indicating FEEL was having difficulty in estimating force of impact under the new loading conditions. This is further backed by Figure 5.48 which gives the 99% confidence interval for force magnitude estimation error as 16.2% ± 8.4%. In conclusion, the transfer functions should be re-calibrated when significant furniture rearrangement is done.

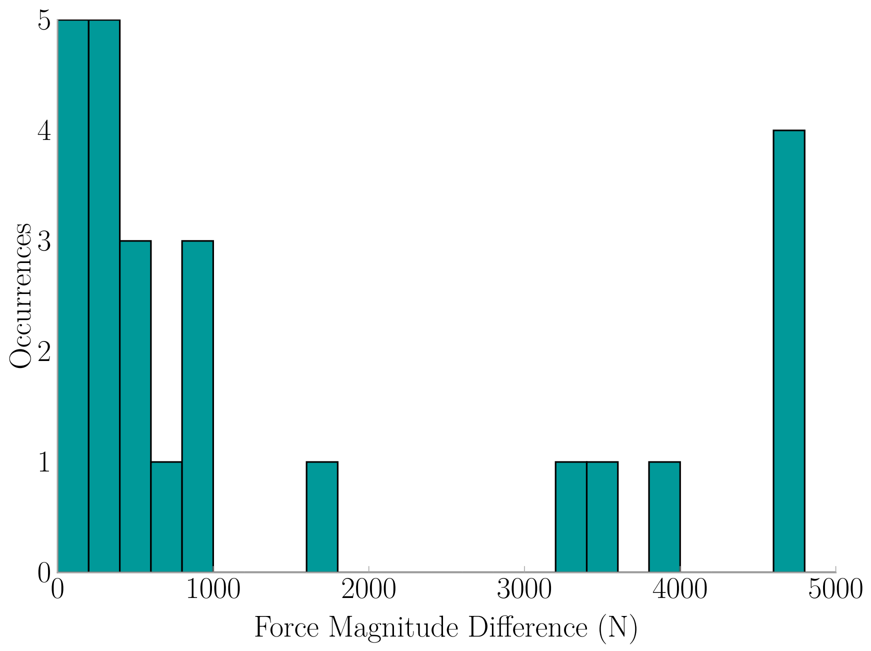

Figure 5.47: Difference Between Force Magnitude Estimation And Measured Hammer Force for Implementation Retest Experiment

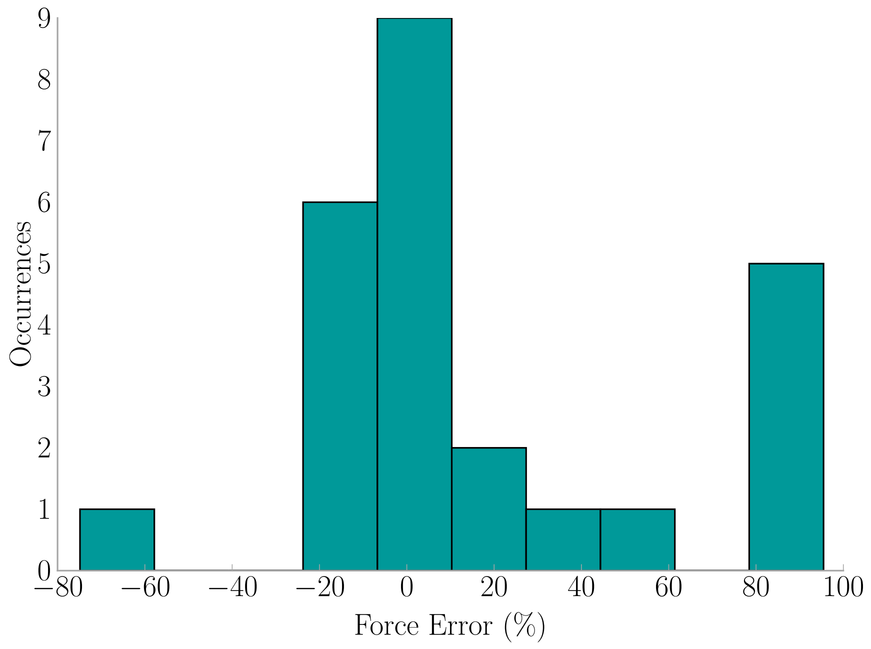

Figure 5.48: Error Between Force Magnitude Estimation And Measured Hammer Force for Implementation Retest Experiment

5.8 Conclusion

Most of the challenges faced by current detection systems based in structural vibrations are overcome through the application of the Force Estimation and Event Localization (FEEL) Algorithm. Structural vibrations, which naturally contain the dynamic attributes of the structure, are directly related to the impact force and location. Challenges arising from structural property variation are thus eliminated, and challenges of distance between a sensor and an event are overcome. Time synchronization is not required for applying FEEL, making implementation easier than other methods.

The algorithm exhibits great performance with 96.4% average accuracy in recognizing impact location in over 3575 impacts of eight different types, and having a force magnitude estimation error of -2.0% $\pm$ 1.3% for the 99% confidence interval. A brief look how FEEL works at a lower sampling rate, 400 Hz in this case, indicates that location accuracy decreases and force magnitude estimation accuracy increases when compared to a higher sampling rate of 1651.7 Hz. However, the force actually experienced by the structure is larger than what the signal captured at the lower sampling rate sees. Data can be captured at a low sampling rate and upsampled to close the gap between the force magnitude estimation and the force experienced by the structure to alleviate this problem. Upsampling, however, does not increase localization accuracy, but instead decreases it. In addition for long term implementations, there is a need to re-calibrate the transfer functions when significant furniture rearranging in an area is done to maintain FEEL's high accuracy.

Chapter 6

EFFECT Active Learning Module For The Frequency Domain

6.1 Introduction

Traditionally research dissertations focus on reporting a contribution to a specific area. However, the job of an academician goes beyond the discovery of new knowledge to disseminating that knowledge through education. Dr. Juan M. Caicedo encourages doctoral students that are interested in academia to apply to programs such as the Preparing Future Faculty program and explore other aspects of the academic life such as teaching and service [47]. He also encourages students to explore the use of effective teaching techniques by including a chapter in their dissertation focusing in education rather than research. This chapter should not be an island of the dissertation, and the topics should be relevant to those covered in the rest of the work. This chapter discusses the use of active learning, "defined as any instructional method that engages students in the learning process" [48], to teach concepts that are difficult to conceptualize in structural dynamics. These concepts are particularly important to understand the rest of the work presented herein.

Material such as that provided within this work can be difficult to grasp for students without prior knowledge in dynamics due to the complexity of many of the basic concepts. The Environments For Fostering Effective Critical Thinking (EFFECT) framework is used here to engage critical thinking skills and improve the transfer of knowledge [49, 50, 51]. EFFECT was originally created in 2008 with a focus on freshmen engineering students to increase retention and improve outcomes in the aforementioned areas and has since seen expansion to other college levels [49, 52, 53, 54]. Accreditation Board for Engineering and Technology (ABET) and American Society of Civil Engineers (ASCE) student outcomes can be addressed by each full EFFECT making it a natural choice for engineering education, particularly in the realms of communication skills, teamwork, and knowledge of contemporary issues [53]. The EFFECT developmental framework provides a procedure that guides instructors in creation of an EFFECT. The framework, in summary, follows this procedure: (1) critical concepts should be identified, (2) active learning modules are developed for those concepts, (3) context provided for the EFFECT, and (4) a driving question and supporting question for a decision worksheet are developed [55]. It is highly recommended that instructors test and perfect the active learning modules before continuing with providing a context and designing a decision worksheet.

In this work, only the first two steps are completed. The outcome is an active learning module for the concept of frequency domain representation of signals, a concept heavily used in the FEEL Algorithm seen in Chapter 5. The module provides a foundation on which to expand into a full EFFECT for areas that work with frequency domain based analysis, and will be provided on the EFFECT website (https://sdii.ce.sc.edu/effects/).

6.2 The EFFECT Pedagogical Framework

EFFECT's pedagogical framework, presented in Figure 6.1, "links the two critical elements of active learning and reflective writing" [51] to stimulate the learner to think critically about a topic presented [49, 51] and is what students experience in class. An EFFECT begins with a decision worksheet where students thoughts are framed in a design problem individually and then in concert with a group. The groups discuss their varying opinions and provide support for their arguments. Everyone has a different knowledge set, thus this encourages students to think through each others' ideas which in itself requires critical thinking or meta-cognition of what factors they do not know. Driving questions are then supported by any number of interchangeable active learning modules designed to give hands on experience to explore topics. The modules can challenge students' preconceived notions which may vary well be misconceptions, encouraging self-discovery of knowledge. After each module, students submit journal entries about class activities addressing the hows and whys the new material can aid them in the design problem. This further directs students to think deeply about a concept. The end of an EFFECT is a group and class discussion about everything that was learned to come up with their new answers to the driving question after they have corrected any misconceptions and expanded their knowledge base. Afterwards, students submit final reports with their designs [49, 50, 51].

6.3 The EFFECT Developmental Framework

The developmental framework, outlined in Figure 6.2, takes a "think big, start small" approach to creating a full EFFECT [55]. Individual elements of an EFFECT are implemented first, and then refined in an iterative process based on feedback from students and teacher evaluations of both self and the class. Items like how well did the activity work in getting the understanding across or was the activity engaging enough to encourage students to use critical thinking are of particular interest. Over time, all the individual components of an EFFECT are combined to create the full EFFECT and are linked together through a decision worksheet which has a context and a set of driving and guiding questions to direct students on the learning process [55].

The first step to creating a full EFFECT begins by the instructor identifying concepts to be taught. Following this, active learning modules are created to demonstrate the concepts through hands-on experiences, jigsaw class, or other engaging

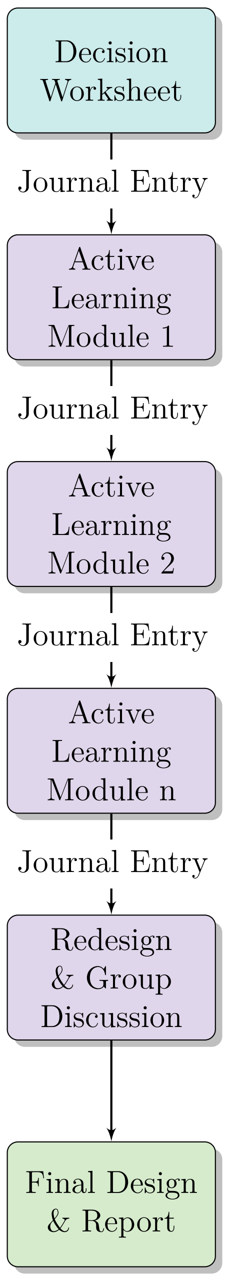

Figure 6.1: EFFECT Pedagogical Structure [49, 50, 51]

active learning techniques [56, 57, 58, 59, 60, 61, 62, 63]. These two steps are done iteratively for several classes to improve upon the active learning modules so that knowledge transfer is maximized and critical thinking is engaged. The third step is to connect the concepts to a real world application. This aids in deep learning as students link what they are seeing to something they are more familiar with or is more tangible to them. After this, a context for the application is identified, ideally an event or item that is contemporary. Finally, driving and guiding questions are created. These questions serve as a launching point for the full EFFECT to get the student engaged in a problem, and then direct their thinking through the problem. One can think of the driving question as the main goal and the guiding questions as hints to get the student thinking about the details needed to solve the main goal. The combination of the driving question, guiding questions, and context are the decision worksheet, and is what ultimately would begins a full EFFECT [55].

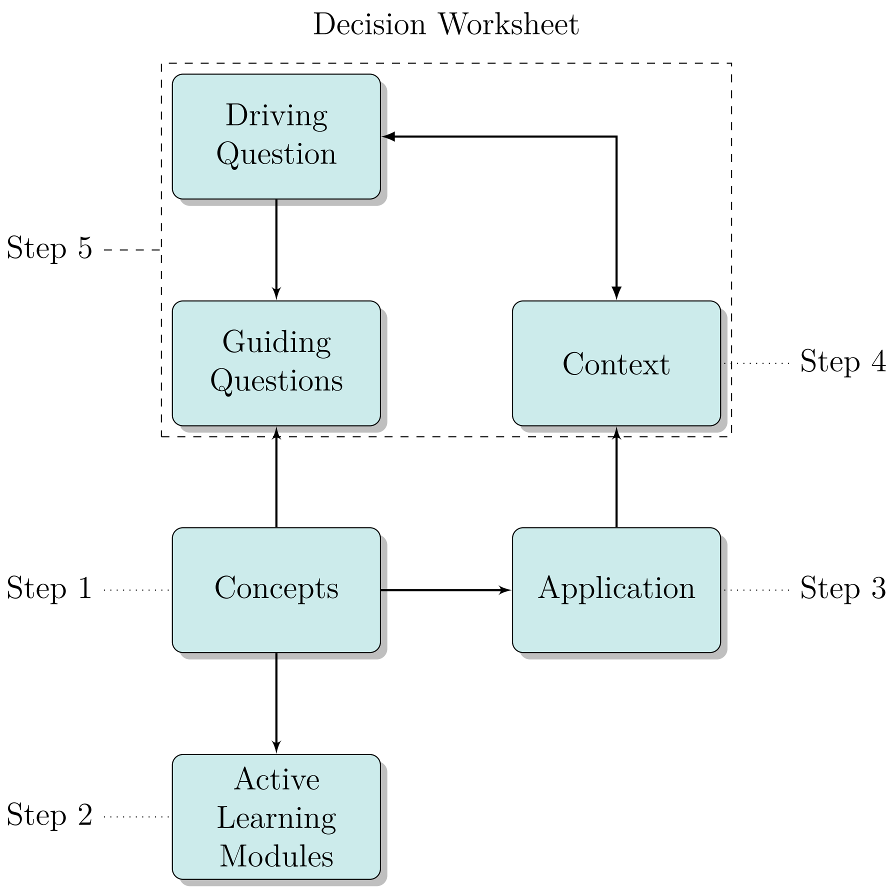

Figure 6.2: EFFECT Developmental Structure [55]

6.4 Concept Selection

Meetings with Dr. Juan M. Caicedo were spent discussing topics explored in this work to select concepts that were, based on his instruction experience, difficult for students to grasp. The concept of frequency domain representation of signals, something used heavily in the FEEL Algorithm, was identified as a difficult concept for students and is the subject of the active learning module presented in Section 6.5 [47]. Frequency domain is not as utilized or explored in basic structural dynamics classes as time domain is, and students typically think in terms of time instead of excitation frequency to the overall signal. Hence, the selected topic was chosen as the subject of an active learning module so that students can learn the concept effectively.

6.5 Active Learning Module

As a step towards creating a full EFFECT, the following active learning module was created based on the format provided from the EFFECT website [54]. The module focuses on the use of a steel frame test structure at the University of South Carolina (USC) seen in Section 5.4; however, any structure can be used provided that it has more visible responses to loading (e.g. large displacements) and one knows or can estimate the first natural frequency. This ensures the students can both feel and see what is happening with the structure. The module additionally provides the opportunity for students to improve communication and teamwork skills through a jigsaw-styled class where some students become ‘experts’ in the mathematical formulas and others in the physical results, enabling the students to teach one another. This method places emphasis on cooperation as the student group is less likely to succeed without everyone coming together as a team, thus encouraging everyone’s engagement with the subject matter [62]. Due to the potential demands of the experience, this module is designed for pairs of ‘experts’ so that students can share the demands for each piece. Students are additionally encouraged to take notes in the focus groups to additionally ease the social demand [57].

Concept Frequency domain representation of signals

Audience College Junior/Senior

Estimated Time 75 minutes

Materials

1. Steel frame (or other structure). See Section 5.4.
2. DAQ. Used NI 9234 Module.
3. Accelerometer. Used PCB 333B50.
4. Computer (to operate DAQ).
5. Hammer (for impulse excitation). Used PCB 086C03.
6. Graph paper.

Description Begin by splitting class into two halves. One half will remain in the classroom where an instructor will introduce the concept using typical classroom instruction. The other half will proceed to the location of the steel frame for a hands on explanation of the concept.

Classroom: Explain what is frequency domain is, and how it differs from the time domain we often see. Talk about how any signal can be broken down into multiple sines and cosines having their own frequency and amplitude. In other words, multiple waveforms combine together to form a signal much like multiple instruments make up an orchestra, and one hears all the instruments together or can focus in on one particular instrument, i.e. a specific waveform within the greater signal. Talk about the math for converting a time domain signal into frequency domain through the

Fourier Transform. A handout to aid with instruction on the topic is provided in Appendix J.

Laboratory: Start by explaining what frequency domain is, and how it differs from the time domain we often see. Talk about how any signal can be broken down into multiple waveforms having their own frequency. Have the students plot their prediction of what a 1 Hz harmonic loading would look like in the frequency domain. Then ask the students to push the frame at an approximate rate of 1 Hz, recording the accelerations. Using software such as Signal Express, convert the recorded time domain data into frequency domain and plot for the students to see. Prompt them to talk about the differences between their predictions and the result from the experiment. Repeat the prediction and experiment for two other excitation frequencies: 5 Hz and 10 Hz.

If using a different structure than the steel frame, choose three rates where one is less than the first natural frequency, one about the first natural frequency, and finally, one after the first natural frequency. This will give the same outcome as the steel frame.

Combined Groups: After each respective group (classroom and laboratory) is done, bring the laboratory group back to the classroom. Take groups of four with two from the initial classroom group and two from the initial laboratory group. Have the student groups relate the classroom instruction to the instruction the laboratory students had. Have the students come up with an idea of what is happening in various parts of the graph. Students will then present what they have learned to the class, with the instructors prompting for other groups who have different explanations.

The groups will then be asked to come up with an estimate of what would happen if the steel frame came under simultaneous loadings, one loading at each of the rates used previously (1 Hz, 5 Hz, 10 Hz). Then ask them what they would expect a hammer hit would look like in the frequency domain. Each group should generate a new set of response vs. frequency plots for the two cases. Instructor prompts for groups to describe their plots and reasoning for their expected results.

Take the whole class back to the laboratory with the steel frame. Have three different students apply a loading at the three rates simultaneously. On Signal Express, the frequency representation of the signal can be updated in real time so that the students may compare their estimates to reality. Ask them about the differences between what they thought and what the results are showing. Why do the results look that way?

Repeat the experiment using the hammer to excite the structure. Plot the frequency domain representation of the signal. Ask the students about the differences between what they thought and what the results are showing. Why do the results look that way? What do the peaks in the frequency domain mean? Discuss what the students observed and how/why their thinking differs from reality.

Expected Outcomes The expected outcomes include students learning about that signals can be represented in different domains, the frequency domain in particular. Students are expected to begin to understand a relationship between structural response in the time domain and power in the frequency domain, and that one signal can be broken into multiple sinusoidals that have their own frequencies. The concept of superposition can be reinforced with discussions on why multiple signals can be combined into one as well.

Students are expected to begin answering questions about the frequency domain as if it is the time domain. After a few experiments and discuss, students then are expected to realize the frequency domain operates differently than the time domain and be able to correctly predict what the signal representation in the frequency domain looks like.

6.6 Conclusion

The active learning module was used in a structural vibrations engineering class at USC having fifteen students. In the class period after the module, an anonymous survey (see Appendix K) was administered to gain feedback from students on how to improve the module and nine students responded. Survey responses are provided in Appendix L, and a summary of scores is provided in Table 6.1 where a score of one is not conducive/confident and a score of five is conducive/confident.

A post-class interview with the instructor indicated that the scores presented in Table 6.1 were representative of exam performance in each topic [64]. Confidence scores for Single Degree of Freedom (SDOF) Periodic Excitation and Frequency Domain Signal Representation confirms that they are topics that are challenging for students, i.e. they perceive the topics as being challenging, as thought by the instructor. Surveys were not taken in prior years, so a similar survey needs to be done in subsequent years (longitudinal study) to see if student mean confidence increases.

The breakdown of scores by students' expected grades are displayed in Figure 6.3. All students regardless of expected grade thought the class lectures were all very conducive to their learning. In-class homeworks were not regarded as conducive with a student commenting on how he felt the format was more like a quiz than a homework with the instructor not providing much aid. The project was considered conducive, however, some students wanted more guidance or instruction before tackling the assignment.

Experiments and lab visits were regarded as conducive, with student responses to Question 6 (Did the lab visit make the connection between math and physics easier to understand? How or why?) reinforcing scores in Question 3 (Indicate how conducive to learning the following course activities were.). Figure 6.4 displays the breakdown of responses for Question 6.a where students were asked if the lab visit allowed them to

Table 6.1: Question Statistics for Conducive/Confidence Questions

Question	Mean	St. Dev.
Indicate how conducive to learning the following course activities were.		
(a) Lectures	5.0	0.0
(b) In-Class Homework	4.0	1.2
(c) Experiments and Lab Visits	4.1	0.8
(d) Project	4.2	0.7
How confident do you feel about the following topics?		
(a) SDOF Free Vibration	4.7	0.5
(b) SDOF Harmonic Excitation	4.7	0.5
(c) SDOF Periodic Excitation	2.7	1.2
(d) SDOF Impulse Excitation	4.2	1.1
(e) SDOF Arbitrary Excitation	4.1	1.1
(f) Applying the Central Difference Method	3.1	1.1
(g) Frequency Domain Signal Representation	2.0	0.9

*number of survey responses = 9

grasp the connection between math and physics. Seven out of nine students indicated 'yes' with comments suggesting that seeing the structure respond to the excitation and then seeing the recorded data displayed graphically gave a better sense of the physics that the math was describing. The two students answering 'no' indicated they felt like they did not have enough time to discuss what was happening and did not get to see the whole experiment. These two students were likely in the classroom group who only got to see half of the experiments. What group the survey taker participated in was not asked for on the survey but should be added in future surveys so further insights can be made. Interestingly enough, students who thought they would receive a grade of C or D in the class responded 'yes' along with all of the students expecting a grade of A suggesting hands-on learning is an effective teaching tool. Potentially by adding more hands-on activities to classes, students who otherwise would expect a low grade (i.e. <B) would become more engaged with the material [65, 66].

When looking at Question 4 (How confident do you feel about the following top-

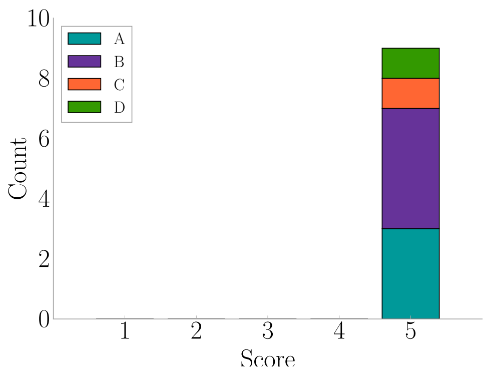

(a) Lectures

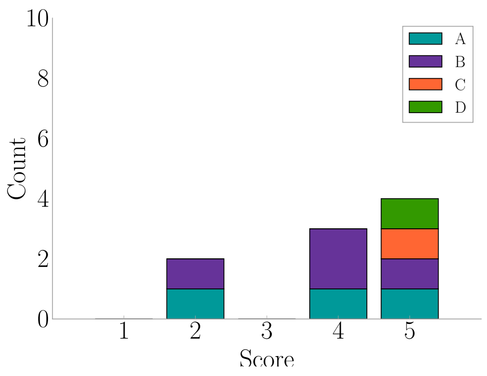

(b) In-Class Homework

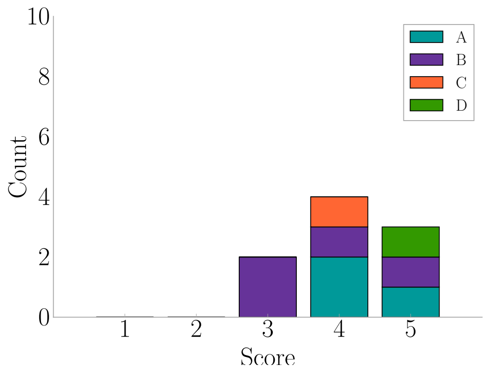

(c) Experiments and Lab Visits

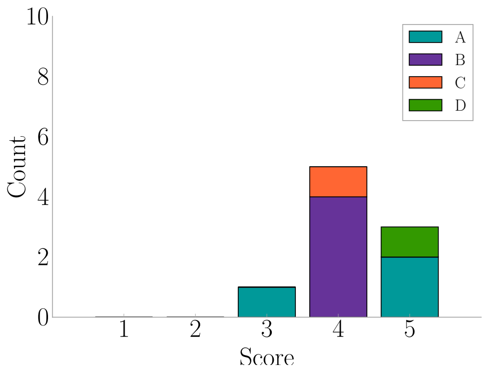

(d) Project

Figure 6.3: Distribution of Responses Broken Down by Students' Expected Grade for Question 3 "Indicate How Conducive to Learning The Following Course Activities Were"

ics.) which served to indicate how confident students felt on their grasp of concepts presented in the class, there were mixed results as seen in Figure 6.5. Free vibration and harmonic excitation are topics the students felt confident about, and are also topics taught at the beginning of the semester. Periodic and impulse excitation are more complex topics, with the students reporting varying levels of confidence levels. Students reported having more confidence with arbitrary excitation even though this topic is 'an extension' of impulse excitation. The central difference method had an mean score of 3.1 showing students had a moderate confidence level about the topic. Of particular interest to the author is the scores for the frequency domain representation which was only taught through the active learning module for a single class period. Students reported not being very confident (score ≤ 3) which suggests some

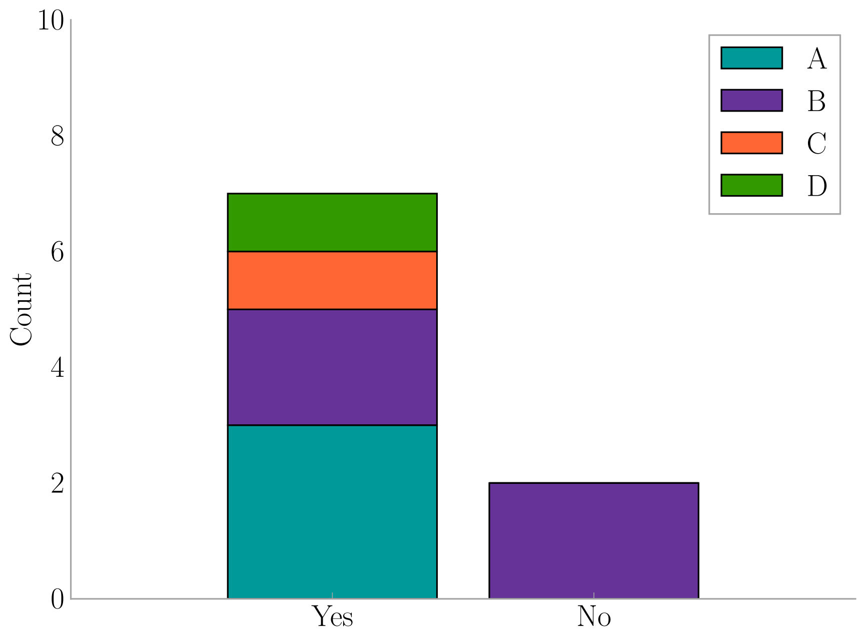

Figure 6.4: Distribution of Responses Broken Down by Students' Expected Grade for Question 6.a "Did The Lab Visit Make The Connection Between Math and Physics Easier to Understand?"

refinement in the module or additional modules are required to aid learning in the subject. In addition, the survey should be administered in the future to determine how the active learning module affects students perceptions on this topic.

Student responses to Question 2 (What have you learned in this class?) provided some insight into what topics students retained. There were many mentions of learning about various types of excitation and structural properties, which were taught throughout the semesters. Interestingly, a student mentioned the Fourier Transform by name, another about experimentally testing structures, and another about what causes failure in a structure. These are things taught in the single class period using the active learning module, which suggests the module aided in engaging students.

When asked to suggest improvements to the class, some students responded with praise for the hands-on activities finding "them useful and engaging" and the "extracurricular feel [...] adds to the course." Other suggestions included for the instructor to give an overview of concepts to be thinking about during the experiments or to have more class discussion in addition to the 'expert' groups. A few responses asked for more time to work with the material and to get to see all of the experiments. This thought is further backed by instructors' observation that the classroom group of students asked more questions to gain understanding of the base concepts whereas the experiment group was able to piece the concepts together and ask more application

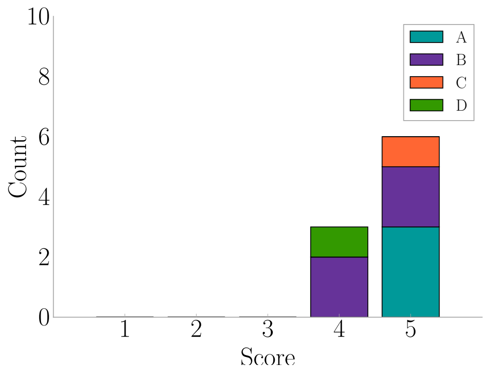

(a) SDOF Free Vibration

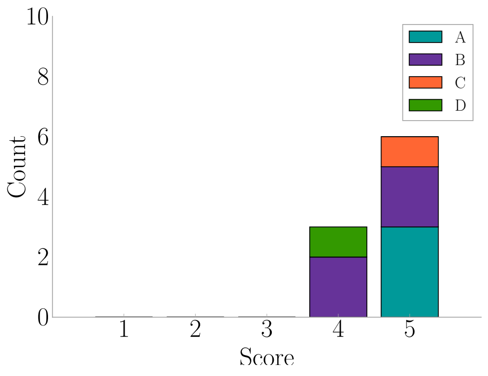

(b) SDOF Harmonic Excitation

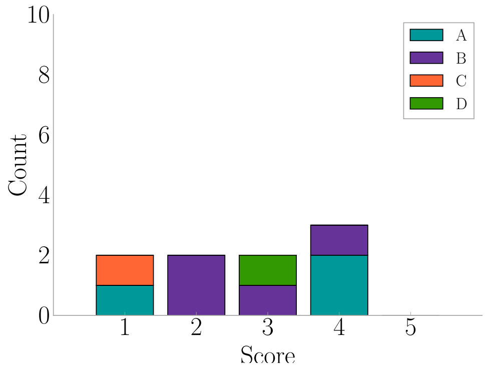

(c) SDOF Periodic Excitation

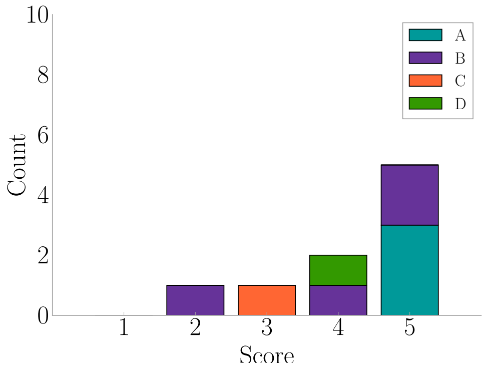

(d) SDOF Impulse Excitation

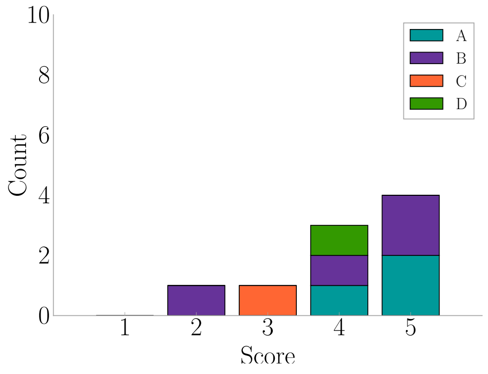

(e) SDOF Arbitrary Excitation

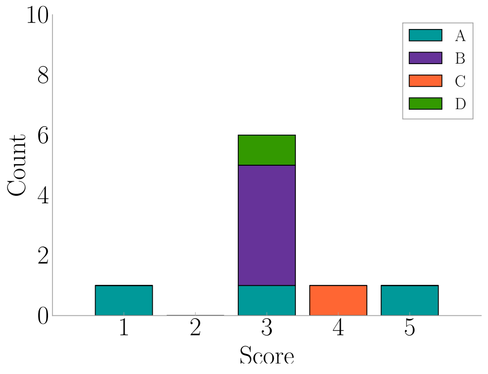

(f) Applying the Central Difference Method

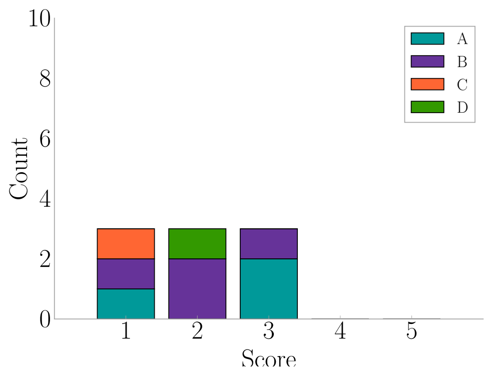

(g) Frequency Domain Signal Representation

Figure 6.5: Distribution of Responses Broken Down by Students' Expected Grade for Question 4 "How Confident Do You Feel About The Following Topics?"

questions. In the future, it is suggested to split the module across two class periods where the whole class can have a chance to do all the experiments and get all of the classroom instruction before teams are formed for the final experiment. This will enable each student to gain more experience and time with the concepts presented.

Another outcome of the class is that the students were able to connect the concept of superposition to why signals can be broken down into multiple sinusoidals having their own frequency, and further acknowledge that superposition only works in the case of linear structures. They continued this thinking and asked questions about if a structure will fail if an earthquake with large enough amplitude, as shown in the frequency domain representation, excites the structure.

Students were observed in the experimental group progressively understanding that the frequency domain works differently from the time domain. For the first experiment to excite the structure, students predicted the time domain response with a signal having a sinusoidal shape and the frequency domain response as having much the same look. The third experiment (harmonic excitation of about 10 Hz) saw predictions for the time domain and frequency domain being correct, with the experimental results validating the students predictions. One of the whole class experiments was not performed due to time constraints, but the impulse experiment saw students connecting how an impulse excites the natural frequencies of a structure and further seeing students realize a structure has many natural frequencies, not just one.

Overall, the active learning module appears to have encouraged students' critical thinking and engagement. Future iterations to better refine the module are suggested to (1) expand the module over two class periods, (2) to allow the entire class to cycle through the experiments, and (3) provide ample time for discussion and demonstrations during classroom instruction.

Chapter 7
Conclusion

Wireless smart accelerometers were implemented in system boasting a star network topology which allowed for each sensor to operate independently to dynamically adjust to their respective local environment. The sensors themselves, had a success rate of 62% in capturing the falls reported by the study participants. Falls missed by the sensors were likely due to low-force impacts that would not have resulted in severe injury. The remaining fall events missed were due to several failures modes, the most predominant of which being the power supply to the sensors being mistaken for a phone charger. Together, the accelerometers experienced a wear out failure trend with a $5.06 \times 10^{-3} \frac{\text{failures}}{\text{hour}}$ failure rate and a 197.7 hours Mean Time Between Failure (MTBF). This equates to a 4.9% chance to capture a human fall in a year. A successful system would instead need a 99% chance to capture a fall, which means a MTBF of 8642.4 hours is required for the sensors.

Other characteristic recommendations for the wireless accelerometers emerged when working with the vibration monitoring system. The 16 human fall events captured by the system indicate a buffer size of 3 s suggested by Yu is sufficient to capture the full waveform, and important aspect when dealing with limited resources of an embedded sensor [6]. A sampling rate of 316 Hz was used by the Camp Hill/Agua Mansa and worked well. The more common sampling rate of 400 Hz is suggested as it is a more typical rate and will provide more definition in the signal. Installed sensors operated using 0.25 mg resolution and ± 2 g range. The range proved to be large enough based on the falls recorded. The resolution, however, was not sharp enough in several cases and may have contributed to the sensors missing low-force falls. A resolution of 1 µg would provide greater definition, and a better chance for registering human falls resulting in low amplitude accelerations. These three general characteristics were chosen as they are applicable in any situation. Sensor characteristics like operational temperature range are not explored since they are related to the environment a sensor would be in, thus making those characteristics better chosen by case.

Large amounts of data were generated whilst monitoring structural vibrations at both the hospital and private home. A data management plan was developed using a relation database architecture and online tools, and accompanied by a Python package to streamline access to the information. The plan proved to be robust and provided much needed infrastructure to handle the information generated by the study. In fact, the infrastructure allowed for the researchers to discover the possible connection between vibrations and human activity.

The installed systems recorded data that demonstrated a potential way to analyze human activity patterns from the structural vibrations produced. General schedules of those in the hospital and private residence closely relate to the amount of accelerations seen by installed sensors, indicating the possibility. This area of study could result in predictive activity models that could create more intelligent infrastructure to adjust to the needs of the human residing.

A way to choose quality acceleration signals became of interest in the face of a human activity database comprising 536,686 acceleration records. Machine learning through Support Vector Machine (SVM) utilizing typical and new signal metrics were used with high accuracy in the classification results. The radial basis function (RBF) kernel was the most robust of the kernels tested, reaching a mean accuracy of 96.8% with a standard deviation of 3.4% in 100 trials. The linear kernel came in second, reaching a mean accuracy of 95.7% with a standard deviation of 3.2% in 100 trials.

Of the metric combinations used, the Dispersion Ratio (DR) proved to be the best one its own. DR scored higher than the other metrics when used on its own in the linear and RBF kernels, and increased the score of the metric combinations it was involved in. When looking at the score distributions for each metric combination, this becomes apparent as one can see that combinations with DR have distributions like that of DR alone, placing accuracy scores almost entirely in the 95%-100% range.

The RBF kernel was used in combination with the DR metric to classify all the acceleration records in the human activity database using only 200 manually classified records for training - a mere 0.04% of the entire database. The small amount of training records required make this machine learning method very time-efficient to implement. Preprocessing of records with sensor errors or records with missing data points resulted in the removal of 273,422 records from the dataset. The remaining were classified as exhibiting lots of noise with little to no data (category one: 203,964), having some activity but indistinct peaks or shape (category two: 33,972), and having distinct peaks or shape (category three: 25,321). Seven records were ignored as their value of DR was infinity indicating a signal having one value for every time step. This, and the low computational cost of SVMs and the DR metric, indicates the possibility that the SVM could also be implemented at the sensor level to great effect, reducing the amount of data to be processed at a centralized hub.

Investigating how the SVM classified researcher's identified human fall vibration events was of particular interest to the author. The fall records were classified primarily as category two and category three, which, in an implementation scenario, would indicate the data was good for analysis. A few acceleration records were ignored as preprocessing identified them as having a missing data point. The effectiveness of the SVM could still be high if the rule on missing data points was relaxed some, and is something to be explored in the future.

The development of the Force Estimation and Event Localization (FEEL) Algorithm furthers knowledge of structural dynamics and overcomes most challenges of other fall detection techniques based in structural vibrations, including the estimation of structural characteristics such as stiffness and acceleration amplitudes experienced by the sensors being affected by distance to the impact. FEEL operates by first calibrating likely fall locations around a structure and directly relating structural vibrations, which naturally contain the dynamic characteristics of the structure, to force and location of an impact - thus overcoming the aforementioned challenges. Additionally, sensors do not need to be time-synchronized as FEEL primarily operates in the frequency domain, which makes the algorithm easier to implement and less costly, computation-wise, to use.

FEEL was tested using more than 3500 combined impacts on a concrete floor at five different locations and of eight different types (e.g. ball drop, human jump), showing great performance. Impact location was identified with an average of 96.4% accuracy, and the force magnitude estimate error was -2.0% $\pm$ 1.3% for the 99% confidence interval.

Sampling rates were shown to have an effect on performance of FEEL. Lower rates reduce location accuracy and increase force magnitude accuracy, yet, the force actually experienced by the structure is larger than that recorded at a lower sampling rate. This is because the lower sampling rate can miss part of the true signal. To alleviate this issue, data can be resampled to a higher rate to get closer to the true force magnitude quantity. Upsampling from the lower rate does not improve location accuracy however.

The Environments For Fostering Effective Critical Thinking (EFFECT) active learning module on the frequency domain representation of signals had interesting outcomes. Students surveyed found experiments and lab visits to be conducive to learning. A large majority additionally indicated that lab visits made the connection between math and physics easier to understand, suggesting hands-on learning is an effective teaching tool. Instructor observations reinforce this idea as they noticed students who were in the lab group grasped the concepts better based on their responses to questions. Yet, frequency domain signal representation on a scale of 1 (not confident) to 5 (confident) scored the lowest of all the topics surveyed having a mean confidence score of 2 and a 0.9 standard deviation. Students found the activity “useful and engaging” while that having an “extracurricular feel [...] adds to the course”, with a few responses indicating students would like more time with the material which could possibly increase their confidence with the concept. In the future, splitting the module across multiple class periods so that each student group gets time in the classroom and the lab could be beneficial to learning.

Another outcome of the module was that students connected the concept of superposition to why the Fourier Transform can break a signal down into multiple sinusoidals each having its own frequency, and they further were able to acknowledge that superposition can only be used in linear structures. More thinking on the topic and students arrived at questions about if a structure will fail during an earthquake if a large enough amplitude, shown in the frequency domain representation, excites the structure. Students also began to realize that structures have multiple natural frequencies, not just one as they had seen previously in Single Degree of Freedom (SDOF) cases.

The whole of this contribution provides deeper knowledge into vibrations from human activity, and in particular, human fall detection using force of impact. The system design and data management plans pave the way for implementation and enable further collection of vibration-based analysis of human activity, whilst serving as guidelines for other projects. The human activity database housed at the Structural Dynamics and Intelligent Infrastructure Laboratory (SDII) at the University of South Carolina (USC) provides a large conglomerate of structural vibration records, including 16 human fall events, for future researchers to analyze and test new algorithms against. Acceleration event classification reduces the amount of data to be processed, so a system can operate more efficiently or relevant data can be chosen effectively. Information provided by FEEL can reduce response times to fall events and give doctors more insight to the incident, and, more broadly, enable analysis of other types of impacts on structures.

7.1 Future Work

Research into modeling human activity from structural vibrations would provide avenues for predicting a condition change of the user, such as the possibility of an oncoming fall. More work into using SVM classifiers for signal selection, such as manually categorizing more records in the human activity database and comparing to the SVM results, would provide more insight into effectiveness of the method. Exploring how to optimize signal preprocessing before applying the SVM, would also be of interest. Forays into how to best place and use calibration points for FEEL would be a great addition to it's body of knowledge. Finally, capturing falls in a room calibrated by FEEL and applying the algorithm, would validate FEEL in regards to human fall detection.

References

[1] Robert Frost. “The Road Not Taken”. In: *Mountain Interval*. 1916.

[2] Centers for Disease Control and Prevention. *The State of Aging and Health in America*. Report. Atlanta, GA: US Department of Health and Human Services, 2013.

[3] Centers for Disease Control and Prevention. *Falls Among Older Adults*. Tech. rep. US Department of Health and Human Services, Sept. 2014. URL: http://www.cdc.gov/HomeandRecreationalSafety/Falls/adultfalls.html.

[4] *Learn Not To Fall*. Philips Lifeline. Dec. 2014. URL: http://www.learnnottofall.com/ (visited on 12/18/2014).

[5] Majd Alwan et al. “A Smart and Passive Floor-Vibration Based Fall Detector for Elderly”. In: *Information and Communication Technologies, 2006. ICTTA '06. 2nd*. Vol. 1. 2006, pp. 1003–1007. DOI: 10.1109/ICTTA.2006.1684511.

[6] Xinguo Yu. “Approaches and Principles of Fall Detection for Elderly and Patient”. In: *10th Annual IEEE International Conference on e-Health Networking, Applications, and Service*. IEEE, July 2008, pp. 42–47. DOI: 10.1109/HEALTH.2008.4600107.

[7] *Saving a Life from Potential Catastrophe Every 10 Minutes*. Life Alert. 2014. URL: http://www.lifealert.com/ (visited on 12/19/2014).

[8] Michael Belshaw et al. “Towards a Single Sensor Passive Solution for Automated Fall Detection”. In: *Annual International Conference of the IEEE Engineering in Medicine and Biology Society*. IEEE Engineering in Medicine and Biology Society, 2011, pp. 1773–1776. DOI: 10.1109/IEMBS.2011.6090506.

[9] Andrew Sixsmith and Neil Johnson. “A Smart Sensor to Detect the Falls of the Elderly”. In: *Pervasive Computing, IEEE* 3.2 (2 Apr. 2004), pp. 42–47. ISSN: 1536-1268. DOI: 10.1109/MPRV.2004.1316817.

[10] Kateryna Rybina, Maksym Ternovoy, and Waltenegus Dargie. *Expressiveness of Time Domain Features for Detecting Different Types of Human Movements*. Conference. Lviv-Slaske, Ukraine: TCSET, Feb. 2010.

[11] Waltenegus Dargie. "Analysis of Time and Frequency Domain Features of Accelerometer Measurements". In: *International Conference on Computer Communications and Networks*. San Francisco, CA: IEEE, Aug. 2009, pp. 1–6. ISBN: 978-1-4244-4581-3. DOI: 10.1109/ICCCN.2009.5235366.

[12] Jin Wang et al. "Recognizing Human Daily Activities from Accelerometer Signal". In: *Advanced in Control Engineering and Information Science* 15 (2011), pp. 1780–1786. DOI: 10.1016/j.proeng.2011.08.331.

[13] Yaniv Zigel, Dima Litvak, and Israel Gannot. "A Method for Automatic Fall Detection of Elderly People using Floor Vibrations and Sound - Proof od Concept on Human Mimicking Doll Falls". In: *IEEE Transactions on Biomedical Engineering* 56.12 (Dec. 2009). DOI: 10.1109/TBME.2009.2030171.

[14] Tom Irvine. *An Introduction to the Shock Response Spectrum*. July 2012. URL: http://www.vibrationdata.com/tutorials2/srs_intr.pdf (visited on 12/18/2014).

[15] Benjamin T. Davis et al. "Use of Wireless Smart Sensors for Detecting Human Falls through Structural Vibrations". In: *Civil Engineering Topics*. Ed. by Tom Proulx. Vol. 4. Conference Proceedings of the Society for Experimental Mechanics Series. Springer New York, 2011, pp. 383–389. DOI: 10.1007/978-1-4419-9316-8_37.

[16] Shinae Jang and Jennifer Rice. *Calibration Guide for Wireless Sensors*. Illinois Structural Health Monitoring Project. 2009.

[17] Rahul C. Shah et al. "Data MULEs: Modeling and Analysis of a Three-Tier Architecture for Sparse Sensor Networks". In: *Ad Hoc Networks* (2003), pp. 215–233.

[18] Eric E. Ungar. "Vibration Criteria for Healthcare Facility Floors". In: *Journal of Sound and Vibration* (Sept. 2007), pp. 26–27.

[19] NIST. *SEMATECH e-Handbook of Statistical Methods*. U.S. Department of Commerce. Oct. 2013. URL: http://www.itl.nist.gov/div898/handbook/ (visited on 11/10/2015).

[20] Scott Speaks. *Reliability and MTBF Overview*. Vicor Power. URL: http://www.vicorpower.com/documents/quality/Rel_MTBF.pdf (visited on 11/10/2015).

[21] *SciPy*. The Scipy Community. Sept. 2015. URL: http://scipy.org/ (visited on 03/21/2016).

[22] *Data Curation*. English. Council on Library and Information Resources. 2014. URL: http://www.clir.org/initiatives-partnerships/data-curation (visited on 03/01/2016).

[23] Dries Buyaert. *Drupal*. English. Drupal. Mar. 2016. URL: https://www.drupal.com/ (visited on 03/23/2016).

[24] *MySQL: The world's most popular open source database*. English. Oracle. Mar. 2016. URL: https://www.mysql.com/ (visited on 03/21/2016).

[25] Bernhard E. Boser, Isabelle M. Guyon, and Vladimir N. Vapnik. "A Training Algorithm for Optimal Margin Classifiers". In: *Proceedings of the Fifth Annual Workshop on Computational Learning Theory*. COLT '92. Pittsburgh, Pennsylvania, USA: ACM, 1992, pp. 144–152. ISBN: 0-89791-497-X. DOI: 10.1145/130385.130401. URL: http://doi.acm.org/10.1145/130385.130401.

[26] I. Guyon, B. Boser, and V. Vapnik. "Automatic Capacity Tuning of Very Large VC-Dimension Classifiers". In: *Advances in Neural Information Processing Systems*. Morgan Kaufmann, 1993, pp. 147–155.

[27] Corinna Cortes and Vladimir Vapnik. "Support-Vector Networks". In: *Machine Learning* 20.3 (Sept. 1995), pp. 273–297. ISSN: 0885-6125. DOI: 10.1023/A:1022627411411. URL: http://dx.doi.org/10.1023/A:1022627411411.

[28] Martin Sewell. *Support Vector Machines (SVMs)*. 2006. URL: http://www.svms.org/ (visited on 04/12/2016).

[29] Youn-Jung Son et al. "Application of Support Vector Machine For Prediction of Medication Adherence in Heart Failure Patients". In: *Healthcare Informatics Research* 16 (4 2010), pp. 253–259. DOI: 10.4258/hir.2010.16.4.253.

[30] R. Han et al. "Application of Support Vector Machine to Mobile Communications in Telephone Traffic Load of Monthly Busy Hour Prediction". In: *2009 Fifth International Conference on Natural Computation*. Vol. 3. 2009, pp. 349–353. DOI: 10.1109/ICNC.2009.96.

[31] William S. Noble. “What is a Support Vector Machine”. In: *Nature Biotechnology. Computational Biology* 24.12 (2006), pp. 1565–1567. DOI: 10.1038/nbt1206-1565.

[32] Scikit-Learn Developers. *Support Vector Machines*. Scikit-Learn. 2015. URL: http://scikit-learn.org/stable/modules/svm.html# (visited on 07/01/2015).

[33] Ting-Fan Wu, Chih-Jen Lin, and Ruby C. Weng. “Probability Estimates for Multi-Class Classification by Pairwise Coupling”. In: *Journal of Machine Learning Research* 5 (Aug. 2004). Ed. by Yoram Singer, pp. 975–1005.

[34] Nick Bunkley. *Joseph Juran, 103, Pioneer in Quality Control, Dies*. New York Times. May 3, 2008. URL: http://www.nytimes.com/2008/03/03/business/03juran.html?_r=0 (visited on 10/05/2016).

[35] Benjamin T. Davis and Juan M. Caicedo. “Impact Force Estimation and Event Localization”. Pat. 62/324,468 (United States of America). University of South Carolina. Apr. 19, 2016.

[36] D. J. Erwins. *Modal Testing: Theory, Practice and Application*. 2nd. Philadelphia: Research Studies Press Ltd., 2003. ISBN: 0863802184.

[37] Julius S. Bendat and Allan G. Peirsol. *Random Data: Analysis and Measurement Procedures*. 3rd. John Wiley & Sons, Inc., 2000. ISBN: 0471317330.

[38] Frank Parker Stockbridge. “How Far Off Is That German Gun”. In: *Popular Science* (Dec. 1918), p. 39. URL: https://books.google.com/books?id=EikDAAAAMBAJ&pg=PA39#v=onepage&q&f=false.

[39] Yiu-Tong Chan et al. “Time-of-Arrival Based Localization Under NLOS Conditions”. In: *IEEE Transactions on Vehicular Technology* 55.1 (Jan. 2006), pp. 14–24. DOI: 10.1109/TVT.2005.861207.

[40] Explorable.com. *Pearson Product-Moment Correlation*. Oct. 8, 2009. URL: https://explorable.com/pearson-product-moment-correlation (visited on 04/10/2016).

[41] *Resampling*. English. The MathWorks, Inc. 2016. URL: http://www.mathworks.com/help/signal/ug/resampling.html (visited on 03/21/2016).

[42] Andrew Greensted. *FIR Filter by Windowing*. English. The Lab Book Pages. May 2010. URL: http://www.labbookpages.co.uk/audio/firWindowing.html (visited on 03/21/2016).

[43] Nguyen Huu Phuong. *FIR Filter Design: The Window Design Method*. English. Rice University. Mar. 2016. URL: http://cnx.org/contents/2YEHwQYh@1/FIR-FILTER-DESIGN-THE-WINDOW-D (visited on 03/22/2016).

[44] J. F. Kaiser. “Nonrecursive Digital Filter Design Using the I_0-sinh Window Function”. In: *IEEE International Symposium on Circuits & Systems*. IEEE. 1974.

[45] William G. Hawkins. “Fourier Transform Resampling: Theory and Application”. In: *IEEE Transactions on Nuclear Science* 44.4 (Aug. 1997), pp. 1543–1550.

[46] Diego Arocha. “Time Domain Methods to Study Human-Structure Interation”. Master. Columbia, SC: University of South Carolina, 2013.

[47] Juan M. Caicedo. *Discussion on EFFECTs*. Personal Communication. Feb. 20, 2016.

[48] *Active Learning*. English. Everett Community College. URL: https://www.everettcc.edu/files/administration/institutional-effectiveness/institutional-research/outcomeassess-active-learning.pdf (visited on 04/19/2016).

[49] Juan M. Caicedo et al. “Environments For Fostering Effective Critical Thinking (EFFECTs)”. In: *2008 ASEE Annual Conference and Exposition*. ASEE. Pittsburgh, PA, June 2008.

[50] Juan M. Caicedo et al. “Assessment of Environments For Fostering Effective Critical Thinking (EFFECTs) on a first year Civil Engineering course”. In: *2009 ASEE Annual Conference and Exposition*. ASEE. Austin, TX, June 2009.

[51] Charlie Pierce, Juan M. Caicedo, and Joe Flora. “Engineering EFFECTs: Strategies and Successes in Introduction to Civil Engineering”. In: *4th First Year Engineering Experience (FYEE) Conference*. Pittsburgh, PA, Aug. 2012.

[52] Juan M. Caicedo. “Active Learning Activities in Structural Model Updating”. In: *120th ASEE Annual Conference and Exposition*. ASEE. Atlanta, GA, June 2013.

[53] Charlie Pierce et al. “Integrating Professional and Technical Engineering Skills with the EFFECTs Pedagogical Framework”. In: *International Journal of Engineering Education* 30 (2014), pp. 1579–1589.

[54] *Environments for Fostering Critical Thinking (EFFECTs).* University of South Carolina. Mar. 2016. URL: http://sdii.ce.sc.edu/effects/.

[55] Charlie Pierce. *EFFECTs Developmental Framework.* English. University of South Carolina. Mar. 15, 2013. URL: https://sdii.ce.sc.edu/effects/?q=node/90 (visited on 02/20/2016).

[56] Thomas A. Angelo and K. Patricia Cross. *Classroom Assessment Techniques.* 2nd ed. San Francisco: Jossey-Bass, 1993.

[57] J. Clarke. *Pieces of the Puzzle: The Jigsaw Method.* Westport, CT: Greenwood Press, 1994.

[58] Melvin L. Silberman. *Active Learning: 101 Strategies to Teach Any Subject.* Boston: Allyn and Bacon, 1996.

[59] Alison Morrison-Sheltar and Mary Marwitz. *Teaching Creatively.* Eden Prairie: Outernet, 2001.

[60] Ryan Watkins. *75 E-Learning Activities: Making Online Learning Interactive.* San Francisco: Pfeiffer, 2005.

[61] Arthur VanGundy. *101 Activities For Teaching Creativity and Problem Solving.* San Francisco: Pfeiffer, 2005.

[62] Schreyer Institute. *Jigsaw Strategy.* English. Penn State. 2007. URL: https://www.schreyerinstitute.psu.edu/pdf/alex/jigsaw.pdf.

[63] Center For Teaching & Learning. *Active Learning Techniques.* English. Brigham Young University. URL: http://ctl.byu.edu/tip/active-learning-techniques (visited on 04/19/2016).

[64] Juan M. Caicedo. *Post ECIV 524 Discussion on Class Performance.* Personal Communication. Apr. 25, 2016.

[65] Michael Prince. “Does Active Learning Work? A Review Of The Research”. In: *Journal of Engineering Education* 93.3 (July 2004), pp. 223–231.

[66] Joel Michael. “Where’s The Evidence That Active Learning Works?” In: *Advances in Physiology Education* 30.4 (2006), pp. 159–167. DOI: 10.1152/advan.00053.2006. eprint: http://advan.physiology.org/content/30/4/159.full.pdf. URL: http://advan.physiology.org/content/30/4/159.

[67] Miroslav Pastor, Michal Binda, and Tomas Harcarik. “Modal Assurance Criterion”. In: *Procedia Engineering* 48 (2012), pp. 543–548. DOI: 10.1016/j.proeng.2012.09.551.

Appendix A

Hospital Reported Falls and Descriptions

Table A.1: Hospital Reported Fall Events

ID	Reported Time	Description	Active Sensors	Record (±1 hr)
1	2013-01-18 11:00	Slid down from chair	0	
2	2013-01-24 06:50	Fell against wall when trying to sit on toilet	0	
3	2013-01-26 11:25	Slid off wheelchair	0	
4	2013-01-27 01:45	-	0	
5	2013-04-11 00:30	-	0	
6	2013-04-17 06:00	-	4	
7	2013-04-19 08:55	-	0	
8	2013-04-25 05:00	-	0	
9	2013-04-25 07:05	-	0	
10	2013-04-28 15:45	-	0	
11	2013-05-17 08:55	-	0	
12	2013-05-23 11:30	-	0	
13	2013-05-27 13:05	-	5	
14	2013-05-27 18:10	-	6	
15	2013-06-06 13:45	-	6	
16	2013-06-17 22:00	Putting right sandal on and lost balance	4	x

continued on next page...

ID	Reported Time	Description	Active Sensors	Record (±1 hr)
17	2013-06-20 13:00	Patient fell forward in bed hitting his lower chest	4	
18	2013-06-20 17:15	CNA was helping patient to bathroom and he fell and hit his head	4	x
19	2013-06-20 21:30	Patient fell in bathroom	4	
20	2013-06-28 23:20	Observed on his knees with both hands holding onto the bed. Side rails were up. Patient stated he just wanted to get out bed and walk	7	x
21	2013-07-02 21:00	Patient got up from BCS unassisted and fell	0	
22	2013-07-05 18:25	Patient found on floor	7	
23	2013-07-07 19:15	Patient found on floor at beside his bed	3	
24	2013-07-13 21:00	Shower head railing broke and patient fell to BSC in shower	7	
25	2013-07-24 19:45	Patient had incontinent episode while going to bathroom and slipped on urine on the floor	0	
26	2013-07-25 18:00	Transferring from bed to chair and fell on buttocks	5	x
27	2013-07-26 13:10	Did not lock rollator while putting on clothes	3	
28	2013-07-30 04:50	Patient found on floor in room	6	x
29	2013-07-30 10:50	Patient was using bathroom and left the bathroom where his legs gave out	0	
30	2013-08-02 23:20	Patient found on floor at the foot of the bed	0	
31	2013-08-04 01:00	Patient found on floor beside of his bed	?	

continued on next page...

ID	Reported Time	Description	Active Sensors	Record (±1 hr)
32	2013-08-27 11:00	Patient was found on the floor by a Med Student. Patient states that he was walking, slipped, and then fell	5	x
33	2013-08-29 14:40	Nurse was helping patient to the bedside commode from a chair and she could not make it. The nurse then eased her to floor	7	x
34	2013-08-31 18:08	Patient was observed falling down, face first onto bathroom floor	7	x
35	2013-09-22 03:05	Patient went to bathroom where he slipped and fell	5	x
36	2013-10-03 12:55	Patient found sitting on floor next to bed	6	x
37	2013-10-17 14:45	Slid to floor while trying to transfer from wheelchair to bed	0	
38	2013-10-20 04:30	Patient stated he was on his way back from bathroom when his leg gave out	0	
39	2013-10-22 20:10	Patient fell while trying to put on pajamas	5	x
40	2013-10-25 11:30	Patient reported he was trying to stand and leg gave out	0	
41	2013-10-26 07:30	Patient stated he walked to door, when he turned around his foot got locked	4	x
42	2013-10-28 23:23	Patient was pulling his pants down when walker slipped and he fell	5	x
43	2013-11-22 22:20	Patient found sitting on floor next to bed	0	
44	2013-11-25 17:45	Bent over to pick up trash off floor, lost balance, and fell	7	x
45	2013-12-03 02:40	Found patient on floor beside bed	0	

continued on next page...

ID	Reported Time	Description	Active Sensors	Record (±1 hr)
46	2013-12-03 03:55	Patient stated he was trying to go to the sink and fell	8	x
47	2013-12-06 11:45	Patient stated he stumbled when returning to bed from bathroom	0	
48	2013-12-09 04:15	Patient's top half on bed facing mattress, legs on floor	7	x
49	2013-12-09 12:00	Patient had sitter in room but wanted to use the bathroom. Sitter was outside bathroom when he heard a thump. Found on floor	0	
50	2013-12-28 12:00	Found bedside bed on all fours	0	

Appendix B

Captured Human Fall Acceleration Records

The following are acceleration versus time plots of the signals corresponding to events highlighted in Table 2.2 that were recorded using sensors in the flooring. Sensor signals showing little to no data are not displayed. The full list of reported falls and their descriptions are found in Table A.1.

B.1 Fall Reported on 2013-06-17 22:00 (ID 16)

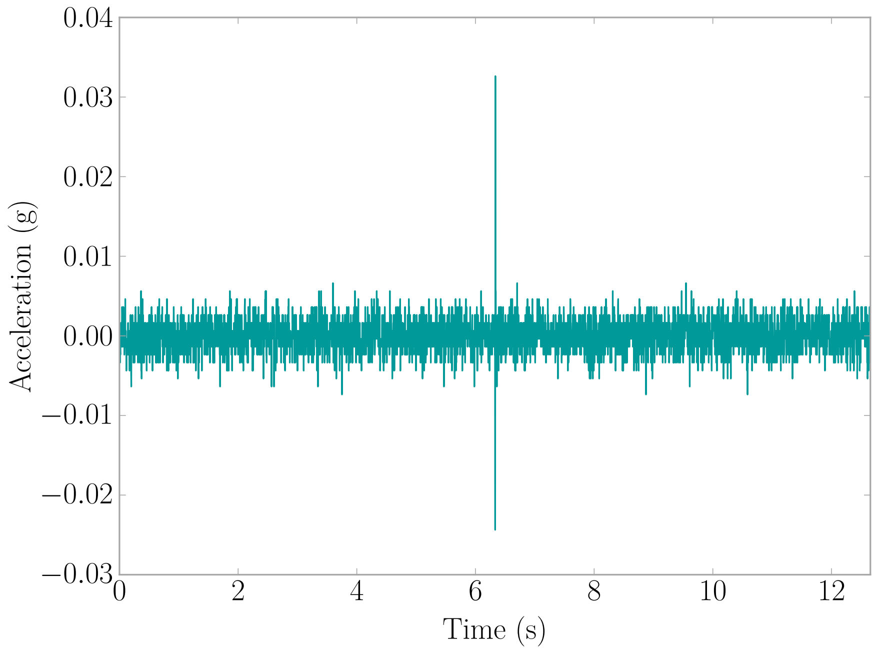

Figure B.1: Fall Event 2013-06-17 21:57:19 | Sensor D4E1

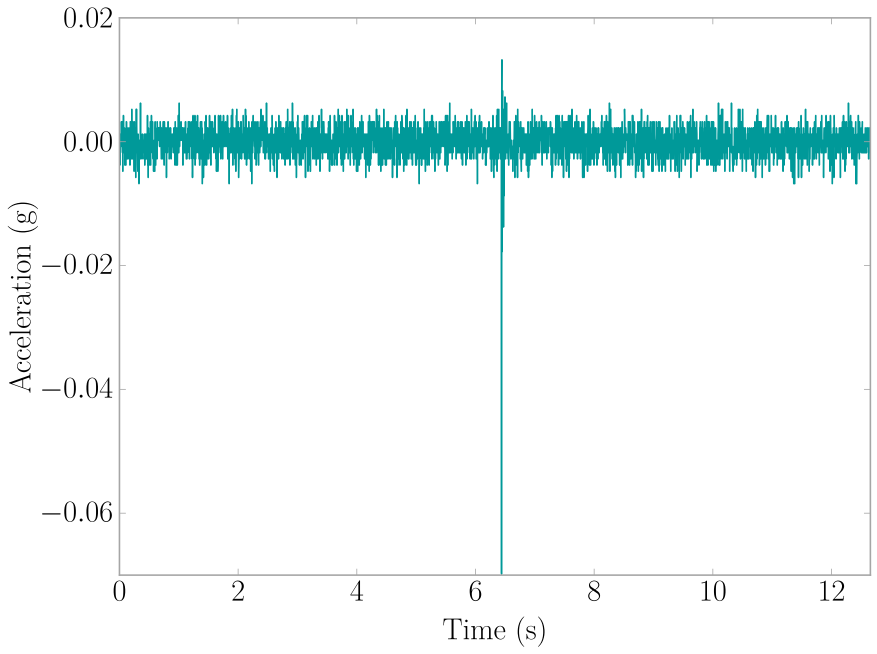

Figure B.2: Fall Event 2013-06-17 21:57:19 | Sensor B3B0

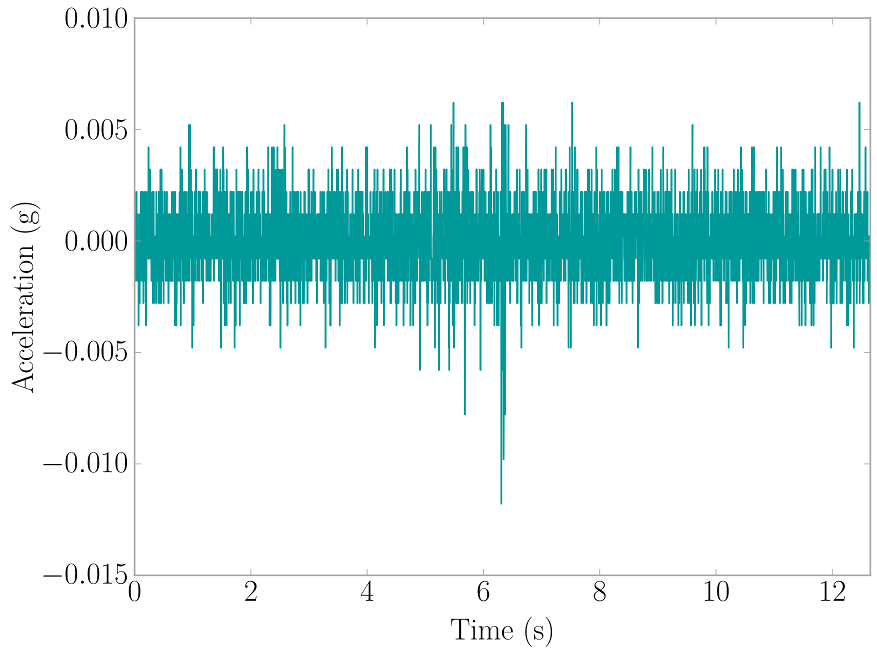

Figure B.3: Fall Event 2013-06-17 21:58:54 | Sensor BB46

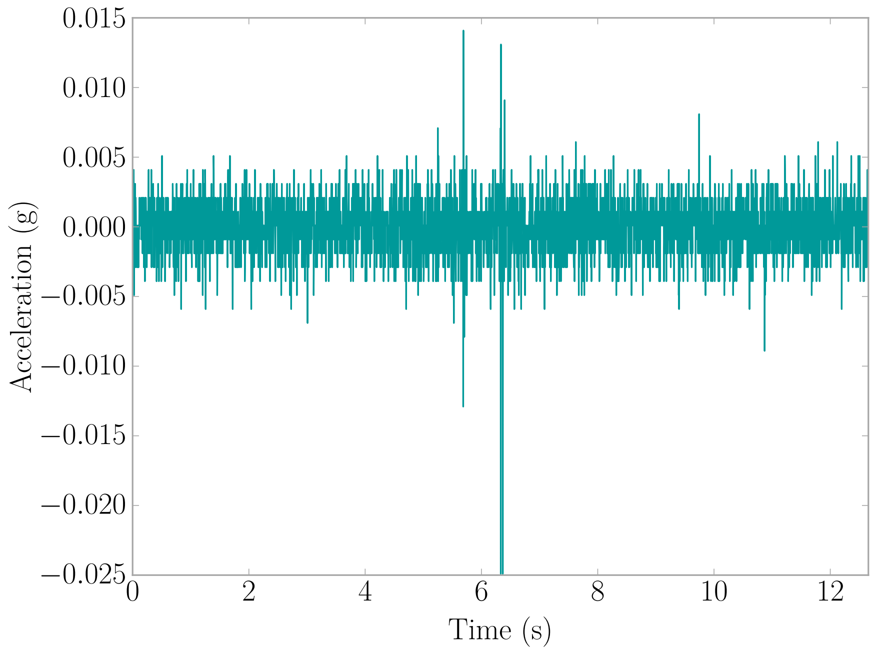

Figure B.4: Fall Event 2013-06-17 21:58:54 | Sensor BB87

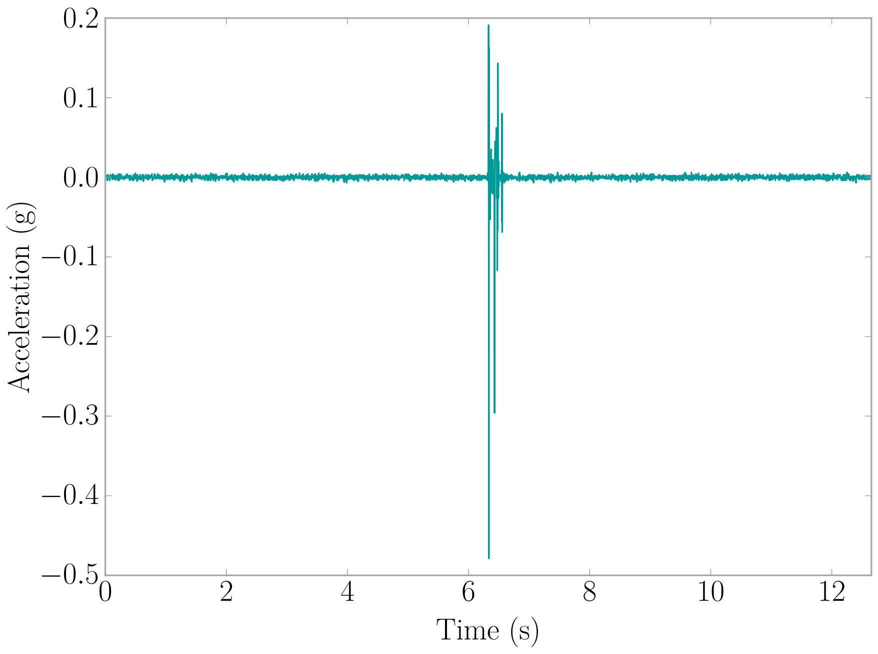

Figure B.5: Fall Event 2013-06-17 22:03:19 | Sensor BB87

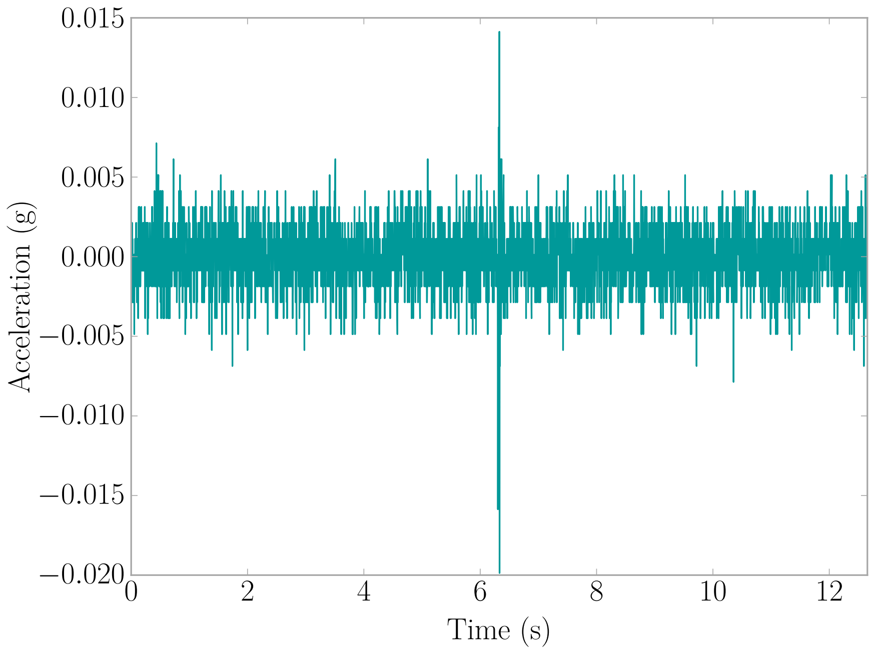

Figure B.6: Fall Event 2013-06-17 22:10:07 | Sensor BB87

B.2 Fall Reported on 2013-06-20 17:15 (ID 18)

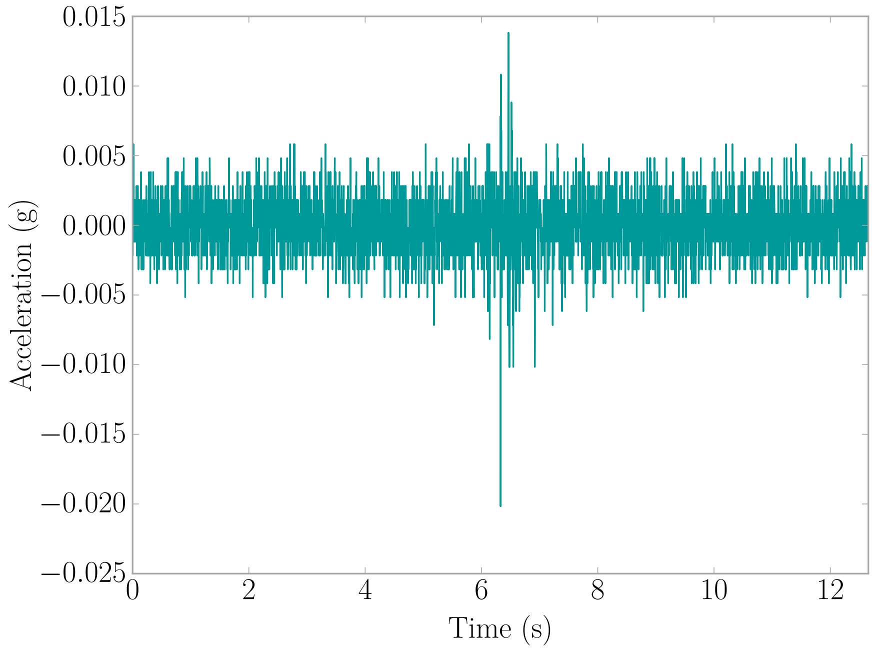

Figure B.7: Fall Event 2013-06-20 17:14:23 | Sensor D4E1

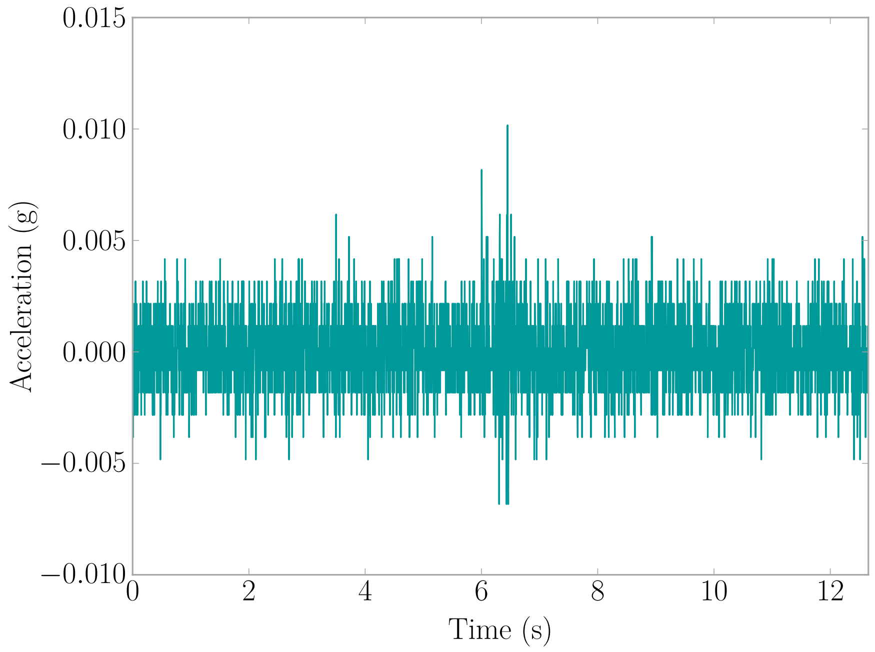

Figure B.8: Fall Event 2013-06-20 17:14:23 | Sensor BB46

B.3 Fall Reported on 2013-06-28 23:20 (ID 20)

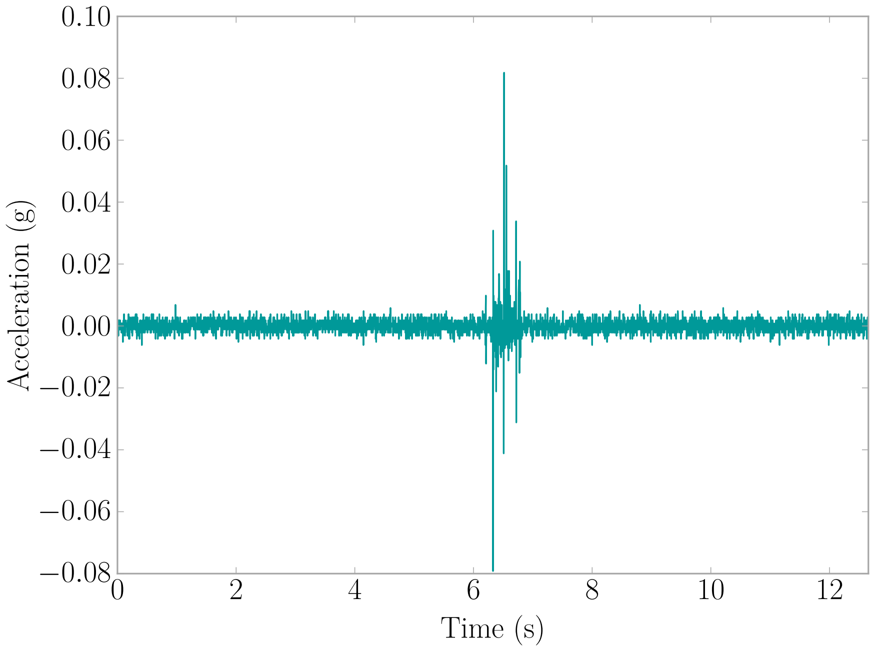

Figure B.9: Fall Event 2013-06-28 23:23:57 | Sensor 8D2C

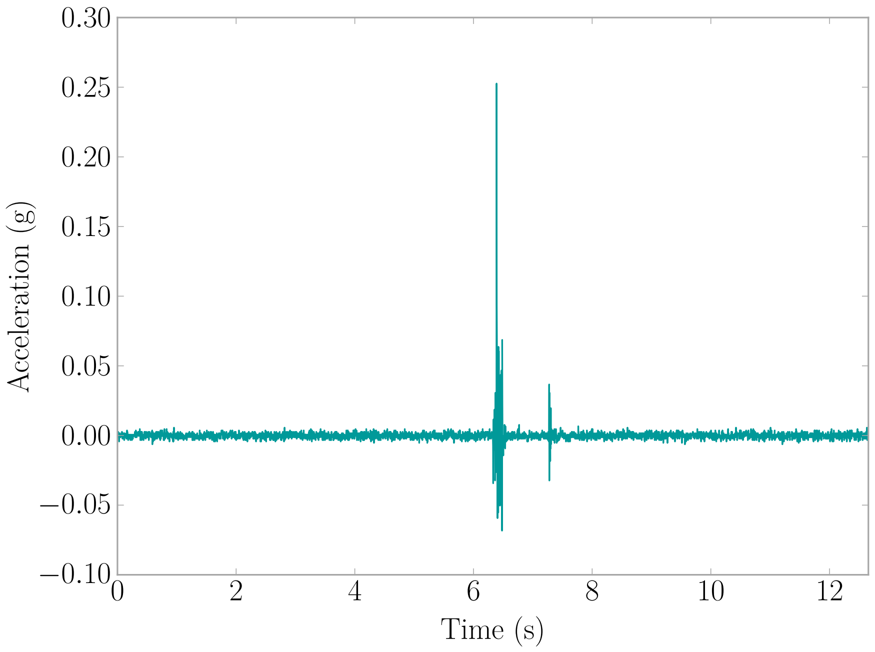

Figure B.10: Fall Event 2013-06-28 23:24:42 | Sensor 8D2C

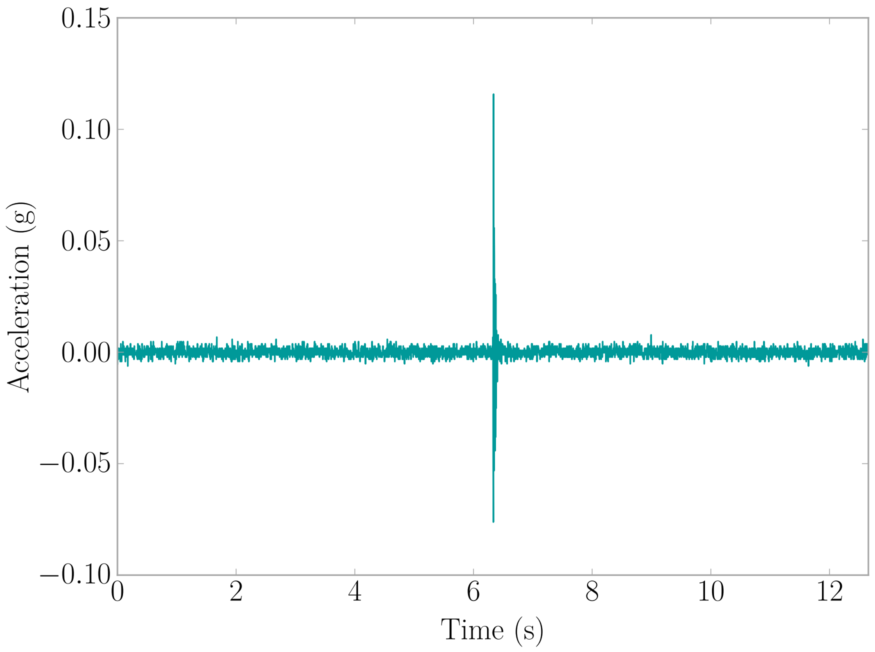

Figure B.11: Fall Event 2013-06-28 23:28:42 | Sensor 8D2C

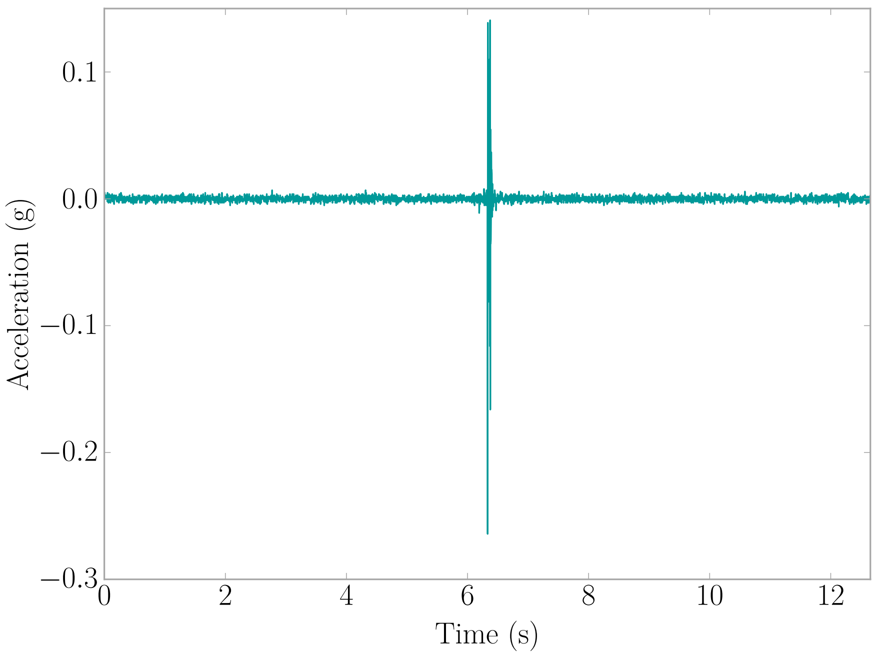

Figure B.12: Fall Event 2013-06-28 23:30:38 | Sensor 8D2C

B.4 Fall Reported on 2013-07-25 18:00 (ID 26)

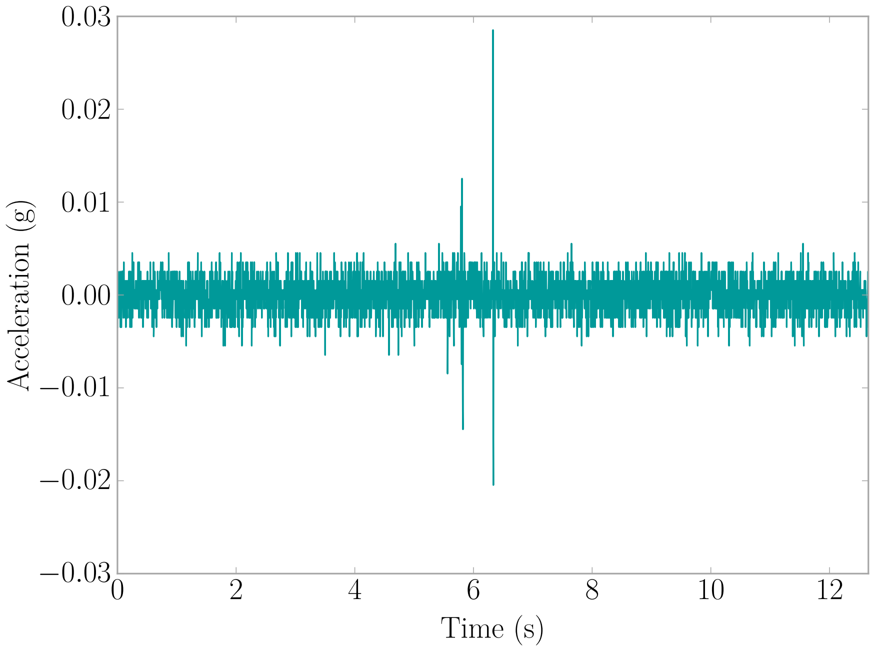

Figure B.13: Fall Event 2013-07-25 17:49:29 | Sensor B3A1

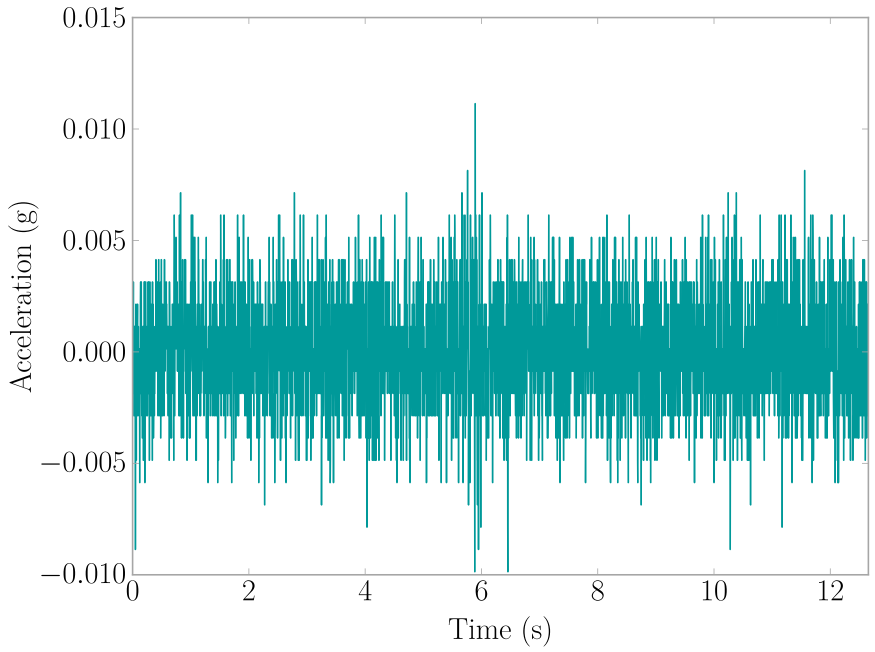

Figure B.14: Fall Event 2013-07-25 17:49:29 | Sensor BB7E

B.5 Fall Reported on 2013-07-30 04:50 (ID 28)

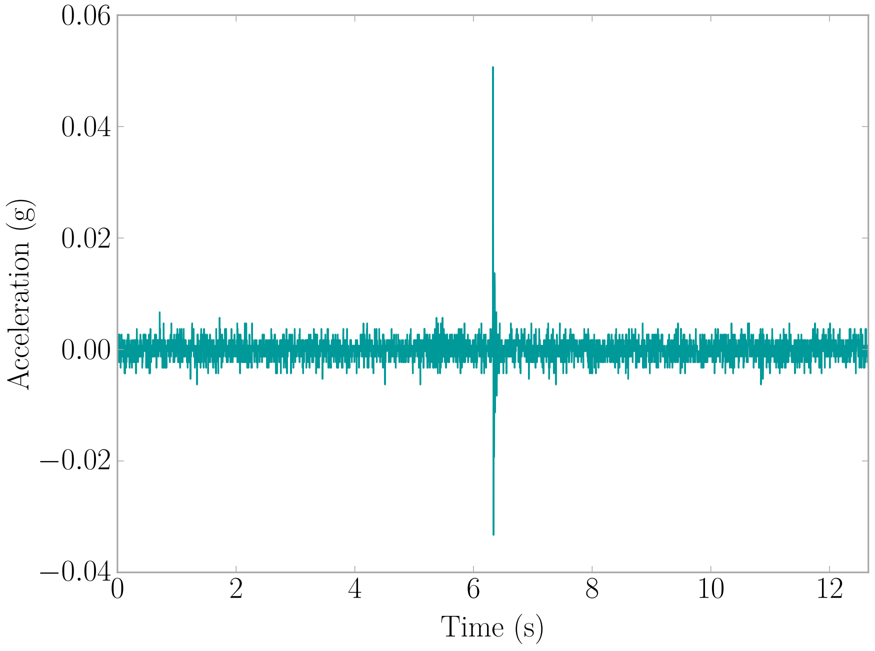

Figure B.15: Fall Event 2013-07-30 04:45:49 | Sensor BB48

B.6 Fall Reported on 2013-08-27 11:00 (ID 32)

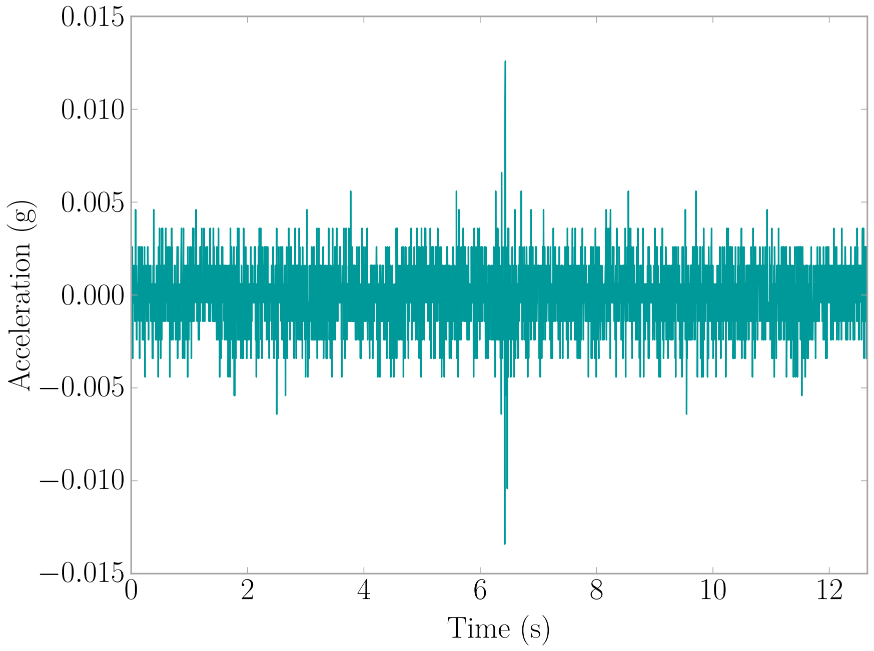

Figure B.16: Fall Event 2013-08-27 10:58:35 | Sensor BB48

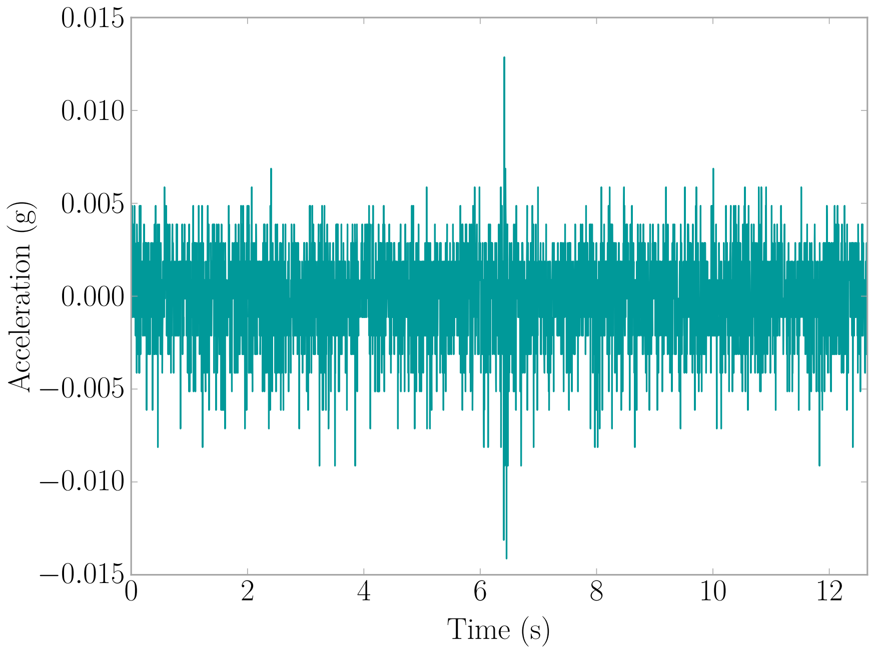

Figure B.17: Fall Event 2013-08-27 10:58:35 | Sensor E0A8

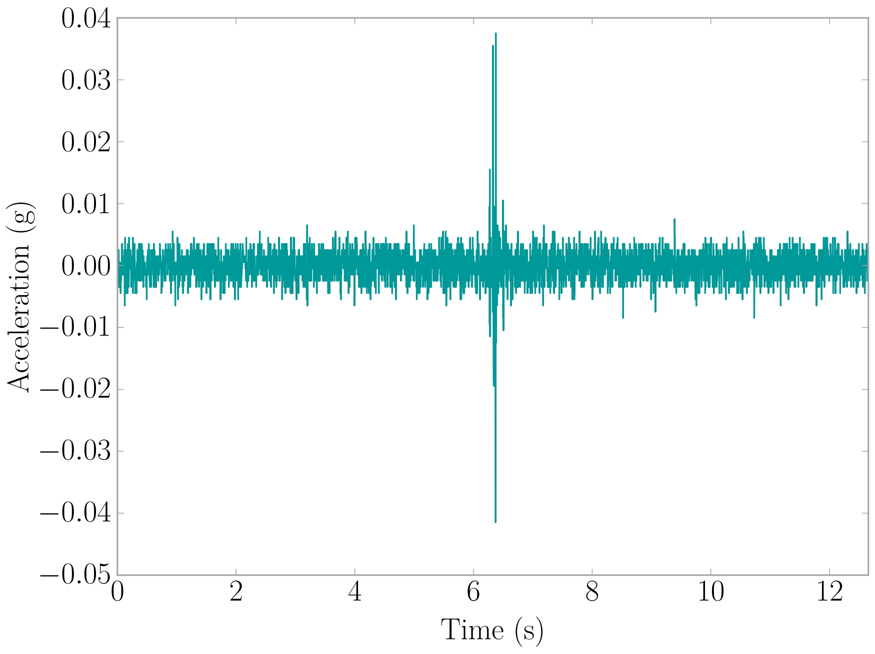

Figure B.18: Fall Event 2013-08-27 10:58:35 | Sensor E7EC

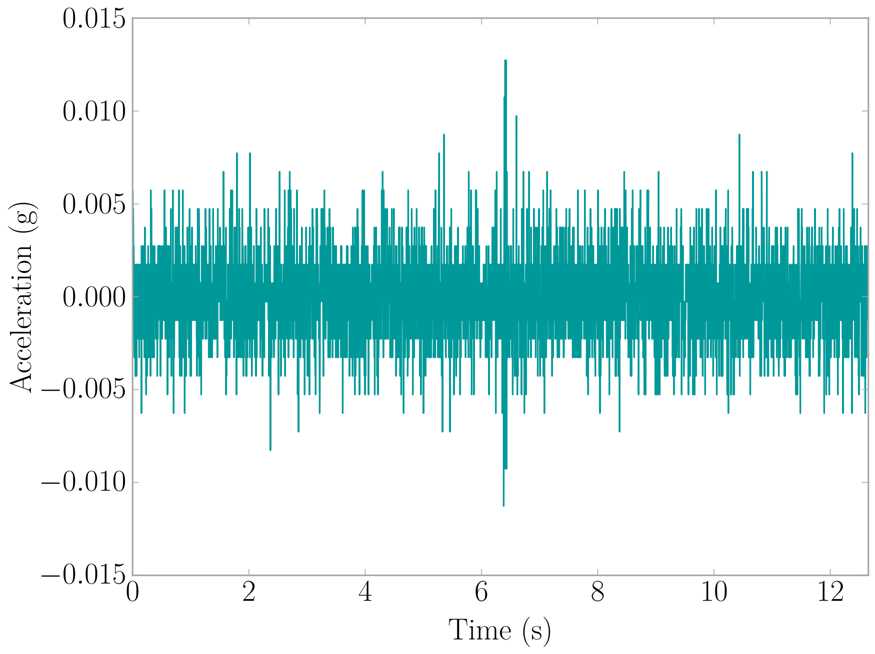

Figure B.19: Fall Event 2013-08-27 10:58:35 | Sensor 3496

B.7 Fall Reported on 2013-08-29 14:40 (ID 33)

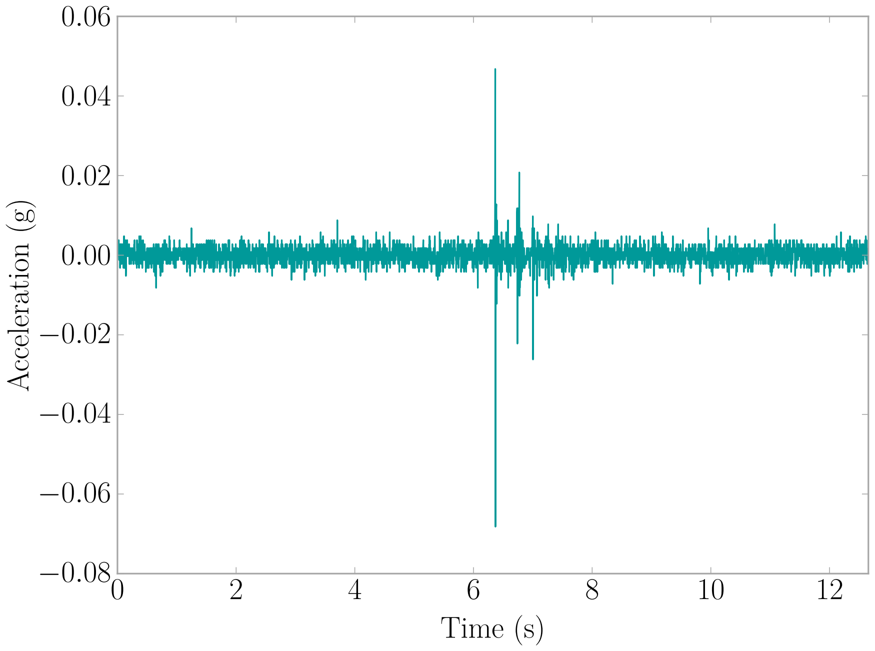

Figure B.20: Fall Event 2013-08-29 14:48:57 | Sensor E7DB

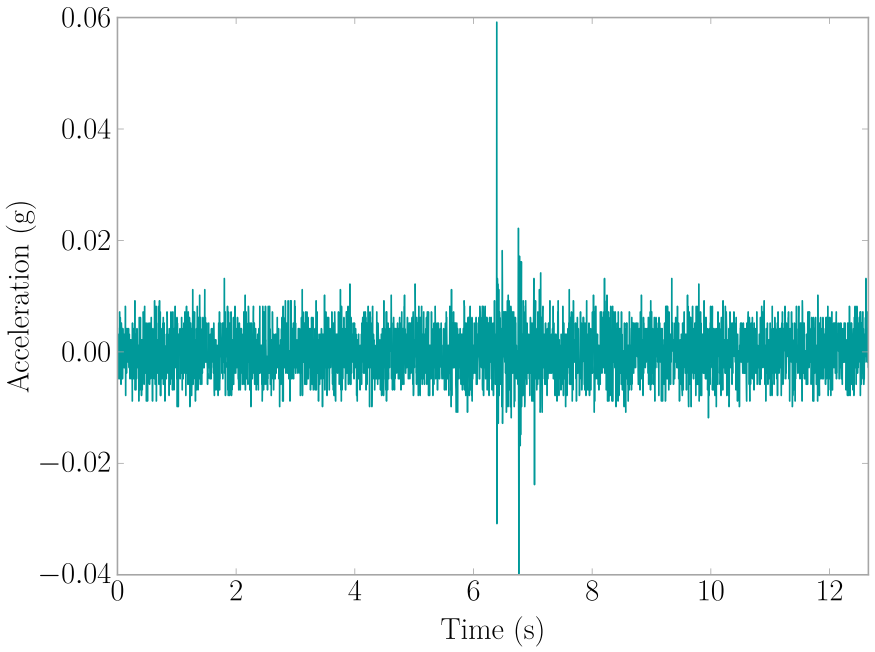

Figure B.21: Fall Event 2013-08-29 14:48:57 | Sensor 3493

B.8 Fall Reported on 2013-08-31 18:08 (ID 34)

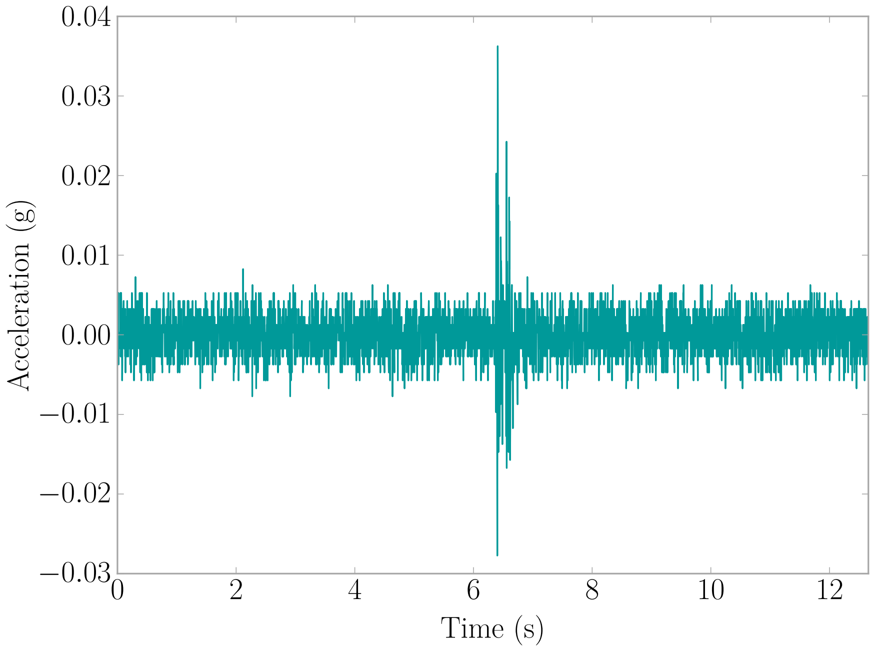

Figure B.22: Fall Event 2013-08-31 18:07:07 | Sensor B3A5

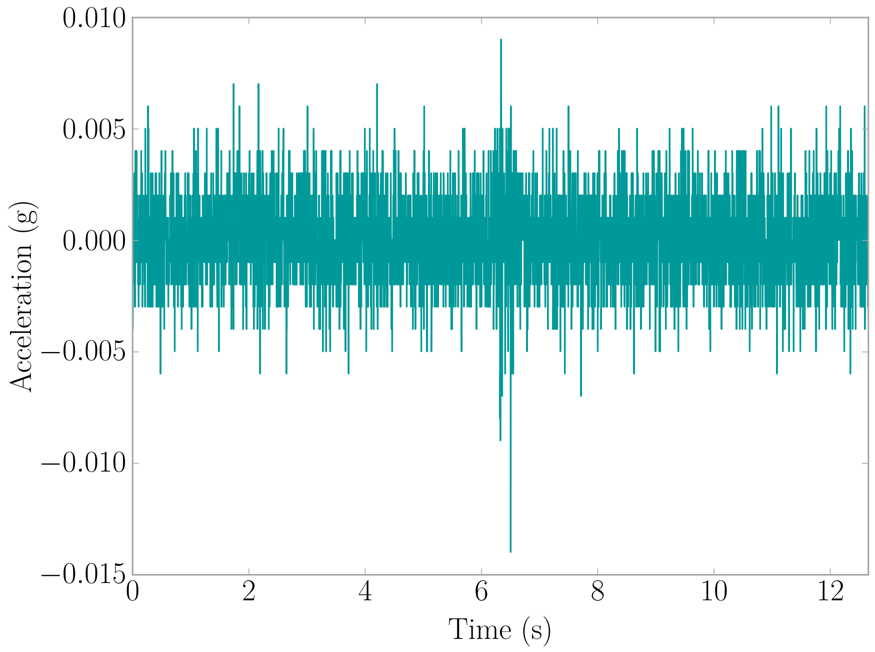

Figure B.23: Fall Event 2013-08-31 18:07:07 | Sensor E7DB

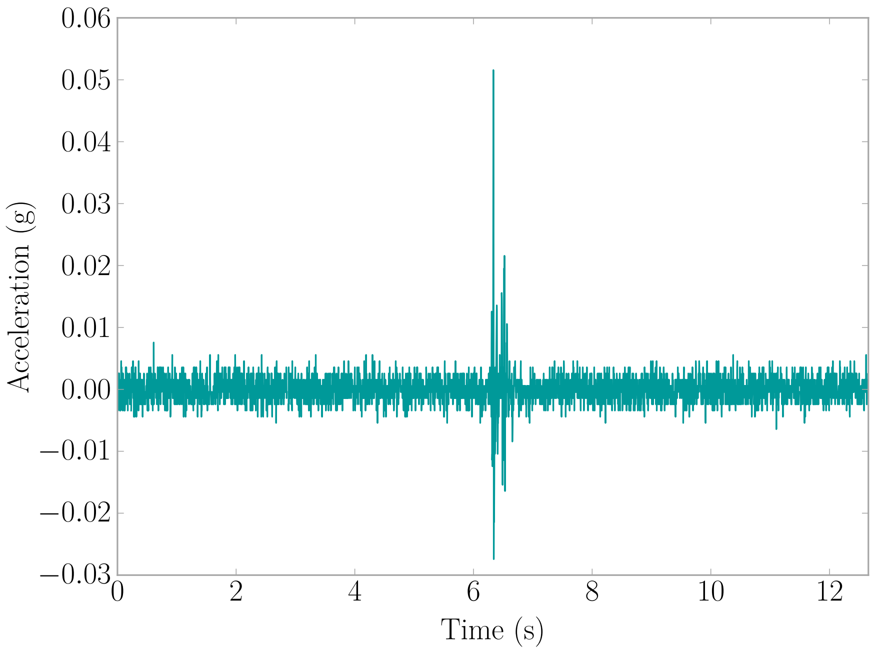

Figure B.24: Fall Event 2013-08-31 18:07:07 | Sensor 8D2C

B.9 Fall Reported on 2013-09-22 03:05 (ID 35)

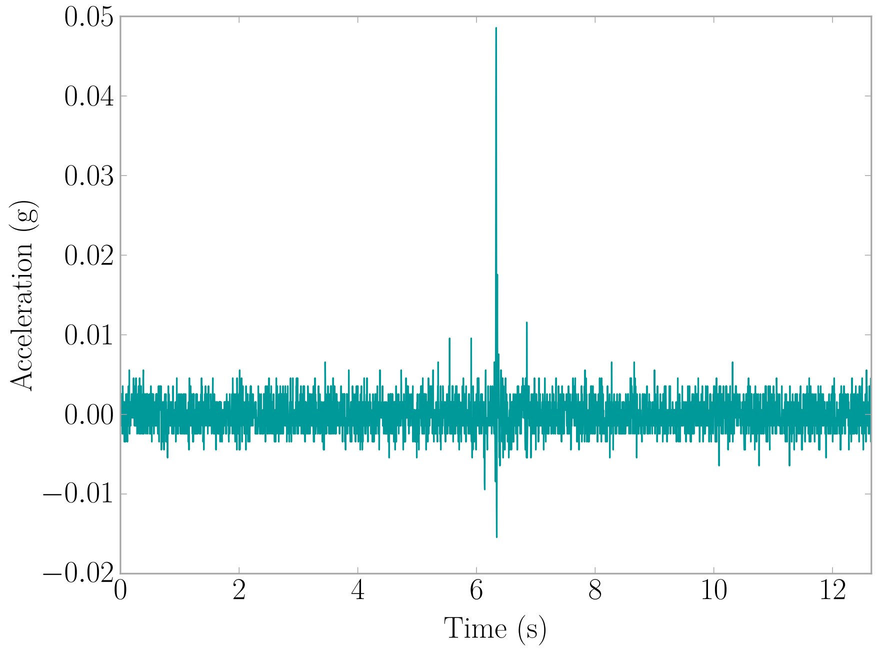

Figure B.25: Fall Event 2013-09-22 02:45:21 | Sensor C7AE

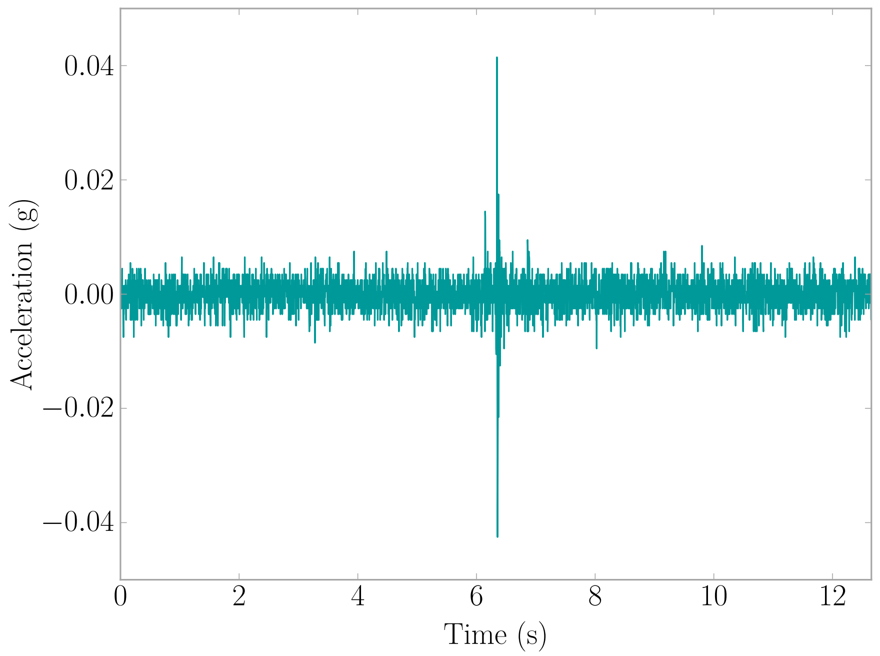

Figure B.26: Fall Event 2013-09-22 02:45:21 | Sensor DC67

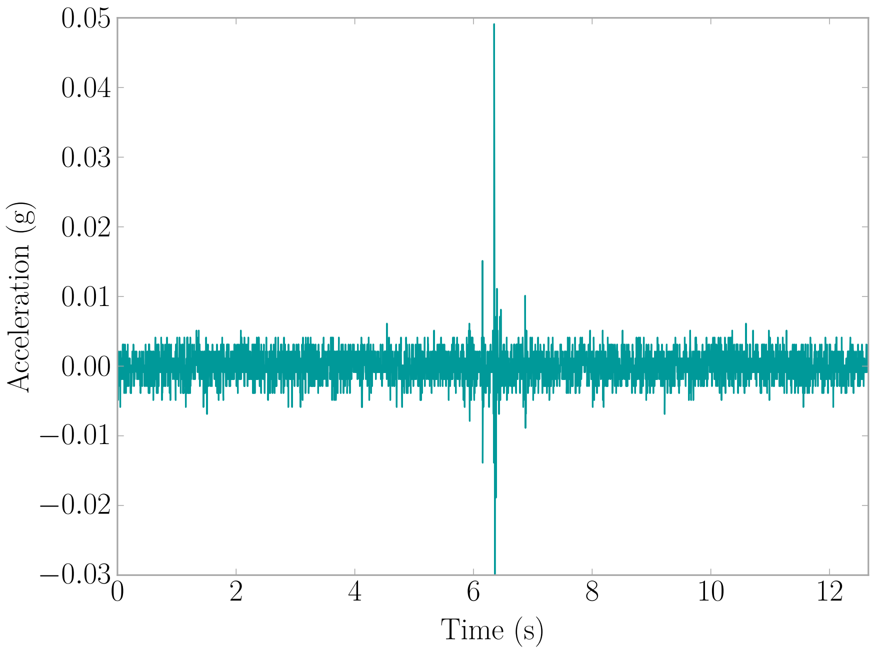

Figure B.27: Fall Event 2013-09-22 02:45:21 | Sensor 2E73

B.10 Fall Reported on 2013-10-03 12:55 (ID 36)

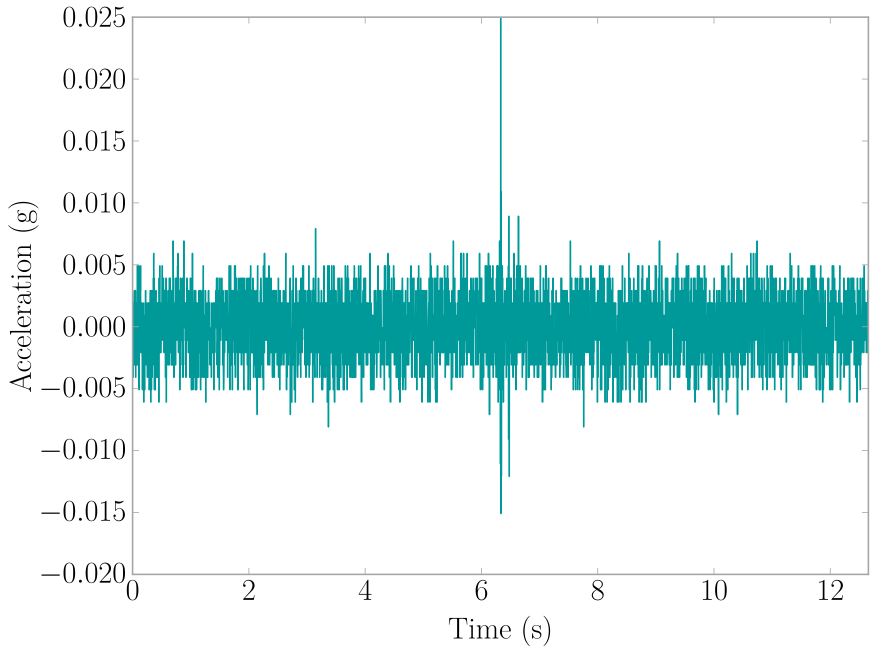

Figure B.28: Fall Event 2013-10-03 12:34:31 | Sensor B3A5

B.11 Fall Reported on 2013-10-22 20:10 (ID 39)

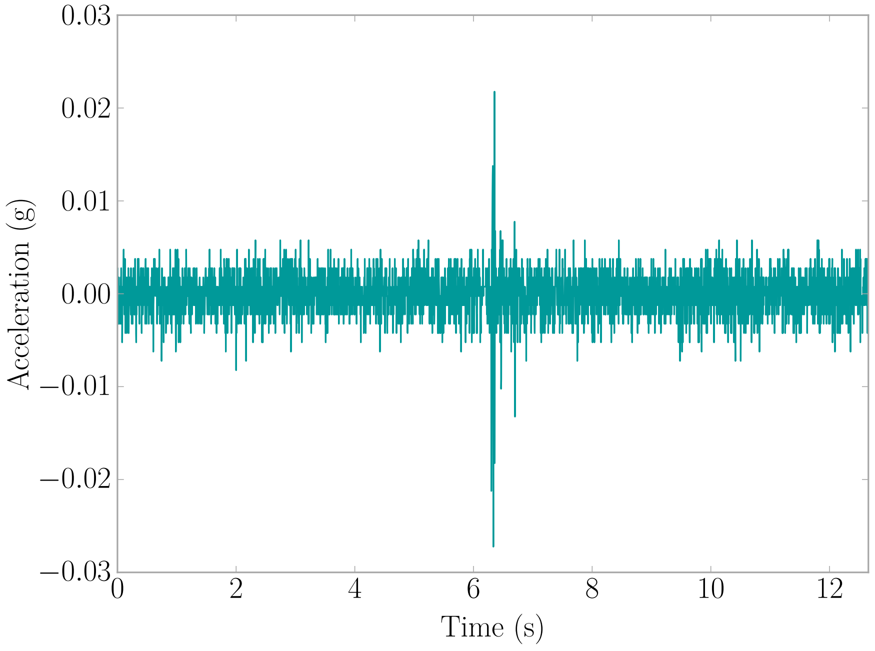

Figure B.29: Fall Event 2013-10-22 20:02:20 | Sensor E7EC

B.12 Fall Reported on 2013-10-26 07:30 (ID 41)

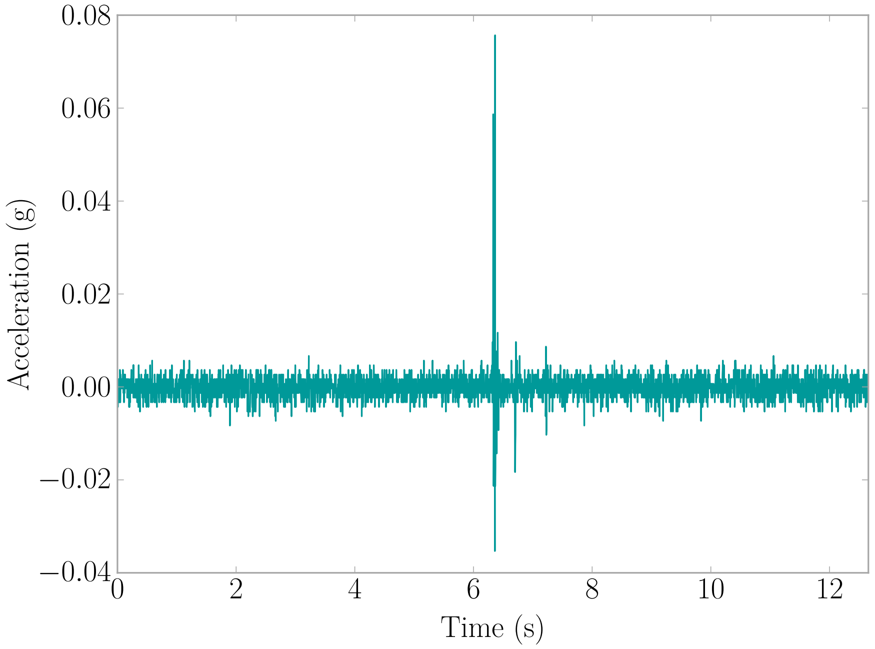

Figure B.30: Fall Event 2013-10-26 07:34:28 | Sensor E7EC

B.13 Fall Reported on 2013-10-28 23:23 (ID 42)

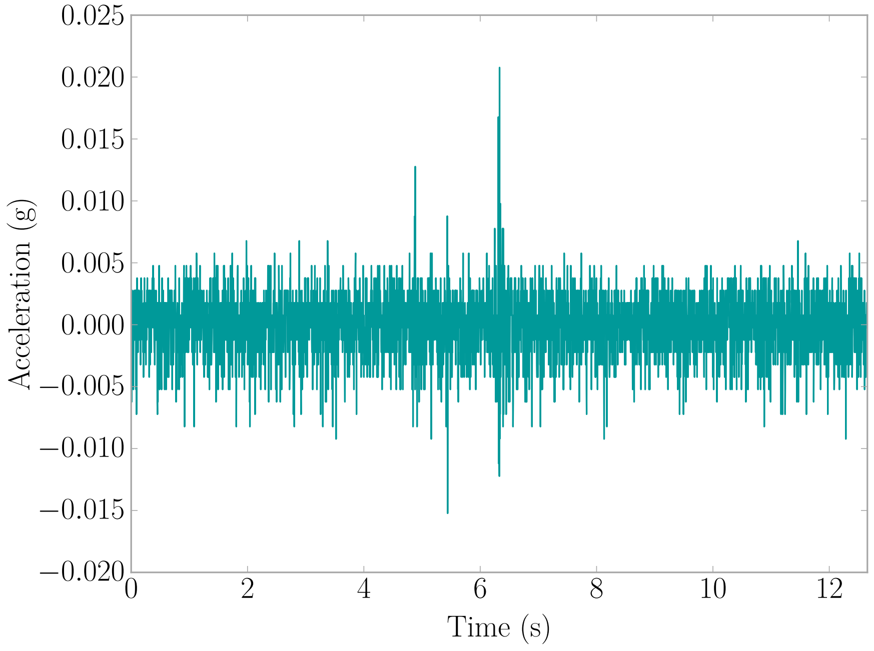

Figure B.31: Fall Event 2013-10-28 23:25:33 | Sensor E0A8

B.14 Fall Reported on 2013-11-25 17:45 (ID 44)

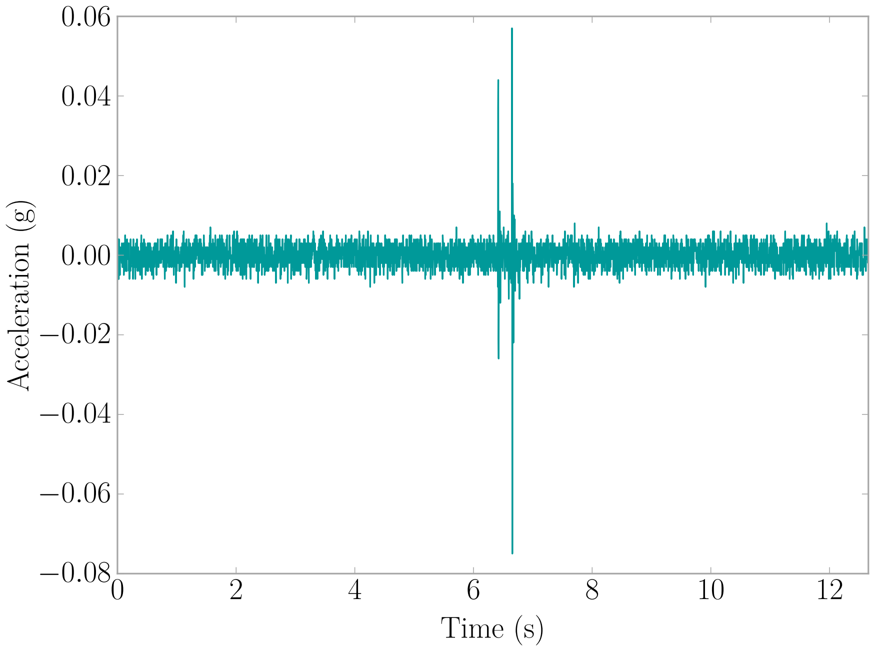

Figure B.32: Fall Event 2013-11-25 17:33:49 | Sensor B3A5

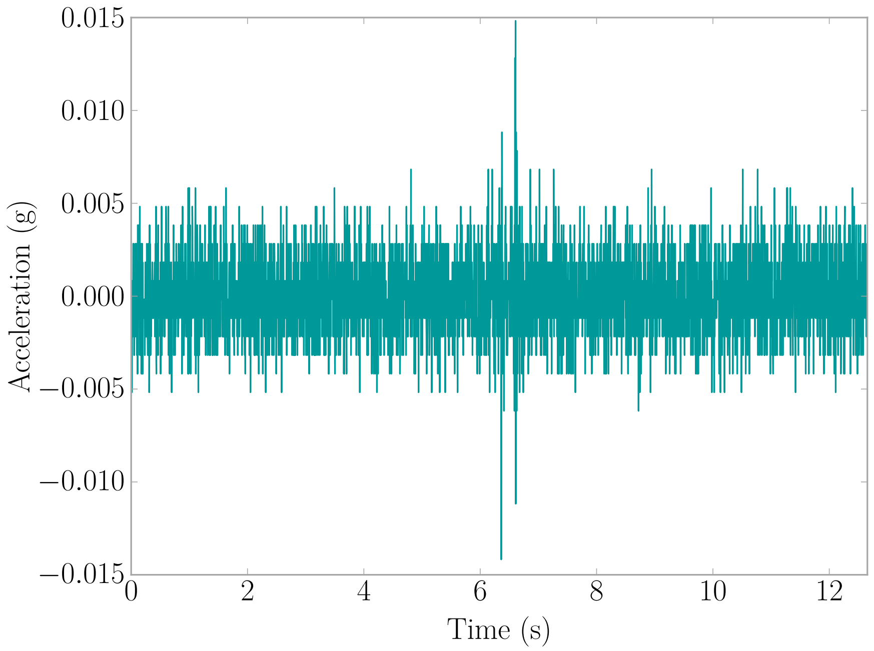

Figure B.33: Fall Event 2013-11-25 17:33:49 | Sensor BB7C

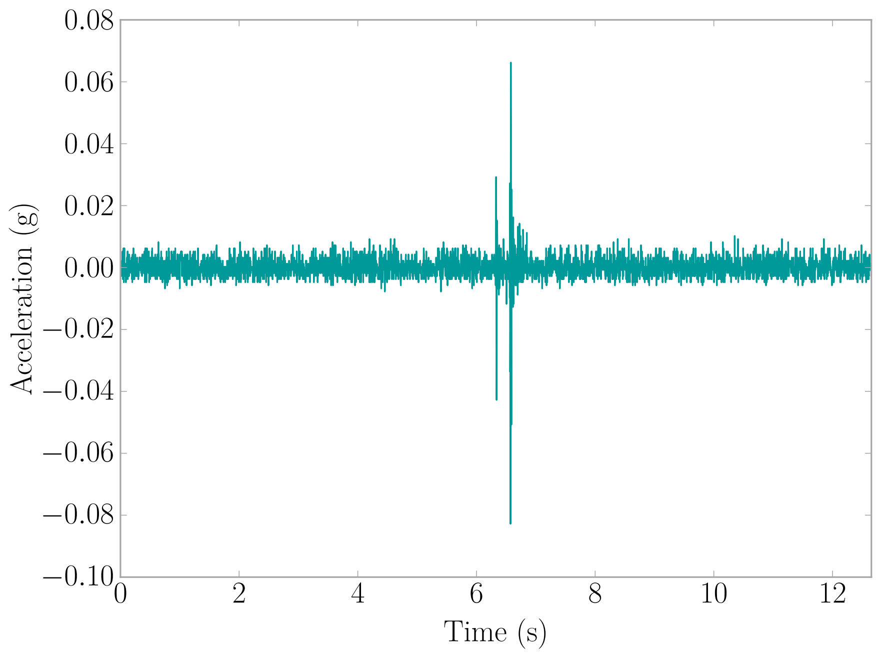

Figure B.34: Fall Event 2013-11-25 17:33:49 | Sensor 3087

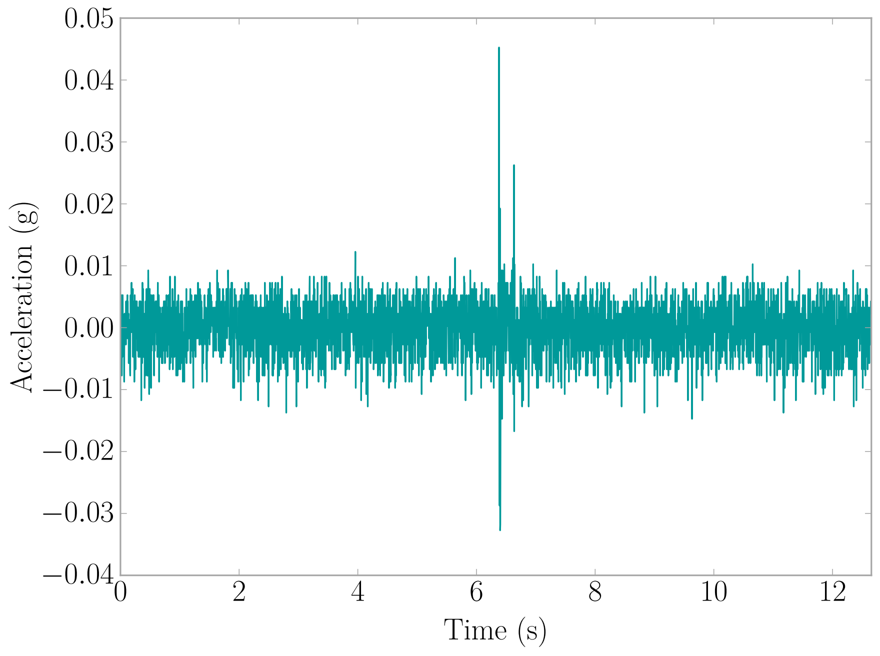

Figure B.35: Fall Event 2013-11-25 17:33:49 | Sensor 3493

B.15 Fall Reported on 2013-12-03 03:55 (ID 46)

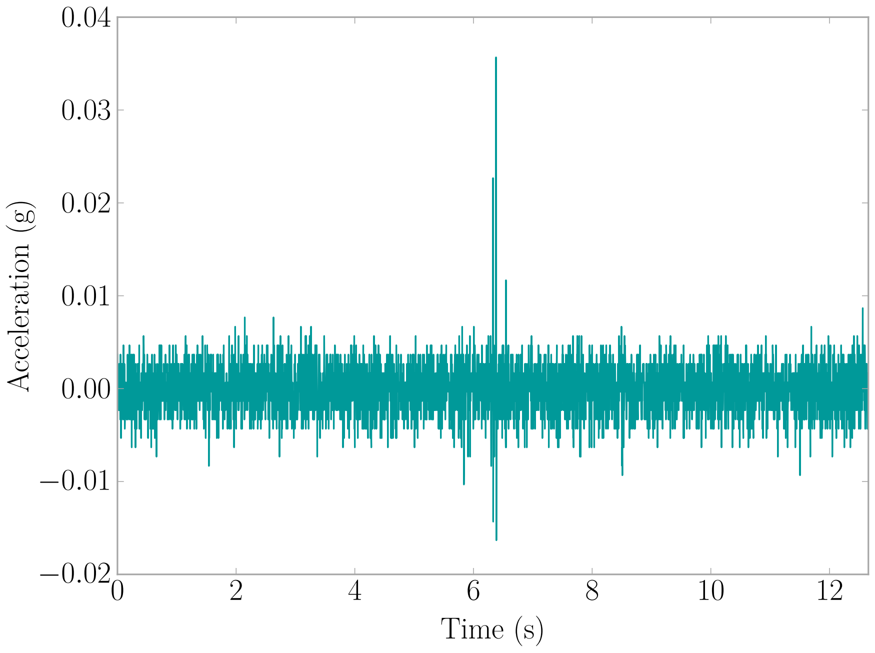

Figure B.36: Fall Event 2013-12-03 03:47:22 | Sensor B3A5

B.16 Fall Reported on 2013-12-09 04:15 (ID 48)

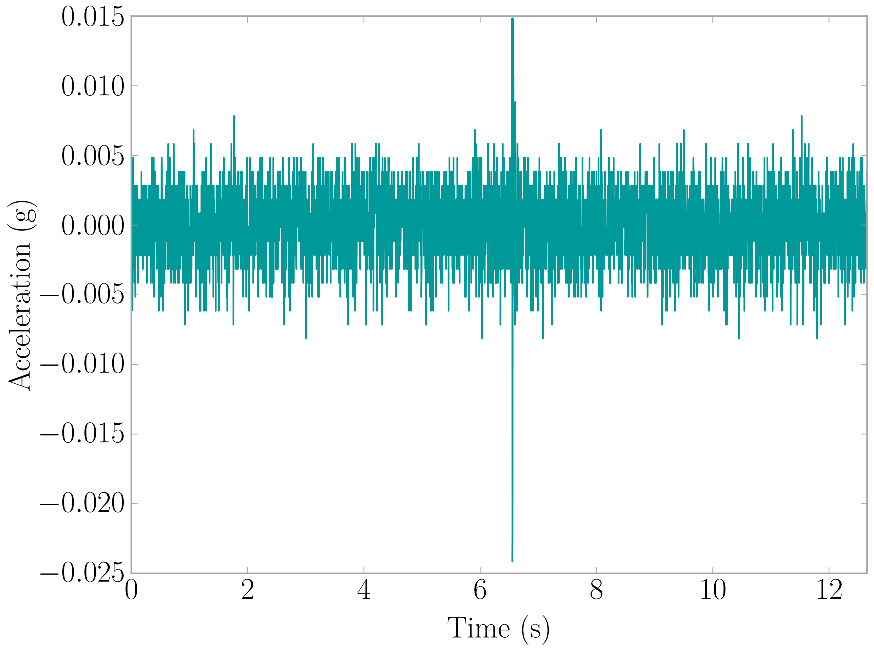

Figure B.37: Fall Event 2013-12-09 04:59:04 | Sensor B3A5

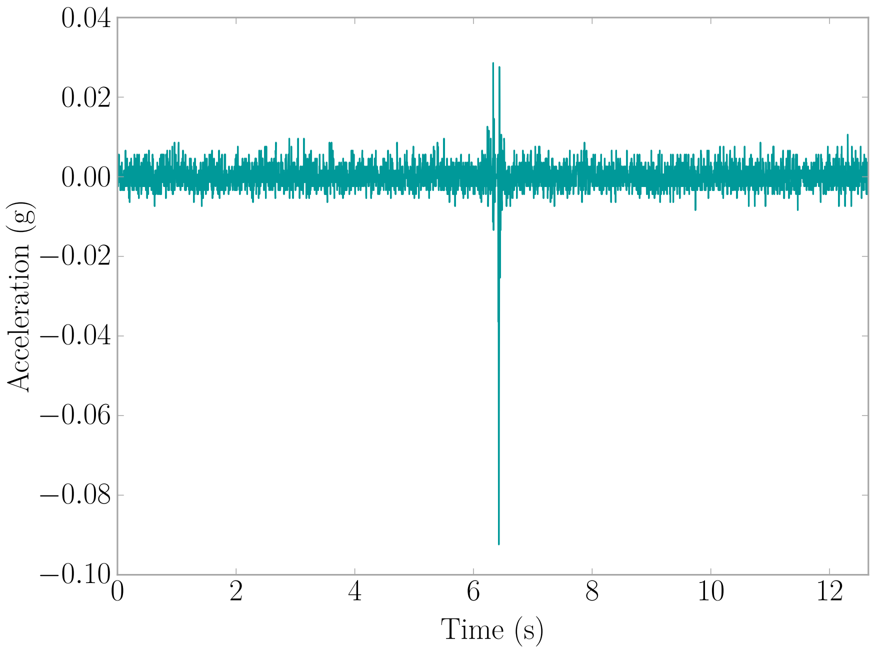

Figure B.38: Fall Event 2013-12-09 04:59:04 | Sensor BB45

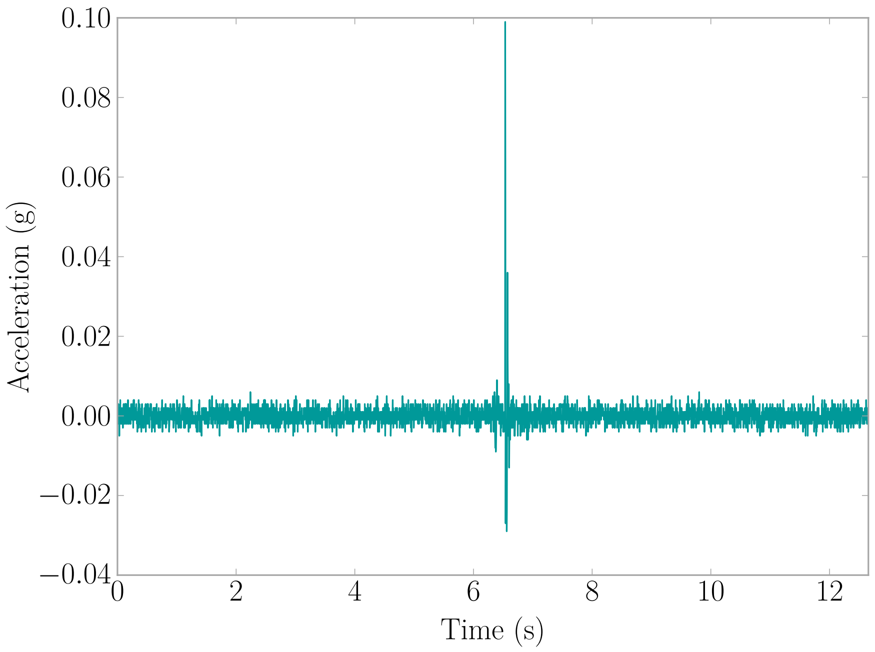

Figure B.39: Fall Event 2013-12-09 04:59:04 | Sensor 8D2C

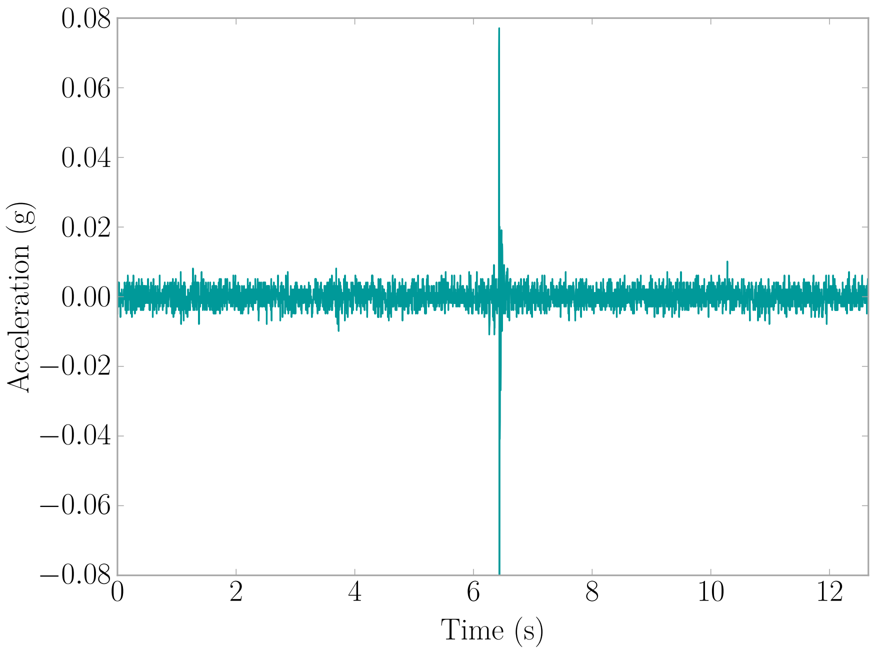

Figure B.40: Fall Event 2013-12-09 04:59:04 | Sensor 8F1E

Appendix C

Sample Human Activity Database Queries

The following presents example Human Activity Database queries grouped by informational type. This is part of the data management plan discussed in Chapter 3.

C.1 Database Table Information

Getting a list of column names in a database table. If another table is desired, simply replace *accel_events* with your desired table.

Code Snippet C.1: List Columns of a Table

```
SELECT COLUMN_NAME
FROM INFORMATION_SCHEMA.COLUMNS
WHERE TABLE_SCHEMA = "main_ssh"
     AND TABLE_NAME = "accel_events";
```

C.2 Sensor Related Queries

Find calibration records for a particular sensor. Replace the *sensor_mac* value with the Media Access Control Address (MAC Address) of the sensor desired.

Code Snippet C.2: Find The Calibration Record of a Sensor

```
SELECT *
FROM calibration
WHERE sensor_mac = "0006661495C0";
```

To cross reference max amplitude of an event with specific sensors for a date use the following. This is particularly useful when trying to find out which room an event occurred in when a system computer services multiple rooms.

Code Snippet C.3: Find Which Sensor Was Closest to The Acceleration Event

```
SELECT *
FROM accel_events t1
INNER JOIN (SELECT system, event_date, mac
            FROM event_parameters t3
            WHERE parameter="ampmax"
                 AND value = (SELECT MAX(value+0.0)
                              FROM event_parameters t4
                              WHERE t3.system = t4.system
                              AND t3.event_date = t4.event_date
                              AND t3.parameter = t4.parameter)) t2
ON t1.system = t2.system
     AND t1.date = t2.event_date
     AND t1.sensor_mac = t2.mac
WHERE t1.date = "2014-03-02 09:29:39"
     AND (t1.sensor_mac="000666303492"
          OR t1.sensor_mac="00066614E241"
          OR t1.sensor_mac="00066614998E");
```

To find the number of sensor monitored hours, use the following. Adjust the date range by replacing the values for *date*, and replace the *system* value for the system of interest. Note this assumes an hour offset in between system log saves.

Code Snippet C.4: Find Number of Sensor Monitored Hours For a Date Range and System

```
SELECT SUM(t1.nsensor)
FROM (SELECT YEAR(date) AS y,
             MONTH(date) AS m,
             DAY(date) AS d,
             HOUR(date) AS h,
             COUNT(DISTINCT mac) AS nsensor
      FROM system_log
      WHERE date>="2013-01-23"
           AND date<="2013-07-09"
           AND system="SSH-5"
      GROUP BY y, m, d, h
      ORDER BY y, m, d, h) AS t1;
```

Determine sensor activity by day for the period requested. Gives an idea of how well the sensors were operating. The *date* parameters can be replaced to choose a specific range, and the *system* parameter can be changed to choose an a different system or can be left out to get all systems. The *mac* parameter must include that is currently there as to ignore *system_logs* pertaining to the base station. If one wishes to specific a MAC Address for a sensor, use the *OR* MySQL command to add onto the *mac* argument.

Code Snippet C.5: Determine Sensor Activity by Day For a Period

```
SELECT DAY(date) AS d,
       MONTH(date) AS m,
       YEAR(date) AS y,
       COUNT(DISTINCT mac),
       SUBSTRING(MONTHNAME(date),1,3)
FROM system_log
WHERE date >= "2013-01-23"
     AND date <= "2013-07-09"
     AND mac != ""
     AND system = "SSH-15"
GROUP BY y, m, d
ORDER BY y, m, d;
```

C.3 System Related Queries

Getting a list of systems.

Code Snippet C.6: List Systems

```
SELECT DISTINCT(system)
FROM accel_events;
```

Getting a list of sensors and their associated systems. Note that this assumes each sensor only sees use with one system.

Code Snippet C.7: List Sensors And Their Systems

```
SELECT DISTINCT(sensor_mac), system
FROM accel_events;
```

Find the parameter names available in the system logs. These are not permanently set, so new parameters may be added over time.

Code Snippet C.8: Available System Log Parameters

```
SELECT DISTINCT(parameter)
FROM system_log;
```

Access system logs for a particular sensor.

Code Snippet C.9: Access System Logs For a Sensor

```
SELECT *
FROM system_log
WHERE mac = "00066614B3A1";
```

Access system logs for the system base station.

Code Snippet C.10: Access System Logs For a Sensor

```
SELECT *
FROM system_log
WHERE system = "SSH-36"
AND mac = "";
```

Access download information for a particular system. Gives insight into how the data was sent to the database.

Code Snippet C.11: Access Download Information For a System

```
SELECT *
FROM downloads
WHERE system = "SSH-5";
```

C.4 Acceleration Event Related Queries

Determine the number of available events in the database. This is useful as the database is expected to grow with time.

Code Snippet C.12: Find The Number of Events

```
SELECT COUNT(DISTINCT date)
FROM accel_events;
```

Grab a specific acceleration event. Replace *date* with the desired event's date.

Code Snippet C.13: Access a Specific Acceleration Event

```
SELECT *
FROM accel_events
WHERE date = "2013-01-18 13:54:55";
```

Get the available parameters used to describe the acceleration signals.

Code Snippet C.14: Get Event Parameters For Describing Acceleration Signals

```
SELECT *
FROM parameters;
```

Gather the metrics for a specific event and sensor. Replace the *sensor_mac* value with the MAC Address of the sensor desired, and replace the value of *event_date* with the specific event desired.

Code Snippet C.15: Find the Signal Metrics For an Event and Sensor

```
SELECT *
FROM event_parameters
WHERE mac = "00066614B3AA"
     AND event_date = "2013-07-20 02:44:25";
```

To find a flat signal (i.e. one with little to no excitation), set the amplitude value low for ampmax like in the following.

Code Snippet C.16: Find a Flat Acceleration Signal

```
SELECT t1.*, t2.value AS ampmax
FROM accel_events t1
INNER JOIN event_parameters t2 ON m1.date = t2.event_date
        AND t1.sensor_mac = t2.mac
WHERE t2.parameter = "ampmax"
        AND t2.value < 0.0125;
```

Find a spike signal (i.e. a sensor error that reads only one high value). See Section 2.4.2 for more details.

Code Snippet C.17: Find a Spike Acceleration Signal

```
SELECT t1.*
FROM event_parameters t1
INNER JOIN event_parameters t2 ON t1.event_date = t2.event_date
     AND t1.mac = t2.mac
INNER JOIN accel_events ON accel_events.date = t1.event_date
     AND accel_events.sensor_mac = t1.mac
WHERE t1.parameter = "metric1"
     AND t2.parameter = "ampmax"
     AND t2.value > 0.5
     AND t1.value/t2.value > 0.95;
```

Find the maximum parameter value for a period, simply replace *ampmax* with the desired parameter, replace the *event_date* ranges, and replace the *system*.

Code Snippet C.18: Find Maximum Parameter Value For a System and Date Range

```
SELECT tt.*
FROM event_parameters tt
INNER JOIN (SELECT system,
                   event_date,
                   mac,
                   parameter,
                   MAX(value+0.0) AS MaxVal
                FROM event_parameters
                WHERE parameter= "ampmax"
                         AND event_date >= "2013-01-18"
                         AND event_date <= "2014-06-14"
                         AND system = "SSH-36"
                GROUP BY event_date) groupedtt
ON tt.event_date = groupedtt.event_date
     AND tt.value = groupedtt.MaxVal
ORDER BY event_date;
```

Getting the number of events by day can give a sense of how activity is distributed across a period of time. The *date* parameters can be replaced to choose a specific range, and the *system* parameter can be changed to choose an a different system or can be left out to get all systems. The *mac* parameter must include that is currently there as to ignore *system_logs* pertaining to the base station. If one wishes to specific a MAC Address for a sensor, use the *OR* MySQL command to add onto the *mac* argument.

Code Snippet C.19: Get The Acceleration Events by Day

```
SELECT YEAR(date) AS y
       MONTH(date) AS m,
       DAY(date) AS d,
       COUNT(DISTINCT date),
       SUBSTRING(MONTHNAME(date),1,3)
FROM accel_events
WHERE date >= "2013-01-23"
     AND date <= "2013-07-09"
     AND mac != ""
     AND system = "SSH-39";
```

Vibration activity in an area can be useful for determining patterns. The activity density information can be determined using the following database query.

Code Snippet C.20: Get The Acceleration Activity Density

```
SELECT DAYOFWEEK(date),
       HOUR(date),
       COUNT(HOUR(date))
FROM accel_events
WHERE system = "SSH-36"
     AND date >= "2013-01-23"
     AND date <= "2013-07-09"
GROUP BY DAYOFWEEK(date), HOUR(date);
```

Signals collected can have a variety of errors in them due hardware and wireless communication problems. Thus it is desirable to find signals without any errors. The following query enables the user to find and error-free signal based on the definition outlined in Chapter 4.

Code Snippet C.21: Find Error-Free Signals

```sql
SELECT ae.sensor_mac, ae.date, ae.data
FROM accel_events ae
WHERE NOT EXISTS (
     SELECT NULL
     FROM event_parameters ep1
     INNER JOIN event_parameters ep2
          ON ep1.mac = ep2.mac
          AND ep1.event_date = ep2.event_date
     INNER JOIN event_parameters ep3
          ON ep1.mac = ep3.mac
          AND ep1.event_date = ep3.event_date
     WHERE ae.date = ep1.event_date
          AND ae.sensor_mac = ep1.mac
          AND ep1.parameter = "nandensity"
          AND ep2.parameter = "ampmax"
          AND ep3.parameter = "mad"
          AND (ep1.value+0.0 > 0.0
               OR (ep3.value+0.0)/(ep2.value+0.0) > 0.95
               OR LOWER(ep2.value) = "nan"
               OR LOWER(ep3.value) = "nan")
     )
     AND ae.data <> 'No Data'
```

Appendix D

SVM 3rd Degree Polynomial Kernel Results for Event Filtering

The polynomial kernel was also evaluated as a possibility for acceleration event filtering as seen in Chapter 4. The following figures and tables present the results for the kernel.

Table D.1: SVM 3rd Degree Polynomial Kernel Metric Combination Stats (100 Trials)

	Accuracy (%)	
Metric Combinations	Mean	St. Dev.
A_{max}	82.7	5.8
RoD	79.9	6.3
DR	69.9	27.5
A_{max}, RoD	82.7	5.8
RoD, DR	81.4	16.7
A_{max}, DR	84.8	15.1
A_{max}, RoD, DR	87.0	11.0

Table D.2: SVM 3rd Degree Polynomial Kernel Best Training Set for Each Metric Combination

Metric Combinations	C1	C2	C3	Accuracy (%)
A_{max}	121	21	18	97.5
RoD	121	21	18	97.5
DR	125	18	17	97.5
A_{max}, RoD	121	21	18	100.0
RoD, DR	126	21	13	100.0
A_{max}, DR	121	21	18	100.0
A_{max}, RoD, DR	125	19	16	100.0

Table D.3: SVM 3rd Degree Polynomial Kernel Worst Training Set for Each Metric Combination

Metric Combinations	C1	C2	C3	Accuracy (%)
A_{max}	134	11	15	67.5
RoD	134	15	11	65.0
DR	121	21	18	0.0
A_{max}, RoD	134	11	15	67.5
RoD, DR	130	17	13	15.0
A_{max}, DR	127	17	16	17.5
A_{max}, RoD, DR	126	21	13	10.0

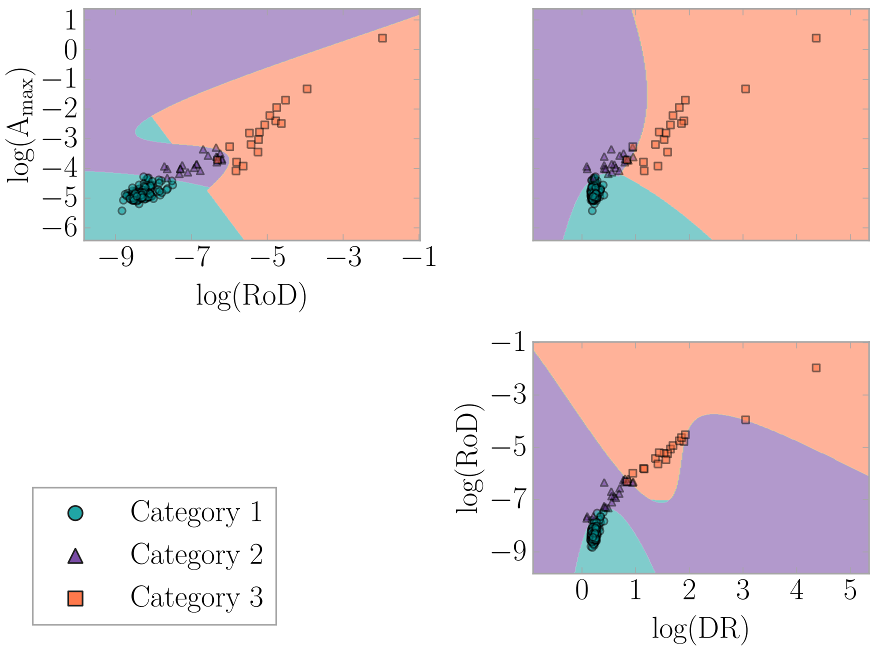

Figure D.1: SVM 3rd Degree Polynomial Kernel Metric Combination Hyperplanes

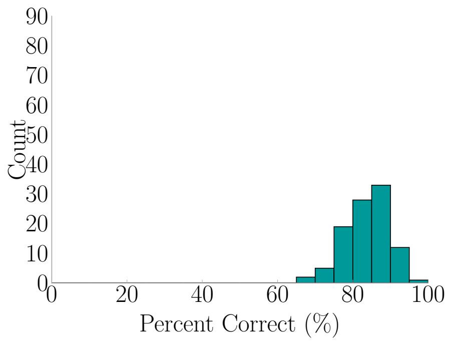

(a) A_{max}

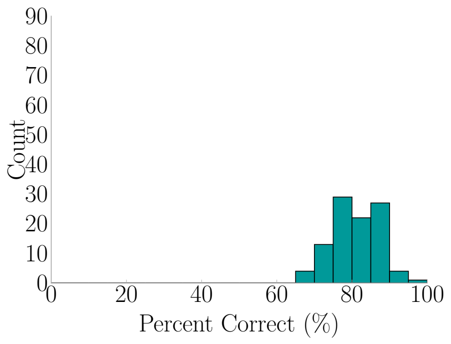

(b) RoD

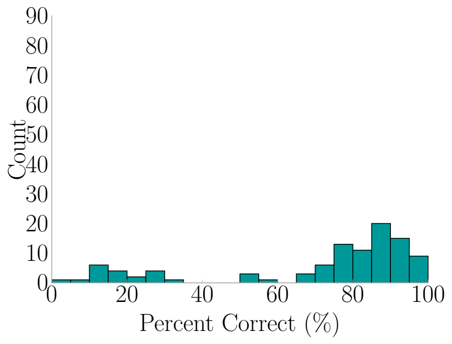

(c) DR

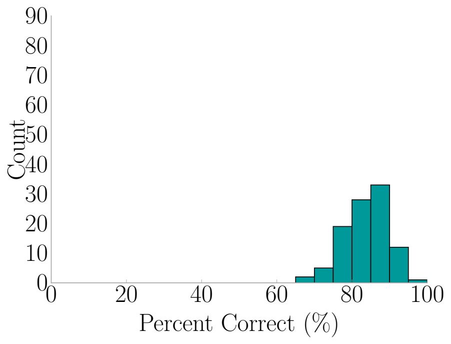

(d) A_{max} and RoD

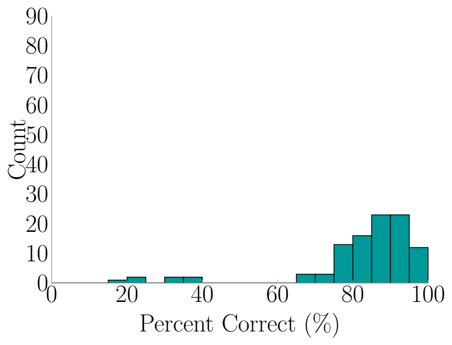

(e) RoD and DR

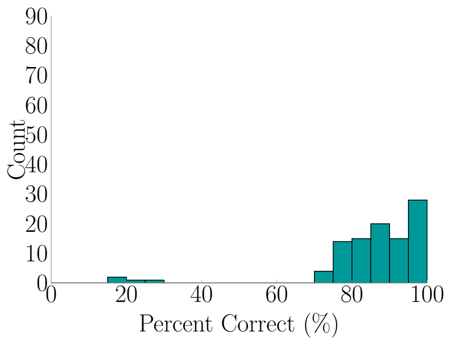

(f) A_{max} and DR

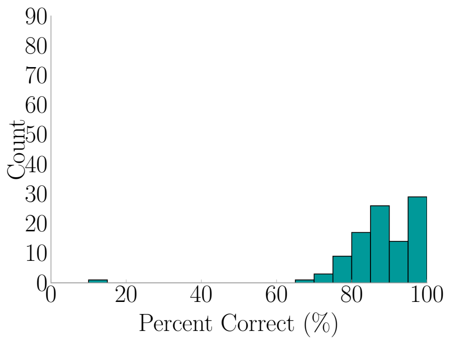

(g) A_{max}, RoD, and DR

Figure D.2: Score Distribution for 3rd Degree Polynomial Kernel Metric Combinations (100 Trials)

Appendix E

SVM Sigmoid Kernel Results for Event Filtering

The sigmoid kernel was also evaluated as a possibility for acceleration event filtering as seen in Chapter 4. The following figures and tables present the results for the kernel.

Table E.1: SVM Sigmoid Kernel Metric Combination Stats (100 Trials)

	Accuracy (%)	
Metric Combinations	Mean	St. Dev.
A_{max}	93.6	3.7
RoD	81.3	6.1
DR	79.9	6.3
A_{max}, RoD	93.4	3.7
RoD, DR	79.9	6.3
A_{max}, DR	79.9	6.3
A_{max}, RoD, DR	79.9	6.3

Table E.2: SVM Sigmoid Kernel Best Training Set for Each Metric Combination

Metric Combinations	C1	C2	C3	Accuracy (%)
A_{max}	121	21	18	100.0
RoD	121	21	18	97.5
DR	121	21	18	97.5
A_{max}, RoD	121	21	18	100.0
RoD, DR	121	21	18	97.5
A_{max}, DR	121	21	18	97.5
A_{max}, RoD, DR	121	21	18	97.5

Table E.3: SVM Sigmoid Kernel Worst Training Set for Each Metric Combination

Metric Combinations	C1	C2	C3	Accuracy (%)
A_{max}	132	16	12	82.5
RoD	134	11	15	67.5
DR	134	15	11	65.0
A_{max}, RoD	132	16	12	82.5
RoD, DR	134	15	11	65.0
A_{max}, DR	134	15	11	65.0
A_{max}, RoD, DR	134	15	11	65.0

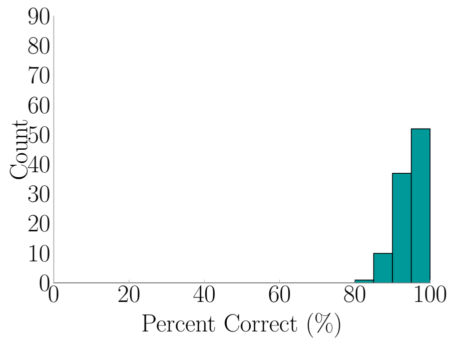

(a) A_{max}

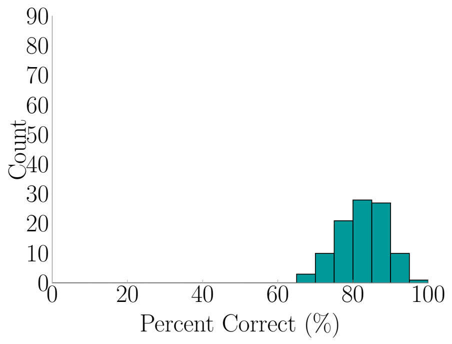

(b) RoD

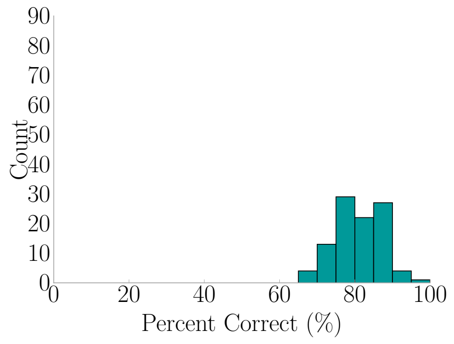

(c) DR

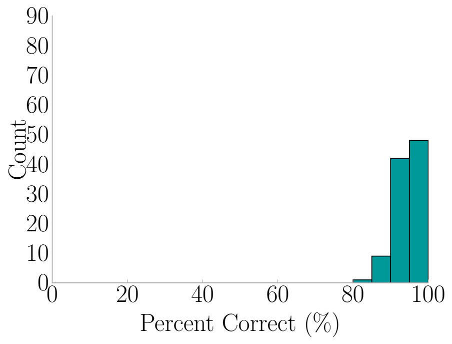

(d) A_{max} and RoD

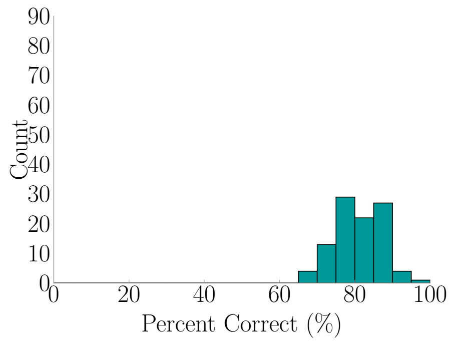

(e) RoD and DR

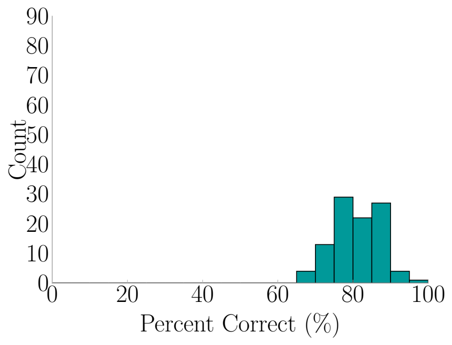

(f) A_{max} and DR

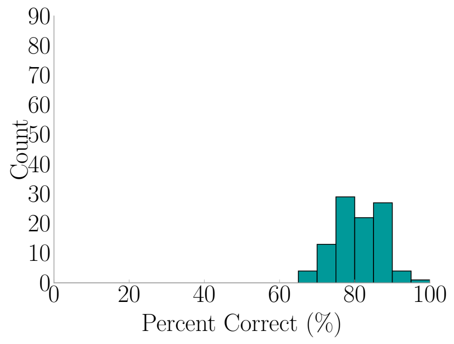

(g) A_{max}, RoD, and DR

Figure E.1: Score Distribution for Sigmoid Kernel Metric Combinations (100 Trials)

Appendix F

Manual Vs. SVM Classified Categories for Recorded Fall Events

The recorded fall data presented in Appendix B were manually filtered. To get an idea of the effectiveness of the Support Vector Machine (SVM) when filtering acceleration events for a fall detection application, the SVM's classified category is compared against the manual classification in Table F.1. More discussion is available in Chapter 4.

Table F.1: Recorded Fall Events SVM Classified Categories

ID	Records ±1 hr	Sensor	Category	Figures
16	2013-06-17 21:57:19	D4E1	2	Figure B.1
		B3B0	2	Figure B.2
		others	1	-
	2013-06-17 21:58:54	BB46	2	Figure B.3
		BB87	2	Figure B.4
	2013-06-17 22:03:19	BB87	2	Figure B.5
		others	1	-
	2013-06-17 22:10:07	BB87	2	Figure B.6
		others	1	-

continued on next page...

ID	Records ±1 hr	Sensor	Category	Figures
18	2013-06-20 17:14:23	D4E1	2	Figure B.7
		BB46	2	Figure B.8
		others	1	-
20	2013-06-28 23:23:57	8D2C	3	Figure B.9
		others	1	-
	2013-06-28 23:24:42	8D2C	-	Figure B.10
		others	1	-
	2013-06-28 23:28:42	8D2C	-	Figure B.11
		others	1	-
	2013-06-28 23:30:38	8D2C	3	Figure B.12
		others	1	-
26	2013-07-25 17:49:29	B3A1	2	Figure B.13
		BB7E	-	Figure B.14
		others	1	-
28	2013-07-30 04:45:49	BB48	3	Figure B.15
		others	1	-
32	2013-08-27 10:58:35	BB48	2	Figure B.16
		E0A8	2	Figure B.17
		E7EC	3	Figure B.18
		3496	1	Figure B.19
		others	1	-
33	2013-08-29 14:48:57	E7DB	3	Figure B.20
		3493	2	Figure B.21
		others	1 or 2	-
34	2013-08-31 18:07:07	B3A5	2	Figure B.22
		E7DB	-	Figure B.23
		8D2C	-	Figure B.24
		others	1	-

continued on next page...

ID	Records ±1 hr	Sensor	Category	Figures
35	2013-09-22 02:45:21	C7AE	3	Figure B.25
		DC67	3	Figure B.26
		2E73	3	Figure B.27
		others	-	-
36	2013-10-03 12:34:31	B3A5	2	Figure B.28
		others	1	-
39	2013-10-22 20:02:20	E7EC	-	Figure B.29
		others	1	-
41	2013-10-26 07:34:28	E7EC	-	Figure B.30
		others	2	-
42	2013-10-28 23:25:33	E0A8	2	Figure B.31
		others	-	-
44	2013-11-25 17:33:49	B3A5	3	Figure B.32
		BB7C	2	Figure B.33
		3087	3	Figure B.34
		3493	2	Figure B.35
		others	2	-
46	2013-12-03 03:47:22	B3A5	2	Figure B.36
		others	1,2	-
48	2013-12-09 04:59:04	B3A5	2	Figure B.37
		BB45	3	Figure B.38
		8D2C	3	Figure B.39
		8F1E	-	Figure B.40
		others	1	-

Appendix G

Event Localization Method Attempts

This section describes the attempted methods towards determine the location of an impact from a force estimate generated by Equation 5.5 whilst developing the FEEL Algorithm. All methods have the flexibility of window choice like in the Correlated Force Estimates Method of Section 5.2.3.

G.1 Deviation Method

Following the selection of a window, the standard deviation is taken between the resulting real portions of the force estimations from each sensor to each location, point by point within the window. Equation G.1 demonstrates this step with $\{L_i\}$ being a vector of maximum standard deviations σ for each location, $\hat{F}_{i,j}(k)$ being the force estimate for the i-th location and j-th sensor, k being the point within the force estimate vector being compared, and n being the number of points in the force estimate window.

$$\{L_i\} = \max \left\{ \begin{array}{llllll} \sigma(& \hat{F}_{i,1}(k) & \hat{F}_{i,2}(k) & \cdots & \hat{F}_{i,j}(k) &) \\ \sigma(& \hat{F}_{i,1}(k+1) & \hat{F}_{i,2}(k+1) & \cdots & \hat{F}_{i,j}(k+1) &) \\ \vdots & \vdots & \vdots & \ddots & \vdots & \\ \sigma(& \hat{F}_{i,1}(k+n) & \hat{F}_{i,2}(k+n) & \cdots & \hat{F}_{i,j}(k+n) &) \end{array} \right\} \tag{G.1}$$

The maximum standard deviation of the force at each location is then compared in Equation G.2 where $\hat{L}$ is the lowest standard deviation, which indicates the impact location estimation, and min() is the minimum value function.

$$\hat{L} = \min(\{L_i\}) \tag{G.2}$$

The reasoning is that the location's force estimates that more closely match in magnitude for the specified window, indicates the location of impact. This works very well for impulse forces, but begins to have challenges when applied to other force impacts such as a person jumping as seen in the following tables.

Table G.1: Confusion Matrix for Locating Ball-Low Impacts Using The Deviation Method

		Identified				
		Location 1	Location 2	Location 3	Location 4	Location 5
Actual	Location 1	**100**	0	0	0	0
	Location 2	0	**100**	0	0	0
	Location 3	0	0	**100**	0	0
	Location 4	0	0	0	**100**	0
	Location 5	0	1	0	0	**99**

Table G.2: Confusion Matrix for Locating Ball-High Impacts Using The Deviation Method

		Identified				
		Location 1	Location 2	Location 3	Location 4	Location 5
Actual	Location 1	**100**	0	0	0	0
	Location 2	0	**100**	0	0	0
	Location 3	0	1	**99**	0	0
	Location 4	0	0	0	**100**	0
	Location 5	0	0	0	0	**100**

Table G.3: Confusion Matrix for Locating Bag-Low Impacts Using The Deviation Method

		Identified				
		Location 1	Location 2	Location 3	Location 4	Location 5
Actual	Location 1	**91**	0	0	9	0
	Location 2	2	**98**	0	0	0
	Location 3	60	0	**4**	36	0
	Location 4	1	1	0	**98**	0
	Location 5	20	65	0	0	**15**

Table G.4: Confusion Matrix for Locating Bag-High Impacts Using The Deviation Method

		Identified				
		Location 1	Location 2	Location 3	Location 4	Location 5
Actual	Location 1	**84**	1	0	15	0
	Location 2	0	**100**	0	0	0
	Location 3	51	0	**6**	43	0
	Location 4	2	8	0	**90**	0
	Location 5	24	70	0	0	**6**

Table G.5: Confusion Matrix for Locating D-Jump Impacts Using The Deviation Method

		Identified				
		Location 1	Location 2	Location 3	Location 4	Location 5
Actual	Location 1	**89**	0	0	9	2
	Location 2	1	**99**	0	0	0
	Location 3	0	0	**97**	3	0
	Location 4	0	0	0	**100**	0
	Location 5	0	0	0	4	**96**

Table G.6: Confusion Matrix for Locating J-Jump Impacts Using The Deviation Method

		Identified				
		Location 1	Location 2	Location 3	Location 4	Location 5
Actual	Location 1	**95**	0	1	4	0
	Location 2	17	**79**	1	3	0
	Location 3	1	0	**95**	4	0
	Location 4	2	0	0	**98**	0
	Location 5	29	10	0	24	**37**

Table G.7: Confusion Matrix for Locating W-Jump Impacts Using The Deviation Method

		Identified				
		Location 1	Location 2	Location 3	Location 4	Location 5
Actual	Location 1	**54**	0	0	46	0
	Location 2	86	**11**	0	3	0
	Location 3	30	0	**56**	14	0
	Location 4	0	0	0	**100**	0
	Location 5	34	0	0	53	**13**

G.2 Deviation of Normalized Force Estimates

This method is similar to the Deviation Method discussed in Section G.1, but normalizes the force before making the standard deviation calculations. Equation G.3 normalizes each force estimate where $\hat{F}_{i,j}$ is the force estimate for the i-th location and j-th sensor, and max() is the maximum value function.

$$||\hat{F}_{i,j}|| = \frac{\hat{F}_{i,j}}{\max\left(\left|\hat{F}_{i,j}\right|\right)} \tag{G.3}$$

The standard deviation is then taken point by point for a chosen window in Equation G.4 where $\{L_i\}$ is a vector of maximum standard deviations σ for each location, $||\hat{F}_{i,j}||$ being the normalized force estimate for the i-th location and j-th sensor, k being the point within the force estimate vector being compared, and n being the number of points in the normalized force estimate window.

$$\{L_i\} = \max \begin{Bmatrix} \sigma(& ||\hat{F}_{i,1}(k)|| & ||\hat{F}_{i,2}(k)|| & \cdots & ||\hat{F}_{i,j}(k)|| &) \\ \sigma(& ||\hat{F}_{i,1}(k+1)|| & ||\hat{F}_{i,2}(k+1)|| & \cdots & ||\hat{F}_{i,j}(k+1)|| &) \\ \vdots & \vdots & \vdots & \ddots & \vdots & \\ \sigma(& ||\hat{F}_{i,1}(k+n)|| & ||\hat{F}_{i,2}(k+n)|| & \cdots & ||\hat{F}_{i,j}(k+n)|| &) \end{Bmatrix} \tag{G.4}$$

Finally, the location is identified as being the location with lowest standard deviation value as seen in Equation G.5.

$$\hat{L} = \min(\{L_i\}) \tag{G.5}$$

Since the peak magnitudes varied a lot between the sensors, the thought became to normalized each signal so that the maximum value was one. In theory, this would move the shapes of the force closer together for the actual location. See the confusion matrices below for results.

Table G.8: Confusion Matrix for Locating Ball-Low Impacts Using The Deviation of Normalized Force Estimates Method

		Identified				
		Location 1	Location 2	Location 3	Location 4	Location 5
Actual	Location 1	**100**	0	0	0	0
	Location 2	0	**100**	0	0	0
	Location 3	0	0	**100**	0	0
	Location 4	0	0	0	**100**	0
	Location 5	0	0	0	0	**100**

Table G.9: Confusion Matrix for Locating Ball-High Impacts Using The Deviation of Normalized Force Estimates Method

		Identified				
		Location 1	Location 2	Location 3	Location 4	Location 5
Actual	Location 1	**100**	0	0	0	0
	Location 2	0	**100**	0	0	0
	Location 3	0	1	**99**	0	0
	Location 4	0	0	0	**100**	0
	Location 5	0	0	0	0	**100**

Table G.10: Confusion Matrix for Locating Bag-Low Impacts Using The Deviation of Normalized Force Estimates Method

		Identified				
		Location 1	Location 2	Location 3	Location 4	Location 5
Actual	Location 1	**100**	0	0	0	0
	Location 2	0	**96**	0	4	0
	Location 3	0	25	**11**	55	0
	Location 4	0	1	0	**99**	0
	Location 5	0	3	0	2	**95**

Table G.11: Confusion Matrix for Locating Bag-High Impacts Using The Deviation of Normalized Force Estimates Method

		Identified				
		Location 1	Location 2	Location 3	Location 4	Location 5
Actual	Location 1	**95**	4	1	0	0
	Location 2	0	**98**	0	1	1
	Location 3	0	23	**21**	48	8
	Location 4	0	5	0	**95**	0
	Location 5	0	2	0	5	**93**

Table G.12: Confusion Matrix for Locating D-Jump Impacts Using The Deviation of Normalized Force Estimates Method

		Identified				
		Location 1	Location 2	Location 3	Location 4	Location 5
Actual	Location 1	**62**	0	0	3	35
	Location 2	1	**97**	1	1	0
	Location 3	2	0	**96**	1	1
	Location 4	0	0	0	**98**	2
	Location 5	0	0	0	0	**100**

Table G.13: Confusion Matrix for Locating J-Jump Impacts Using The Deviation of Normalized Force Estimates Method

		Identified				
		Location 1	Location 2	Location 3	Location 4	Location 5
Actual	Location 1	**65**	2	4	6	23
	Location 2	5	**71**	2	17	5
	Location 3	0	0	**79**	6	15
	Location 4	0	0	0	**93**	7
	Location 5	3	0	2	14	**81**

Table G.14: Confusion Matrix for Locating W-Jump Impacts Using The Deviation of Normalized Force Estimates Method

		Identified				
		Location 1	Location 2	Location 3	Location 4	Location 5
Actual	Location 1	**38**	1	8	49	4
	Location 2	30	**54**	1	14	1
	Location 3	2	1	**72**	21	4
	Location 4	1	0	0	**99**	0
	Location 5	2	0	0	12	**86**

G.3 Modal Assurance Criterion of Force Estimates

Taking an idea from the modal analysis play book that looks at the similarity of mode shapes, the Modal Assurance Criterion (MAC) was adapted to be applied to pairs of force estimates in a similar manner as that of the Correlated Force Estimates Method in Section 5.2.3. Equation G.6 is the original equation for MAC [67]. This was adapted so that $\{A\}$ is one force estimate and $\{X\}$ is another, with n being the number of points within the force estimate window being considered.

$$\text{MAC}(A, X) = \frac{\left|\sum_{j=1}^{n} \{A_j\}\{X_j\}\right|}{\left(\sum_{j=1}^{n} \{A_j\}^2\right)\left(\sum_{j=1}^{n} \{X_j\}^2\right)} \tag{G.6}$$

Using the MAC equation, all force estimate combinations would be compared and the maximum value taken as that location's MAC value. Equation G.7 shows this procedure where $\{L_i\}$ is the maximum MAC value of all the combinations of the i-th location, max() is the maximum value function, $\hat{F}_{i,j}$ is the force estimate of the i-th location at the j-th sensor, and n is the number of points within the window.

$$\{L_i\} = \max \begin{bmatrix} 0 & \text{MAC}\left(\hat{F}_{i,1}(n), \hat{F}_{i,2}(n)\right) & \cdots & \text{MAC}\left(\hat{F}_{i,1}(n), \hat{F}_{i,j}(n)\right) \\ & 0 & \cdots & \text{MAC}\left(\hat{F}_{i,2}(n), \hat{F}_{i,j}(n)\right) \\ & & \ddots & \vdots \\ \text{sym.} & & & \text{MAC}\left(\hat{F}_{i,j}(n), \hat{F}_{i,j}(n)\right) \end{bmatrix} \tag{G.7}$$

The location is then determined by whichever location has the largest MAC value as in Equation G.8.

$$\hat{L} = \max(\{L_i\}) \tag{G.8}$$

MAC is used in Modal Analysis to compare the shapes of multiple mode shapes. As experiments continued to more varied impacts, the shape of the force became more important that then magnitude for localization. Hence, MAC was adapted for the Force Estimation and Event Localization (FEEL) Algorithm. The results are presented below in confusion matrices.

Table G.15: Confusion Matrix for Locating Ball-Low Impacts Using The MAC of Force Estimates Method

		Identified				
		Location 1	Location 2	Location 3	Location 4	Location 5
Actual	Location 1	**100**	0	0	0	0
	Location 2	0	**100**	0	0	0
	Location 3	0	0	**100**	0	0
	Location 4	0	0	0	**100**	0
	Location 5	0	1	0	0	**99**

Table G.16: Confusion Matrix for Locating Ball-High Impacts Using The MAC of Force Estimates Method

		Identified				
		Location 1	Location 2	Location 3	Location 4	Location 5
Actual	Location 1	**100**	0	0	0	0
	Location 2	0	**100**	0	0	0
	Location 3	0	0	**99**	0	1
	Location 4	0	0	0	**100**	0
	Location 5	0	0	0	0	**100**

Table G.17: Confusion Matrix for Locating Bag-Low Impacts Using The MAC of Force Estimates Method

		Identified				
		Location 1	Location 2	Location 3	Location 4	Location 5
Actual	Location 1	**77**	4	11	3	5
	Location 2	0	**100**	0	0	0
	Location 3	5	2	**50**	1	42
	Location 4	0	0	0	**99**	1
	Location 5	1	0	0	0	**99**

Table G.18: Confusion Matrix for Locating Bag-High Impacts Using The MAC of Force Estimates Method

		Identified				
		Location 1	Location 2	Location 3	Location 4	Location 5
Actual	Location 1	**77**	2	12	2	7
	Location 2	0	**100**	0	0	0
	Location 3	2	3	**69**	0	26
	Location 4	0	0	0	**99**	1
	Location 5	0	1	0	0	**99**

Table G.19: Confusion Matrix for Locating D-Jump Impacts Using The MAC of Force Estimates Method

		Identified				
		Location 1	Location 2	Location 3	Location 4	Location 5
Actual	Location 1	**68**	0	0	2	30
	Location 2	0	**100**	0	0	0
	Location 3	0	0	**97**	2	1
	Location 4	0	0	0	**97**	3
	Location 5	0	5	0	1	**94**

Table G.20: Confusion Matrix for Locating J-Jump Impacts Using The MAC of Force Estimates Method

		Identified				
		Location 1	Location 2	Location 3	Location 4	Location 5
Actual	Location 1	**69**	10	0	3	18
	Location 2	5	**88**	1	4	2
	Location 3	4	14	**75**	0	7
	Location 4	1	1	3	**74**	21
	Location 5	5	9	1	3	**82**

Table G.21: Confusion Matrix for Locating W-Jump Impacts Using The MAC of Force Estimates Method

		Identified				
		Location 1	Location 2	Location 3	Location 4	Location 5
Actual	Location 1	**32**	5	8	21	34
	Location 2	4	**84**	2	4	6
	Location 3	4	1	**81**	3	11
	Location 4	0	1	0	**91**	8
	Location 5	1	4	0	1	**94**

G.4 Time Shift Method

Time shifting looks at the location of peaks within the force estimates, and if the peaks of the sensors align. The thought is that the location whose force estimates have peaks that more closely align is where the impact occurred since the FEEL Algorithm is time-independent. The standard deviation σ is taken of each point in time $\tau_{\hat{F}_i,j}$ where the peak in the force estimate occurred as in Equation G.9 where i is the location, and j is the sensor.

$$\{L_i\} = \sigma \begin{Bmatrix} \tau_{\hat{F}_i,1} \\ \tau_{\hat{F}_i,2} \\ \vdots \\ \tau_{\hat{F}_i,j} \end{Bmatrix} \tag{G.9}$$

The location of impact is consequently the location having the lowest standard deviation value as this indicates the time in the force estimate the peaks occur are more closely aligned as in Equation G.10.

$$\hat{L} = \min(\{L_i\}) \tag{G.10}$$

Results of this method are presented in the following confusion matrices.

Table G.22: Confusion Matrix for Locating Ball-Low Impacts Using The Time Shift Method

		Identified				
		Location 1	Location 2	Location 3	Location 4	Location 5
Actual	Location 1	**100**	0	0	0	0
	Location 2	0	**99**	0	0	1
	Location 3	0	0	**100**	0	0
	Location 4	0	0	0	**100**	0
	Location 5	0	0	0	0	**100**

Table G.23: Confusion Matrix for Locating Ball-High Impacts Using The Time Shift Method

		Identified				
		Location 1	Location 2	Location 3	Location 4	Location 5
Actual	Location 1	**100**	0	0	0	0
	Location 2	0	**100**	0	0	0
	Location 3	0	0	**100**	0	0
	Location 4	0	0	0	**98**	2
	Location 5	0	0	0	0	**100**

Table G.24: Confusion Matrix for Locating Bag-Low Impacts Using The Time Shift Method

		Identified				
		Location 1	Location 2	Location 3	Location 4	Location 5
Actual	Location 1	**87**	3	2	7	1
	Location 2	0	**91**	3	3	3
	Location 3	9	72	**13**	2	4
	Location 4	0	0	0	**98**	2
	Location 5	2	7	5	3	**83**

Table G.25: Confusion Matrix for Locating Bag-High Impacts Using The Time Shift Method

		Identified				
		Location 1	Location 2	Location 3	Location 4	Location 5
Actual	Location 1	**81**	10	1	4	4
	Location 2	0	**99**	0	0	1
	Location 3	16	62	**20**	1	1
	Location 4	1	2	1	**94**	2
	Location 5	6	9	12	4	**69**

Table G.26: Confusion Matrix for Locating D-Jump Impacts Using The Time Shift Method

		Identified				
		Location 1	Location 2	Location 3	Location 4	Location 5
Actual	Location 1	**73**	5	2	14	6
	Location 2	0	**99**	0	0	1
	Location 3	1	2	**76**	10	11
	Location 4	6	4	5	**82**	3
	Location 5	10	2	0	6	**82**

Table G.27: Confusion Matrix for Locating J-Jump Impacts Using The Time Shift Method

		Identified				
		Location 1	Location 2	Location 3	Location 4	Location 5
Actual	Location 1	**81**	1	8	3	7
	Location 2	11	**75**	4	7	3
	Location 3	20	7	**55**	14	4
	Location 4	1	0	3	**86**	10
	Location 5	29	3	24	16	**28**

Table G.28: Confusion Matrix for Locating W-Jump Impacts Using The Time Shift Method

		Identified				
		Location 1	Location 2	Location 3	Location 4	Location 5
Actual	Location 1	**51**	10	2	15	22
	Location 2	5	**93**	0	2	0
	Location 3	5	4	**87**	3	1
	Location 4	1	0	3	**86**	10
	Location 5	20	2	0	2	**76**

G.5 Residual Analysis Method

Residuals consist of interpreting if the dispersion of the data matches the model. In this case, it is used to compare the real portion of the force estimates to each other in order to indicate how well they match with the thought being the actual location would have the best coherence, and thus lowest covariance, between all its force estimates. Equation G.11 demonstrates the procedure with cov() being the covariance function, $\hat{F}_{i,j}$ being the force estimate of the i-th location at the j-th sensor, k is the point being considered in the force estimate, and μ is the average of the force estimate vector.

$$\{L_i\} = \text{cov}\begin{bmatrix} \hat{F}_{i,1}(k) - \mu_{\hat{F}_{i,1}} & \hat{F}_{i,2}(k) - \mu_{\hat{F}_{i,2}} & \cdots & \hat{F}_{i,j}(k) - \mu_{\hat{F}_{i,j}} \\ \hat{F}_{i,1}(k+1) - \mu_{\hat{F}_{1,j}} & \hat{F}_{i,2}(k+1) - \mu_{\hat{F}_{i,2}} & \cdots & \hat{F}_{i,j}(k+1) - \mu_{\hat{F}_{i,j}} \\ \vdots & \vdots & \vdots & \vdots \\ \hat{F}_{i,1}(k+n) - \mu_{\hat{F}_{1,j}} & \hat{F}_{i,2}(k+n) - \mu_{\hat{F}_{i,2}} & \cdots & \hat{F}_{i,j}(k+n) - \mu_{\hat{F}_{i,j}} \end{bmatrix} \tag{G.11}$$

The location of impact is thus the location with the lowest covariance value as seen in Equation G.12 where min() is the minimum value function.

$$\hat{L} = \min(\{L_i\}) \tag{G.12}$$

Table G.29: Confusion Matrix for Locating Ball-Low Impacts Using The Residual Analysis Method

		Identified				
		Location 1	Location 2	Location 3	Location 4	Location 5
Actual	Location 1	**100**	0	0	0	0
	Location 2	1	**99**	0	0	0
	Location 3	0	0	**100**	0	0
	Location 4	0	0	0	**100**	0
	Location 5	43	57	0	0	**0**

Table G.30: Confusion Matrix for Locating Ball-High Impacts Using The Residual Analysis Method

		Identified				
		Location 1	Location 2	Location 3	Location 4	Location 5
Actual	Location 1	**100**	0	0	0	0
	Location 2	0	**100**	0	0	0
	Location 3	0	1	**99**	0	0
	Location 4	0	0	0	**100**	0
	Location 5	13	87	0	0	**0**

Table G.31: Confusion Matrix for Locating Bag-Low Impacts Using The Residual Analysis Method

		Identified				
		Location 1	Location 2	Location 3	Location 4	Location 5
Actual	Location 1	**93**	0	0	7	0
	Location 2	13	**87**	0	0	0
	Location 3	93	1	**6**	0	0
	Location 4	13	4	0	**83**	0
	Location 5	57	43	0	0	**0**

Table G.32: Confusion Matrix for Locating Bag-High Impacts Using The Residual Analysis Method

		Identified				
		Location 1	Location 2	Location 3	Location 4	Location 5
Actual	Location 1	**90**	0	0	10	0
	Location 2	6	**94**	0	0	0
	Location 3	93	0	**7**	0	0
	Location 4	5	11	0	**84**	0
	Location 5	51	49	0	0	**0**

Table G.33: Confusion Matrix for Locating D-Jump Impacts Using The Residual Analysis Method

		Identified				
		Location 1	Location 2	Location 3	Location 4	Location 5
Actual	Location 1	**96**	0	0	4	0
	Location 2	44	**46**	0	10	0
	Location 3	69	0	**17**	14	0
	Location 4	4	0	0	**96**	0
	Location 5	53	45	0	2	**0**

Table G.34: Confusion Matrix for Locating J-Jump Impacts Using The Residual Analysis Method

		Identified				
		Location 1	Location 2	Location 3	Location 4	Location 5
Actual	Location 1	**94**	0	0	6	0
	Location 2	77	**21**	0	2	0
	Location 3	61	0	**36**	3	0
	Location 4	21	0	0	**79**	0
	Location 5	99	0	0	1	**0**

Table G.35: Confusion Matrix for Locating W-Jump Impacts Using The Residual Analysis Method

		Identified				
		Location 1	Location 2	Location 3	Location 4	Location 5
Actual	Location 1	**98**	0	0	2	0
	Location 2	93	**0**	0	7	0
	Location 3	99	0	**0**	1	0
	Location 4	98	0	0	**2**	0
	Location 5	100	0	0	0	**0**

Appendix H

Verification Experiments Additional Results

The following presents results from impacts that occurred on the remaining nodes from the steel frame eight node trial in Section 5.4.2. Force estimates and force correlations are presented for each case. FEEL Algorithm was successful in force and location estimation in all cases.

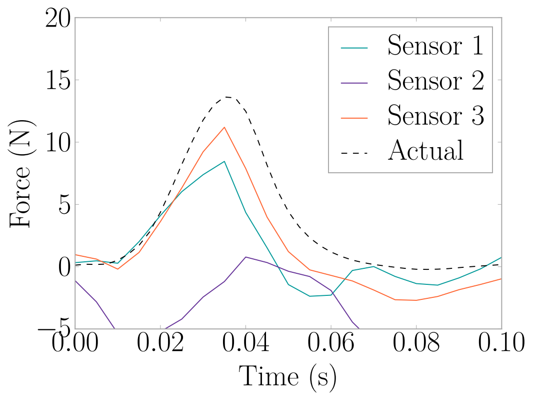

(a) $\hat{F}_{14,j}$

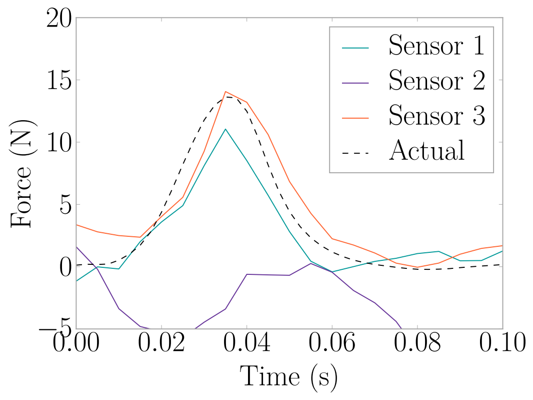

(b) $\hat{F}_{15,j}$

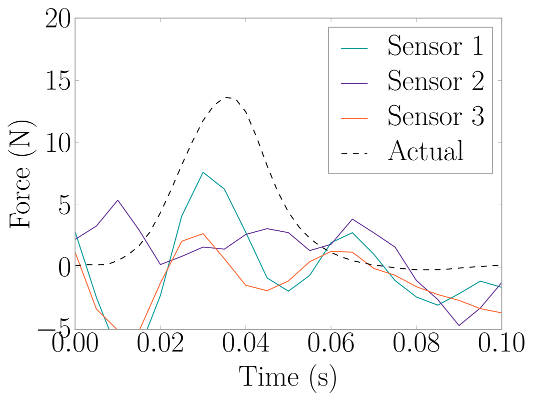

(c) $\hat{F}_{10,j}$

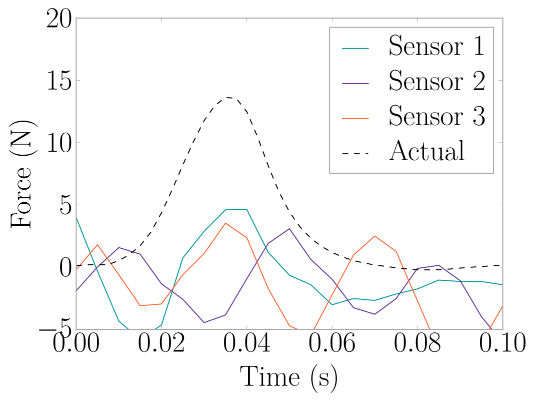

(d) $\hat{F}_{11,j}$

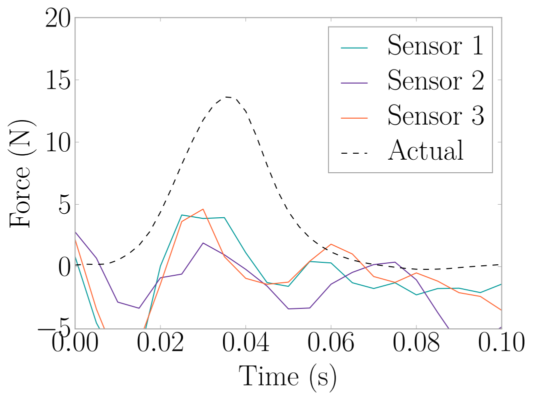

(e) $\hat{F}_{6,j}$

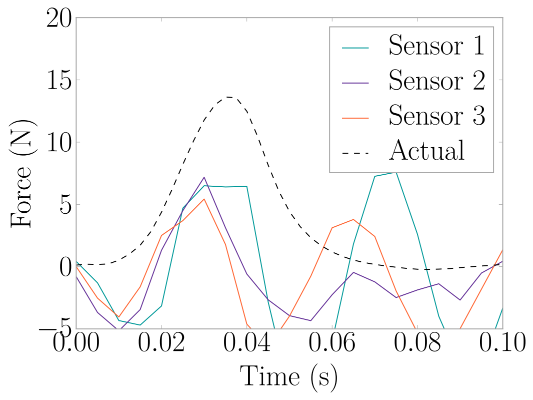

(f) $\hat{F}_{7,j}$

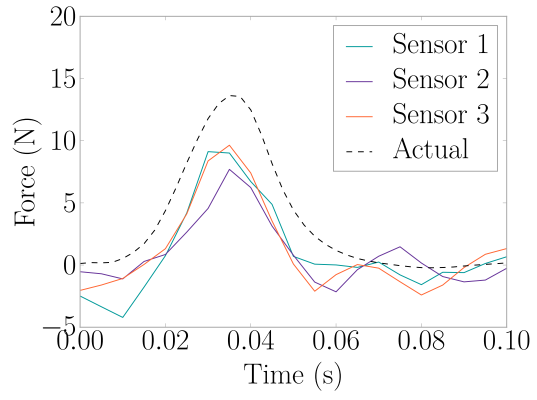

(g) $\hat{F}_{2,j}$

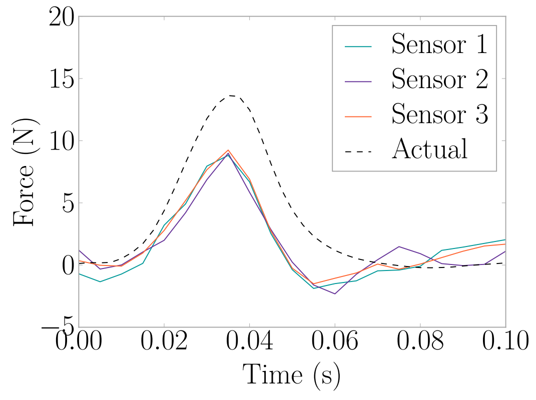

(h) $\hat{F}_{3,j}$

Figure H.1: Force Estimates by Node for an Impact on Node 3

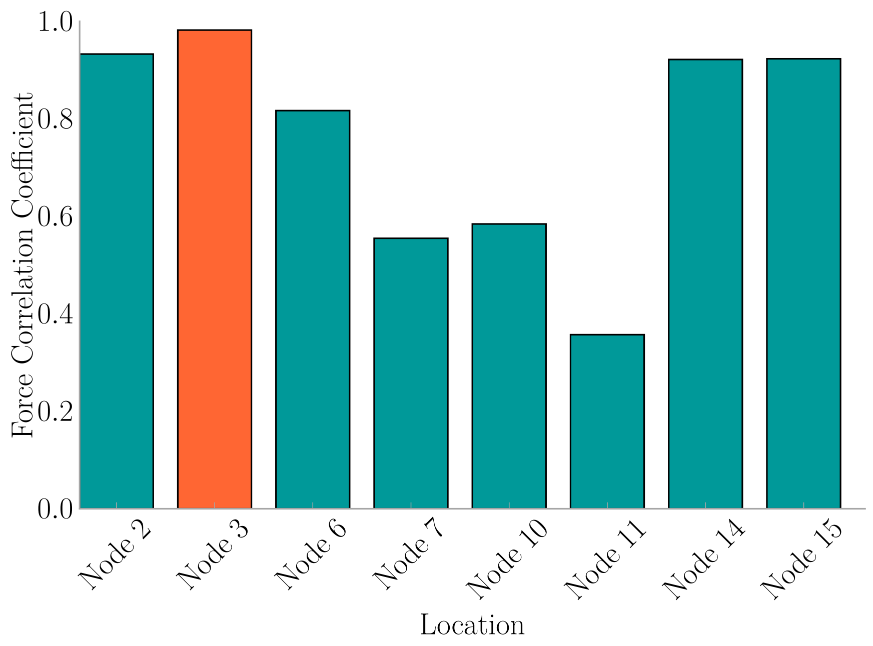

Figure H.2: L_i for an Impact on Node 3

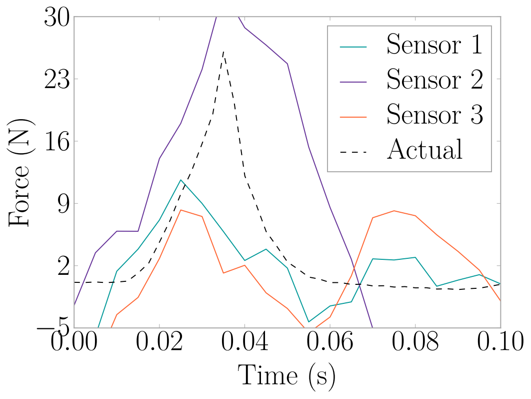

(a) $\hat{F}_{14,j}$

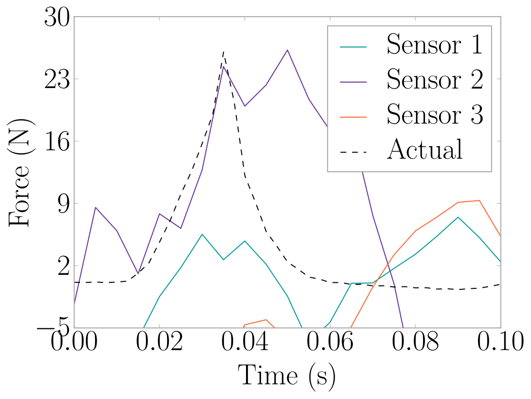

(b) $\hat{F}_{15,j}$

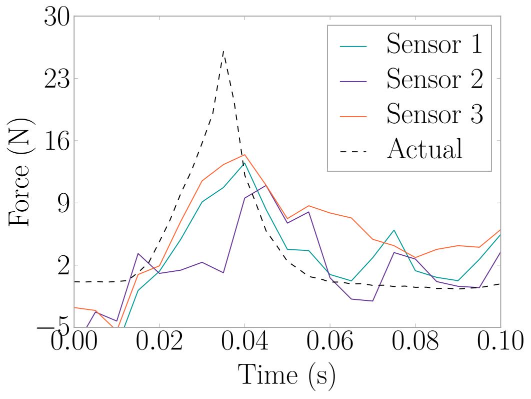

(c) $\hat{F}_{10,j}$

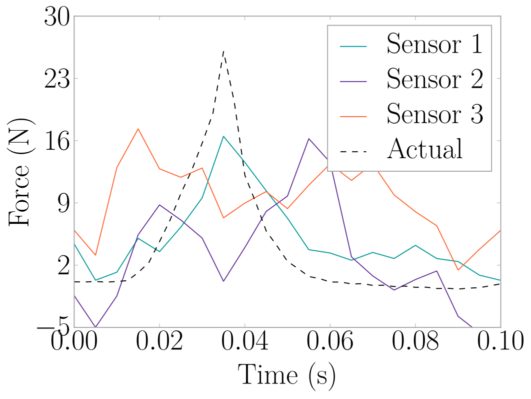

(d) $\hat{F}_{11,j}$

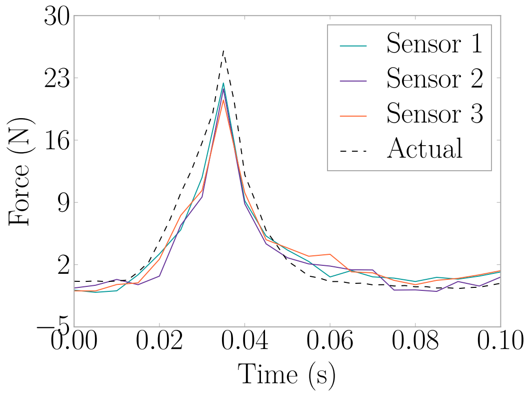

(e) $\hat{F}_{6,j}$

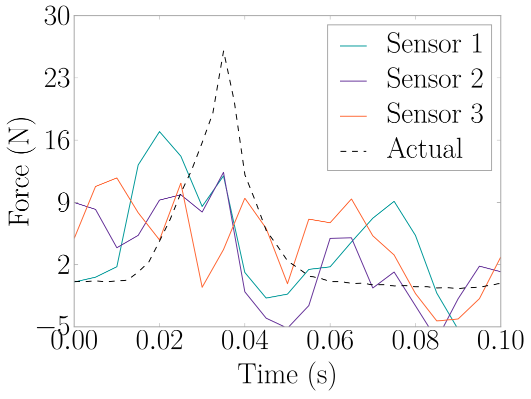

(f) $\hat{F}_{7,j}$

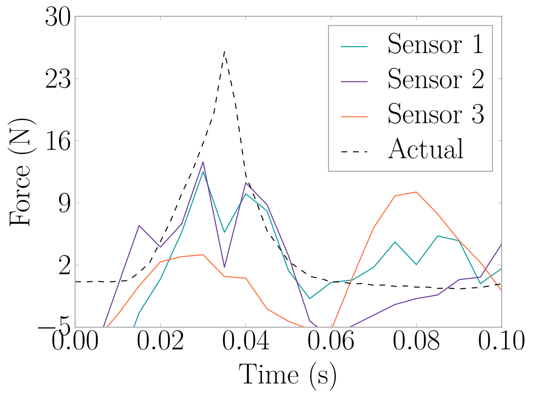

(g) $\hat{F}_{2,j}$

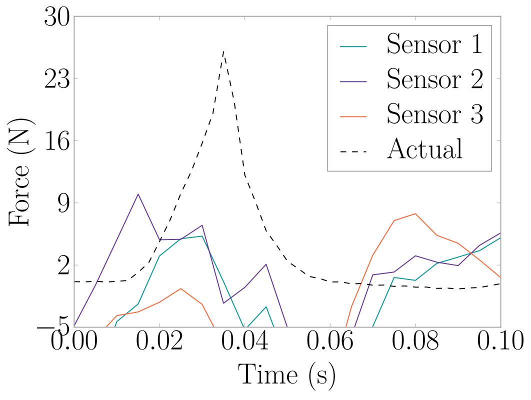

(h) $\hat{F}_{3,j}$

Figure H.3: Force Estimates by Node for an Impact on Node 6

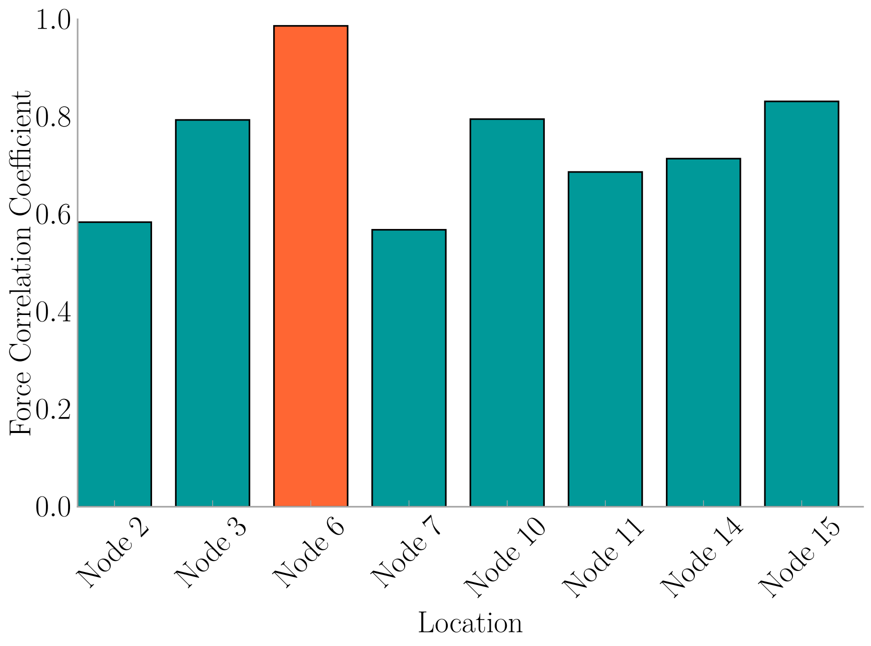

Figure H.4: L_i for an Impact on Node 6

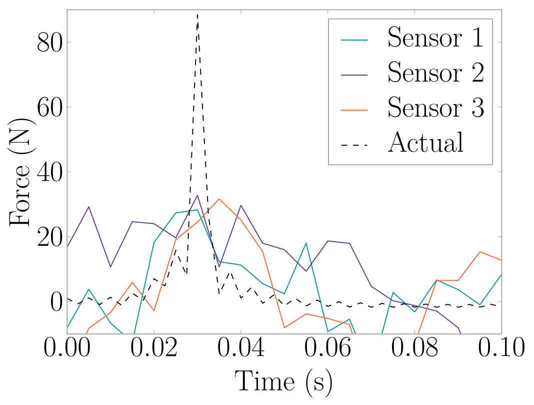

(a) $\hat{F}_{14,j}$

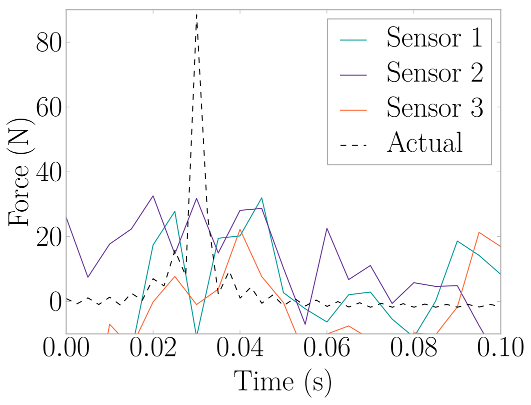

(b) $\hat{F}_{15,j}$

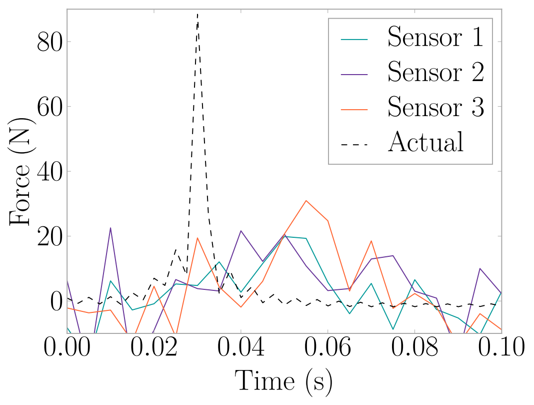

(c) $\hat{F}_{10,j}$

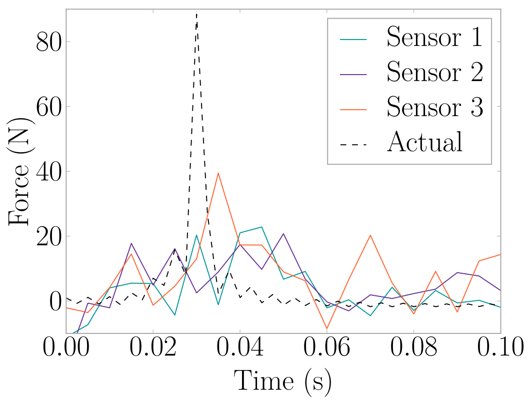

(d) $\hat{F}_{11,j}$

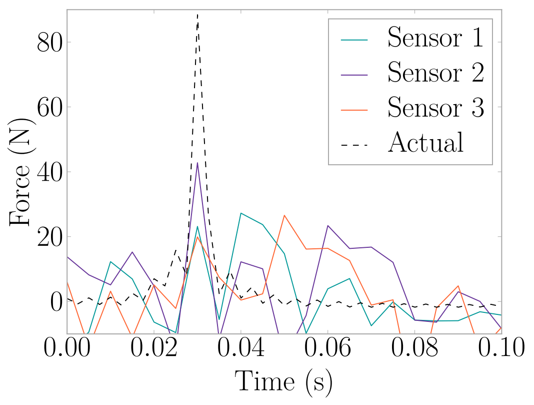

(e) $\hat{F}_{6,j}$

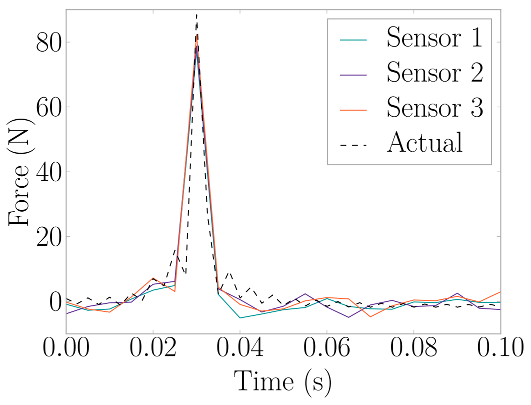

(f) $\hat{F}_{7,j}$

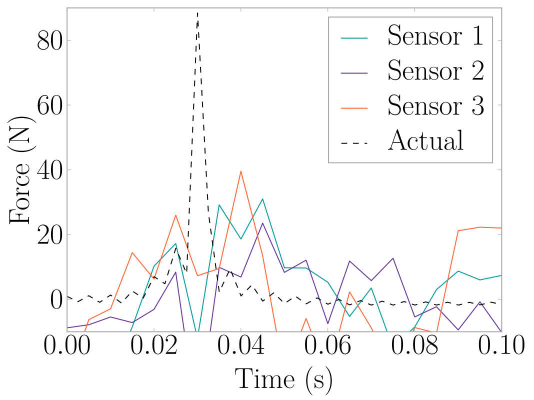

(g) $\hat{F}_{2,j}$

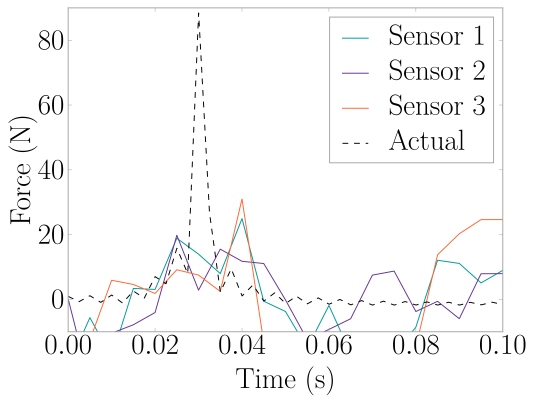

(h) $\hat{F}_{3,j}$

Figure H.5: Force Estimates by Node for an Impact on Node 7

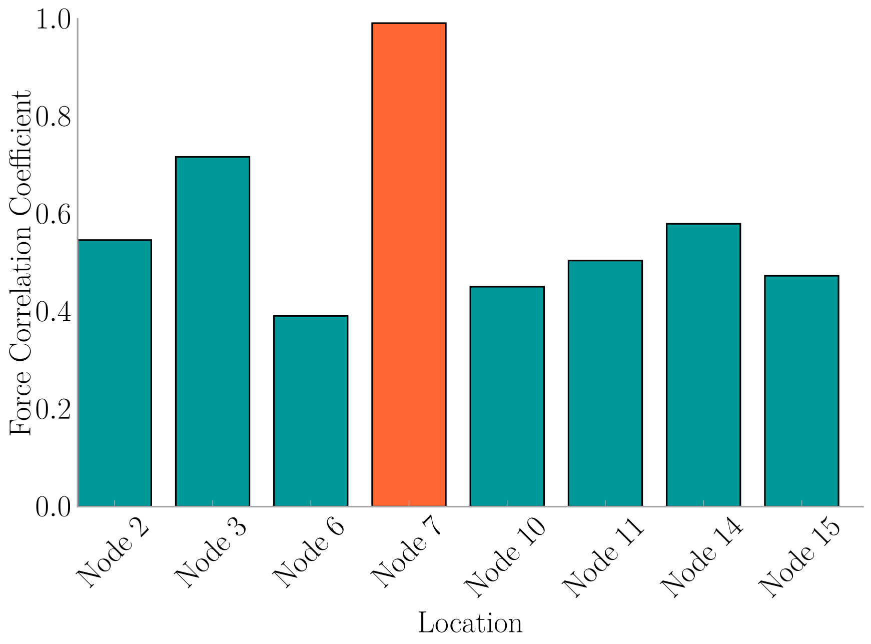

Figure H.6: L_i for an Impact on Node 7

H.4 Node 10 Impact

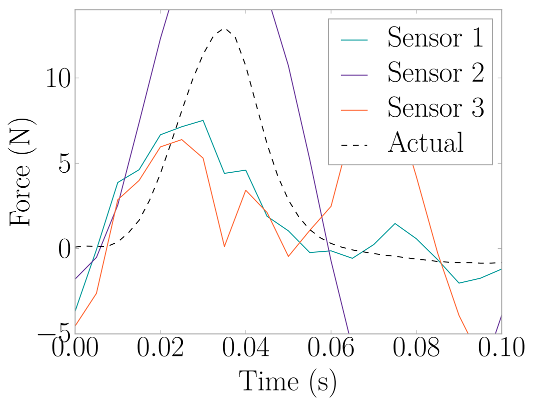

(a) $\hat{F}_{14,j}$

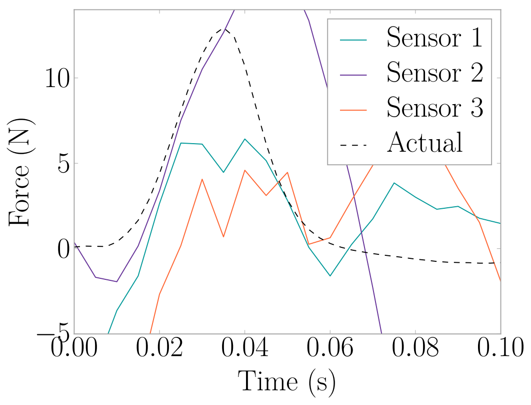

(b) $\hat{F}_{15,j}$

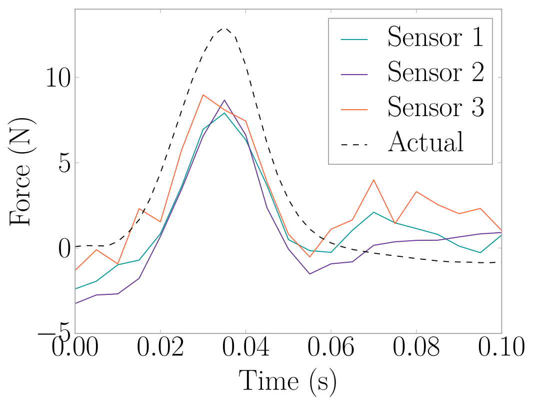

(c) $\hat{F}_{10,j}$

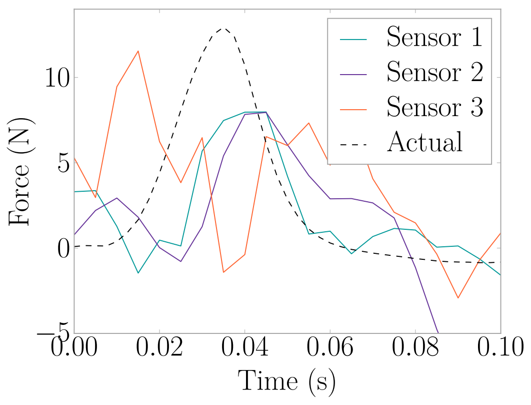

(d) $\hat{F}_{11,j}$

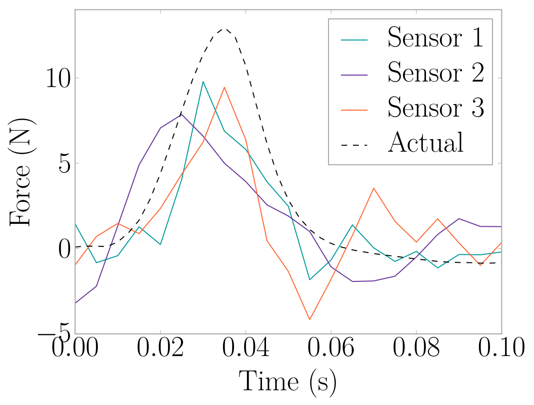

(e) $\hat{F}_{6,j}$

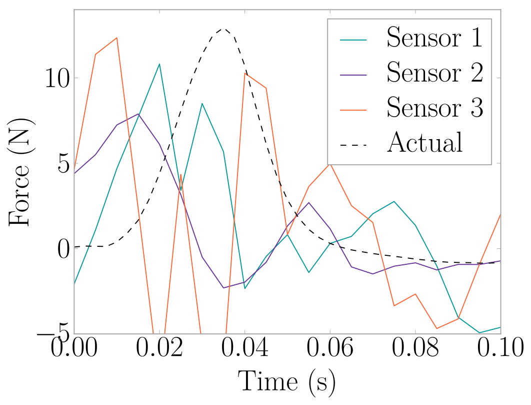

(f) $\hat{F}_{7,j}$

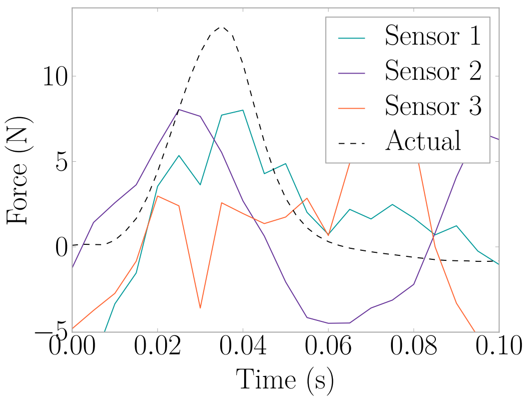

(g) $\hat{F}_{2,j}$

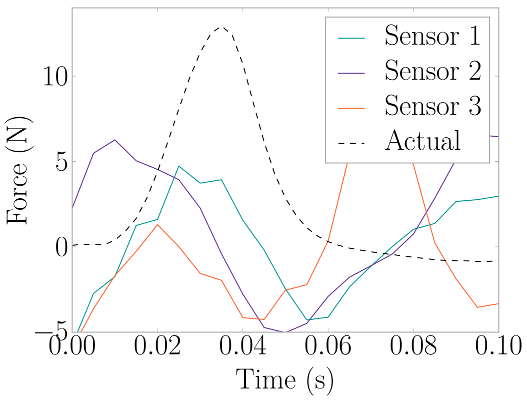

(h) $\hat{F}_{3,j}$

Figure H.7: Force Estimates by Node for an Impact on Node 10

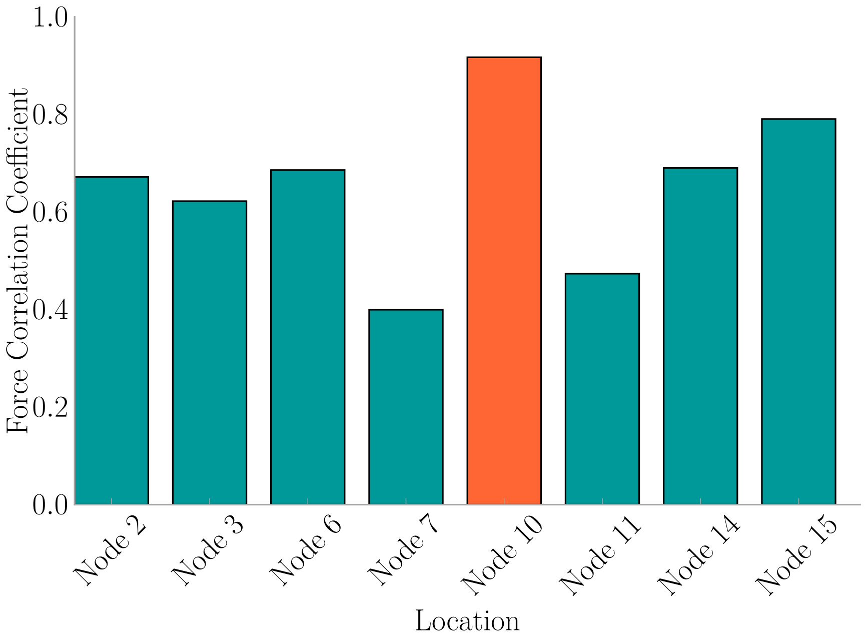

Figure H.8: L_i for an Impact on Node 10

H.5 Node 11 Impact

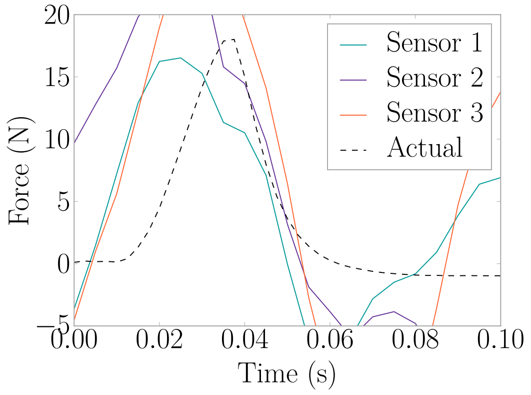

(a) $\hat{F}_{14,j}$

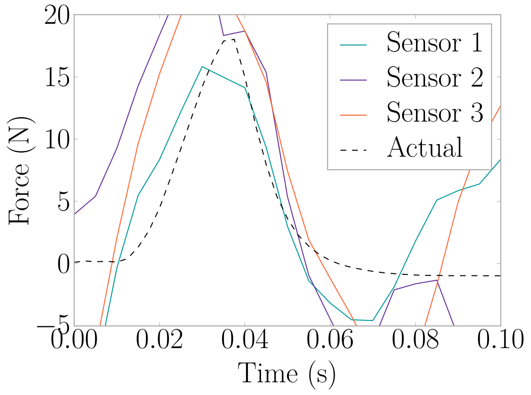

(b) $\hat{F}_{15,j}$

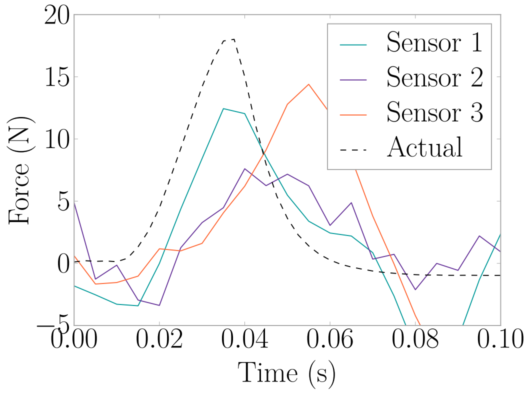

(c) $\hat{F}_{10,j}$

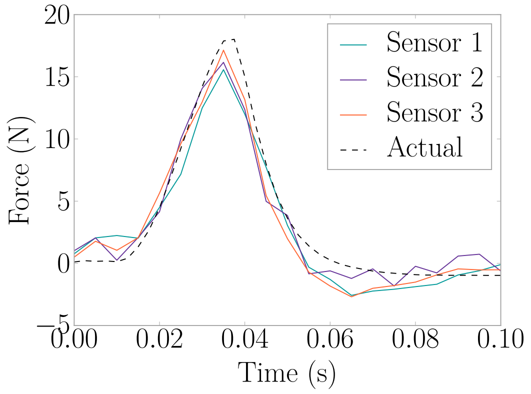

(d) $\hat{F}_{11,j}$

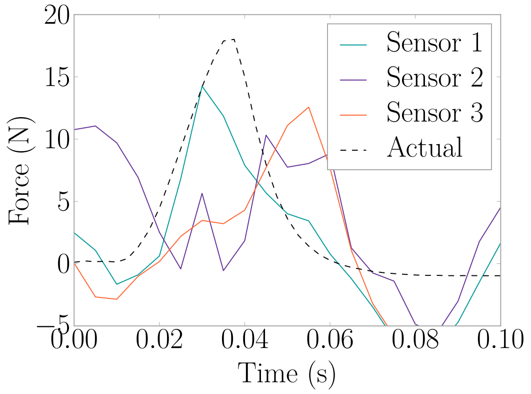

(e) $\hat{F}_{6,j}$

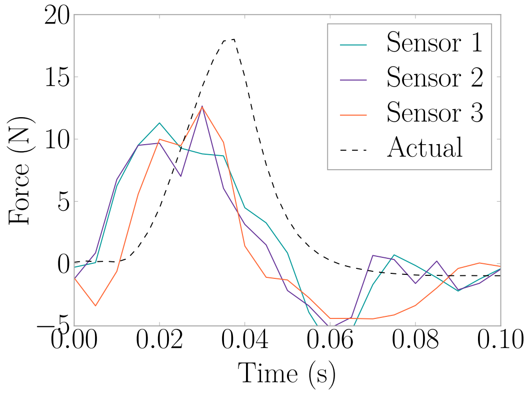

(f) $\hat{F}_{7,j}$

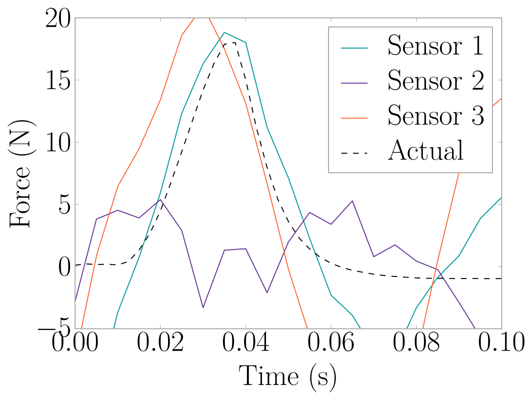

(g) $\hat{F}_{2,j}$

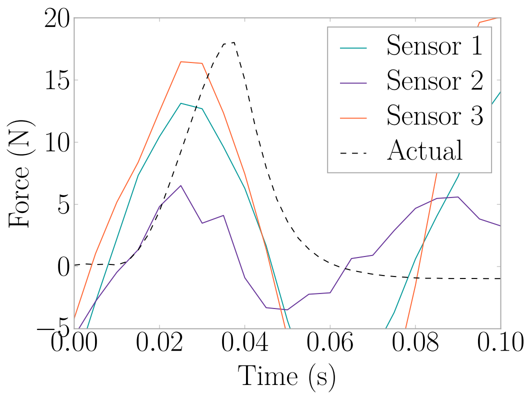

(h) $\hat{F}_{3,j}$

Figure H.9: Force Estimates by Node for an Impact on Node 11

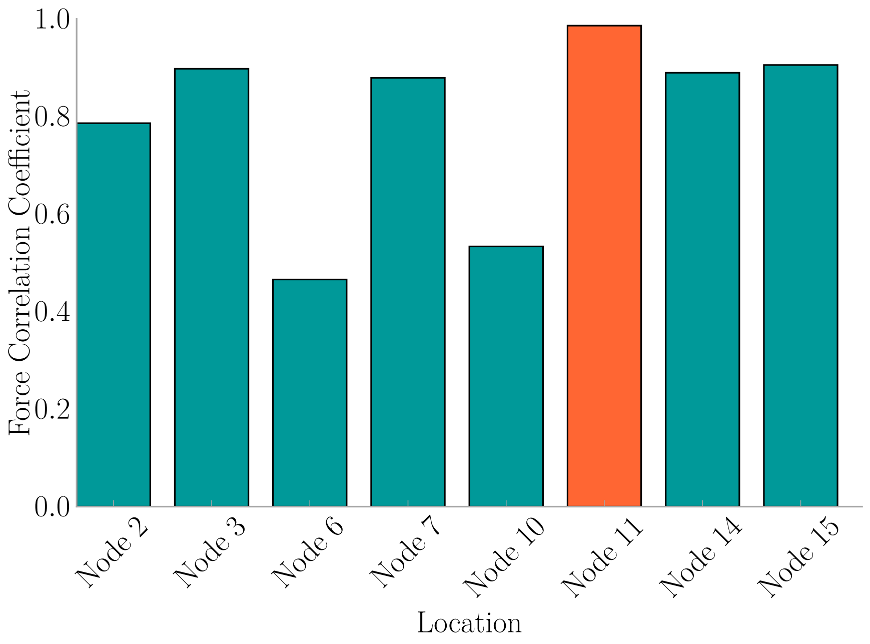

Figure H.10: L_i for an Impact on Node 11

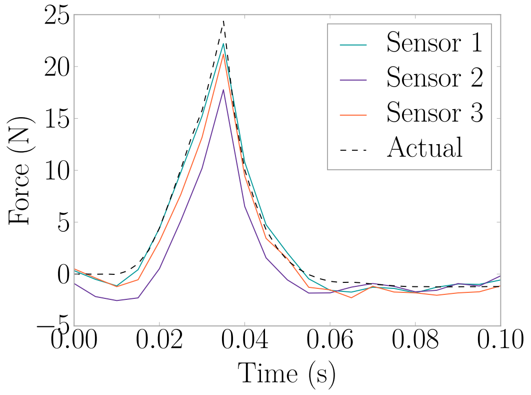

(a) $\hat{F}_{14,j}$

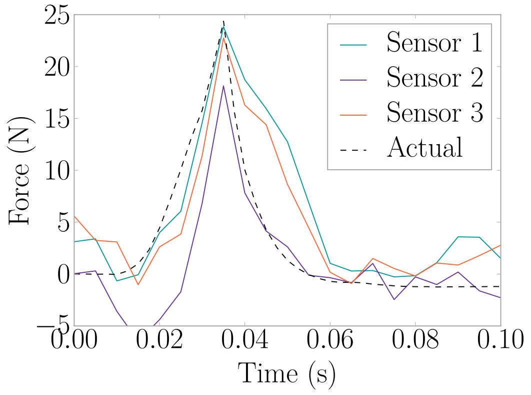

(b) $\hat{F}_{15,j}$

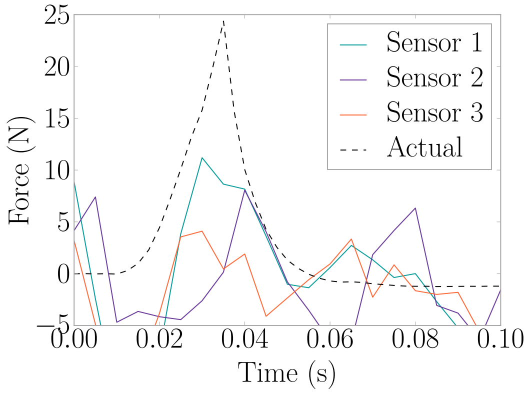

(c) $\hat{F}_{10,j}$

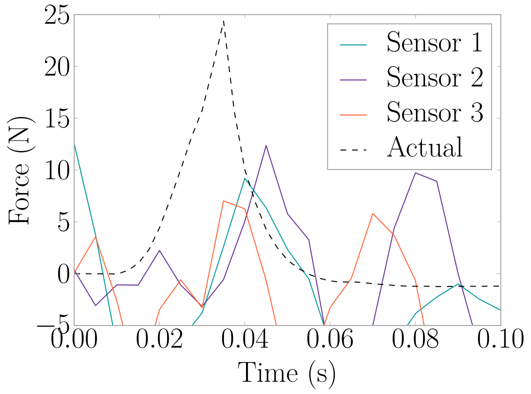

(d) $\hat{F}_{11,j}$

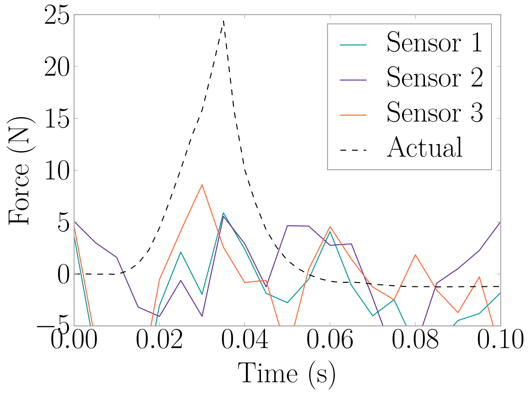

(e) $\hat{F}_{6,j}$

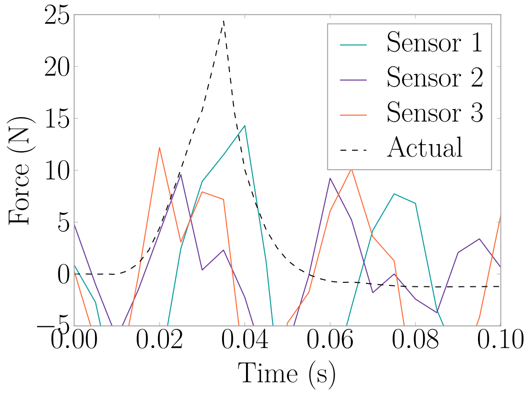

(f) $\hat{F}_{7,j}$

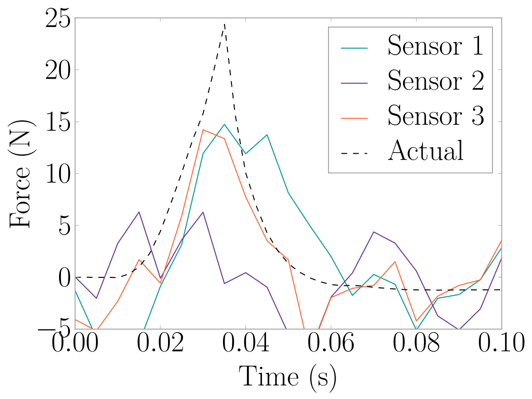

(g) $\hat{F}_{2,j}$

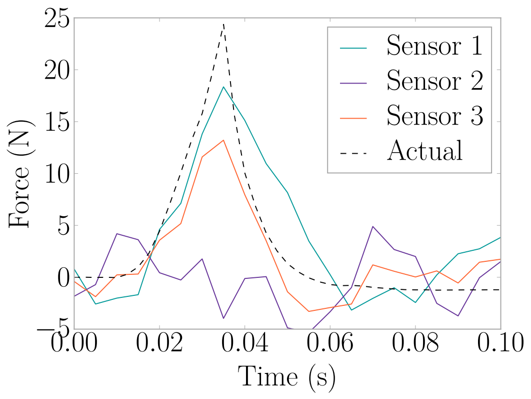

(h) $\hat{F}_{3,j}$

Figure H.11: Force Estimates By Node for An Impact On Node 14

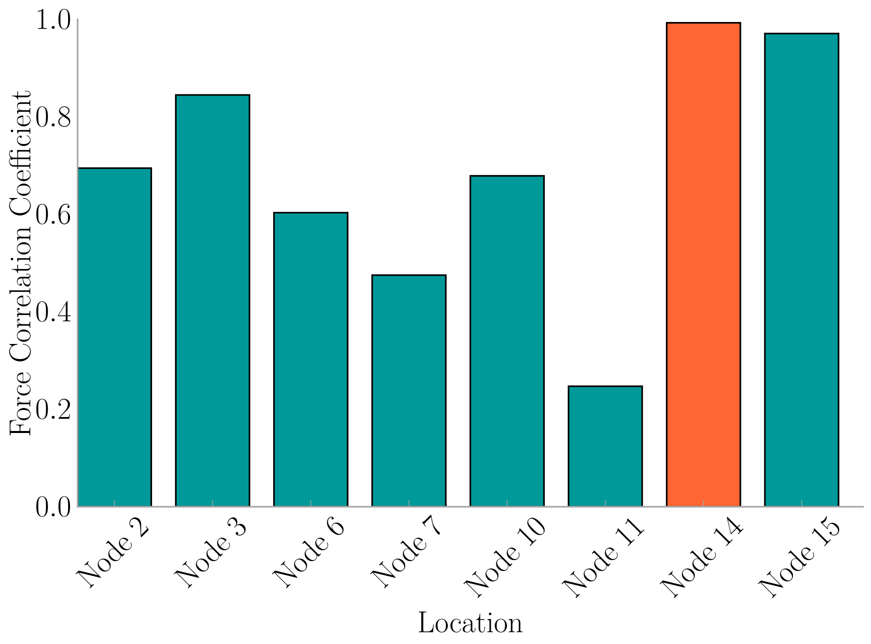

Figure H.12: L_i for an Impact on Node 14

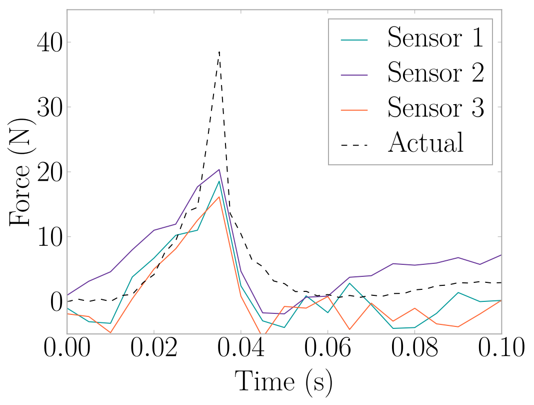

(a) $\hat{F}_{14,j}$

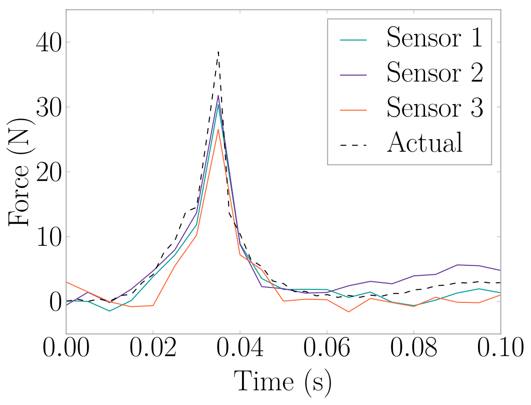

(b) $\hat{F}_{15,j}$

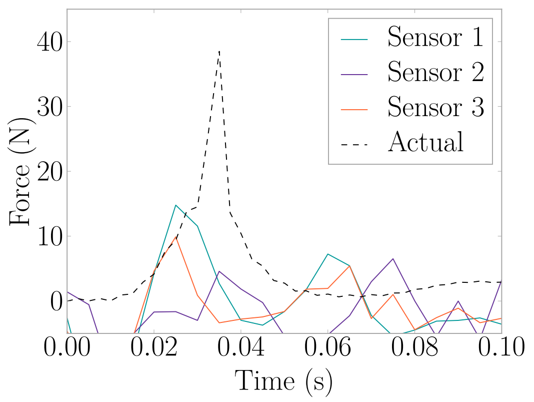

(c) $\hat{F}_{10,j}$

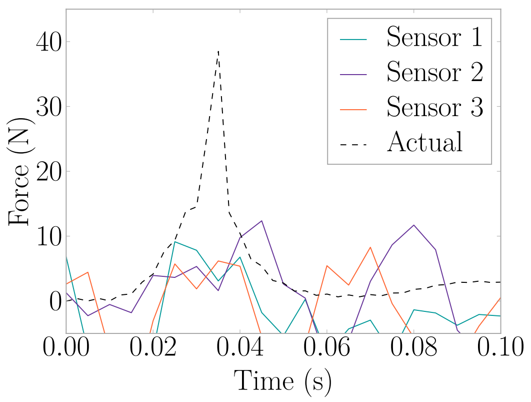

(d) $\hat{F}_{11,j}$

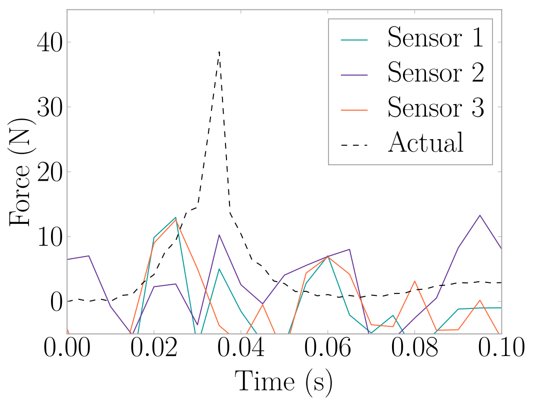

(e) $\hat{F}_{6,j}$

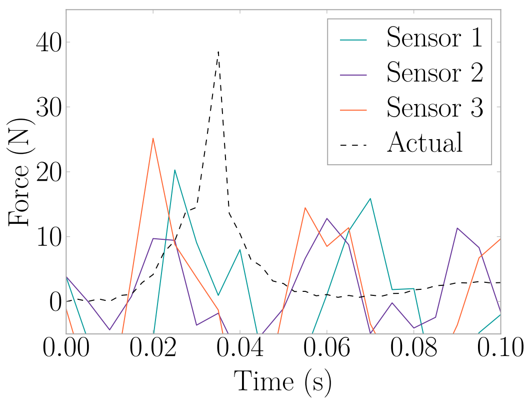

(f) $\hat{F}_{7,j}$

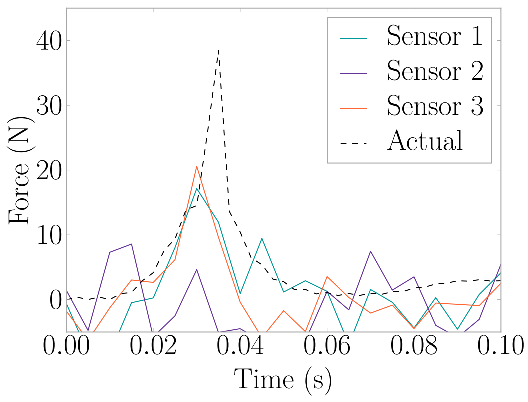

(g) $\hat{F}_{2,j}$

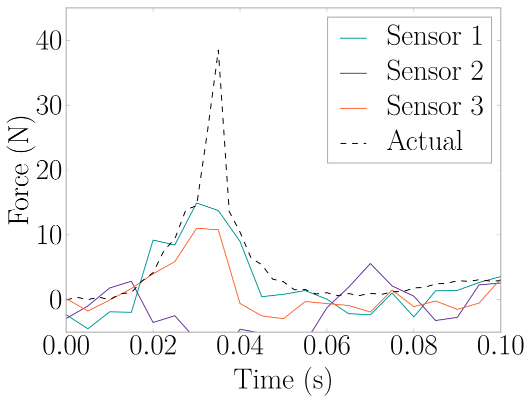

(h) $\hat{F}_{3,j}$

Figure H.13: Force Estimates by Node for an Impact on Node 15

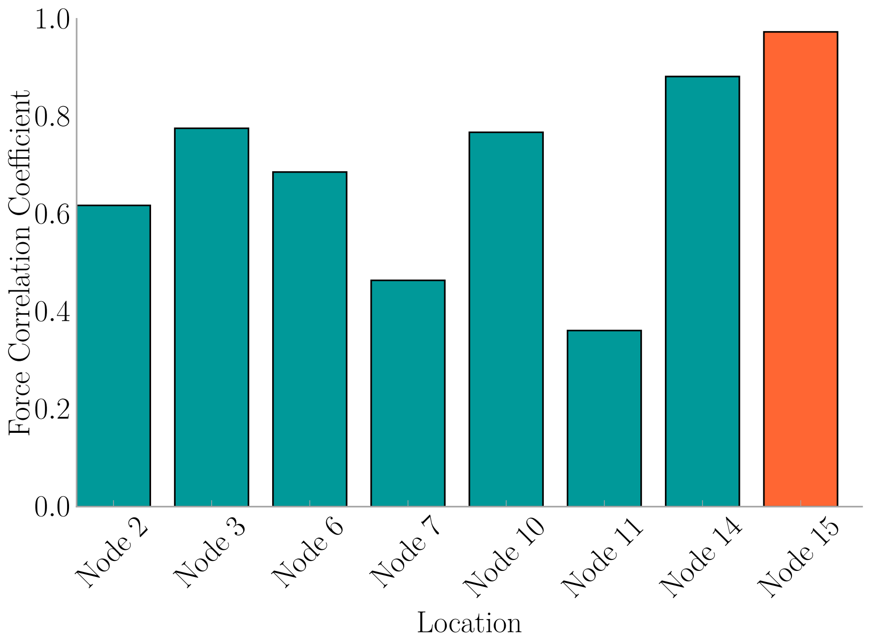

Figure H.14: L_i for an Impact on Node 15

Appendix I

Implementation Experiment Force Hammer Trial Additional Results

The following presents results from impacts that occurred on the remaining locations in the force hammer trial of the implementation experiments in Section 5.5.1. Force estimates and force correlations are presented for each case. The FEEL Algorithm was successful in force and location estimation in all cases.

I.1 Location 2 Impact

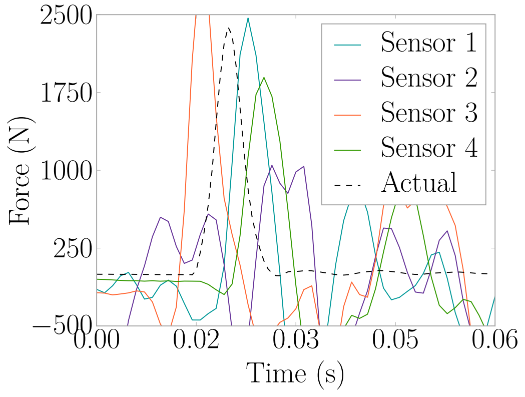

(a) $\hat{F}_{1,j}$

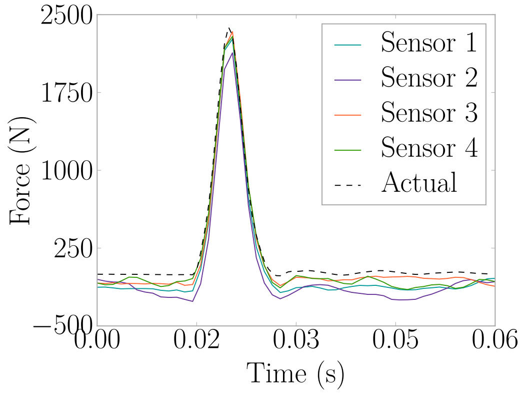

(b) $\hat{F}_{2,j}$

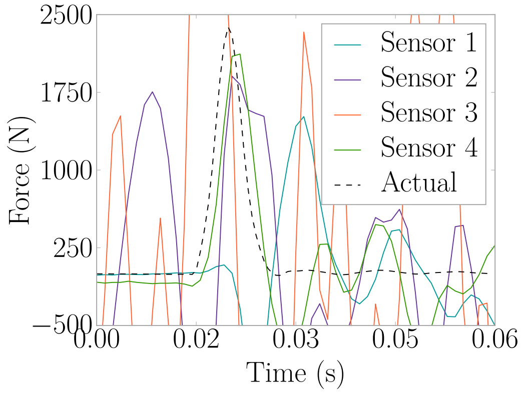

(c) $\hat{F}_{3,j}$

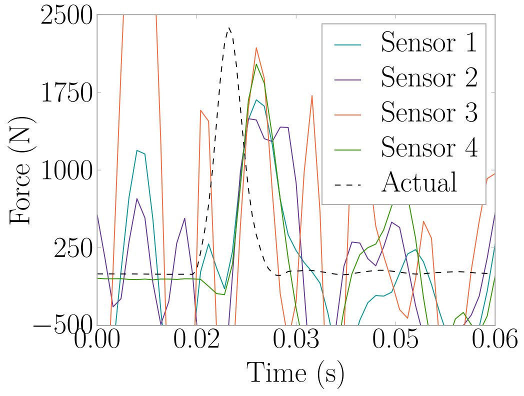

(d) $\hat{F}_{4,j}$

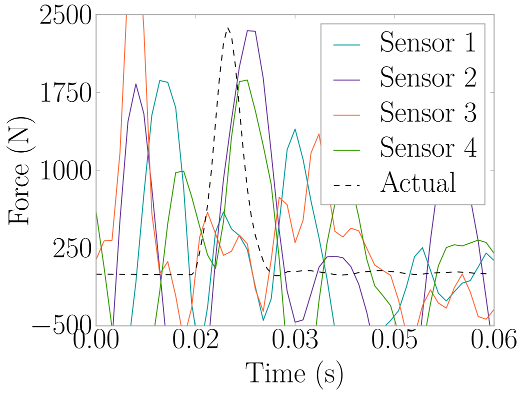

(e) $\hat{F}_{5,j}$

Figure I.1: Hammer Impact Force Estimations for an Impact on Location 2

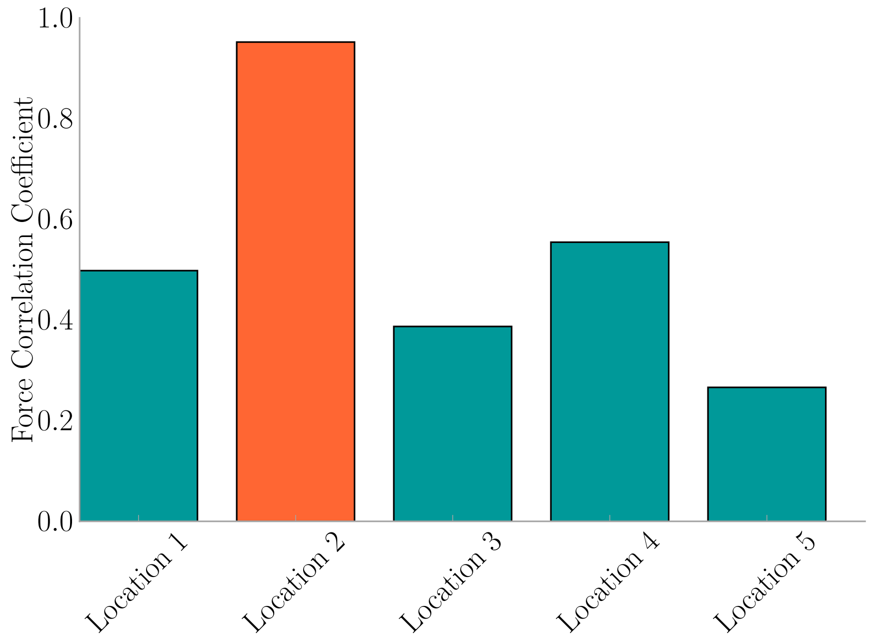

Figure I.2: Hammer Impact L_i for an Impact on Location 2

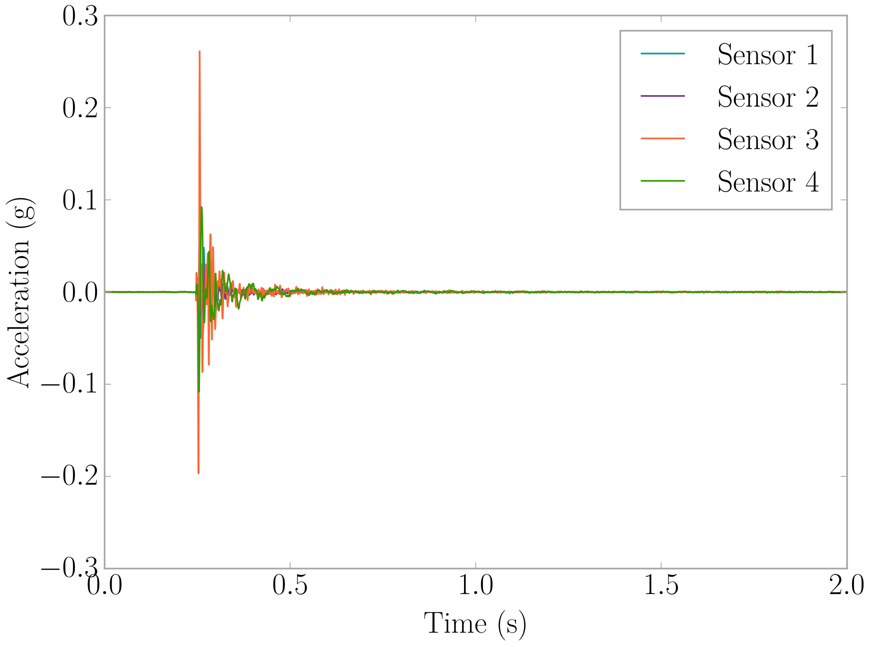

Figure I.3: Hammer on Location 2 Accelerations

I.2 Location 3 Impact

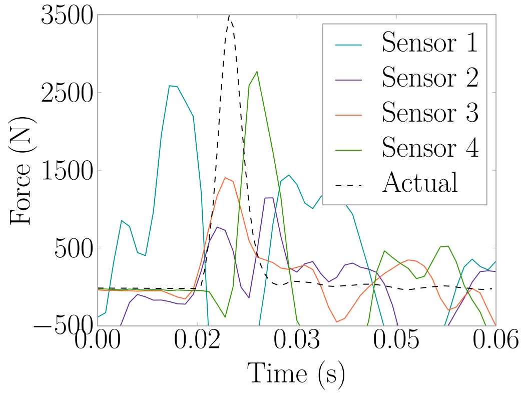

(a) $\hat{F}_{1,j}$

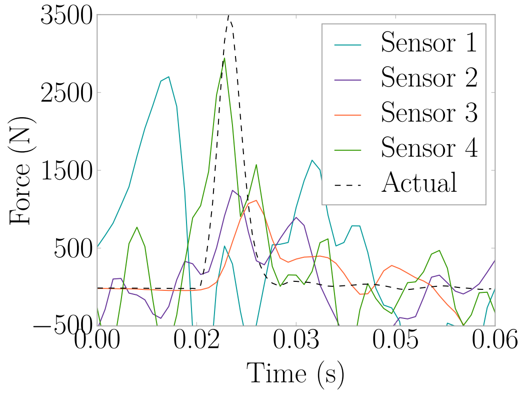

(b) $\hat{F}_{2,j}$

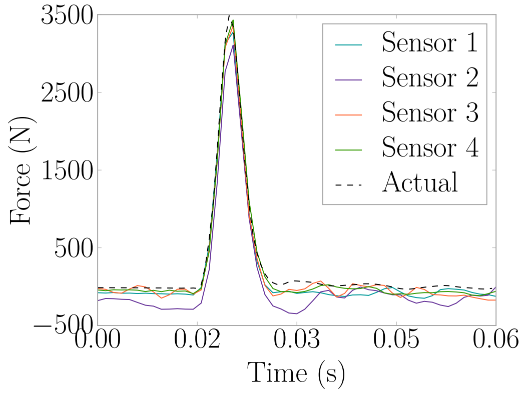

(c) $\hat{F}_{3,j}$

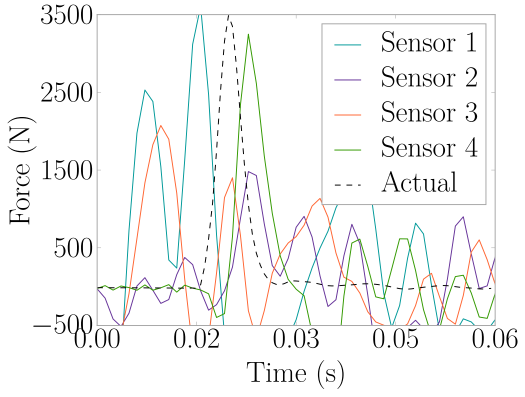

(d) $\hat{F}_{4,j}$

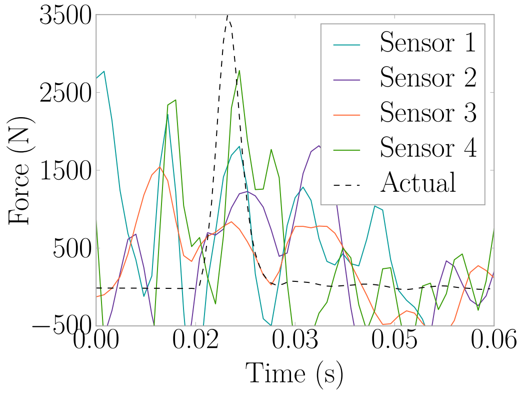

(e) $\hat{F}_{5,j}$

Figure I.4: Hammer Impact Force Estimations for an Impact on Location 3

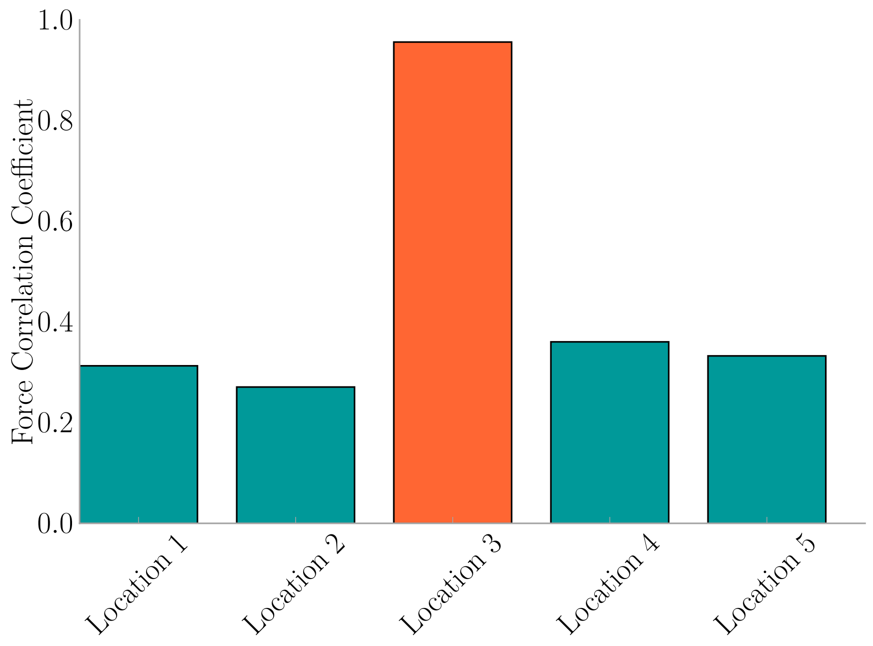

Figure I.5: Hammer Impact L_i for an Impact on Location 3

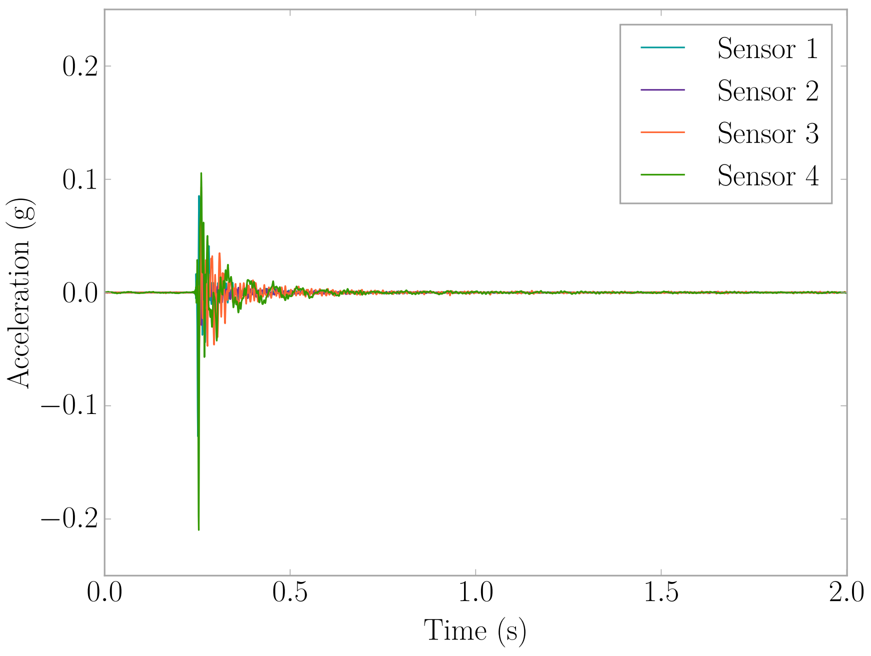

Figure I.6: Hammer on Location 3 Accelerations

I.3 Location 4 Impact

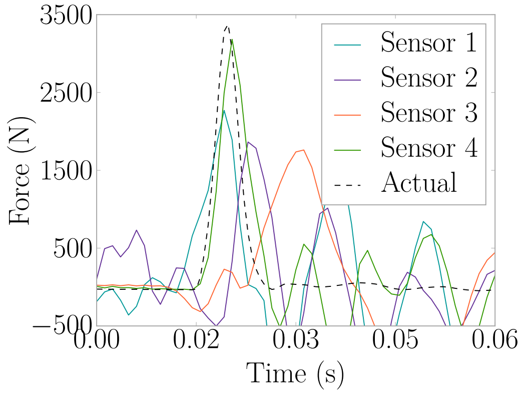

(a) $\hat{F}_{1,j}$

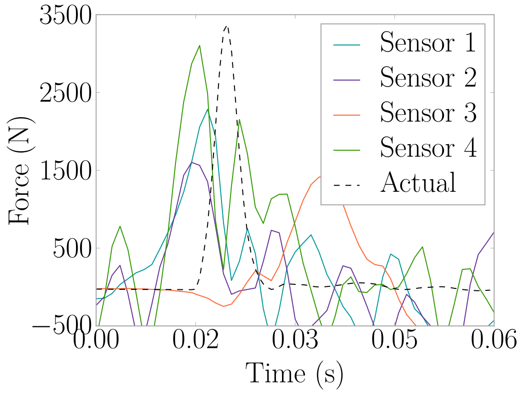

(b) $\hat{F}_{2,j}$

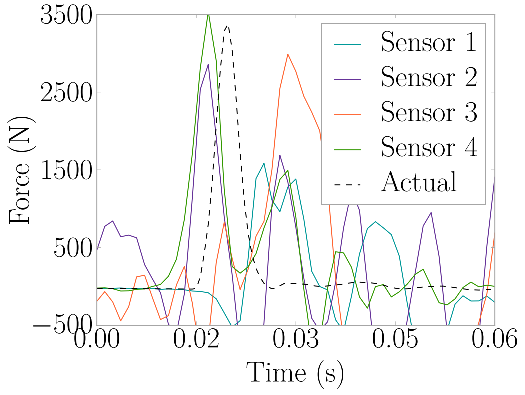

(c) $\hat{F}_{3,j}$

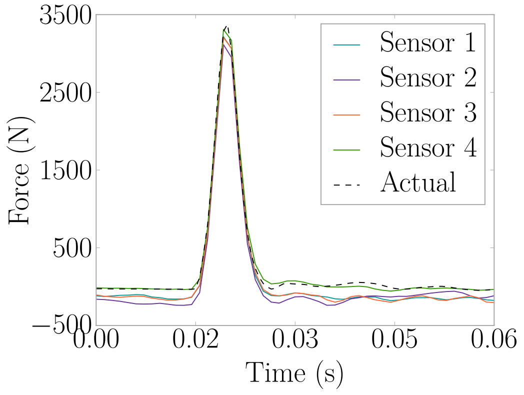

(d) $\hat{F}_{4,j}$

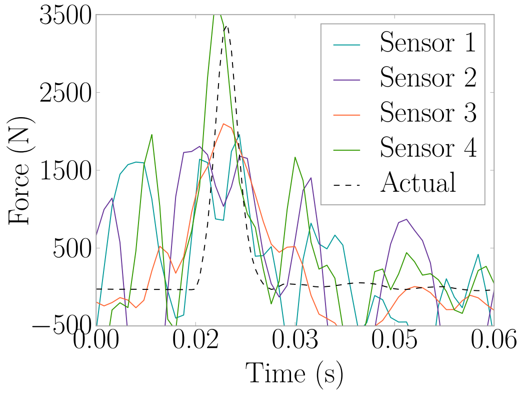

(e) $\hat{F}_{5,j}$

Figure I.7: Hammer Impact Force Estimations for an Impact on Location 4

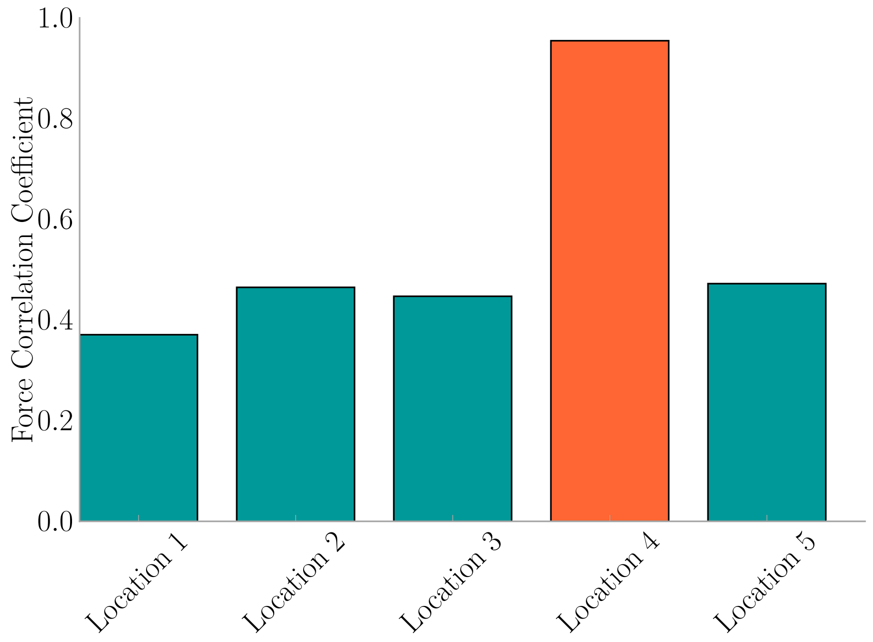

Figure I.8: Hammer Impact L_i for an Impact on Location 4

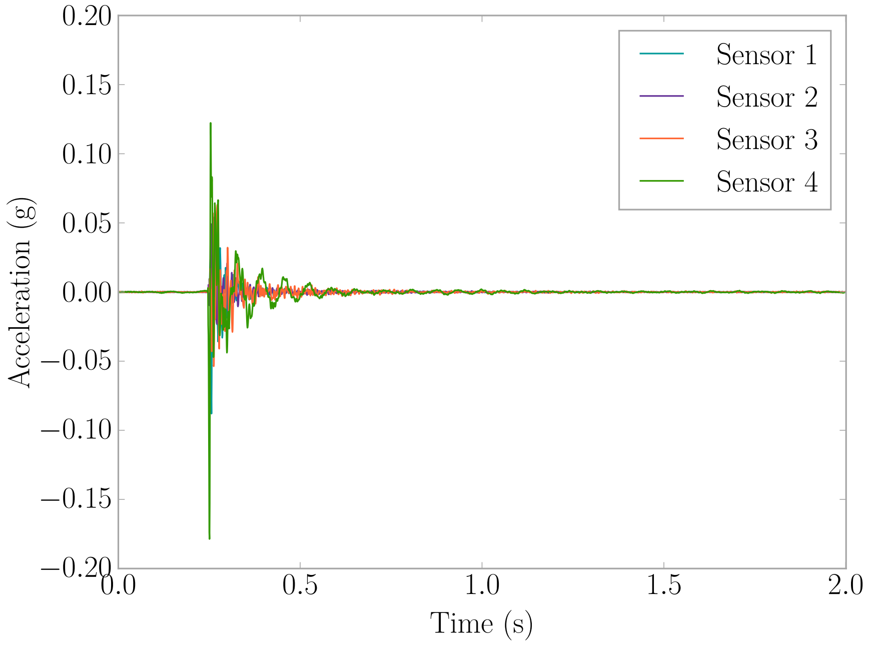

Figure I.9: Hammer on Location 4 Accelerations

I.4 Location 5 Impact

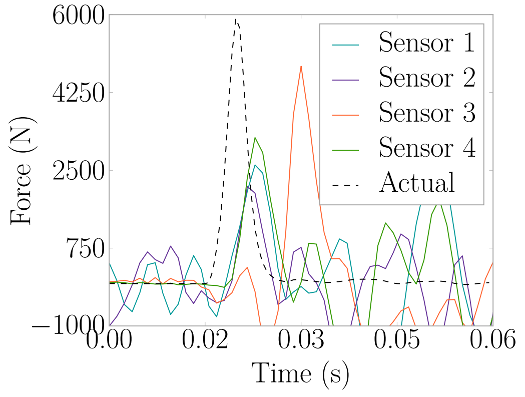

(a) $\hat{F}_{1,j}$

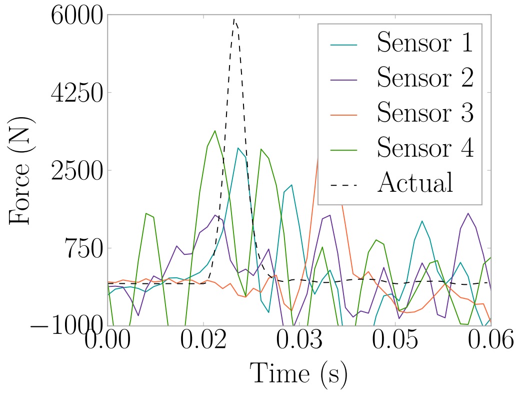

(b) $\hat{F}_{2,j}$

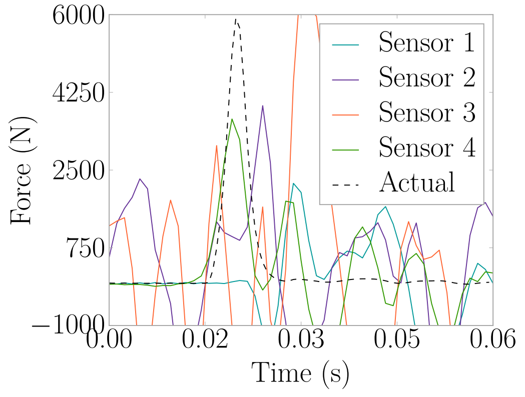

(c) $\hat{F}_{3,j}$

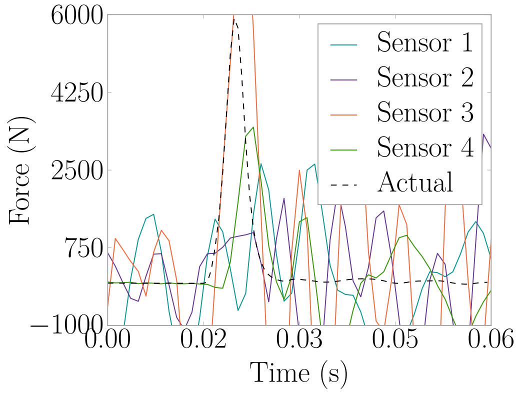

(d) $\hat{F}_{4,j}$

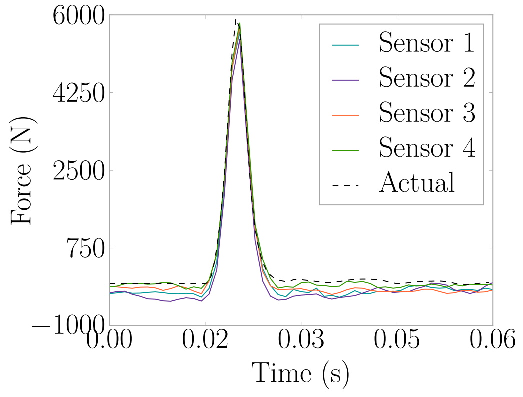

(e) $\hat{F}_{5,j}$

Figure I.10: Hammer Impact Force Estimations for an Impact on Location 5

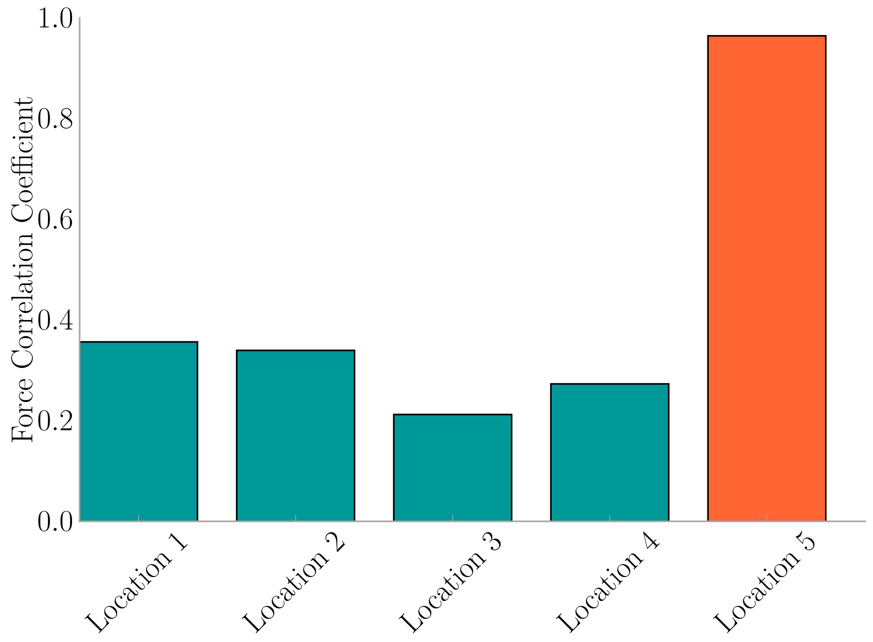

Figure I.11: Hammer Impact L_i for an Impact on Location 5

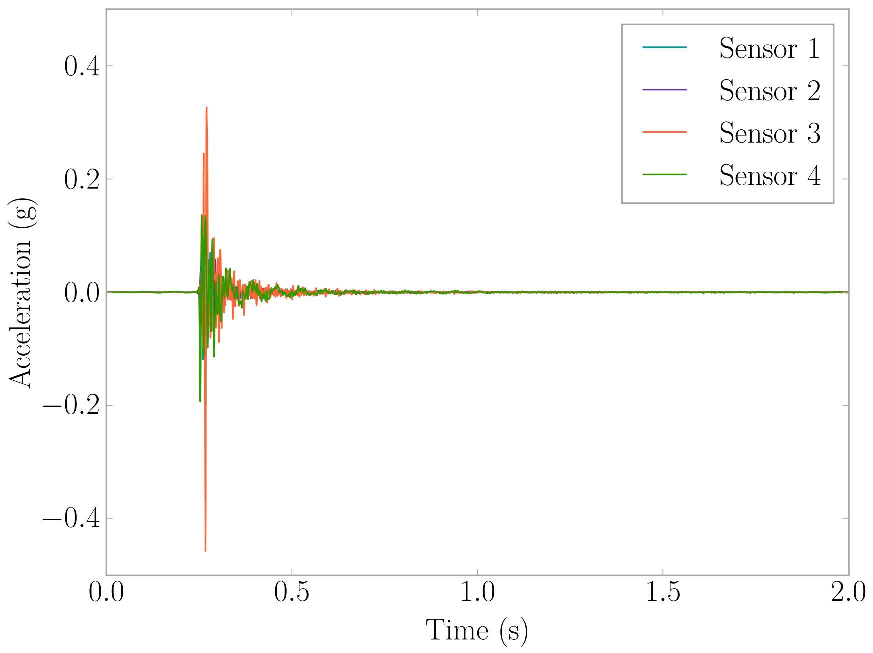

Figure I.12: Hammer on Location 5 Accelerations

Appendix J

EFFECT Active Learning Module Frequency Domain Handout

This section contains a handout used in the EFFECT active learning module discussed in Chapter 6.

What is frequency domain?

"Put simply, a time-domain graph shows how a signal changes over time, whereas a frequency-domain graph shows how much of the signal lies within each given frequency band over a range of frequencies" [1].

You may have heard of the Fourier Series and its use in representing periodic signals through a summation of cosine and sine terms. As a reminder, Equation 1 presents the Fourier Series [2].

$$S(t) = a_0 + \sum_{j=1}^{\infty} a_j \cos(j\omega_0 t) + \sum_{j=1}^{\infty} b_j \sin(j\omega_0 t) \tag{1}$$

This series is fundamental in creating a function for a periodic signal allowing for further analysis and modeling. Taking a closer look at the series, one can see the theory that signals contain many sinusoidals of varying amplitudes and frequencies. The larger the amplitude, the greater power that particular waveform contributes to overall signal. This concept is what the frequency domain representation of a signal emulates - frequencies present within a signal and how much each frequency contributes to the signal as a whole.

As an example, let's take a sinusoidal loading that has a frequency of 10 Hz and an amplitude of 20 N. In the time domain, this looks like a typical sine wave that has ten cycles in a second as in Figure 1a; however, in the frequency domain (see Figure 1b) the frequency present in the signal, 10 Hz, will create a peak as it is rate with a large contribution (i.e. highest power).

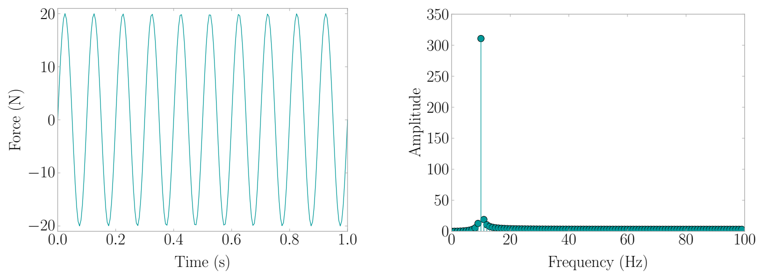

(a) Time Domain (b) Frequency Domain

Figure 1: Signal Representations

Given the frequency domain representation in Figure 2a, can you draw the time domain signal?

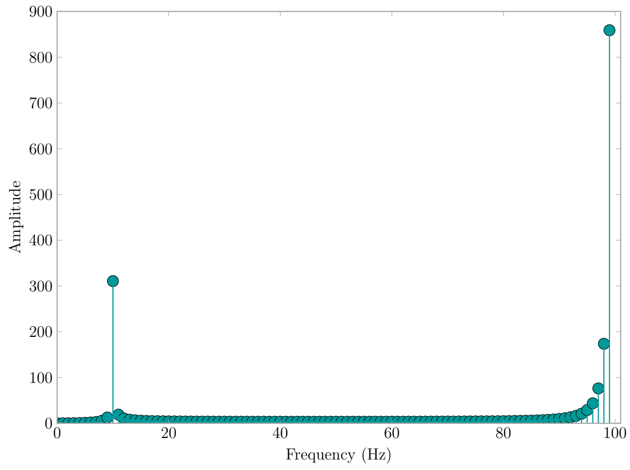

(a) Frequency Domain

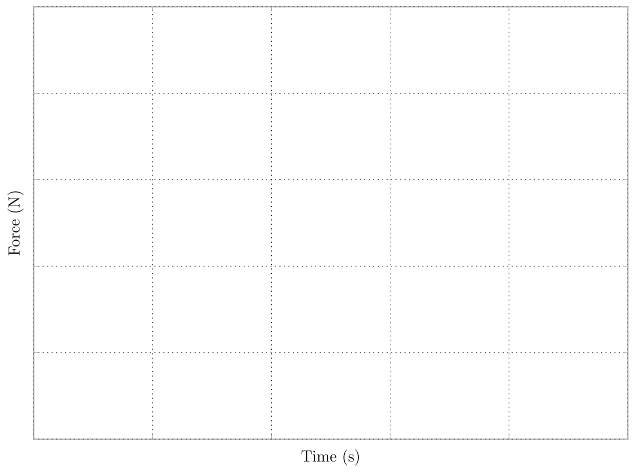

(b) Time Domain

Figure 2: Transforming Frequency Domain into Time Domain Problem

How to transform a time domain signal to frequency domain?

The Fourier Transform "is a generalization of the complex Fourier Series" [3] that enables the decomposition of a periodic signal into its frequency components, or, in other words, "takes a time-based pattern, measures every possible cycle, and returns the overall 'cycle recipe' (the strength, offset, and rotation speed for every cycle that was found)" [4]. One can liken the concept to listening to an orchestra. The orchestra combines multiple waveforms from the many instruments that make up its whole into one audio signal. Now, if you were to focus in on an individual instrument within the orchestra, you would be focusing on one audio signal. This is essentially what the Fourier Transform does. It breaks down the orchestra into individual instruments each having their own frequency to create the frequency domain representation of the entire orchestra's sound. Equation 2 presents the Fourier Transform [3, 5]

$$\mathcal{F}(\xi) = \int_{-\infty}^{\infty} S(t) e^{2\pi i \xi t} dt \tag{2}$$

where

ξ = frequency, Hz
S(t) = signal being evaluated with respect to time t
t = time, s

How to handle transforming more complex signals into the frequency domain?

That first example wasn't so rough, right? What if you had to decompose the signal in Figure 3a? A lot more difficult to do by hand.

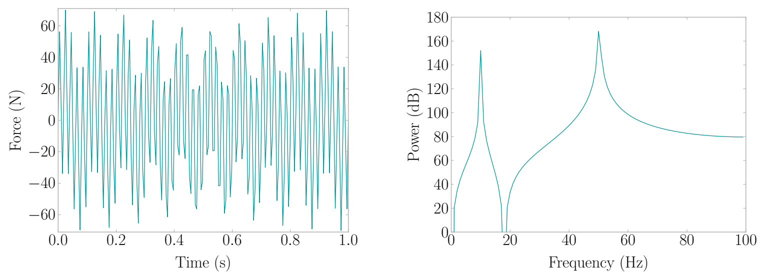

(a) Time Domain (b) Frequency Domain

Figure 3: Complex Signal Example

Enter the Fast Fourier Transform (FFT) for machine calculations created by James Cooley and John Tukey to make the transformation from time domain to frequency domain simple to do by computer [6]. Equation 3 presents the FFT [4, 6]

$$\mathcal{F}(\xi) = \sum_{n=0}^{N-1} S(n) e^{2\pi i \xi (n/N)} \tag{3}$$

where

ξ = frequency, Hz
S(n) = signal being evaluated with respect to point n
n = data point
N = total number of data points

Fortunately for us, a lot of programming languages come with FFT built in. Take a look at the *numpy* package available in Python in Code Snippet 1. Pretty easy, right?

```python
import numpy as np

N = 200      # number of points in signal
dt = 1.0 / N # the time step between each data point of signal for one cycle

x = np.linspace(0, 2*np.pi, N)             # in radians as np.sin() works in radians only
signal = 20*np.sin(10*x) + 50*np.sin(50*x) # the values of your signal
time = np.arange(0, len(signal)/dt, dt)    # the time vector of the signal

sp = np.fft.fft(signal, len(signal))      # calculate the FFT for the discrete signal
freq = np.fft.fftfreq(time.shape[-1], dt) # grab the frequencies FFT evaluated
```

Code Snippet 1: Example of FFT Using Python Package NumPy

Using the code above on the complex signal in Figure 3a transforms the signal in the frequency domain seen in Figure 3b. Notice how there is a peak at both 10 Hz and 50 Hz and that directly comes from the frequencies in the sine functions used to create the signal. Additionally, pay attention to the decibel values of the peaks. How does this relate to the amplitudes of each sine term that composes the signal?

References

[1] *Frequency Domain*. English. Wikipedia. 2015. URL: https://en.wikipedia.org/wiki/Frequency_domain.

[2] Anil K. Chopra. *Dynamics of Structures: Theory and Applications to Earthquake Engineering*. 4th ed. Prentice Hall, 2011.

[3] *Fourier Transform*. English. Wolfram Math World. 2016. URL: http://mathworld.wolfram.com/FourierTransform.html.

[4] Kalid Azad. *An Interactive Guide to the Fourier Transform*. English. Better Explained. 2013. URL: http://betterexplained.com/articles/an-interactive-guide-to-the-fourier-transform/.

[5] *Fourier Transform*. English. Wikipedia. 2016. URL: https://en.wikipedia.org/wiki/Fourier_transform.

[6] James W. Cooley and John W. Tukey. "An Algorithm for the Machine Calculation of Complex Fourier Series". In: *Mathematics of Computation* 19.90 (1965), pp. 297–301. URL: http://www.jstor.org/stable/2003354?seq=1#page_scan_tab_contents.

Appendix K

EFFECT Active Learning Module Survey

This section contains the survey given to evaluate the EFFECT active learning module discussed in Chapter 6.

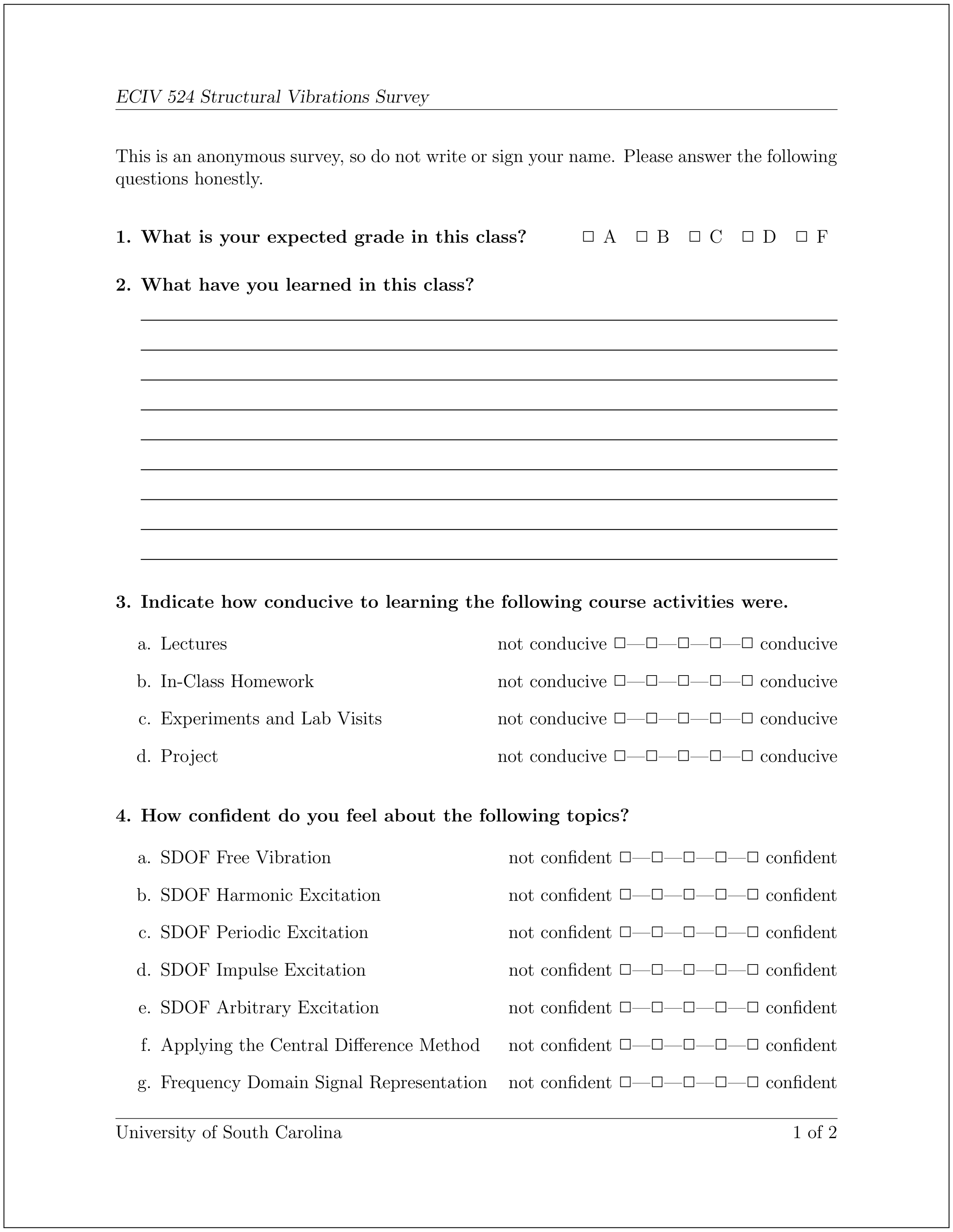

This is an anonymous survey, so do not write or sign your name. Please answer the following questions honestly.

1. What is your expected grade in this class? ☐ A ☐ B ☐ C ☐ D ☐ F

2. What have you learned in this class?

3. Indicate how conducive to learning the following course activities were.

a. Lectures	not conducive ☐—☐—☐—☐—☐ conducive
b. In-Class Homework	not conducive ☐—☐—☐—☐—☐ conducive
c. Experiments and Lab Visits	not conducive ☐—☐—☐—☐—☐ conducive
d. Project	not conducive ☐—☐—☐—☐—☐ conducive

4. How confident do you feel about the following topics?

a. SDOF Free Vibration	not confident ☐—☐—☐—☐—☐ confident
b. SDOF Harmonic Excitation	not confident ☐—☐—☐—☐—☐ confident
c. SDOF Periodic Excitation	not confident ☐—☐—☐—☐—☐ confident
d. SDOF Impulse Excitation	not confident ☐—☐—☐—☐—☐ confident
e. SDOF Arbitrary Excitation	not confident ☐—☐—☐—☐—☐ confident
f. Applying the Central Difference Method	not confident ☐—☐—☐—☐—☐ confident
g. Frequency Domain Signal Representation	not confident ☐—☐—☐—☐—☐ confident

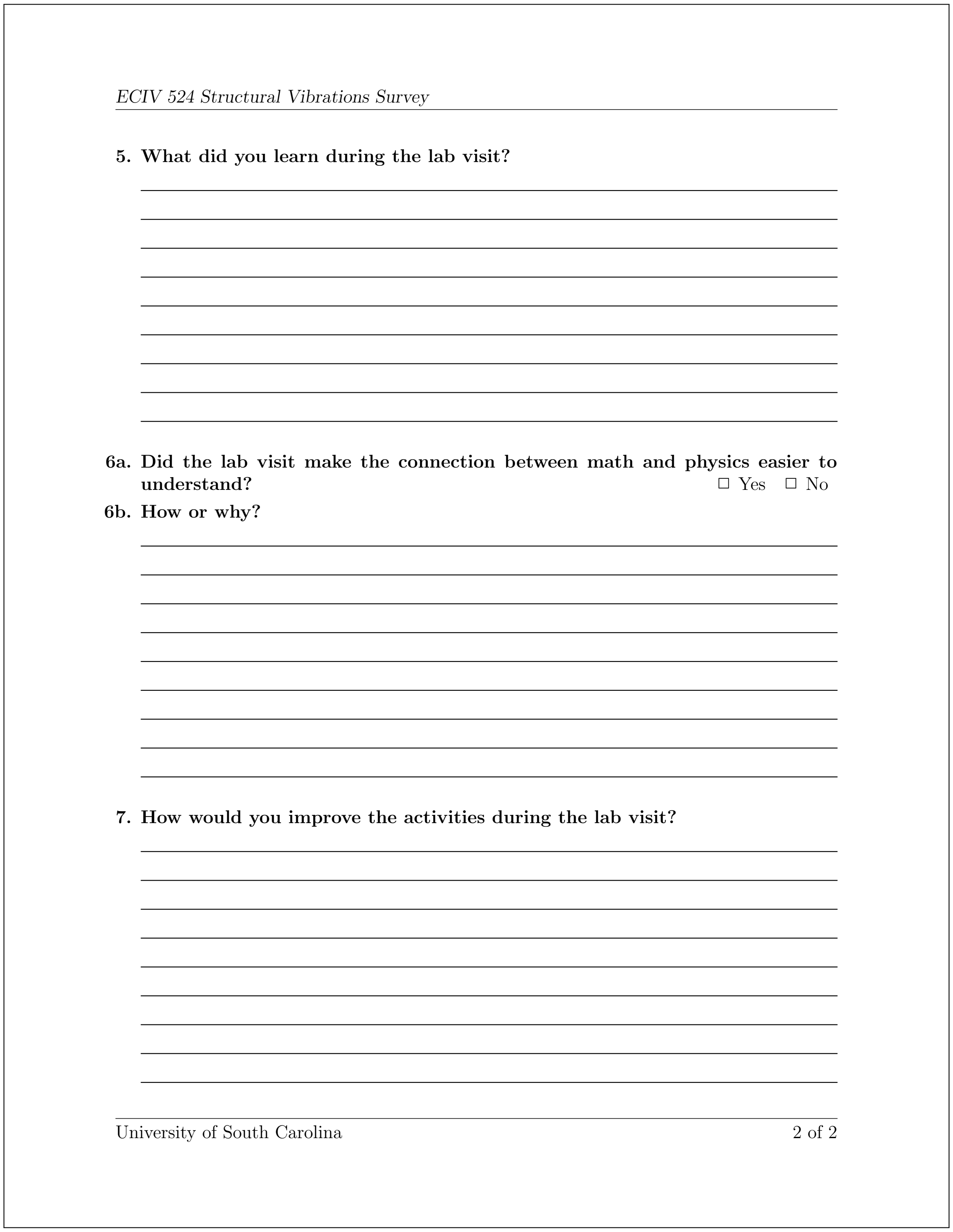

ECIV 524 Structural Vibrations Survey

5. What did you learn during the lab visit?

6a. Did the lab visit make the connection between math and physics easier to understand? ☐ Yes ☐ No

6b. How or why?

7. How would you improve the activities during the lab visit?

University of South Carolina 2 of 2

Appendix L

EFFECT Survey Responses

The following are responses given by students to the survey in Appendix K to evaluate the EFFECT active learning module in Chapter 6. The check boxes for questions three and four were given numeric values where one is not conducive/confident and five is conducive/confident.

L.1 Student A

1. B
2. Structures have a natural frequency and will undergo damping. There are different types of excitations that can be applied to a structure and each one will have a different impact on the structure's properties.
3. a) 5
   b) 4
   c) 3
   d) 4
4. a) 5
   b) 5
   c) 4
   d) 2
   e) 2
   f) 3
   g) 3
5. A structure can have more than one natural frequency, and when these are excited you see peaks on the frequency vs. amplitude graph. A structure can only have so much power done on it before it will break (max amplitude).
6. a) Yes
   b) Seeing the data graphically after an actual experiment helped relate the concepts.
7. Some of the concepts were still pretty confusing, even after some explanation. Maybe give an overview of the basic concepts to keep in mind before doing the actual experiment.

L.2 Student B

1. A
2. We have learned a lot about the response of a SDoF to different forms of excitation including free vibrations, harmonic, impulse, and arbitrary. We studied the displacement, the velocity, and acceleration of the structures in question. I also learned how much this upper level class calls upon information we learned in other classes. I liked that because it makes the effort in previous years feel worth it.
3. a) 5
   b) 2
   c) 4
   d) 3
4. a) 5
   b) 5
   c) 4
   d) 5
   e) 5
   f) 1
   g) 1
5. I was absent the day of the lab visit so I went on my own. I was able to manipulate the structure myself by pushing on it and "felt" how strong it was. I was also able to observe the structure in vibration. Finally, we used a slow motion camera and a ruler to determine displacement at certain time intervals which we used to calculate ζ.
6. a) Yes
   b) It helps to see the actual 3D structure in front of you. It gives you a mental check while performing calculations. You know what the structure should do so you can say your math would or would not match up with what you think it should do.
7. Again, I wasn't there but I feel if the entire class is struggling to calculate stiffness then the teacher should help us out. Our project was made more difficult because we could not find k and neither could anyone else. Also, in class homeworks are awful. Its basically a quiz because the teacher would not answer any questions even if we were totally lost. Take home homework we could bring to the teacher and ask for further explanation (teaching) of a certain topic.

L.3 Student C

1. A
2. I've learned about classifying systems and the process behind solving for those systems. We have gotten a chance to see how you would experimentally test structures and how to take data from them.
3. a) 5
   b) 4
   c) 4
   d) 5
4. a) 5
   b) 5
   c) 4
   d) 5
   e) 4
   f) 3
   g) 3
5. I learned how to test a structure as well as saw how to graph and visualize lab data. From the last visit, I was able to see how a structure can be excited at all frequencies when struck by an impulse hammer.
6. a) Yes
   b) It helped to make the connection because the results nearly mimicked the theoretical numbers and it confirmed that the physics was true and accurately described structures.
7. The last lab was confusing dealing with frequency domain response mainly because I didn't see David run through the simulations with the group that went to the lab. The theory helped solve the problem at the end, but I took a minute to grasp the physics behind exciting certain frequencies.

L.4 Student D

1. B
2. I have learned about different frequencies and how these frequencies come into play when trying to find the displacement, velocity, and acceleration of different structures. Also, how different types of excitations effect the structures differently from each other.
3. a) 5
   b) 2
   c) 4
   d) 4
4. a) 5
   b) 4
   c) 2
   d) 5
   e) 5
   f) 3
   g) 2
5. I learned that without using time in the graphs, it was easier to see how much and how little the different frequencies were.
6. a) Yes
   b) To perform an actual test and see the results was helpful. On the other hand the results from the real world simulation aren't perfect graphs which is what the book usually deals with.
7. I'm sure there is a way to improve, but I found them useful and engaging.

L.5 Student E

1. B (student reported B+ which was not an option; changed to B)
2. Learned about SDOF systems and the many excitations a system can have and the effects of them.
3. a) 5
   b) 4
   c) 3
   d) 4
4. a) 4
   b) 5
   c) 2
   d) 5
   e) 5
   f) 3
   g) 1
5. Learned that superposition is only valid with a linear system.
6. a) No
   b) Because I guess I had not been involved in the lab during the whole duration of the experiment. It's kinda hard to go in and learn in an hour and a half.
7. Not really sure. However, the lab visits do have an extracurricular feel and I feel it adds to the course.

L.6 Student F

1. A
2. How to model a single degree of freedom vibration due to arbitrary excitations.
3. a) 5
   b) 5
   c) 5
   d) 5
4. a) 5
   b) 5
   c) 1
   d) 5
   e) 5
   f) 5
   g) 3
5. How a structure reacts to various frequencies. Natural frequencies can be found with a simple impulse hammer test.
6. a) Yes
   b) It allowed myself to physically see what was going on.
7. Allow more brainstorming among the entire class versus working in pairs.

L.7 Student G

1. C
2. I have learned what damping ratios are, a better understanding of degrees of freedom. I've learned these are different types of vibrations and most can be calculated.
3.
   a) 5
   b) 5
   c) 4
   d) 4
4.
   a) 5
   b) 5
   c) 1
   d) 3
   e) 3
   f) 4
   g) 1
5. I learned that even such a large structure moves when enough force is applied. I also learned the structure moves not only up and down, but left and right slightly.
6.
   a) Yes
   b) We got to physically see the vibrating of the structure happen.
7. I cannot think of anything at the moment.

L.8 Student H

1. D
2. The concepts of vibrations in structures with single degrees of freedom. The tools/methods to use to analyze structural vibrations and what counts as failure.
3. a) 5
   b) 5
   c) 5
   d) 5
4. a) 4
   b) 4
   c) 3
   d) 4
   e) 4
   f) 3
   g) 2
5. That there are other methods/data to analyze experiments with rather than just something with time domain.
6. a) Yes
   b) The actual observation of the experiment allowed a firm connection between the concept and the math.
7. Perhaps a different experiment included, maybe a small demonstration in excel on what was one can analyze the data to reach conclusions for the key variables necessary for the math equations.

L.9 Student I

1. B
2. Dynamics of Structures, SDOF, free vibrations through undamped structures, viscously damped, and coloumb damped. SDOF harmonic excitations on structures. Arbitrary and impulse responses. The central difference method and Fourier series (a little bit).
3.
   a) 5
   b) 5
   c) 5
   d) 4
4.
   a) 4
   b) 4
   c) 3
   d) 4
   e) 4
   f) 3
   g) 2
5. We learned about frequency-domain responses. Basically, the representation of a response of a system through amplitudes and frequency.
6.
   a) No
   b) I thought we didn't have a lot of time to further discuss the subject.
7. Make it a two-three day lecture/lab visit so we have more time for questions/examples.

Appendix M

SSH Database Utilities Documentation

This presents the documentation for the Python package for interacting with the database presented in Chapter 3.

SDII
UNIVERSITY OF SOUTH CAROLINA

SSH Database Utilities Documentation

Release 1.0.0

Benjamin T. Davis

May 04, 2016

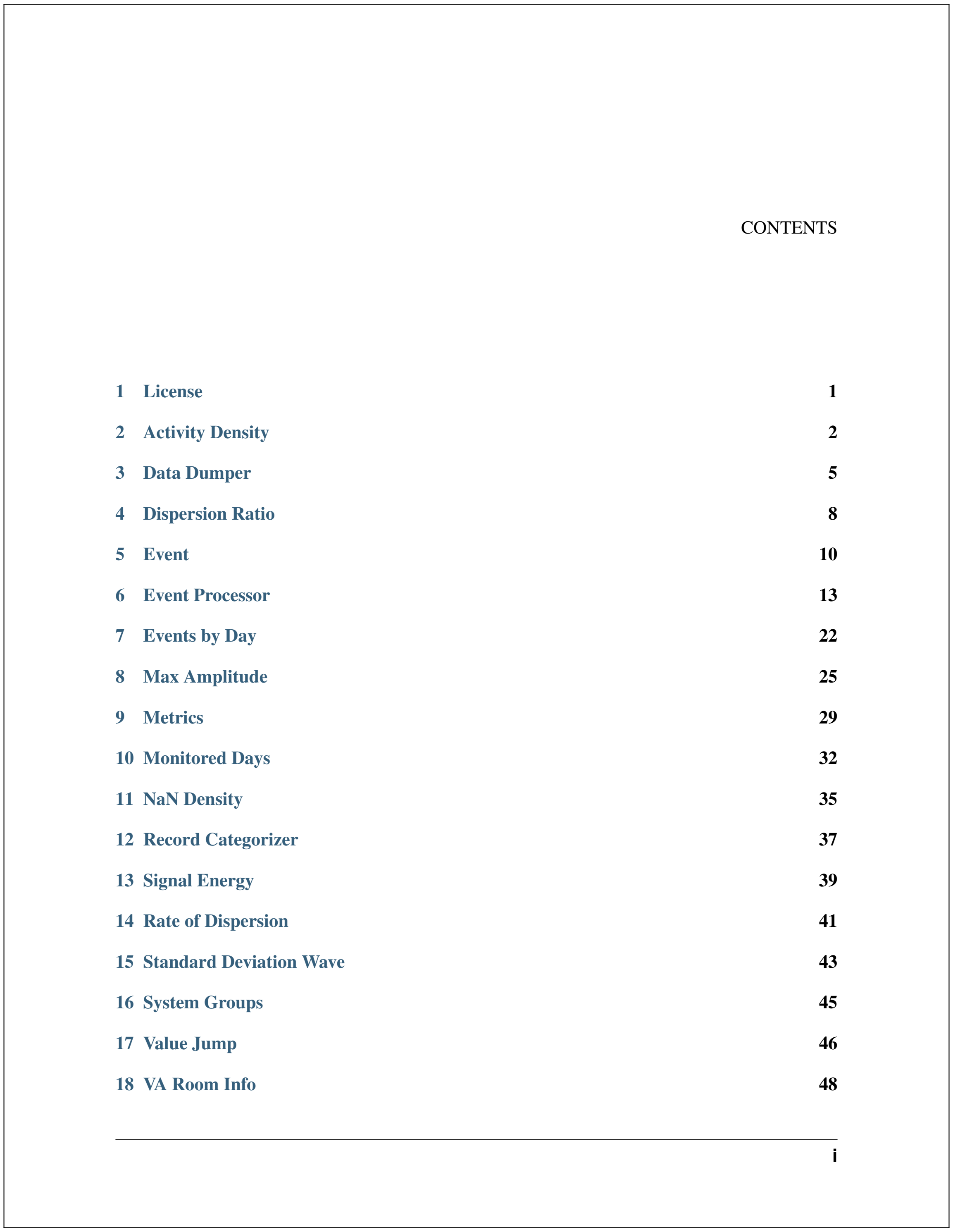

CONTENTS

i

CHAPTER

ONE

LICENSE

CHAPTER

TWO

ACTIVITY DENSITY

Authors: Benjamin T. Davis, NSF Graduate Research Fellow

Date: 2014 August 20

Activity density is a tool to show how activity and area is by compressing acceleration events into an hour by week format. This allows the user to easily see patterns of activity and give the user and idea of how dense a time is for activity.

`activity_density.`**`get`**(*sys='all'*, *start='2010-01-01'*, *end=None*, *mac=None*)

Collects the activity density data from the SSH Database for specified systems for the specified dates and specified sensor macs

Parameters

- **sys** (*str or list*) – The system group as a string being either
  - va : VA Hospital Systems
  - ph : Palmetto Health Systems
  - all : all available systems

  or a custom list of strings with each string having the form SSH-##
- **start** (*str or datetime | default = '2010-01-01'*) – The starting date to consider with form YYYY-MM-DD or YYYY-MM-DD HH:MM:SS
- **end** (*str or datetime | default = '2010-01-01'*) – The ending date to consider with form YYYY-MM-DD or YYYY-MM-DD HH:MM:SS
- **mac** (*list | default = None*) – The unique machine address of the sensor if only a specific sensors are requested. Otherwise all sensors corresponding to a specific date will be returned

Returns **activity** (*list*) – The activity density information with row being and entry and columns having form [0]dayOfWeekNumber, [1]hour, [2]numberOfEvents

Notes

- uses the 'accel_events' table
- adapted from *SSH Data analysis/Database_utils_py/ActivityDensity/*

`activity_density.plot`(*activity*)

Plots the data received from activity_density.get() as a heatmap

Parameters activity (*list*) – The activity density information with row being and entry and columns having form [0]dayOfWeekNumber, [1]hour, [2]numberOfEvents

Returns axis (<*matplotlib.axes.AxesSubplot*>) – The handle for the plot axis

Notes

- The axis default to light gray in color
- Change various features of the plot using axis; e.g.

```
>>> pyplot.setp(axis.lines, color='r', linewidth=2.0, linestyle='-')
```

- adapted from *SSH Data analysis/Database_utils_py/ActivityDensity/*

CHAPTER

THREE

DATA DUMPER

Authors: Benjamin T. Davis, NSF Graduate Research Fellow

Date: 2016 April 07

Grabs the specified system group's data and saves to a csv file.

`data_dumper.`**`run`**(*username, password, sys='all', tables=['accel_events', 'system_log', 'downloads', 'events'], nrows=2000, savedir='./'*)

Dumps the database into a series of csv files, each file containing *nrows* of data

Parameters

- **username** (*str*) – The username having admin rights for the human activity database
- **password** (*str*) – The password for the *username*
- **sys** (*list | default = 'all'*) – The system group as a string being either
  - va : VA Hospital Systems
  - ph : Palmetto Health Systems
  - all : all available systems

  or a custom list of strings with each string having the form SSH-##
- **tables** (*list | default = ['accel_events', 'system_log', 'downloads', 'events']*) – A list of table name strings that should be dumped
- **nrows** (*int | default = 2000*) – The number of rows to dump into the csv file at a time; this prevents possible errors from server timeouts on large datasets
- **savedir** (*str | default = './'*) – The directory to save in csv files in; string should end with '/'

Notes

- Saves the csv files to the server housing the MySQL database based on the *savedir* directory `data_dumper.`**`make_system_options`**(*systems*)

Makes the MySQL where clause for choosing selected systems

Parameters **systems** (*list*) – the system names

CHAPTER

FOUR

DISPERSION RATIO

Authors: Benjamin T. Davis, NSF Graduate Research Fellow

Date: 2015 March 24

`dispersion_ratio.`**`calc`**(*data*, *window=250*, *noverlap=249*)

Calculates the dispersion ratio which is defined as max(std_wave) / min(std_wave)

Parameters

- **data** (*list*) – data to perform the operation on (e.g. accelerometer data)
- **window** (*int | default = 250*) – the number of points to use per operation; must be less than len(data)
- **noverlap** (*int | default = 249*) – number of points to overlap per window; must be less than window

Returns **dr** (*float*) – the dispersion ratio

Notes

- performs calculation as if NaN was not present. Meaning that data=[1,2,3,NaN,4,5] and x=[0,1,2,3,4,5] would be treated as data=[1,2,3,4,5] and x=[0,1,2,4,5], respectively
- adapted from *SSH Data Analysis/Database_utils_py/StandardDeviationSNR/*

CHAPTER FIVE

EVENT

Author: Benjamin T. Davis, NSF Graduate Research Fellow <btdavis@email.sc.edu>

Date: 2015 July 2

`event.`**`get`**(*system*, *event_date*, *mac=None*)

Grabs an acceleration event from the SSH database

Parameters

- **system** (*str*) – The system that saw the event using the format SSH-##. Systems may be obtained from the sys_group module
- **event_date** (*str or datetime*) – The full string or datetime object of form YYYY-MM-DD HH:MM:SS
- **mac** (*str | default = None*) – The unique machine address of the sensor if only a specific sensor is requested. Otherwise all sensors corresponding to a specific date will be returned.

Returns event (*list*) – where each slot contains a sublist of the form [0]event_date, [1]sensor_mac, [2]vertical_axis, [3]accelerationData, [4]system, [5]system_activation

Notes

- uses the 'accel_events' table
- only returns one event at a time
- adapted from *SSH Data analysis/Database_utils_py/AccelEventPlot/*

`event.plot` (*event*, *fs=1*, *one_plot=False*)

Plots the event gathered by event.get()

Parameters

- **event** (*list*) – The list of event data features from event.get()
- **fs** (*float | default = 1*) – The sampling rate of the data in Hz
- **one_plot** (*boolean | default = False*) – If you want the data to be plotted in one window or each sensor to be plotted in its own window

Returns axis (*list or <matplotlib.axes.AxesSubplot>*) – If one_plot was set to True, this will be a list of <matplotlib.axes.AxesSubplot> objects, one for each sensor's plot. Otherwise this will be a single object

Notes

•The axis default to light gray in color

•Change various features of the plot using axis; e.g.

```
>>> pyplot.setp(axis.lines, color='r', linewidth=2.0, linestyle='-')
```

•adapted from *SSH Data analysis/Database_utils_py/AccelEventPlot/*

CHAPTER

SIX

EVENT PROCESSOR

Authors: Benjamin T. Davis, NSF Graduate Research Fellow

Date: 2016 February 09

The event processor works through records processes said records for the various metrics. The results are stored in the human-induced vibration activity database.

`event_processor.`**`insert_or_update_parameter`**(*cursor*, *system*, *event_date*, *mac*, *parameter*, *value*)

Attempts to insert, or failing that update, the parameter value in the *event_parameters* table

Parameters

- **cursor** (*pymysql.cursors.Cursor*) – The pymysql cursor object for executing queries
- **system** (*str*) – The system relating to the parameter
- **event_date** (*str or datetime*) – The event date with form YYYY-MM-DD or YYYY-MM-DD HH:MM:SS
- **mac** (*str*) – The MAC address relating to this parameter
- **parameter** (*str*) – The parameter to insert or update
- **value** (*str*) – The value of the parameter

`event_processor.`**`mark_event_parameter_processed`**(*cursor*, *event_date*, *mac*, *parameter*)

Marks an event's parameter as processed in *event_processing* table

Parameters

- **cursor** (*pymysql.cursors.Cursor*) – The pymysql cursor object for executing queries
- **event_date** (*str or datetime*) – The event date with form YYYY-MM-DD or YYYY-MM-DD HH:MM:SS
- **mac** (*str*) – The MAC address relating to this parameter
- **parameter** (*str*) – The parameter to insert or update

Note:

- Switching the value of 'processed' from 0 to 1 indicates the event has has been processed. In other words, 0 indicated unprocessed and 1 indicates processed.

`event_processor.`**`all_records`**(*metric='ampmax'*, *start='2010-01-01'*, *end=None*)

Generates processing information in the *event_processing* table for all acceleration records in *accel_events* for a date range

Parameters

- **metric** (*str | default = 'ampmax'*) – The metric to process. Metrics are defined in the *parameters* table
- **start** (*str or datetime | default = '2010-01-01'*) – The starting date to consider with form YYYY-MM-DD or YYYY-MM-DD HH:MM:SS
- **end** (*str or datetime | default = None*) – The ending date to consider with form YYYY-MM-DD or YYYY-MM-DD HH:MM:SS

Note:

•Ignores records saying 'No Data'

`event_processor.`**`all_records_category_svm`**(*start='2010-01-01'*, *end=None*)

Adds all records processing information to the *event_processing* table for generated the SVM-defined category

Parameters

- **start** (*str or datetime | default = '2010-01-01'*) – The starting date to consider with form YYYY-MM-DD or YYYY-MM-DD HH:MM:SS
- **end** (*str or datetime | default = None*) – The ending date to consider with form YYYY-MM-DD or YYYY-MM-DD HH:MM:SS

Note:

- Ignores records saying 'No Data'
- Ignores records with 'NaN' present, i.e. incomplete records
- Ignores records with a MADr greater than 0.95 as these are considered sensor errors
- Ignores records that have already been categorized with *category-manual* as these are considered training records for the SVM

`event_processor.`**`records_missing_metric`**(*metric='ampmax'*, *start='2010-01-01'*, *end=None*)

Looks for records missing the specified metric in the *events_parameters* table and then generates processing information in the *event_processing* table

Parameters

- **metric** (*str | default = 'ampmax'*) – The metric to process. Metrics are defined in the *parameters* table
- **start** (*str or datetime | default = '2010-01-01'*) – The starting date to consider with form YYYY-MM-DD or YYYY-MM-DD HH:MM:SS
- **end** (*str or datetime | default = None*) – The ending date to consider with form YYYY-MM-DD or YYYY-MM-DD HH:MM:SS

Note:

•Ignores records saying 'No Data'

`event_processor.`**`records_missing_category_svm`**(*start='2010-01-01'*, *end=None*)

Looks for records missing an SVM-defined category in the *events_parameters* table and then generates processing information in the *event_processing* table

Parameters

- **start** (*str or datetime | default = '2010-01-01'*) – The starting date to consider with form YYYY-MM-DD or YYYY-MM-DD HH:MM:SS
- **end** (*str or datetime | default = None*) – The ending date to consider with form YYYY-MM-DD or YYYY-MM-DD HH:MM:SS

Note:

- Ignores records saying 'No Data'
- Ignores records with 'NaN' present, i.e. incomplete records
- Ignores records with a MADr greater than 0.95 as these are considered sensor errors
- Ignores records that have already been categorized with *category-manual* as these are considered training records for the SVM

`event_processor.`**`generate_metric`**(*metric='ampmax'*, *fs=316.0*, *window=250*, *noverlap=249*)

Generates the specified metric based on the table *event_processing* which is generated using `all_records()` or `records_missing_metric()`

Parameters

- **metric** (*str | default = 'ampmax'*) – The metric to process. Metrics are defined in the *parameters* table
- **fs** (*float | default = 316.0*) – The sampling rate (Hz) of the records being evaluated. This is set to 316 Hz which was shown by Benjamin T. Davis in his PhD dissertation to be the frequency of the Camp Hill sensor; used for *senergy*
- **window** (*int | default = 250*) – The number of points to use per operation; must be less than len(data); used for *stdsnr*
- **noverlap** (*int | default = 249*) – Number of points to overlap per window; must be less than window; used for *stdsnr*

`event_processor.`**`svm_categorize`**`()`

Categorizes records using a SVM from Benjamin T. Davis's dissertation, Characterization of Human-Induced Vibrations, that learns based on *category-manual*. It operates using the table *event_processing* which is generated using `records_missing_category_svm()`

Note:

- The SVM learns based on *category-manual*. The radial basis function kernel using the Disperion Ratio metric was found to be the best, and is what the SVM provided here utilizes.
- if DR = infinity, category is marked as 0 for unsure. These are typically signals containing all the same values.

CHAPTER

SEVEN

EVENTS BY DAY

Authors: Benjamin T. Davis, NSF Graduate Research Fellow

Date: 2014 August 14

Events by day shows how many acceleration events occur on each month of each day which gives the viewer an idea of how active an area is. This is a version of Activity Density.

`events_by_day.`**`get`**(*sys='all'*, *start='2010-01-01'*, *end=None*, *mac=None*)

Collects the event data from the SSH Database specified systems for the specified dates and specified sensor macs

Parameters

- **sys** (*str or list*) – The system group as a string being either
  - va : VA Hospital Systems
  - ph : Palmetto Health Systems
  - all : all available systems

  or a custom list of strings with each string having the form SSH-##
- **start** (*str or datetime | default = '2010-01-01'*) – The starting date to consider with form YYYY-MM-DD or YYYY-MM-DD HH:MM:SS
- **end** (*str or datetime | default = '2010-01-01'*) – The ending date to consider with form YYYY-MM-DD or YYYY-MM-DD HH:MM:SS
- **mac** (*list | default = None*) – The unique machine address of the sensor if only a specific sensors are requested. Otherwise all sensors corresponding to a specific date will be returned

Returns events (*list*) – events by day with columns having the form [0]year, [1]month, [2]day, [3]event count, [4]month abbreviation

Notes

- uses the 'accel_events' table
- adapted from *SSH Data analysis/Database_utils_py/EventsByDay/*

events_by_day.**plot** (*events*, *logscale=False*)

Plots the data received from events_by_day.get() as a heatmap

Parameters

- **events** (*list*) – events by day with columns having the form [0]year, [1]month, [2]day, [3]event count, [4]month abbreviation
- **logscale** (*boolean | default = False*) – determines if output should be in log scale

Returns **axis** (<*matplotlib.axes.AxesSubplot*>) – The handle for the plot axis

Notes

•The axis default to light gray in color

•Change various features of the plot using axis; e.g.

```
>>> pyplot.setp(axis.lines, color='r', linewidth=2.0, linestyle='-')
```

•adapted from *SSH Data analysis/Database_utils_py/ActivityDensity/*

CHAPTER

EIGHT

MAX AMPLITUDE

Authors: Benjamin T. Davis, NSF Graduate Research Fellow

Date: 2015 January 16

`max_amplitude.`**`calc`**`(`*data*`)`

Finds the maximum amplitude of the data determined by *max(abs(data))*

Parameters data (*list*) – data to perform the operation on (e.g. accelerometer data)

Returns max_amplitude (*float*) – the maximum amplitude present in the data `max_amplitude.`**`difference`**`(`*data*`)`

Finds the maximum amplitude difference (MAD) of the data which is the max change of the absolute values of the descending sorted data

Parameters data (*numpy.array*) – data to perform the operation on (e.g. accelerometer data)

Returns mad (*float*) – the maximum amplitude difference present in the data `max_amplitude.get`(*systemDate*)

Finds the maximum amplitudes of the events given based on metric2 in the SSH Database

Parameters systemDate (*2D list*) – a list with system names as the first column and an event date as the second column

```
>>> systemDate = [[['SSH-36'], ['2013-04-25 16:48:03']],
                  [['SSH-37'], ['2014-06-01 00:32:24']]]
```

Returns amplitudes (*2D array*) – an array containing the results for all the system and date combinations from systemDate with each row having the form [[0] system, [1] date, [2] mac, [3] amplitude]. The mac slot corresponds to the mac of the sensor that has the maximum amplitude. The amplitude slot contains the max amplitude value.

Notes

•adapted from *SSH Data Analysis/Database_utils_py/maxAmplitude/*

CHAPTER

NINE

METRICS

Authors: Benjamin T. Davis, NSF Graduate Research Fellow

Date: 2015 November 05

Metrics provides functions for grabbing signal metric information that is stored in the database.

`metrics.get`(*sys='all'*, *start='2010-01-01'*, *end=None*, *param='all'*, *mac=None*)

Collects the specified signal metrics

Parameters

- **sys** (*str or list*) – The system group as a string being either
  - va : VA Hospital Systems
  - ph : Palmetto Health Systems
  - all : all available systems

  or a custom list of strings with each string having the form SSH-##
- **start** (*str or datetime | default = '2010-01-01'*) – The starting date to consider with form YYYY-MM-DD or YYYY-MM-DD HH:MM:SS
- **end** (*str or datetime | default = '2010-01-01'*) – The ending date to consider with form YYYY-MM-DD or YYYY-MM-DD HH:MM:SS
- **param** (*list | default = 'all'*) – The name of the metrics in the database to retrieve or 'all' to grab everything
- **mac** (*list | default = None*) – The unique machine address of the sensor if only a specific sensors are requested. Otherwise all sensors corresponding to a specific date will be returned

Returns metrics (*list*) – The list of metrics requested where [0]system, [1]date [2]sensor mac, [3]param1 value, [4]param2 value,...

Notes

- uses the 'event_parameters' table
- uses the 'parameters' table
- adapted from *SSH Data analysis/Database_utils_py/SignalMetricPlot/*

`metrics.getGrouped`(*sys='all'*, *start='2010-01-01'*, *end=None*, *param='all'*, *mac=None*)

Collects the specified signal metrics as a group. The grouping only returns records that contain the metrics listed after applying a filter to the values to ignore "NaN" and empty.

Parameters

- **sys** (*str or list*) – The system group as a string being either
  - va : VA Hospital Systems
  - ph : Palmetto Health Systems
  - all : all available systems

  or a custom list of strings with each string having the form SSH-##
- **start** (*str or datetime | default = '2010-01-01'*) – The starting date to consider with form YYYY-MM-DD or YYYY-MM-DD HH:MM:SS
- **end** (*str or datetime | default = '2010-01-01'*) – The ending date to consider with form YYYY-MM-DD or YYYY-MM-DD HH:MM:SS
- **param** (*list | default = 'all'*) – The name of the metrics in the database to retrieve or 'all' to grab everything
- **mac** (*list | default = None*) – The unique machine address of the sensor if only a specific sensors are requested. Otherwise all sensors corresponding to a specific date will be returned

Returns **metrics** (*list*) – The list of metrics requested where [0]system, [1]date [2]sensor mac, [3]param1 value, [4]param2 value,...

Notes

- uses the 'event_parameters' table
- uses the 'parameters' table
- adapted from *SSH Data analysis/Database_utils_py/SignalMetricPlot/*

CHAPTER

TEN

MONITORED DAYS

Authors: Benjamin T. Davis, NSF Graduate Research Fellow

Date: 2014 September 29

Monitored Days displays how many sensors were active by day. Gives user an idea of how well a system and its sensors are operating.

`monitored_days.`**`get`** (*sys='all'*, *start='2010-01-01'*, *end=None*, *mac=None*)

Collects the monitored day data from the SSH Database for specified systems for the specified dates and specified sensor macs

Parameters

- **sys** (*str or list*) – The system group as a string being either
  - va : VA Hospital Systems
  - ph : Palmetto Health Systems
  - all : all available systems

  or a custom list of strings with each string having the form SSH-##
- **start** (*str or datetime | default = '2010-01-01'*) – The starting date to consider with form YYYY-MM-DD or YYYY-MM-DD HH:MM:SS
- **end** (*str or datetime | default = '2010-01-01'*) – The ending date to consider with form YYYY-MM-DD or YYYY-MM-DD HH:MM:SS
- **mac** (*list | default = None*) – The unique machine address of the sensor if only a specific sensors are requested. Otherwise all sensors corresponding to a specific date will be returned

Returns **sensors_active** (*list*) – The monitored day information with row being and entry and columns having form [0]day, [1]month, [2]year, [3]numberOfSensors, [4]monthName

Notes

- uses the 'system_log' table
- adapted from *SSH Data Analysis/Database_utils_py/MonitoredDays/*

`monitored_days.plot(`*sensors_active*`)`

Plots the data received from monitored_days.get() as a heatmap

Parameters sensors_active (*list*) – The monitored day information with row being and entry and columns having form [0]day, [1]month, [2]year, [3]numberOfSensors, [4]monthName

Returns axis (<*matplotlib.axes.AxesSubplot*>) – The handle for the plot axis

Notes

- The axis default to light gray in color
- Change various features of the plot using axis; e.g.

```
>>> pyplot.setp(axis.lines, color='r', linewidth=2.0, linestyle='-')
```

- adapted from *SSH Data Analysis/Database_utils_py/MonitoredDays/*

CHAPTER

ELEVEN

NAN DENSITY

Authors: Benjamin T. Davis, NSF Graduate Research Fellow

Date: 2015 March 20

`nan_density.`**`calc`**(*data*)

Calculates the density of nan values in a data set. The equation is # nan / total points

Parameters data (*list*) – data to perform the operation on (e.g. accelerometer data)

Returns density (*float*) – the density of NaN in the data

Notes

- adapted from *SSH Data Analysis/Database_utils_py/nanDensity/*

CHAPTER

TWELVE

RECORD CATEGORIZER

Authors: Benjamin T. Davis, NSF Graduate Research Fellow

Date: 2015 March 26

Browses falls database at random and allows user to categorize the signal `record_categorize.run()`

Runs the categorizer and guides the user through the process while saving the user's responses to the database in table *event_parameters* with the parameter name being *category-manual*

Notes

- uses the 'accel_events' table
- adapted from *SSH Data analysis/Database_utils_py/manualRecordCategorizer/*

CHAPTER

THIRTEEN

SIGNAL ENERGY

Authors: Benjamin T. Davis, NSF Graduate Research Fellow

Date: 2015 April 02

`signal_energy.calc`(*y*, *x=None*, *dx=1.0*)

Determines the signal energy (signal processing version). This is defined to be integral(data^2).The integration scheme used here is the trapezoidal rule.

Parameters

- **y** (*list*) – the y values of the signal
- **x** (*list | default = None*) – the x coordinates corresponding to data
- **dx** (*float | default = 1.0*) – the spacing between elements of data; if *x* is not specified, *dx* is used

Returns **senergy** (*float*) – the signal energy

Notes

- https://en.wikipedia.org/wiki/Energy_(signal_processing))
- performs integration as if NaN was not present. Meaning that data=[1,2,3,NaN,4,5] and x=[0,1,2,3,4,5] would be treated as data=[1,2,3,4,5] and x=[0,1,2,4,5], respectively
- adapted from *SSH Data Analysis/Database_utils_py/signalEnergy/*

CHAPTER

FOURTEEN

RATE OF DISPERSION

Author: Benjamin T. Davis, NSF Graduate Research Fellow <btdavis@email.sc.edu>

Date: 2015 March 05

`rate_of_dispersion.`**`calc`**(*data*, *window=250*, *noverlap=249*, *offset=100*, *rv='rod'*)

Calculates the Rate of Dispersion (RoD) which is defined as max(jumps) / max(abs(data))

Parameters

- **data** (*1D array like*) – data to perform the operation on (i.e. accelerometer data)
- **window** (*int | default = 250*) – the number of points to use per operation; must be less than *len(data)*
- **noverlap** (*int | default = 249*) – number of points to overlap per window; must be less than window
- **offset** (*int | default = 100*) – the number of points to offset for calculating value jumps
- **rv** (*str | default = 'cd'*) – values to return from the following options:
  - cd : Coefficient of Deviation
  - all : stdwave, jumps, cnd

Returns

- **rod** (float | if ‘rv = ‘cd’) – the rate of dispersion
- **info** (dict | if ‘rv = ‘all’) – dictionary containing the results of all the calculations with the keys
  - stdwave : standard deviation wave output
  - jumps : the value jump output
  - rod : Rate of Dispersion

CHAPTER

FIFTEEN

STANDARD DEVIATION WAVE

Author: Benjamin T. Davis, NSF Graduate Research Fellow <btdavis@email.sc.edu>

Date: 2015 March 05

`std_wave.`**`calc`**(*data*, *window=250*, *noverlap=249*)

Windows the data and takes the standard deviation of those windows creating a wave like effect moving through the data.

Parameters

- **data** (*1D array like*) – data to perform the operation on (e.g. accelerometer data)
- **window** (*int | default = 250*) – the number of points to use per operation; must be less than *len(data)*
- **noverlap** (*int | default = 249*) – number of points to overlap per window; must be less than window

Returns **std_wave** (*list*) – contains the standard deviation wave through the signal of size *len(signal)-noverlap*

CHAPTER

SIXTEEN

SYSTEM GROUPS

The module provides some system groupings for various deployments. These groups are:

Group Name	Variable
All Systems	all
Palmetto Health Systems	ph
VA Hospital Systems	va

Here is the list of systems in each group in Python code.

```
all = ['SSH-1','SSH-2','SSH-3','SSH-4','SSH-5','SSH-6','SSH-7','SSH-9',
       'SSH-10','SSH-11','SSH-12','SSH-13','SSH-14','SSH-15','SSH-16',
       'SSH-17','SSH-18','SSH-19','SSH-20','SSH-21','SSH-22','SSH-23',
       'SSH-24','SSH-25','SSH-26','SSH-27','SSH-28','SSH-29','SSH-30',
       'SSH-31','SSH-32','SSH-33','SSH-34','SSH-35','SSH-36','SSH-37',
       'SSH-38','SSH-39','SSH-40','SSH-41','SSH-42']

ph = ['SSH-1','SSH-2','SSH-3','SSH-4','SSH-5','SSH-6','SSH-7','SSH-9',
      'SSH-10','SSH-11','SSH-12','SSH-13','SSH-14','SSH-15','SSH-16',
      'SSH-17','SSH-18','SSH-19','SSH-20','SSH-21','SSH-22','SSH-23',
      'SSH-24','SSH-25','SSH-26','SSH-27','SSH-28','SSH-29','SSH-30',
      'SSH-31','SSH-32','SSH-33','SSH-34','SSH-35']

va = ['SSH-36','SSH-37','SSH-38','SSH-39','SSH-40','SSH-41','SSH-42']
```

These are all automatically loaded for you when you import the package and can be accessed like so.

```
>>> ssh_database_utils.sys_groups.ph
```

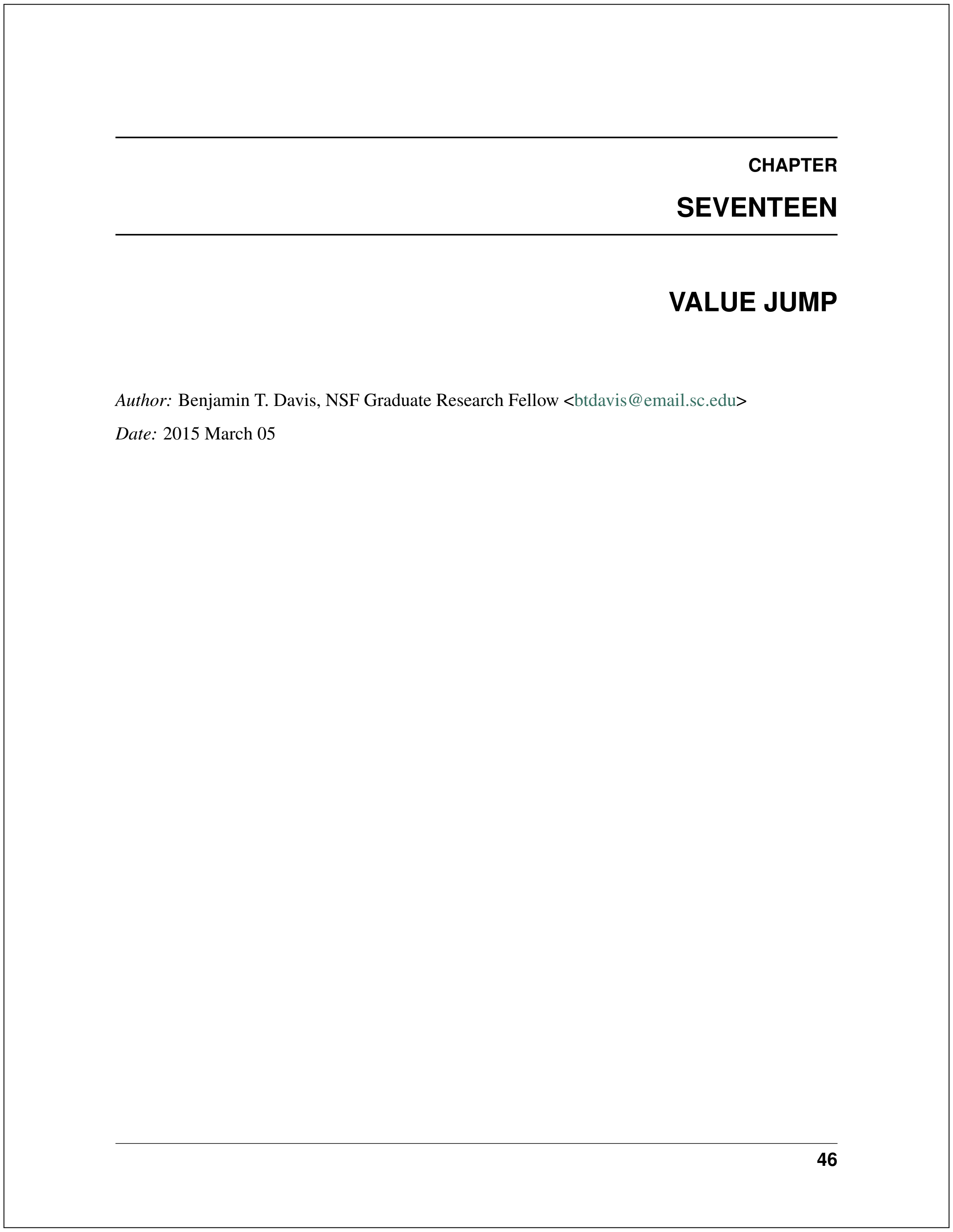

CHAPTER

SEVENTEEN

VALUE JUMP

Author: Benjamin T. Davis, NSF Graduate Research Fellow <btdavis@email.sc.edu>

Date: 2015 March 05

46

`value_jump.`**`calc`**(*data*, *offset=100*)

Calculates value jumps between points with an offset defining which points to use.

Parameters

- **data** (*1D array_like*) – data to perform the operation on (i.e. standard deviation wave data)
- **offset** (*int | default = 100*) – the number of points to offset

Returns jumps (*list*) – contains the value jumps through the data; list of size *data-offset*

CHAPTER

EIGHTEEN

VA ROOM INFO

Authors: Benjamin T. Davis, NSF Graduate Research Fellow

Date: 2014 July 24

Groups sensors by room for the VA installation from 2013-01-18 to 2014-06-13.

The following shows the break down by room for the VA installation as seen in python code. This is loaded as a variable when importing the package and can be accessed using the variable *va_room_info*.

```
va_room_info =  {103:{'system':'SSH-41',
                      'sensor':['00066614BB46',
                                '00066614E6AB',
                                '0006661405B2',
                                '000666149989',
                                '000666149946']
                   },

                 104:{'system':'SSH-41',
                      'sensor':['00066614B3B0',
                                '00066614B3BC',
                                '00066614E7E5',
                                '00066614B15A']
                   },

                 105:{'system':'SSH-41',
                      'sensor':['00066613D4E1',
                                '00066614BB87',
                                '00066614E2CC']
                   },

                 106:{'system':'SSH-40',
                      'sensor':['00066614BB81',
                                '00066614B3A9']
                   },

                 107:{'system':'SSH-40',
                      'sensor':['00066614E7EC',
                                '00066614E0A8',
                                '0006661438F5']
                   },

                 108:{'system':'SSH-40',
                      'sensor':['00066614BB48',
                                '000666303496',
                                '000666138D07',
                                '00066614E7E9',
                                '00066614986D']
                   },

                 109:{'system':'SSH-39',
                      'sensor':['000666303493',
                                '00066614E2CC',
                                '00066614E7DB',
                                '000666143087',
                                '0006661497E3']
                    },

                 110:{'system':'SSH-39',
                      'sensor':['00066614BB7C',
                                '00066614E272',
                                '00066614B3A5',
                                '00066614394B',
                                '00066614996F',
                                '0006661497E8']
                    },

                 111:{'system':'SSH-39',
                      'sensor':['000666138F1E',
                                '000666138D2C',
                                '000666143081']
                    },

                 112:{'system':'SSH-39',
                      'sensor':['00066614B3B3',
                                '00066614BB45',
                                '00066614999F']
                    },

                 113:{'system':'SSH-38',
                      'sensor':['0006661400E5',
                                '00066614BB89',
                                '000666142F31',
                                '000666303486',
                                '00066614B3B5']
                    },

                 114:{'system':'SSH-38',
                      'sensor':['00066614C7AE',
                                '000666138D9C']
                    },

                 115:{'system':'SSH-38',
                      'sensor':['00066614DC67',
                                '000666142E73']
                    },

                 116:{'system':'SSH-37',
                      'sensor':['00066614BB90',
                                '00066613C925',
                                '0006661499A6']
```

```
    },

117:{'system':'SSH-37',
     'sensor':['00066613D665',
               '000666303495',
               '0006661499B5',
               '000666142F24']
    },

118:{'system':'SSH-37',
     'sensor':['00066614E6D0',
               '00066614D0A3',
               '000666139700',
               '00066614B3B1',
               '000666149983']
    },

119:{'system':'SSH-37',
     'sensor':['000666143B49',
               '00066614B94A',
               '0006661499B5',
               '00066614B3A1',
               '0006661499B6',
               '0006661497A5']
    },

120:{'system':'SSH-36',
     'sensor':['000666303492',
               '00066614E241',
               '00066614998E']
    },

120:{'system':'SSH-36',
     'sensor':['000666303492',
               '00066614E241',
               '00066614998E']
    },

121:{'system':'SSH-36',
     'sensor':['00066614BB8F',
               '00066614BB7E',
               '000666303485',
               '0006661499AF']
    },

122:{'system':'SSH-36',
     'sensor':['00066614E687',
                                    '00066614B3A1',
                                    '00066614E687',
                                    '000666149981']
                        },
                    }
```

Appendix N

FEEL Python Package Documentation

This presents the documentation for the Python package that implements the FEEL Algorithm presented in Chapter 5.

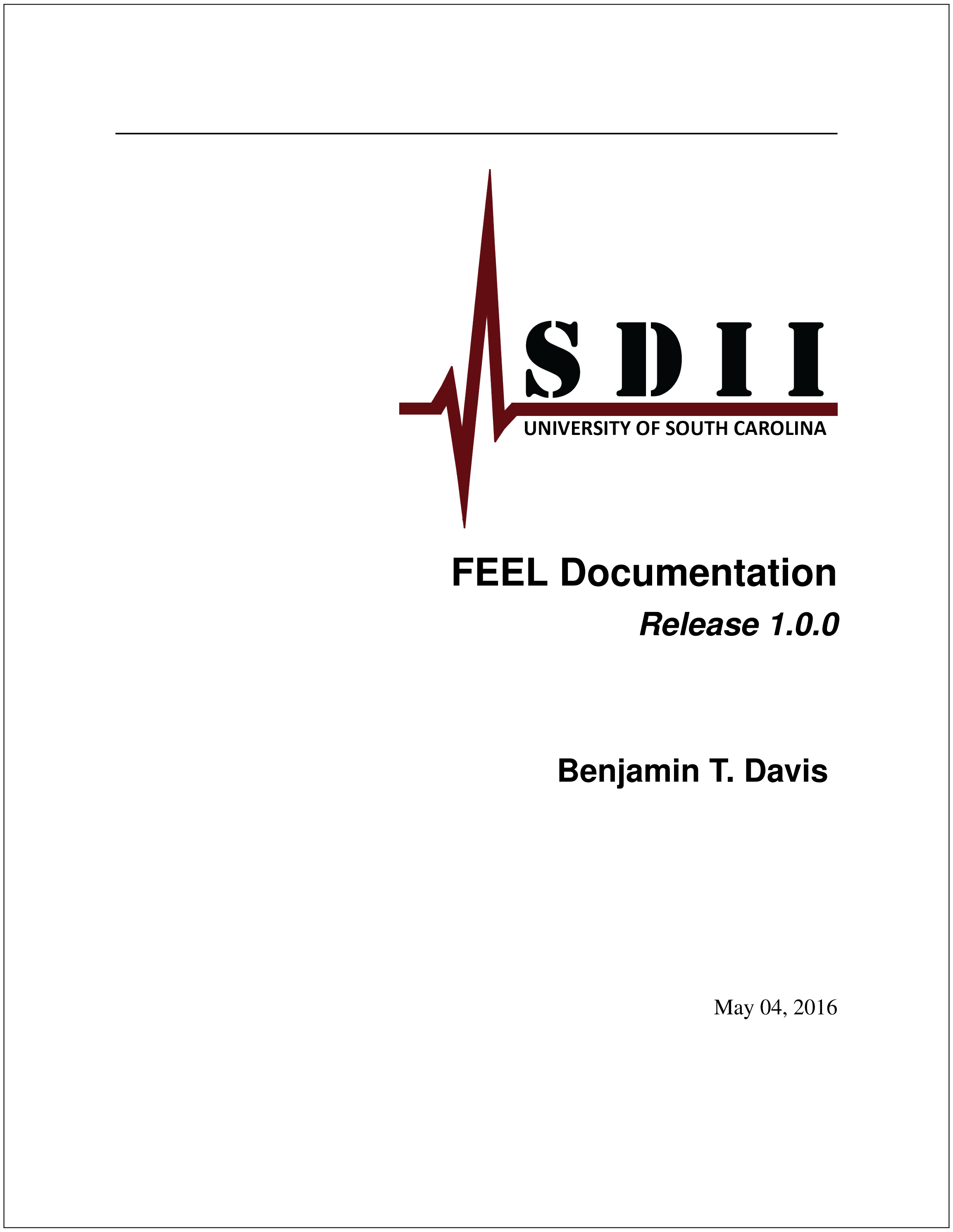

SDII
UNIVERSITY OF SOUTH CAROLINA

FEEL Documentation

Release 1.0.0

Benjamin T. Davis

May 04, 2016

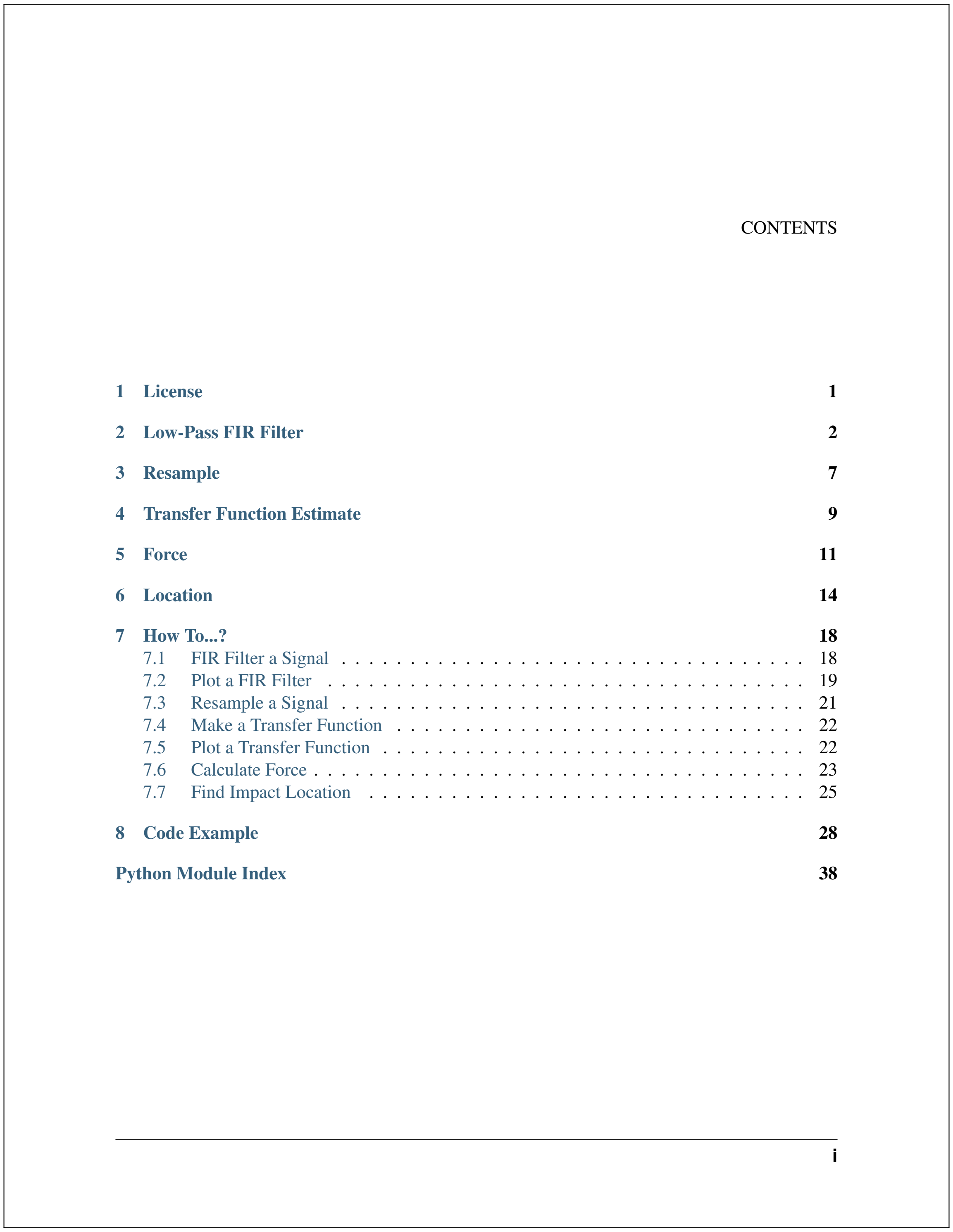

CONTENTS

CHAPTER

ONE

LICENSE

CHAPTER

TWO

LOW-PASS FIR FILTER

Author: Benjamin T. Davis, NSF Graduate Research Fellow <btdavis@email.sc.edu>

Date: 2015 May 1

`lowpassfir.`**`applyfilter`**(*data*, *taps*, *a*)

Applies a low-pass finite impulse response filter to clean digital acceleration and force data

Parameters

- **data** (*array-like*) – The detrended data captured from a system (e.g. force) where column is the sensor and row is time step
- **taps** (*1D array-like*) – The values of the taps of the low pass FIR filter; can get the taps using `design()`
- **a** (*float*) – The denominator coefficient for the filter; can get the taps using `design()`

Returns

- **fdata** (*array*) – The filtered data
- **delay** (*float*) – The phase delay in points from the beginning of the signal; to get the delay in seconds, divide value by sampling frequency; the filtering process corrupts part of the record, so shift the record by this value like this `fdata[delay:]`

Notes

- The way the record shift is calculated here differs from that of the reference material. This is due to some experimenting with the shifting value that determined force estimations are more accurate with the version presented here.

References

http://wiki.scipy.org/Cookbook/FIRFilter `lowpassfir.`**`design`** (*fs*, *trans_hz=10*, *ripple_db=160*, *cutoff_hz=208*, *rv='filter'*)

Designs a low-pass finite impulse response filter for cleaning digital acceleration and force data

Parameters

- **fs** (*float*) – Sampling frequency for the data in Hz
- **trans_hz** (*int or float | optional | default = 10*) – Transition width from pass to stop of the filter in Hz
- **ripple_db** (*int or float | optional | default = 160*) – Desired attenuation of the stop band in dB
- **cutoff_hz** (*int or float | optional | default = 208*) – Cut off frequency for the filter in Hz; it is recommended that this value is slightly higher than the desired Nyquist Rate, e.g. (0.5*fs)+8
- **rv** (*str | optional | default = 'filter'*) – Specified return values the user wants `filter` -> taps, a `params` -> taps, a, width, beta

Returns

- **taps** (*1D array-like*) – The values of the taps of the low pass FIR filter
- **a** (*float*) – The denominator coefficient for the filter
- **width** (*float*) – Transition width relative to Nyquist Rate
- **beta** (*float*) – Kaiser window beta parameter used

References

http://wiki.scipy.org/Cookbook/FIRFilter `lowpassfir.`**`plotfiltercoeff`**`(`*taps*`)`

Plots the FIR filter coefficients

Parameters taps (*1D array-like*) – The values of the taps of the low pass FIR filter; can get the taps using design()

Returns axis (*<matplotlib.axes.AxesSubplot>*) – The axis handle for the current plot; can be used to adjust the plot visuals

Notes

- The axis default to light gray in color
- Change various features of the plot using axis; e.g.

```
>>> pyplot.setp(axis.lines, color='r', linewidth=2.0, linestyle='-')
```

References

http://wiki.scipy.org/Cookbook/FIRFilter

http://matplotlib.org/users/pyplot_tutorial.html `lowpassfir.`**`plotfreqresponse`**`(`*taps*, *fs*`)`

Plots the FIR filter frequency response

Parameters

- **taps** (*1D array-like*) – The values of the taps of the low pass FIR filter; can get the taps using `design()`
- **fs** (*int or float*) – Sampling frequency for the data; same as used in `design()`

Returns **axis** (<*matplotlib.axes.AxesSubplot*>) – The axis handle for the current plot; can be used to adjust the plot visuals

Notes

- The axis default to light gray in color
- Change various features of the plot using axis; e.g.

```
>>> pyplot.setp(axis.lines, color='r', linewidth=2.0, linestyle='-')
```

References

http://wiki.scipy.org/Cookbook/FIRFilter

http://matplotlib.org/users/pyplot_tutorial.html

CHAPTER

THREE

RESAMPLE

Author: Benjamin T. Davis, NSF Graduate Research Fellow <btdavis@email.sc.edu>

Date: 2015 May 1

`resample.`**`resample`**(*data*, *oldfs*, *newfs*, *trans_hz=10*, *ripple_db=160*, *cutoff_hz=208*)

Resamples data from and old rate to a new rate using the Fourier Method, after applying a FIR filter to clean the data

Warning: Function has only been tested to work for downsampling!

Parameters

- **data** (*array-like*) – The detrended data captured from a system (e.g. force) where column is the sensor and row is time step
- **oldfs** (*float*) – Original sampling frequency for the data in Hz
- **newfs** (*float*) – New sampling frequency for the data in Hz
- **trans_hz** (*int or float | optional | default = 10*) – Transition width from pass to stop of the filter in Hz
- **ripple_db** (*int or float | optional | default = 160*) – Desired attenuation of the stop band in dB
- **cutoff_hz** (*int or float | optional | default = 208*) – Cut off frequency for the filter in Hz; it is recommended that this value is slightly higher than the desired Nyquist Rate, e.g. (0.5*fs)+8

Returns **rdata** (*1D array*) – The resampled data that has been adjusted for phase delay

Notes

- function has only been tested and verified to work when downsampling
- if you are interested in seeing more specifics about the filter, refer to lowpassfir functions

References

http://docs.scipy.org/doc/scipy-0.15.1/reference/generated/scipy.signal.resample.html

CHAPTER

FOUR

TRANSFER FUNCTION ESTIMATE

Author: Benjamin T. Davis, NSF Graduate Research Fellow <btdavis@email.sc.edu>

Date: 2015 April 30

`tfestimate.`**`tfestimate`**(*x*, *y*, *fs*, *nfft=2048*, *noverlap=1024*)

Estimates the transfer function using the average of two different methods to calculate the transfer function

Parameters

- **x** (*1D array-like*) – The input for the system (e.g. force)
- **y** (*1D array-like*) – The output of the system (e.g. accelerations) corresponding to the input x
- **fs** (*int or float*) – Sampling frequency for both the input and output
- **nfft** (*int | optional | default = 2048*) – Number of data points used in each block for FFT
- **noverlap** (*int | optional | default = 1024*) – Number of overlapping data points used for Welch's Average Periodogram Method

Returns

- **freq** (*1D array*) – The frequencies corresponding to each point of the transfer function estimate
- **tfe** (*1D array*) – The values of the transfer function estimate

Notes

- x and y should be captured at the same sampling frequency
- utilizes Welch‘s Average Periodogram Method
- typically one would want to display the transfer function in decibel units; to convert to dB perform 20*log10(tfe)

References

http://matplotlib.org/api/mlab_api.html?highlight=psd#matplotlib.mlab.psd

http://matplotlib.org/api/mlab_api.html?highlight=psd#matplotlib.mlab.csd

Bendat, J. S., and Piersol, A. G. (2000). Random Data: Analysis and Measurement Procedures. Wiley. New York.

Ewins, D.J. (2000). Modal Testing: Theory, Practice, and Application. Research Studies Press Ltd. p.238-239.

CHAPTER

FIVE

FORCE

Author: Benjamin T. Davis, NSF Graduate Research Fellow <btdavis@email.sc.edu>

Date: 2015 April 30

`force.estimate`(*accel*, *tfe*, *nfft=2048*, *rmtrend=False*)

Estimates the force of impact from acceleration data

Parameters

- **accel** (*1D array-like*) – The detrended accelerations captured from a system
- **tfe** (*1D array-like*) – The values of the transfer function estimate relating force and acceleration; these are found using feel.tfestimate()
- **nfft** (*int | optional | default = 2048*) – Number of data points used in the FFT
- **rmtrend** (*boolean | optional | default = False*) – Whether or not to remove trend (detrend) of the force estimate before returning the data; uses scipy.signal.detrend() with default settings

Returns **f_hat** (*array*) – The detrended impact force estimate

Notes

- Only uses the first n points of the acceleration signal, where n is the number of points of the tfe

References

http://docs.scipy.org/doc/numpy/reference/routines.fft.html

http://docs.scipy.org/doc/scipy-0.15.1/reference/generated/scipy.signal.detrend.html `force.`**`magnitude`**(*f_hat*)

Determines the magnitude of the force estimate. Grabs the two best matching force estimate pairs (based on correlations) and uses the real part of the complex conjugate to calculate the magnitude.

Parameters **f_hat** (*array*) – The force estimates for a location with rows being the sensor and columns being the data points

Returns **f** (*float*) – The force estimate magnitude

Notes

- it is easiest to take the outputs from force_estimate and use `numpy.vstack((force1, force2))` to create the f_hats array

CHAPTER SIX

LOCATION

Author: Benjamin T. Davis, NSF Graduate Research Fellow <btdavis@email.sc.edu>

Date: 2015 June 10

`location.`**`forcedev`**(*f_hats*)

Calculates the deviation of force estimates for each provided location using real portion of the estimate only

Parameters **f_hats** (*dict*) – The detrended impact force estimates for each sensor at each location of form

```
>>> f_hats = {1: [force11 force12], 2:[force21 force22]}
```

where the dict key is the location designation, and the dict value is an array where rows indicate sensor and column indicate points in the force estimates

Returns

L (*dict*) – The values for each location in f_hats of form

```
>>> L = {1: dev1, 2: dev2}
```

where lowest deviation value is the location of impact

Notes

- It is easiest to take the outputs from force_estimate and use numpy.vstack((force11, force12)) to create each dictionary value
- It is also best to use this method by first taking a window around the peak of the force estimate for each sensor record in f_hats

`location.`**`forcecorr`** (*f_hats*)

Calculates the correlation of force estimates for each provided location by calculating the correlation coefficents of pairs of signals and grabbing the largest coefficient as the correlation for the location

Parameters f_hats (*dict*) – The detrended impact force estimates for each sensor at each location of form

```
>>> f_hats = {1: [force11 force12], 2:[force21 force22]}
```

where the dict key is the location designation, and the dict value is an array where rows indicate sensor and column indicate points in the force estimates

Returns

L (*dict*) – The values for each location in f_hats of form

```
>>> L = {1: corr1, 2: corr2}
```

where highest correlation value is the location of impact

Notes

- It is easiest to take the outputs from force_estimate and use `numpy.vstack((force11, force12))` to create each dictionary value `location.`**`locate`**(*L*, *ctype='corr'*)

Determines the location of impact

Parameters

- **L** (*dict*) – The values for each location in f_hats of form {1: dev1, 2: dev2}
- **ctype** (*str*) – The force comparision type used

  `std` -> if results are from forcedev

  `corr` -> if results are from forcecorr

Returns **L_hat** (*any type*) – The location of impact; type is dependent on the key type given in the dictionary L

CHAPTER

SEVEN

HOW TO...?

Here are various topics to help you on your way to using the **feel** package to its fullest.

7.1 FIR Filter a Signal

Sometimes a signal contains a lot of high-frequency noise that is unnecessary for the FEEL Algorithm and it just creates *noisy* transfer functions which in turn skew results. The **feel** package provides a simple way to clean these signals using `lowpassfir()`.

Let's say you have acceleration data, named *signal*, collected at a rate of 2000 Hz, sees a lot of noise once it passes the 500 Hz frequency. We would filter it like in the following.

```python
from feel.lowpassfir import design, applyfilter

# design the filter
taps, a = design(fs=2000,
                 trans_hz=10,
                 ripple_db=160,
                 cutoff_hz=1008,
                 rv='filter')

# apply the filter
fdata, delay = applyfilter(data=signal,
                           taps=taps,
                           a=a)
```

FIR Filters have a linear phase delay which allows one to easily remove the phase from the filtered signal. This is done like in the following.

```python
s = fdata[delay:]
```

A good tip is to make the cut-off frequency slightly higher than the Nyquist Frequency, or in other words slightly higher than half of the *fs*.

7.2 Plot a FIR Filter

When reporting about the filter one used, it is sometimes beneficial to provide plots showing the the filter coefficients and frequency response. The **feel** package provides a simple way to clean these signals using *lowpassfir()*.

7.2.1 Filter Coefficents

To plot the filter coefficients, do the following.

```
from feel.lowpassfir import design, plotfiltercoeff

# design the filter
taps, a = design(fs=2000,
                 trans_hz=10,
                 ripple_db=160,
                 cutoff_hz=208,
                 rv='filter')

# now for plotting
axis = plotfiltercoeff(taps)
```

Figure 7.1 shows an example of what the filter coefficients look like when plotted.

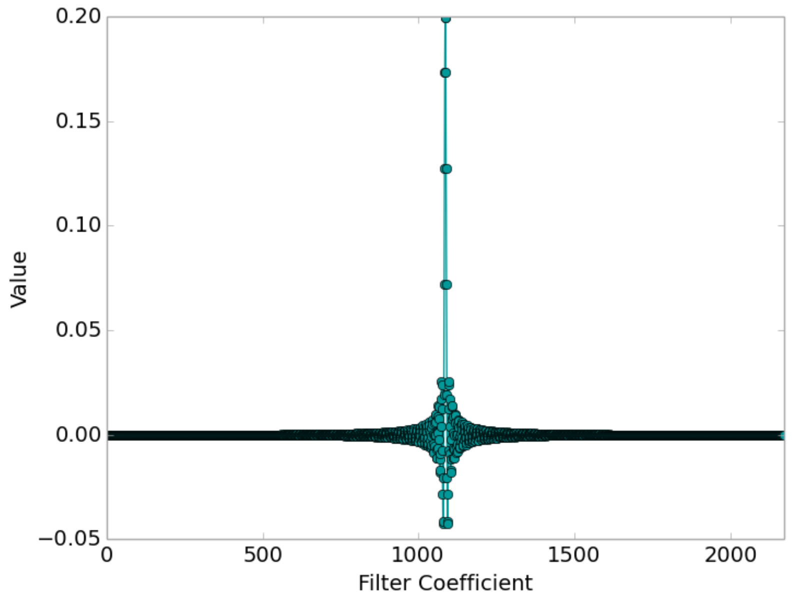

Fig. 7.1: Example Filter Coefficients

7.2.2 Frequency Response

To plot the frequency response, do the following.

```
from feel.lowpassfir import design, plotfreqresponse

fs = 2000

# design the filter
taps, a = design(fs=fs,
                 trans_hz=10,
                 ripple_db=160,
                 cutoff_hz=208,
                 rv='filter')

# now for plotting
axis = plotfreqresponse(taps,fs)
```

Figure 7.2 shows an example of what the frequency response looks when plotted.

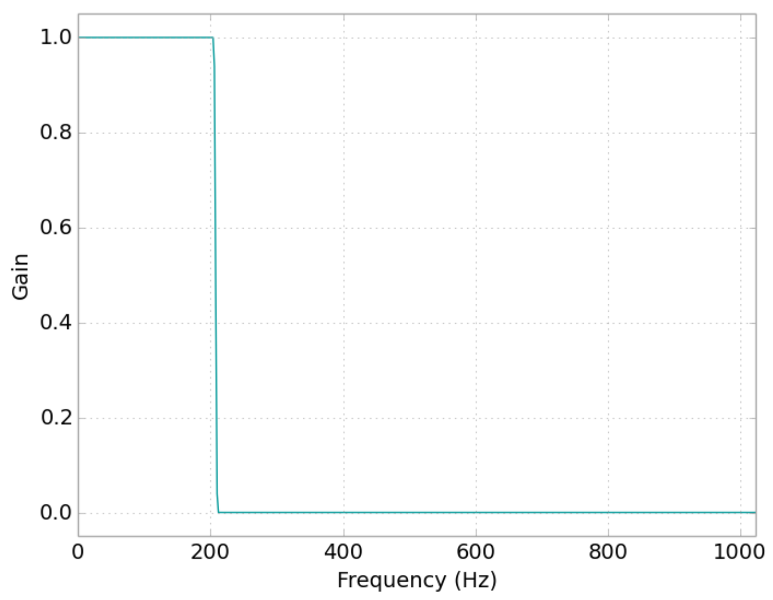

Fig. 7.2: Example Frequency Response

7.2.3 Editing Plots

If you do not like the default display of the plots, you can adjust it using *pyplot.setp()* like below.

```
pyplot.setp(axis.lines, color='r', linewidth=2.0, linestyle='-')
```

7.3 Resample a Signal

If a lower sampling rate is desired, one can use *scipy.signal.resample()* which does not apply a filter before resampling, or one can use `resample()` provided by the **feel** package. Using `resample()`, applies the filters available from `lowpassfir()` and then resamples using *scipy.signal.resample()*.

For example, consider the following code where we want to resample the data from 2000 Hz to 400 Hz.

```
from feel import resample

rdata = resample(data,
                 oldfs=2000,
                 newfs=400,
                 trans_hz=10,
                 ripple_db=160,
                 cutoff_hz=208)
```

A good tip is to make the cut-off frequency slightly higher than the Nyquist Frequency, or in other words slightly higher than half of the *newfs*.

7.4 Make a Transfer Function

The basis of the FEEL Algorithm is based in manipulation of transfer functions. So naturally a function, called `tfestimate()`, to easily generate said function is provided in the package. See the code snippet below where the variable *input* would the exciter of the system, and the variable *output* would be the measured response of the system.

```
from feel import tfestimate

freq, tfe = tfestimate(x=input,
                       y=output,
                       fs=500,
                       nfft=2048,
                       noverlap=1024)
```

Typically you would want to have an *noverlap* of half of the *nfft* which helps smooth out the transfer function.

7.5 Plot a Transfer Function

Transfer functions are often displayed using decibels for the power value and Hertz for the frequency values. The code above gives *freq* in Hertz, but not *tfe* in decibels. For example, here is how you would simply plot the output from `tfestimate()`.

```
import numpy as np
from matplotlib import pyplot as plt

tfe_db = 20 * np.log10(tfe)
```

```
plt.figure()
plt.plot(freq, tfe_db)
plt.ylabel('Power (dB)')
plt.xlabel('Frequency (Hz)')
plt.show()
```

Figure 7.3 shows an example of what a transfer function looks when plotted.

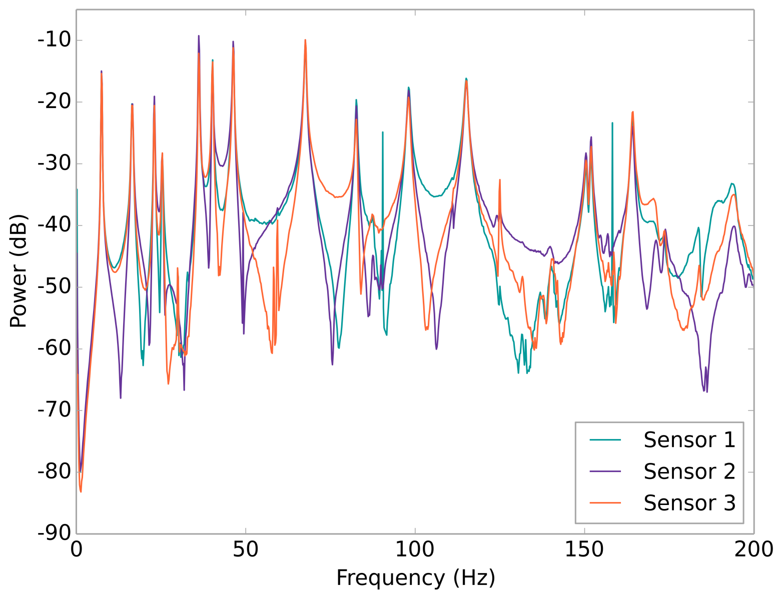

Fig. 7.3: Example Transfer Function Plot

7.6 Calculate Force

Force calculations are made simple using `force()`.

7.6.1 Force Vector

The force vector is calculated as seen in the example below. This output will have a time step equivalent to that of the transfer function *tfe* used to generate it. The acceleration signal should have the same sampling rate as the data used to generate the transfer functions, and the nfft should be the same as used to generate the *tfe*.

```
from feel import force

force = force.estimate(accel=signal,
                       tfe=tfe,
                       nfft=2048,
                       rmtrend=False)
```

Sometimes it may be desirable to utilize the *scipy.signal.detrend* function to straighten out the force vector, be advised that this can return weird results.

Figure 7.4 shows an example of what force vectors look like when plotted. The force vectors calculated for each sensor match the actual measured force.

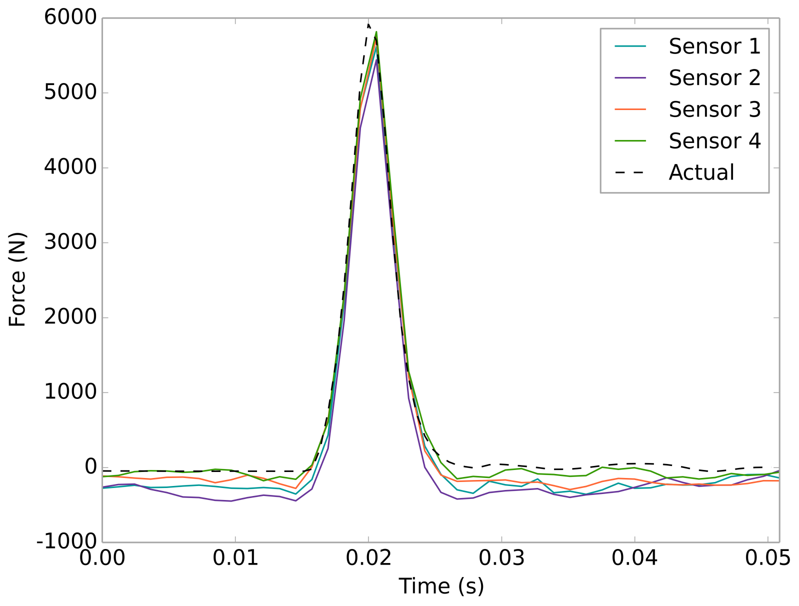

Fig. 7.4: Example Force Vector Plot

7.6.2 Force Magnitude

Each force vector has a peak magnitude which is considered to be the force of impact. This is calculated by taking the minimum value of the local peak area and subtracting it from the maximum value of the local peak area. Luckily, **feel** provides a function to do just that. See the example below.

```
from feel import force

magnitude = force.magnitude(force)
```

7.7 Find Impact Location

The location of impact can be determined using the force vectors from each sensor which experience the event. This method requires a minimum of two sensor's force vectors to work. Two techniques are shipped with the package. The author recommends the Force Correlation Method provided by *location.forcecorr()* as it is more robust, and will be the example presented. Alternatively, a second choice is to use the Force Deviation Method available from *location.forcedev()*.

7.7.1 Force Correlation Method

The author's recommended method is demonstrated in the example below. Let's start by getting the force vectors (see *force.estimate()*) of two sensors who are s1 and s2 respectively, for all two locations l1 and l2 using the transfer functions estimates (see *tfestimate()*) for each of the locations to each of the sensors.

```
import numpy as np
from feel import force, location

# location 1
force_s1_l1 = force.estimate(accel=s1,
                             tfe=tfe_s1_l1,
                             nfft=2048,
                             rmtrend=False)

force_s2_l1 = force.estimate(accel=s2,
                             tfe=tfe_s2_l1,
                             nfft=2048,
                             rmtrend=False)

# location 2
force_s1_l2 = force.estimate(accel=s1,
                             tfe=tfe_s1_l2,
                             nfft=2048,
                             rmtrend=False)

force_s2_l2 = force.estimate(accel=s2,
                             tfe=tfe_s2_l2,
                             nfft=2048,
                             rmtrend=False)
```

Then we make the *f_hats* dictionary where keys are location names and the values are the force vectors of each sensor for that location.

```
f_hats = {l1: np.vstack((force_s1_l1, force_s1_l1))
          l2: np.vstack((force_s1_l2, force_s1_l2))}
```

Once that is done, invoke the function for the Force Correlation Method (see *location.forcecorr()*) to get correlation values for each location.

```
L = location.forcecorr(f_hats)
```

This will give a dictionary back where key is the location label and value is the correlation for that location. Now apply the *location.locate()* function which will tell you which location the impact occurred.

```
L_hat = location.locate(L,
                        ctype='corr')
```

7.7.2 Plotting the Force Correlation Method

To visualize the location correlations, the author suggests using a bar plot where the x axis is the location labels (i.e. the keys of the *L* dictionary), and the y axis is the correlation value (i.e. the values of the *L* dictionary). Highlighting the location where the algorithm thinks the event occurred helps make the location's bar pop. Something like in Figure 7.5.

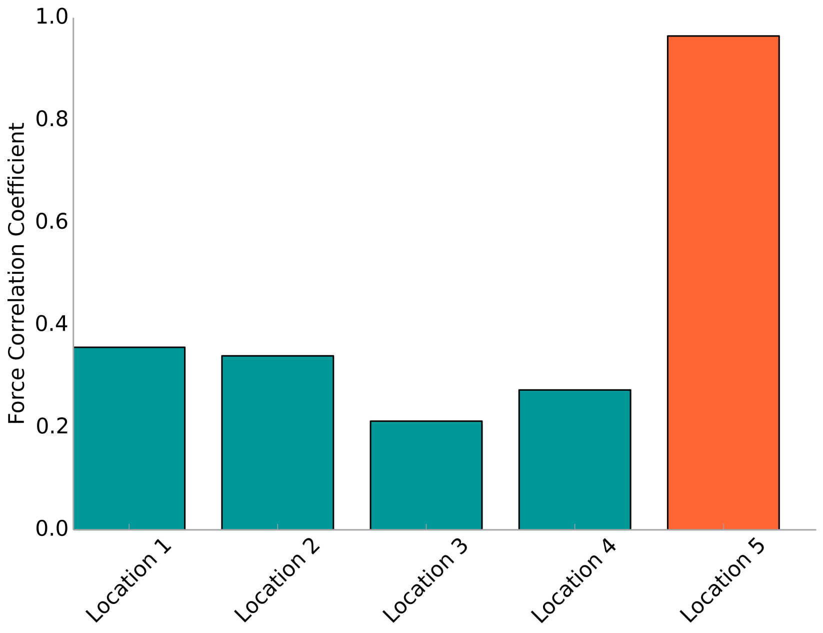

Fig. 7.5: Example Force Correlation Location Plot

CHAPTER

EIGHT

CODE EXAMPLE

A working example is provided along with the **feel** package that demonstrates its use. Look in the directory */feel/example/* for the Python code and the data files.

filename: example.py

```
"""
Example using the FEEL Algorithm toolsuite

Author: Benjamin T. Davis, NSF Graduate Research Fellow
Date Created: 2015 May 1
"""

import sys
import os
sys.path.insert(0, os.path.abspath('../../')) # path to feel package
                                              # relative to example.py

import numpy as np
import scipy.signal as signal
from matplotlib import pyplot as plt

from feel import resample, tfestimate, force, location


#%% set constants
dt = 0.000488 # time step between samples


#%% Load data
'''
Location 1 Data
'''
# Acceleration
filename = './loc1/Acceleration.txt'
loc1_accel = np.loadtxt(fname=filename, dtype=float, skiprows=7)
```

```
# Hammer (i.e. force)
filename = './loc1/Hammer.txt'
loc1_force = np.loadtxt(fname=filename, dtype=float, skiprows=7)


'''
location 2 Data
'''
# Acceleration
filename = './loc2/Acceleration.txt'
loc2_accel = np.loadtxt(fname=filename, dtype=float, skiprows=7)

# Hammer (i.e. force)
filename = './loc2/Hammer.txt'
loc2_force = np.loadtxt(fname=filename, dtype=float, skiprows=7)


#%% Detrend and resample data - this uses the lowpassfir functions
'''
If you did not need to resample, you would instead call

lowpassfir.design()
lowpassfir.applyFilter()

to clean the data.

Also, one can plot the filter using the functions

lowpassfir.plotfiltercoeff()
lowpassfir.plotfreqresponse()

See each function's help for more information
'''
newfs = 400.0 # desired new sampling rate, hz


# location 1
raccel_loc1 = np.empty((25776,3)) # cheating since I know the shape

for i in range(np.shape(loc1_accel)[1]):
    raccel_loc1[:,i] = resample(signal.detrend(loc1_accel[:,i]),
                                oldfs=1.0/dt,
                                newfs=newfs,
                                trans_hz=10,
                                ripple_db=160,
                                cutoff_hz=208)
```

```
rforce_loc1 = resample(signal.detrend(loc1_force),
                       oldfs=1.0/dt,
                       newfs=newfs,
                       trans_hz=10,
                       ripple_db=160,
                       cutoff_hz=208)

rforce_loc1 *= 10.350 # convert from volts to lb of force hammer

# plot location 1 data
plt.figure()
plt.subplot(4,1,1)
plt.plot(raccel_loc1[:,0])
plt.ylim((-0.6,0.6))
plt.xlim((0,len(raccel_loc1[:,0])))
plt.title('Location 1 - ai0')
plt.ylabel('Accel (g)')
plt.subplot(4,1,2)
plt.plot(raccel_loc1[:,1])
plt.ylim((-0.6,0.6))
plt.xlim((0,len(raccel_loc1[:,1])))
plt.title('Location 1 - ai1')
plt.ylabel('Accel (g)')
plt.subplot(4,1,3)
plt.plot(raccel_loc1[:,2])
plt.ylim((-0.6,0.6))
plt.xlim((0,len(raccel_loc1[:,2])))
plt.title('Location 1 - ai2')
plt.ylabel('Accel (g)')
plt.subplot(4,1,4)
plt.xlim((0,len(rforce_loc1)))
plt.plot(rforce_loc1)
plt.title('Location 1 - Force')
plt.ylabel('Force (lb)')
plt.xlabel('Points')
plt.tight_layout()
plt.show()


# location 2
raccel_loc2 = np.empty((25776,3)) # cheating since I know the shape

for i in range(np.shape(loc2_accel)[1]):
    raccel_loc2[:,i] = resample(signal.detrend(loc2_accel[:,i]),
                                oldfs=1.0/dt,
                                newfs=newfs,
                                trans_hz=10,
                                ripple_db=160,
                                cutoff_hz=208)

rforce_loc2 = resample(signal.detrend(loc2_force),
                       oldfs=1.0/dt,
                       newfs=newfs,
                       trans_hz=10,
                       ripple_db=160,
                       cutoff_hz=208)

rforce_loc2 *= 10.350 # convert from volts to lb of force hammer

# plot location 2 data
plt.figure()
plt.subplot(4,1,1)
plt.plot(raccel_loc2[:,0])
plt.ylim((-0.6,0.6))
plt.xlim((0,len(raccel_loc2[:,0])))
plt.title('Location 2 - ai0')
plt.ylabel('Accel (g)')
plt.subplot(4,1,2)
plt.plot(raccel_loc2[:,1])
plt.ylim((-0.6,0.6))
plt.xlim((0,len(raccel_loc2[:,1])))
plt.title('Location 2 - ai1')
plt.ylabel('Accel (g)')
plt.subplot(4,1,3)
plt.plot(raccel_loc2[:,2])
plt.ylim((-0.6,0.6))
plt.xlim((0,len(raccel_loc2[:,2])))
plt.title('Location 2 - ai2')
plt.ylabel('Accel (g)')
plt.subplot(4,1,4)
plt.xlim((0,len(rforce_loc2)))
plt.plot(rforce_loc2)
plt.title('Location 2 - Force')
plt.ylabel('Force (lb)')
plt.xlabel('Points')
plt.tight_layout()
plt.show()


#%% Estimate transfer functions
nfft = 2048 # size of FFT window, typically best as a power of 2
noverlap = nfft / 2 # overlap of Welch method, typically half of nfft
```

```
# Location 1
freq_ai0, loc1_ai0_tf = tfestimate(x=rforce_loc1,
                                   y=raccel_loc1[:,0],
                                   fs=newfs,
                                   nfft=nfft,
                                   noverlap=noverlap)

freq_ai1, loc1_ai1_tf = tfestimate(x=rforce_loc1,
                                   y=raccel_loc1[:,1],
                                   fs=newfs,
                                   nfft=nfft,
                                   noverlap=noverlap)

freq_ai2, loc1_ai2_tf = tfestimate(x=rforce_loc1,
                                   y=raccel_loc1[:,2],
                                   fs=newfs,
                                   nfft=nfft,
                                   noverlap=noverlap)

# plot location 1 TF
plt.figure()
plt.plot(freq_ai0, 20*np.log10(loc1_ai0_tf), label='ai0')
plt.plot(freq_ai1, 20*np.log10(loc1_ai1_tf), label='ai1')
plt.plot(freq_ai2, 20*np.log10(loc1_ai2_tf), label='ai2')
plt.legend()
plt.title('Location 1 Transfer Functions')
plt.xlabel('Frequency (Hz)')
plt.ylabel('Power (dB)')
plt.show()


# Location 2
freq_ai0, loc2_ai0_tf = tfestimate(x=rforce_loc2,
                                   y=raccel_loc2[:,0],
                                   fs=newfs,
                                   nfft=nfft,
                                   noverlap=noverlap)

freq_ai1, loc2_ai1_tf = tfestimate(x=rforce_loc2,
                                   y=raccel_loc2[:,1],
                                   fs=newfs,
                                   nfft=nfft,
                                   noverlap=noverlap)

freq_ai2, loc2_ai2_tf = tfestimate(x=rforce_loc2,
                                   y=raccel_loc2[:,2],
                                    fs=newfs,
                                    nfft=nfft,
                                    noverlap=noverlap)

# plot location 2 TF
plt.figure()
plt.plot(freq_ai0, 20*np.log10(loc2_ai0_tf), label='ai0')
plt.plot(freq_ai1, 20*np.log10(loc2_ai1_tf), label='ai1')
plt.plot(freq_ai2, 20*np.log10(loc2_ai2_tf), label='ai2')
plt.legend()
plt.title('Location 2 Transfer Functions')
plt.xlabel('Frequency (Hz)')
plt.ylabel('Power (dB)')
plt.show()



#%% Estimating the force with an impact at location 1
rlength = 1800
maxpoint = np.argmax(rforce_loc1)
f = rforce_loc1[maxpoint-50:maxpoint+rlength]
a0 = raccel_loc1[maxpoint-50:maxpoint+rlength,0]
a1 = raccel_loc1[maxpoint-50:maxpoint+rlength,1]
a2 = raccel_loc1[maxpoint-50:maxpoint+rlength,2]

# estimating using location 1 transfer functions
# f<location><sensor>
f11 = force.estimate(accel=a0,
                     tfe=loc1_ai0_tf,
                     nfft=nfft)

f12 = force.estimate(accel=a1,
                     tfe=loc1_ai1_tf,
                     nfft=nfft)

f13 = force.estimate(accel=a2,
                     tfe=loc1_ai2_tf,
                     nfft=nfft)

# estimating using location 2 transfer functions
# f<location><sensor>
f21 = force.estimate(accel=a0,
                     tfe=loc2_ai0_tf,
                     nfft=nfft)

f22 = force.estimate(accel=a1,
                     tfe=loc2_ai1_tf,
                     nfft=nfft)

f23 = force.estimate(accel=a2,
                     tfe=loc2_ai2_tf,
                     nfft=nfft)

# form the dictionary for force_location
# location #: array((sensor) x (npoints in force_estimate))
# aka row is sensor, column is point in force estimate for each entry
f_hats = {1:np.vstack((f11,f12,f13)), 2:np.vstack((f21,f22,f23))}

L = location.forcecorr(f_hats) # determines the force correlations

x = []
y = []
for key, val in L.items():
    x.append(key)
    y.append(val)

time1 = np.array(range(0,len(f))) * dt
time2 = np.array(range(0,len(f11))) * dt * 2.0

plt.figure()

# plot actual force of impact
plt.subplot(4,1,1)
plt.plot(time1, f, label='Actual')
plt.title('Actual Impact at Location 1')
plt.xlabel('Time (s)')
plt.ylabel('Force (N)')

# plot location 1 force estimates
plt.subplot(4,1,2)
plt.plot(time2, f11, label='ai0')
plt.plot(time2, f12, label='ai1')
plt.plot(time2, f13, label='ai2')
plt.legend()
plt.title('Location 1 Force Estimates (L1 TF)')
plt.xlabel('Time (s)')
plt.ylabel('Force (N)')

# plot location 2 force estimates
plt.subplot(4,1,3)
plt.plot(time2, f21, label='ai0')
plt.plot(time2, f22, label='ai1')
plt.plot(time2, f23, label='ai2')
plt.legend()
plt.title('Location 2 Force Estimates (L2 TF)')
plt.xlabel('Time (s)')
plt.ylabel('Force (N)')

# event localization
# locate function gives the location number
plt.subplot(4,1,4)
width = 0.8
plt.bar(x,y, width=0.8, align='center')
plt.title('Impact Occured at Location %s' %location.locate(L))
plt.xlabel('Location')
plt.ylabel('Force Correlation')
axis = plt.gca()
axis.xaxis.set_ticks([1,2])
axis.xaxis.set_ticklabels(['Loc %s'%x[0],'Loc %s'%x[1]])

plt.tight_layout()

plt.show()



#%% Estimating the force with an impact at location 2
rlength = 1800
maxpoint = np.argmax(rforce_loc2)
f = rforce_loc2[maxpoint-50:maxpoint+rlength]
a0 = raccel_loc2[maxpoint-50:maxpoint+rlength,0]
a1 = raccel_loc2[maxpoint-50:maxpoint+rlength,1]
a2 = raccel_loc2[maxpoint-50:maxpoint+rlength,2]

# estimating using location 1 transfer functions
# f<location><sensor>
f11 = force.estimate(accel=a0,
                     tfe=loc1_ai0_tf,
                     nfft=nfft)

f12 = force.estimate(accel=a1,
                     tfe=loc1_ai1_tf,
                     nfft=nfft)

f13 = force.estimate(accel=a2,
                     tfe=loc1_ai2_tf,
                     nfft=nfft)

# estimating using location 2 transfer functions
# f<location><sensor>
f21 = force.estimate(accel=a0,
                     tfe=loc2_ai0_tf,
                     nfft=nfft)

f22 = force.estimate(accel=a1,
                     tfe=loc2_ai1_tf,
                     nfft=nfft)

f23 = force.estimate(accel=a2,
                     tfe=loc2_ai2_tf,
                     nfft=nfft)

# form the dictionary for force_location
# location #: array((sensor) x (npoints in force_estimate))
# aka row is sensor, column is point in force estimate for each entry
f_hats = {1:np.vstack((f11,f12,f13)), 2:np.vstack((f21,f22,f23))}

L = location.forcecorr(f_hats) # determines the force correlations

x = []
y = []
for key, val in L.items():
    x.append(key)
    y.append(val)


time1 = np.array(range(0,len(f))) * dt
time2 = np.array(range(0,len(f11))) * dt * 2.0

plt.figure()

# plot actual force of impact
plt.subplot(4,1,1)
plt.plot(time1, f, label='Actual')
plt.title('Actual Impact at Location 1')
plt.xlabel('Time (s)')
plt.ylabel('Force (N)')

# plot location 1 force estimates
plt.subplot(4,1,2)
plt.plot(time2, f11, label='ai0')
plt.plot(time2, f12, label='ai1')
plt.plot(time2, f13, label='ai2')
plt.legend()
plt.title('Location 1 Force Estimates (L1 TF)')
plt.xlabel('Time (s)')
plt.ylabel('Force (N)')
```

```
# plot location 2 force estimates
plt.subplot(4,1,3)
plt.plot(time2, f21, label='ai0')
plt.plot(time2, f22, label='ai1')
plt.plot(time2, f23, label='ai2')
plt.legend()
plt.title('Location 2 Force Estimates (L2 TF)')
plt.xlabel('Time (s)')
plt.ylabel('Force (N)')

# event localization
# locate function gives the location number
plt.subplot(4,1,4)
width = 0.8
plt.bar(x,y, width=0.8, align='center')
plt.title('Impact Occurred at Location %s' %location.locate(L))
plt.xlabel('Location')
plt.ylabel('Force Correlation')
axis = plt.gca()
axis.xaxis.set_ticks([1,2])
axis.xaxis.set_ticklabels(['Loc %s'%x[0],'Loc %s'%x[1]])

plt.tight_layout()

plt.show()
```